Numerical modelling of the coastal processes in Dithmarschen Bight incorporating field data

Dissertation
Zur Erlangung des Doktorgrades
der Mathematisch-Naturwissenschaftlichen Fakultät
der Christian-Albrechts-Universität zu Kiel

vorgelegt von
Maryam Rahbani

Kiel
May 2011

Referent:	Prof. Dr. Roberto Mayerle
Korreferent:	Prof. Dr. Athanasios Vafeidis
Tag der mündlichen Prüfung:	04.05.2011
Zum Druck genehmigt:	04.05.2011

To my mother

Simin

Acknowledgements

Had it not been for the support I have received in the last six years, I doubt that this thesis would be where it is today. Over the years I have been lucky to receive the guidance and encouragement from people who more than generous with their time and knowledge.

Firstly, I would like to thank my supervisor Prof. Dr. Roberto Mayerle, whose patience and full attention have been a blessing. Not only was he there to answer my queries, he also challenged me to produce my best work. I would also like to mention Prof. Dr. Athanasios Vafeidis for being the Korreferent and reviewer of my dissertation.

My time in Germany would never have been possible without the financial support I was given by the General Bureau of Scholarship and Overseas Affairs. More specifically a special gratitude to the University of Hormozgan for granting me the opportunity to study abroad.

I am eternally grateful to Dr. Rangaswami Narayanan, Dr. Hossein Keshavarz and Dr. Peter Weppen for their time, patience and influence in steering me in the right direction. Between them they devoted a lot of time in not only reading and editing my work but also in providing moral support. I also appreciate the support and guidance from my colleagues at the Coastal Research Laboratory. In particular, I am grateful to Dr. Wiwin Windupranata, Dr. Poerbandono, Dr. Karl-Heinz Runte, Dr. Talal Etri, Simon A. van der Wulp, Joaquim Pereira Bento Netto Jr., Katharina Róisín Niederndorfer, Jose Manuel Fernandez Jaramillo, Jana Block, and Robert Osinski.

A special thanks to my friend, Parvaneh Karimi Massoule who did more than enough to fill the void left from being so far from my family. She ended up being the sister that I never had.

And finally, I would like to thank my family. First and foremost my mother Simin, who deserves the biggest acknowledgement. If it was not for her endless encouragement and support throughout whole my life, I doubt I would have been at this level. I cannot forget my father, Rahim as well as my brothers, Mazyar and Sam, who never stopped believing in me.

Maryam Rahbani

Kiel 10.05.2011

Abstract

The main concern of this investigation is to evaluate the use of numerical models in the study of the sediment transport in the Dithmarschen Bight located in the German North Sea coast. The area consists of tidal channels and tidal flats with prevailing semi-diurnal tides with a mean tidal range of about 3.2m. Five independently collected sets of data at different stages of the neap-spring tides were used for the evaluation of numerical models. The employed models were those from the Delft3D package (Delft Hydraulics, The Netherlands) in two and three dimensions. The investigation stages consisted of i) evaluation of the two dimensional model results (2DH) in comparison with the field data, and ii) assessment and comparison of the three dimensional model results (3D) with the field data and with the two dimensional model results.

Following the comparison of the 2DH model results with the field data, it was found that the boundary conditions of the model required adjustment. The adjusted model was used to study the effect of wind induced waves on the performance of the model in providing information on the hydrodynamics and sediment dynamics of the area. It is shown that the effect of waves under moderate winds having velocities less than 11m/s is not significant for this area. It is also shown that the performance of the model in providing the hydrodynamic values in comparison with field data was good, as the mean absolute errors between these values and the data were less than 0.2 m/s. This was not the case in regard to sediment transport values provided by the model.

In the assessment of the performance of the 3D model, the results of the executed model were compared with the field data and the 2DH model results. Over the depth of flow, the uniform distribution of the current velocity and the suspended sediment concentration were comparable with the depth-averaged results obtained from the 2DH model. This confirmed that the coastal water under investigation shows well-mixed conditions. The comparison of the 3D model results and the field data showed some disagreements that were analysed to be due to the measuring devices used in the field measurements and to some model shortcomings. It is shown that the transmissometer device, employed for deriving suspended sediment concentration data, might contribute some error when used in regions of shallow water in the area. The disagreements between the results and the data attributed to the model performance were considered to be mainly due to the input of grain size distribution specifically on the tidal flat area, settling velocity, and critical bed shear stresses. These, in turn, were due to insufficient field data to feed proper values to the model.

Furthermore, it is shown that the critical bed shear stress and settling velocity are not constant for the whole area and the use of variable values on the basis of measurements is necessary. The difficulty in obtaining accurate data on suspended sediment concentrations from field measurements makes the assessment of the accuracy of the results difficult. Besides this, the limits associated with the Delft3D modelling should be included which does not allow the use of variable values of settling velocities over the area.

It is shown that the difference between results, i.e. the current velocity and the suspended sediment concentration from the two and the three dimensional simulations is not significant. Thus, the use of the 3D model may not be justified with the currently available data for the area under investigation. However, the 3D model made it possible to find some weak points and deficiencies in the model; and in the collected data from the field. It has also provided very useful information about the flow and sediment dynamics of the area and the type of data required for further studies if three dimensional simulations are to be used.

Kurzfassung

Das wesentlichste Anliegen dieser Untersuchung ist es, die Eignung und Anwendung numerischer Modelle für bzw. auf das Studium des Sedimenttransportes in der Dithmarscher Bucht, an der deutschen Nordseeküste zu analysieren. Das Gebiet besteht aus Prielen und Wattflächen mit einer vorherrschend halbtägigen Tide mit einem mittleren Tidenhub von 3,2m. Fünf unabhängige Datensätze aus verschiedenen Phasen des Spring-Nipp-Zyklus wurden genutzt, um die numerischen Modelle zu untersuchen, die dem Delft3D-Paket (Delft Hydraulics, Niederlande) in der zwei- und dreidimensionalen Version entstammen. Die Phasen der Untersuchung bestanden aus i) Analyse der Resultate des tiefen-integrierten zweidimensionalen Modells (2DH) im Vergleich zu Naturmessungen; und ii) Bewertung und Vergleich der Resultate des dreidimensionalen (3D) Models mit Naturmessungen und ebenso mit den Ergebnissen aus dem zweidimensionalen Modell.

Als Schlussfolgerung aus dem Vergleich der Resultate des 2DH Modells mit den Naturdaten wurde festgestellt, dass die Randbedingungen an der Offenen Modellgrenze der Modelle eine Anpassung erforderten. Das angepasste Modell wurde genutzt, um den Effekt von Wind-induzierten Wellen auf die Leistungsfähigkeit des Modells zu untersuchen, indem es Informationen über die Hydrodynamik und Sedimentdynamik des Untersuchungsgebietes bereitstellte. Es wird gezeigt, dass der Effekt von Wellen unter moderaten Windbedingungen mit Windgeschwindigkeiten kleiner als 11m/s ohne Bedeutung ist für das Untersuchungsgebiet. Es wird auch gezeigt, dass die Leistungsfähigkeit des Modells für die Produktion hydrodynamischer Daten im Vergleich mit den Feldmessungen gut war, weil die mittleren absoluten Fehler zwischen den Modelldaten und Naturdaten kleiner als 0,2m/s waren. Mit Blick auf die Daten zum Sedimenttransport, die das Modell lieferte, war dies nicht der Fall.

In der Analyse zur Leistungsfähigkeit des 3D-Modells wurden die Resultate des ausgeführten Modells mit den Naturmessungen und den Ergebnissen des 2DH-Modells verglichen. Über das Tiefenprofil für die Strömung war die einheitliche Verteilung der Strömungsgschwindigkeiten und der Konzentration von suspendiertem Sediment (SSC) vergleichbar mit den tiefengemittelten Ergebnissen aus dem 2DH-Modell. Dies bestätigt, dass das untersuchte Küstengewässer gut durchmischte Bedingungen aufweist. Der Vergleich der Resultate des 3D-Modells und der Feldmessungen zeigte gewisse Abweichungen, die sowohl den Eigenschaften der verwendeten Messgeräte, die bei den Feldmessungen eingesetzt wurden, sowie einigen Problemen (shortcommings) des Modells

zugeordnet werden konnten. Es wird gezeigt, dass das Transmissometer-Messsystem, das verwendet wurde, um SSC-Daten herzuleiten, einige (systematische) Fehler aufgewiesen haben könnte, wenn es in Flachwassergebieten im Untersuchungsgebiet eingesetzt wurde. Abweichungen zwischen Modellergebnissen und Naturdaten, soweit sie der Modell-Leistung zugeordnet wurden, wurden ursächlich auf die vorgegebene Korngrössenverteilung, speziell im Bereich der Wattflächen, die Werte für die Sedimentationsgeschwindigkeit und den Wert für den kritischen *Bed Shear Stress* zurückgeführt. Im Umkehrschluss ergeben sich diese Werte aus Naturmessungen, die allerdings zu unzureichend sind, um präzisere Daten in das Modell zuliefern. Darüberhinaus wird demonstriert, dass der kritische *Bed Shear Stress* und die Sedimentationsrate nicht über das gesamte Untersuchungsgebiet konstant sind; die Verwendung von (räumlich) verschiedenen Werten auf der Grundlage von Naturmessungen ist erforderlich. Die Problematik, genaue Werte für die SSC aus Feldmessungen zu erhalten, erschwert die Bewertung der Ergebnisse. Hierzu sollten auch Grenzen im Delft3D-Paket erwähnt werden, die es nicht erlauben, verschiedene Werte für die Sedimentationsgeschwindigkeit im Untersuchungsgebiet zu verwenden.

Es wird gezeigt, dass die Unterschiede zwischen den Ergebnissen, vor allem bei der Strömungsgeschwindigkeit aus dem Vergleich der Resultate des 2DH Modells mit den Naturdaten und SSC, aus den 2DH- und 3D-Simulationen nicht signifikant sind. Deshalb ist die Nutzung des 3D-Modells auf der Grundlage der gegenwärtig verfügbaren Daten zum Untersuchungsgebiet möglicherweise nicht gerechtfertigt. Trotzdem ermöglicht es das 3D-Modell, einige Schwächen und Mängel in dem Modell aufzufinden, auch in den gesammelten Feld-Daten. Es hat sehr nützliche Informationen über Strömungsverhältnisse und Sedimentdynamik im Untersuchungsgebiet geliefert. Ferner Konnten Hinweise auf die Art der Daten gegeben werden, die für 3D-Simulationen erforderlich sind.

Definition of symbols

Symbol	Units	Meaning
A	Kg/m^3	attenuation coefficient
A_{nest}	m	tide amplitude from nesting sequence
A_{meas}	m	measured tide amplitude
a	m	reference level above the mean bed
a_i	-	constant
b_i	-	constant
c	Kg/m^3	suspended sediment concentrations
c_a	Kg/m^3	suspended concentration of the sediment at the reference height a
c_b	Kg/m^3	average sediment concentration in the near bottom computational layer
d_{50}	m	median diameter of sediment
D	$kg/m^2/s$	deposition rate
D_*	-	dimensionless particle diameter
D_{floc}	mm	diameter of the floc
D_P	mm	diameter of the primary particle
D_H	m^2/s	eddy diffusivity in the horizontal
D_V	m^2/s	eddy diffusivity in the vertical
E	$kg/m^2/s$	erosion rate
E_f	$kg/m^2/s$	residual floc erosion rate
EI	dB	acoustic echo intensity
f	1/s	Coriolis parameter
f_{BED}	-	calibration factor
F	kg/ms^2	horizontal Reynolds stress
g	m/s^2	gravity
G	m^2	coefficient used to transform curvilinear to rectangular coordinates
h	m	water depth
H_{adj}	m	adjusted water level at boundaries

H_{nest}	m	water level obtained from the nesting sequence
H_{meas}	m	measured water level
I	Decimal fraction	optical transmission received by transmissometer light detector
k	-	Von Karman constant
k_1	-	constant coefficient
L	cm	transmissometer path length
m	-	coefficient
M	kg/ms^2	external momentum due to sources and sinks
M_{er}	kg/m^2/s	erosion parameter
n	-	constant
n_f	fractal dimension	representative of the number and the linear size of the primary particles
P	kg/ms^2	hydrostatic water pressure
$P_{m,eq}$	-	dimensionless parameter of the ratio between the deposition and erosion flux capacity
Q	m/s	discharge source or sink per unit area
Re_P	-	particle Reynolds number
R^2	-	correlation coefficient
RMAE	-	Relative Mean Absolute Error
s	-	relative density of sediment
S	Kg/m^3/s	source and sink terms per unit area
CBSSE	N/m^2	critical bed shear stress for erosion
SSC	Kg/m^3	Suspended Sediment Concentration
$\lvert S_b \rvert$	kg/m/s	bed load transport rate
t	s	time
t_{adj}	min	adjusted peak occurrence time
t_{nest}	min	peak occurrence time derived from nesting sequence
t_{meas}	min	measured peak occurrence time
T_a	-	dimensionless bed shear stress
TCM	-	Turbulence Closure Module
U	m/s	depth-averaged velocity in x or ξ -direction
U_{GLM}	m/s	Generalized Lagrangian Mean velocity in x direction
u	m/s	Eulerian velocity in x direction
u_s	m/s	Stokes' drift in x direction
u_*'	m/s	effective bed shear velocity
V	m/s	depth-averaged velocity in y or η -direction
V_{GLM}	m/s	Generalized Lagrangian Mean velocity in y direction
v	m/s	Eulerian velocity in y direction
v_s	m/s	Stokes' drift in y direction
w	m/s	vertical velocity
w_s	m/s	settling velocity
$w_{s,r}$	m/s	settling velocity of the floc
x	m	Cartesian co-ordinate

y	m	Cartesian co-ordinate
z	m	Cartesian co-ordinate
z_b	m	elevation above the bed
α_{er}	-	coefficient
α	-	shape parameter
β	-	shape parameter
$\overline{\Delta A}$	m	average amplitude ratio
$\overline{\Delta H}$	m	average difference in the peak water levels
$\overline{\Delta t}$	s	average difference in the peak occurrence time
ℓ	-	fractions of the sediment
ν	m^2/s	eddy viscosity
ν_H	m^2/s	horizontal eddy viscosity
ν_V	m^2/s	vertical eddy viscosity
ρ_s	kg/m^3	sediment density
ρ_w	kg/m^3	water density
σ	-	scaled vertical co-ordinate
σ_c	-	Prandtl-Schmidt number
μ		Dynamic viscosity
τ_b	N/m^2	grain related or effective bed shear stress
τ_{ce}	N/m^2	critical shear stress for erosion
τ_{cd}	N/m^2	critical bed shear stress for deposition
τ_{cw}	N/m^2	maximum bed shear stress
η	-	horizontal curvilinear coordinate
η_{re}	-	relative availability of the sediment fraction in the mixing layer
ω	m/s	velocity in the z-direction in the σ coordinate system
ξ	-	horizontal curvilinear coordinate
ζ	m	free surface elevation above the reference

Contents

ACKNOWLEDGEMENTS ..... **VII**

ABSTRACT ..... **VIII**

KURZFASSUNG ..... **X**

DEFINITION OF SYMBOLS ..... **XII**

CONTENTS ..... **XV**

LIST OF FIGURES ..... **XIX**

LIST OF TABLES ..... **XXIII**

CHAPTER 1. INTRODUCTION **1**

1.1 OVERVIEW 1
1.2 THE SIGNIFICANCE OF MODELLING 2
1.3 THE SIGNIFICANCE OF DATA COLLECTION 4
1.4 SENSITIVITY ANALYSIS, CALIBRATION, AND VALIDATION 6
1.5 OBJECTIVES OF THIS STUDY 7
1.6 SUBJECT AND METHODS 9

CHAPTER 2. LITERATURE REVIEW **11**

2.1 INTRODUCTION 11
2.1.1 Physical models *12*
2.1.2 Numerical Models *12*
2.2 SPATIAL DIMENSIONS OF A NUMERICAL MODEL 13
2.2.1 One-Dimensional Models *14*
2.2.2 Two-dimensional models *14*
2.2.3 Three dimensional models *15*
2.3 FLOW, SEDIMENT TRANSPORT AND MORPHOLOGICAL MODELS 17
2.3.1 Non cohesive sediment model *18*
2.3.2 Cohesive sediment models *18*
2.3.3 Mixture of mud and sand *19*
2.4 EROSION 20

2.4.1 Erosion parameter *22*
2.4.2 Critical Bed Shear Stress for Erosion *23*
2.5 SETTLING VELOCITY 25
2.6 DEPOSITION 28

CHAPTER 3. INTRODUCING THE AREA AND AVAILABLE FIELD DATA 33

3.1 INTRODUCTION 33
3.2 LOCATION OF DITHMARSCHEN BIGHT 33
3.3 GEOLOGICAL, MORPHOLOGICAL AND MORPHODYNAMIC FEATURES OF THE AREA 34
3.4 METEOROLOGY AND WAVE CHARACTERISTIC OF THE AREA 38
3.5 THE HYDRODYNAMICS OF THE AREA 39
3.6 WATER TEMPERATURE, DENSITY, AND SALINITY 41
3.7 SEDIMENT DISTRIBUTION AND SEDIMENT DYNAMICS OF THE AREA 43
3.8 MEASUREMENTS AND DEVICES 45
3.8.1 Current velocity *45*
3.8.2 Suspended sediment concentration (SSC) *46*
3.8.2.1 Niskin bottle 46
3.8.2.2 Transmissometer 47
3.8.2.3 ADCP 48
3.9 MEASURED DATA AT CROSS SECTIONS 49

CHAPTER 4. DELFT3D PACKAGE RELEVANT TO PRESENT APPLICATION 51

4.1 INTRODUCTION TO DELFT3D PACKAGE 51
4.2 DELFT3D-FLOW 51
4.3 MODEL STRUCTURE 52
4.3.1 Model Grids *53*
4.3.2 Vertical Coordinate System *54*
4.3.3 Hydrodynamic equations *55*
4.3.3.1 Continuity Equation 55
4.3.3.2 Momentum Equation 55
4.3.3.3 Hydrostatic pressure assumption 56
4.3.3.4 Vertical Velocity 56
4.3.4 Transport equation *56*
4.3.4.1 Exchange with the Bed 57
4.3.4.2 Bed Load Sediment Transport 59
4.3.4.3 Turbulence Closure Model 59
4.3.5 Boundary Conditions *60*
4.3.5.1 Vertical Boundary Conditions 60
4.3.5.2 Lateral Boundary Conditions 60
4.4 WAVE MODULE 60
4.5 AN OVERVIEW ON THE 2DH SET UP OF THE MODEL FOR CENTRAL DITHMARSCHEN BIGHT 61
4.5.1 Model Border and Grid *61*
4.5.2 Bathymetry *62*
4.5.3 Determination of the Condition along the Boundaries *63*
4.5.4 Monitoring Points *63*
4.6 SEDIMENT AND MORPHOLOGICAL DATA INPUT 64

4.6.1 Grain Size Map *64*
4.6.2 Bed Roughness Map *65*
4.7 SEDIMENT TRANSPORT MODEL OF THE BIGHT 66

CHAPTER 5. PERFORMANCE OF THE 2DH SEDIMENT TRANSPORT MODEL 69

5.1 INTRODUCTION 69
5.2 2DH FLOW MODEL 69
5.2.1 Water level discrepancies *70*
5.2.1.1 Examination of the model bathymetry 71
5.2.1.2 Waves superimposed on water levels 72
5.2.1.3 Water levels along the open sea boundaries 75
5.3 2DH SEDIMENT TRANSPORT MODEL 77
5.3.1 Existing model *77*
5.3.2 Sensitivity studies *84*
5.3.2.1 Relevance of the open sea boundary conditions for flow 84
5.3.2.2 Relevance of waves 84
5.3.3 Model calibration *87*
5.3.4 Model validation *88*
5.3.5 Prediction of current velocity and suspended sediment concentration according to the tidal range *90*
5.4 SUMMARY 91

CHAPTER 6. PERFORMANCE OF THE 3D SEDIMENT TRANSPORT MODEL 93

6.1 INTRODUCTION 93
6.2 SELECTION OF NUMBER OF LAYERS AND TURBULENCE CLOSURE MODULE (TCM) 93
6.3 COMPARISON BETWEEN 3D MODEL RESULTS AND FIELD DATA 98
6.3.1 Performance of the model in regard to the current velocity *98*
6.3.2 Current Velocity and Sediment Concentration Profiles *100*
6.3.2.1 Statistical analyses of results 108
6.3.3 Measured versus Predicted suspended Sediment Concentration (SSC) *110*
6.3.4 The effect of the Flow model performance on the distribution of the SSC *116*
6.4 FURTHER ASSESSMENT OF THE PERFORMANCE OF THE 3D MODEL 119
6.4.1 Distribution of SSC time series across the cross section in various layers of depth *119*
6.4.2 Evolution of the vertical profiles of suspended sediment concentration (SSC) *123*
6.4.3 Snapshots of Suspended Sediment Concentrations in cross sections *127*
6.5 SUMMARY 131

CHAPTER 7. CONCLUSION 133

7.1 PREDICTIVE ABILITY OF TWO-DIMENSIONAL MODELLING 133
7.1.1 Hydrodynamics domain *133*
7.1.2 Sediment transport domain *133*
7.2 PREDICTIVE ABILITY OF THREE-DIMENSIONAL MODELLING 134
7.2.1 Establishment *134*
7.2.2 Comparison between the performance of the 2DH and the 3D models *134*
7.2.3 Comparison the performance of the 3D model with the actual results of the field *134*
7.2.4 Parameters and/or factors responsible for the model deficiency *135*
7.2.5 The choice of the 2DH or the 3D model for the area under investigation *136*

REFERENCES 137

ERKLÄRUNG 156

List of Figures

Figure 1.1 Geographical Location of Central Dithmarschen Bight 2
Figure 2.1 A typical Composite Erosion Rate Variation with Bed Shear Stress at a Mean Density of 1.1 gcm^{-3} for Okeechobee Lake in Florida Experiments (Hwang and Mehta, 1989) 23
Figure 2.2 The influence of sediment concentration on the settling velocity (Brisbane in Australia; Severn, Avonmouth, Thames, and Mersey in England; Western Scheldt in The Netherlands; River Scheldt in Belgium; Chao Paya in Thailand; Demerara in South America) (Source: Van Rijn, 1993)....26
Figure 2.3 Correlation between suspended sediment concentration and median settling velocity from the Danish Wadden Sea (Andersen (2001) 26
Figure 2.4 Illustration of the conceptual difference between the cohesive sediment paradigm of mutually exclusive erosion and deposition and the alternative of stress dependent erosion with continuous deposition possible (Sanford and Halka, 1993) 30
Figure 3.1 Area under the investigation showing the locations of the cross section T1, T2 and T3 (Winter et.al., 2005) 34
Figure 3.2 Morphology of the area (Wilkens, 2004) 35
Figure 3.3 Availability of sediment and EHL positions in the tidal channel (Mayerle et al., 2002) 35
Figure 3.4 Spatial variation of bedforms (Mayerle et al., 2005) 36
Figure 3.5 Sedimentation and erosion in the Dithmarschen Bight between 1977 and 1999. Isobaths shown for 1977 bathymetry (Wilkens and Mayerle, 2005)....37
Figure 3.6 Long term morphological changes of two cross sections in Süderpiep and Piep channel....37
Figure 3.7 Wind rose for the study area, based on data extracted from the synoptic PRISMA meteorological model (Luthardt, 1987). Nautical convention for the direction; the radial axis shows the probability of occurrence per wind speed interval (Wilkens, 2004) 39
Figure 3.8 Locations of water level gauges....40
Figure 3.9 Water level time series in Blauort, Tertius and Büsum stations 40
Figure 3.10 Seasonal variation of vertical temperature profiles in cross-sections T2 and T3 (Toro, et.al. 2005) 42
Figure 3.11 Seasonal variation of vertical salinity profiles in cross-sections T2 and T3 (Toro, et.al. 2005) 42
Figure 3.12 Map of grain size characteristics in the tidal flat area (Ricklefs, K., & Asp Neto, 2005) 43
Figure 3.13 Distribution of sediment types, after Vela Diez (2001)....44
Figure 3.14 Measuring technique along a cross section....48
Figure 4.1 Setting of bed-load transport components at velocity points (DELFT3D-FLOW, user manual) 53
Figure 4.2 An Example of Delft3d-Flow Model Area (DELFT3D-FLOW, user manual) 53
Figure 4.3 Typical Vertical Grid Consisting Of Six Equal Thickness σ-Layers (DELFT3D-FLOW, user manual)....55
Figure 4.4 Boundaries of the Model 62
Figure 4.5 Model bathymetry (Escobar 2007)....62
Figure 4.6 Nesting sequence for the generation of open boundary conditions....63
Figure 4.7 Location of Cross Sections and Monitoring Points in the Model....64

Figure 4.8 Predicted (background) and measured (circles) grain sizes in the study area (Escobar 2007) 65
Figure 4.9 Bedform Roughness Map for Dithmarschen Bight (Escobar 2007) 66
Figure 5.1 Model domain 70
Figure 5.2 Comparison of measured and computed water levels at cross-section T1 in the Norderpiep tidal channel - June 3 to 7, 2000 71
Figure 5.3 Difference between bathymetries in m (measurements– model) 72
Figure 5.4 Comparisons of the bed elevation at selected cross sections 72
Figure 5.5 Comparison of measured and computed water levels from simulations with and without waves - Station G4- Period June 3 to 8, 2000 - Moderate wind conditions..... 73
Figure 5.6 Comparison of the computed water levels at Gauge G4, from simulations with and without the wave model inclusion, for the period from the 2nd to the 7th of December 1999, during which the Storm Anatol had occurred 74
Figure 5.7 Comparison of measured and computed water levels at the centre of cross-section T1 before (a) and after (b) applying the corrections to the open sea boundary conditions–Spring tide, March 20-25, 2000 76
Figure 5.8 Comparison of measured and computed water levels at the centre of cross-section T2 before (a) and after (b) applying corrections to the open sea boundary conditions – Neap tide, Dec 3 to 8, 2000 76
Figure 5.9 Performance of the 2DH Sediment Transport Model for prediction of Suspended Material Concentration at cross-sections T1, T2 and T3 80
Figure 5.10 Performance of the 2DH Sediment Transport Model for prediction of Suspended Material Concentration at cross-section T1 81
Figure 5.11 Performance of the 2DH Sediment Transport Model for prediction of Suspended Material Concentration at cross-section T2 82
Figure 5.12 Performance of the 2DH Sediment Transport Model for prediction of Suspended Material Concentration at cross-section T3 83
Figure 5.13 Effect of waves on the sediment transport for moderate wind conditions June 3 to 8, 2000 85
Figure 5.14 Effect of waves on the sediment transport for extreme wind conditions Storm Anatol 86
Figure 5.15 Validation of the performance of the calibrated 2DH sediment transport model for prediction of suspended material concentration at cross-sections T1, T2 and T3..... 89
Figure 5.16 Comparison of measured and modelled variations of the max. depth averaged current velocities (left) and max. suspended sediment concentration (right) with tidal ranges at cross-sections T1, T2 and T3 91
Figure 6.1 Time series of suspended sediment concentration for different number of layers across the depth for near surface (up) and near bed (down) layers 94
Figure 6.2 Suspended sediment concentration profiles from 3D simulations with equal thicknesses of 5 layers, unequal thicknesses for 5, 7, 10 and 12 layers, together with profiles from 2DH simulations and field data for cross sections T1, T2, and T3. From the left: Flood phase (first row), High slack water (second row), Ebb phase (third row), and Low slack water phase (forth row) 96
Figure 6.3 From the top: water level time series, the field data contours of depth averaged velocity (Poerbandono and Mayerle, 2005), Colour coded contours graphs of the velocity from the model for the near surface, at middle depth, and near bed layers for Cross section T1..... 99
Figure 6.4 From the top: water level time series, the field data contours of depth averaged velocity (Poerbandono and Mayerle, 2005), Colour coded contours graphs of the

velocity from the model for the near surface, at middle depth, and near bed layers for Cross section T2 99
Figure 6.5 From the top: water level time series, the field data contours of depth averaged velocity (Poerbandono and Mayerle, 2005), Colour coded contours graphs of the velocity from the model for the near surface, at middle depth, and near bed layers for Cross section T3 100
Figure 6.6 Current Velocity and Suspended Sediment Concentration Profile derived from 3D model, 2DH model and in situ measurements during the *high slack water* for cross sections T1 (in Norderpiep channel), T2 (in Süderpiep channel), and T3 (Piep channel) 102
Figure 6.7 Current Velocity and Suspended Sediment Concentration Profile derived from 3D model, 2DH model and in situ measurements during the *ebb condition* for cross sections T1 (in Norderpiep channel), T2 (in Süderpiep channel), and T3 (Piep channel) 103
Figure 6.8 Variations of the ratio of observed to predicted SSC along the depth of flow for monitoring points in deep water (shown in red) and in shallow water (shown in blue) at the cross section T2 during one ebb phase (left plots) and one flood phase (right plots) 104
Figure 6.9 Variations of the ratio of observed to predicted SSC along the depth of flow for monitoring points in deep water (shown in red) and in shallow water (shown in blue) at the cross section T3 during one ebb phase (left plots) and one flood phase (right plots) 104
Figure 6.10 Suspended Sediment Concentration Profile derived from 3D model, and in situ measurements using two different devices; transmissometer and ADCP for cross sections T1, T2, and T3 during *high slack water (*first row for each cross section*) and ebb condition* (second row for each cross section) 107
Figure 6.11 Box and Whisker plot of suspended sediment concentration derived from the model (left side plots) and from transmissometer (right side plots) for cross sections T1, T2, and T3 for five tidal periods 109
Figure 6.12 Box and Whisker plot for measured SSC data derived from transmissometer (left side plots) and from Exclusive data set; employing ADCP data in shallow water and transmissometer data in deep water (right side plots) for cross sections T2, and T3 for five tidal periods 110
Figure 6.13 SSC predicted by 3D model versus SSC measured in the field at cross-sections T1, T2 and T3 for five different period of the year 2000 112
Figure 6.14 SSC predicted by 3D model versus SSC measured in the field at cross-sections T1, T2 and T3 for the total depth (shown in gray), for the layer above 25% of depth (Far From Bed Set, shown in green), and for the layer below 25% of depth (Near Bed Set, shown in blue) 113
Figure 6.15 SSC values predicted by the 3D model versus SSC values from conversion of transmissometer data (the graphs on the left) and from the Exclusive data set (the graphs on the right) at cross-sections T2 for five different periods in year 2000 114
Figure 6.16 SSC values predicted by the 3D model versus SSC values from conversion of transmissometer data (the graphs on the left) and from the Exclusive data set (the graphs on the right) at cross-sections T3 for five different periods in year 2000 115
Figure 6.17 The ratio of predicted to measured (observed) suspended sediment concentration versus current velocity for five tidal conditions 117
Figure 6.18 The ratio of predicted to measured (observed) suspended sediment concentration versus current velocity at cross section T1, T2, and T3 118

Figure 6.19 From the top: water level time series, the field data contours of depth averaged sediment concentration (Poerbandono and Mayerle, 2005), Colour coded contours graphs of the sediment concentration from the model for the near surface, at middle depth, and near bed layers for Cross section T1 121
Figure 6.20 From the top: water level time series, the field data contours of depth averaged sediment concentration (Poerbandono and Mayerle, 2005), Colour coded contours graphs of the sediment concentration from the model for the near surface, at middle depth, and near bed layers for Cross section T2 122
Figure 6.21 From the top: water level time series, the field data contours of depth averaged sediment concentration (Poerbandono and Mayerle, 2005), Colour coded contours graphs of the sediment concentration from the model for the near surface, at middle depth, and near bed layers for Cross section T3 122
Figure 6.22 From the top: water level time series at cross section T3, colour coded contours for the variations of the SSC for the near bed layer at cross sections T1, T2, and T3 respectively 123
Figure 6.23 Graphs of the evolution of the vertical profiles of the SSCs respectively at middle point of cross section T1 (C1), T2 (C2), and T3 (C3) 124
Figure 6.24 Graphs of the evolution of the vertical profiles of SSC from the field data (the top graph) and from the model results (the below graph) at the monitoring point C3 of the cross section T3 125
Figure 6.25Graphs of the evolution of the vertical profiles of SSC from the field data (the top graph) and from the model results using low value of critical bed shear stress for erosion for the tidal flat (the below graph) and high value for tidal channel 126
Figure 6.26 Snapshots of SSC distribution for flood, high slack water, ebb, and low slack water phase at cross-section T1. In each pair the top snapshot represents model results and the one below shows field data 129
Figure 6.27 Snapshots of SSC distribution for flood, high slack water, ebb, and low slack water phase at cross-section T2. In each pair the top snapshot represents model results and the one below shows field data 129
Figure 6.28 Snapshots of SSC distribution for flood, high slack water, ebb, and low slack water phase at cross-section T3. In each pair the top snapshot represents model results and the one below shows field data 130
Figure 6.29Snapshots of SSC distribution for flood, high slack water, ebb, and low slack water phase at cross-section T3. In each pair the top snapshot represents the results from the simulation employing two different values of CBSSE for the tidal flat and tidal channel, and the below snapshot shows the field data 130

List of Tables

Table 2.1 Range of Critical Bed Shear Stresses and erosion parameter based on literature Review 24
Table 2.2 Settling velocities w_s of fine suspended particles reported in the literature 28
Table 2.3 Critical bed shear stress for deposition reported in the literature 31
Table 3.1 Number of ADCP transects, transmissometer profiles and water samples are collected during Measurement surveys at cross sections T1, T2, and T3 under the PROMORPH project 50
Table 5.1 Correction factors applied to the water levels along the open sea boundaries 75
Table 5.2 Properties of the mud fraction as proposed by Escobar (2007) 78
Table 5.3 Sand fractions used by Escobar (2007) 78
Table 5.4 RMAE between modeled and measured suspended material concentrations 79
Table 5.5 Properties of the cohesive sediments used in the calibration 87
Table 5.6 Model validation 88
Table 6.1 Sensitivity analysis of the simulations employing different number of layers in regard to the SSC prediction 95
Table 6.2 RMAE values for suspended sediment concentration derived from the field and those of simulated results employing different number of layer configurations 95
Table 6.3 RMAE for suspended sediment concentration derived from field and those of simulated results using different turbulent closure modules 97
Table 6.4 RMAE values between modeled and measured SSC for 2DH and 3D simulations 97

Chapter 1. Introduction

1.1 Overview

Coastal zones, which form a dynamic interface of land and water, own high potential of physical activity and critical economic importance. They encompass immense environmental, social and economic values. The wide variety of purposes by different groups of people results in conflict between the users. Therefore they are to be managed ecologically, ethically and economically. To achieve this aim it requires a thorough understanding of the physical, chemical, biological and other processes involved. Among the physical processes are the hydrodynamics and sediment transport. These processes are ever-changing from the daily fluctuation of tides, to the seasonal variations in weather, winds and waves and also water level rise. The resulting changes of the coastal zone can have tremendous impact on the local community, navigation, fishing and other activities.

Observations and field measurements are necessary but not sufficient to describe these processes precisely because of the size and the nature of the area involved. The demand for models that can incorporate these processes and solve the environmental problems that cannot be achieved using traditional hydraulic and sediment transport dynamics has grown for some decades. The use of physical models of coastal waters are prohibitively expensive to build and to maintain. The choice is numerical modelling in coastal waters and computational techniques. These models involve the simulation of flow and sediment transport conditions based on the formulation and solution of mathematical relationships. When these models and the relevant computational techniques are established, they can be improved and refined as more data and additional or refined parameters become available. The task is to improve our understanding of their limitations and constraints as well as the knowledge of physical processes involved.

Application of models in coastal engineering is reasonably advanced in terms of the prediction of flow hydrodynamics, but it is imprecise in the prediction of sediment transport and morphodynamics. The lack of sufficient and adequate field data on one hand and the lack of universally accepted equations and parameters on the other hand make the prediction of the sediment transport a challenging topic. The main purpose of this thesis is to evaluate the predictive ability of a model from the Delft3D package regarding

hydrodynamics and sediment dynamics for the coastal zone of Central Dithmarschen Bight which is located on the German North Sea as shown in Figure 1.1. The bight is located between the Eider and Elbe estuaries and is situated about 100km north of Hamburg. It consists of tidal channels, tidal flats and sand banks. It is tidally dominated and known as a well-mixed body of water. The sediments in suspension are mainly cohesive consisting of very fine to medium-grain silt (Poerbandono and Mayerle, 2005). As the management and the well being of the bight require a complete understanding of the processes involved, the bight has been the subject of intensive investigations during the past few decades. The investigations consisted of both field measurements and modelling (see Chapters 3 and 4). Detailed information about the location and characteristic of the area under the investigation is presented in chapter 3.

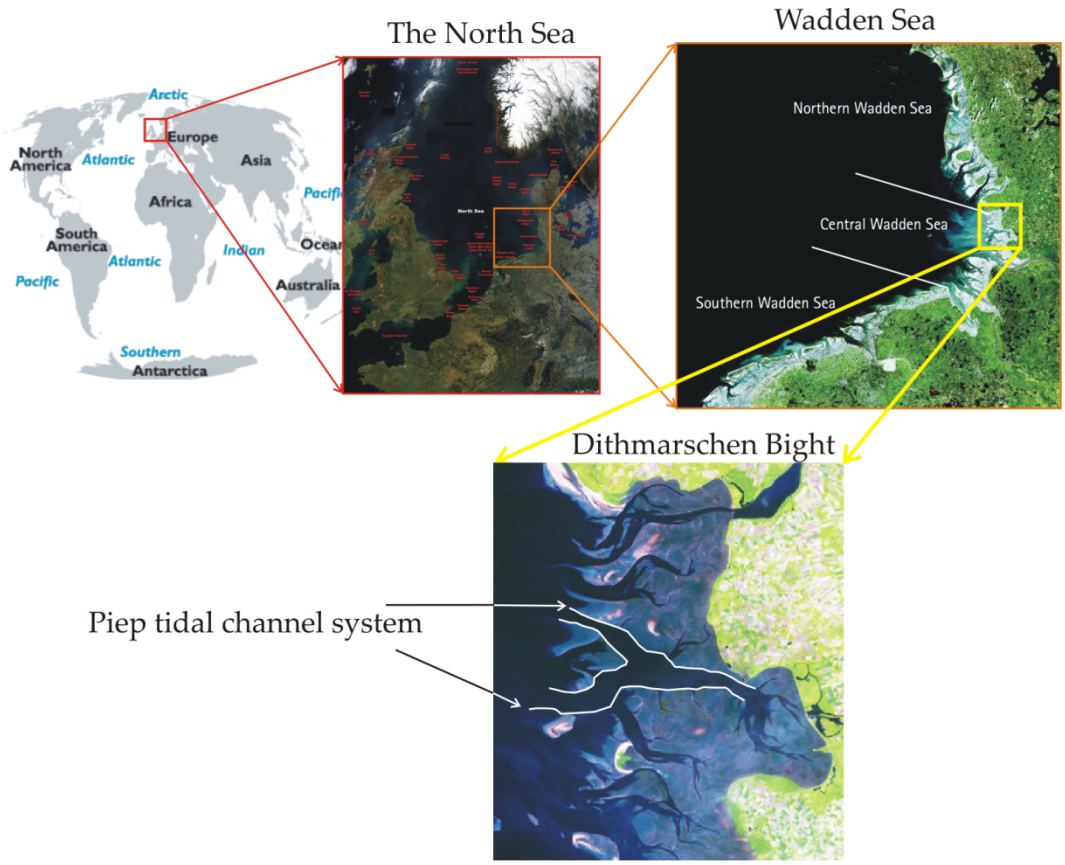

Figure 1.1 Geographical Location of Central Dithmarschen Bight[1]

1.2 The Significance of modelling

Management of coastal zones is specifically important because at this dynamically active intersection of land and the oceans, humans have been building structures throughout

[1] The source of the North Sea map: http://visibleearth.nasa.gov/cgi-bin/viewrecord?25413
*:Wikipedia by user:Southpark {{PD-USGov-NASA}})

history. Ports, harbors and more recently, recreation and tourism at the shoreline are some aspects that make the management of the coastal zones specifically important. There are many examples of mismanagement that have interfered with sediment transport processes, causing severe beach erosion and associated structural damage or, conversely, large accumulations of sand that have rendered some facilities useless. In addition to the ports, human interactions such as constructing navigational channels can adversely impact the shoreline and reduce sand supply to the coast (Dean and Dalrymple, 2004).

During the past several decades however, increasing emphasis has been placed on the coastal zone with the objective of understanding coastal processes and developing strategies to cope effectively with the rapid development of this region and the hazardous effects. Lakhan and Trenhails, (1989) emphasized the importance of numerical modelling of the coasts with a view that such a complex, decomposable, and large scale system cannot be fully comprehended with time limited studies. It is important to keep in mind that no model, however complex, can be more than a representation of reality (Bekey, 1977). While models can be classified as physical, analytical, and numerical ones, the numerical model which has been employed for this investigation is the subject of interest. Some brief information about the different types of model and their specific use are presented in Chapter 2.

According to Dean and Dalrymple (2004) the best understanding of coastal processes, including the nearshore flows and the resulting sediment transport, and the ability to transform this understanding into effective engineering measures require some abilities, among them is to preclude our ability to make models for precise long-term predictions about the coastal zone. They however mentioned that at present time, the mathematical and statistical equations governing the behaviour of the sand and water at the shoreline are not yet fully known thus the modelling results should continuously be compared with the well-documented case studies and field experiments.

On the basis of literature review Schwartz (2005) mentioned an increasing number of researchers who have emphasized the necessity of the use of computer-based models to gain insights into the complex interactions among interdependent entities (e.g., waves, winds, and currents), which have cumulative impacts on the coastal system. These references include Lakhan and Jopling (1987), Briand and Kamphuis (1990), Larson *et al*. (1990), Lakhan (1991), de Vriend (1991), Win-Juinn and Ching-Ton (1991), Abdel-Aal (1992), Horn (1992), Lakhan and LaValle (1992) Lakhan *et al* (1993), Warren (1993), Black (1995), Stive and de Vriend (1995), de Vriend and Ribberink (1996), Holmes and Samarawickrama (1997), LaValle and Lakhan (1997), Sierra *et al* (1997), and Black *et al* (1999). According to Adkins and Pooch (1977) numerical models have certain advantages including: 1) the permission of controlled experimentation in which a simulation experiment can be run a number of times with varying input parameters to test the behaviour of the system under a variety of situations and conditions, 2) the permission of time compression in which operation of the system over extended periods of time can be simulated in only minutes with ultra fast computers, 3) the permission of sensitivity analysis by manipulation of input variables, and 4) not disturbing the real system.

Using a computer to simulate the dynamics of the coastal system however requires that a set of assumptions taking the form of logical or mathematical relationships be developed and formulated into a model. Numerical modelling represents the integrated development of mathematical equations, logical rules, and a computer program embodying the equations, the logical rules and the solutions to them (Schwartz, 2005). According to Lakhan (1989) a realistic and credible simulation model of the coastal system can be formulated by carefully considering each of the following: 1) objective specification, and system definition, 2) model

conceptualization and formulation 3) data collection and model parameterization, 4) model translation or model selection, 5) model verification, 6) model validation, and 7) sensitivity analysis and results interpretation.

After the objective of the model is outlined, the system to be modelled must be defined. For this reason precise knowledge of the system and parameters involved are important. Because the results can strongly be affected by a set of poorly understood components of the model, and the processes that are interacting over time including waves, tides, winds, currents, etc (Lakhan, 1989). As the coastal system is governed by a large number of interdependent elements and their attributes, it is difficult to identify and separate the independent and dependent elements, which control a portion or the whole coastal system. When the system and parameters involved are specified, they should be converted to numerical codes, which could either be a self-developed model or an industry-standard one. The appropriate model depends mainly on the complexity of the problem, on the type of the beach and on the balance between accuracy and computation efficiency (Pechon, 1997).

The use of standard numerical models for coastal area for predicting the hydrodynamic and sediment dynamic processes increasingly grows. However, a comprehensive validation of these models against field data has been hampered because of the lack of field data with sufficient spatial coverage. According to Walstra et al (2001) validation of such models for field condition requires a data set of sufficient length to cover variations in the tidal cycle and varying wave and wind conditions. In addition, they mentioned the importance of availability of dense spatial instrumental coverage within the modelling area in order to obtain an accurate representation of the spatial flow pattern.

Delft3D package developed by Delft Hydraulic is one of the industry-standard models suited to investigate flow, wave, sediment transport and morphology and water quality for fluvial, estuarine and coastal environments in two and three dimensions. This model and its application for this study are discussed comprehensively in Chapter 4. Nicholson et.al. (1997) and Wright and Norton (2000) compared interrelationships of several coastal area morphodynamic models among them Delft3D. They found broad quantitative agreement between the models and also marked discrepancies in the detail. According to Nicholson et al (1997) the variety of factors applied in each modelling among them roughness size, eddy viscosity, smoothing, and sediment transport formulations were the reason for the dissimilarities. They mentioned that in the Delft3D model the bathymetry responds to the gradients in the transport rate, which means that this quantity must be correct for a wide range of depths, current, waves, and breaking conditions. Besides, vast amounts of literature are available concerning the successful usage of the Delft3D package and its evaluated results in different coastal areas. These include Walstra et.al. (2001), Welsch, (2002), van Rijn and Walstra (2003), Lesser, et.al (2004), Maren (2005), Lam, et.al (2007), van Rijn, et.al (2007), Carrivick, (2007), Hsu, et al (2008), Benedet, et al (2008), Cacchione, et al (2008) Hu, et al (2009), Brennan, et al (2008), Tung, et al (2009), Baart et al (2009), and Li, (2010). The package has been employed, and to some extent calibrated and validated for the area under the investigation using hydrodynamic, wave and sediment modules since 2000 (see Chapter 4).

1.3 The significance of data collection

One of the principal tasks in the coastal simulation process is to gain adequate information and data on the parameters and attributes which govern the coast. The data must be collected over a continuous and long period of time, so that the time series provide accurate

insights into the nature of the parameters, which impact on the coastal system. They should also be homogeneous (Schwartz, 2005). According to Furumai (2010) the model development cannot proceed without scientific information and knowledge on coastal activities and the kinetics of associated processes. He also mentioned that monitoring and experiment are fundamental steps to understand these phenomena and processes. Before the model application, the models need to be calibrated and validated using monitoring and experimental data.

Sorensen (2006) on the other hand mentioned about the high cost of field data collection and reasoned that most coastal processes occur over relatively long time spans and have large spatial extents. He also included that the coastal processes are impacted by or involve a variety of coastal factors including waves, wind, the tide and storm surge, currents, and beach sediment properties. Thereafter, he concluded that continued advancement of coastal engineering requires that these costs be anticipated and met.

The challenges and opportunities associated with data collection and management for the hydrologic sciences have become evident in recent years. According to van Rijn (1993) the first stage of a coastal study consists of the analysis of the existing data. He emphasized the importance of the input data for the model and mentioned that there was no point in selecting a sophisticated mathematical model when the input data were of poor quality. According to him, an important phase prior to the actual field survey is the selection of the most appropriate instruments, which usually is rather difficult problem because the available wide range of instruments has various specific advantages and disadvantages. The sort and amount of data collection for modelling a coastal area with regards to hydrodynamic and sediment dynamic depends on the subject and the aim of each project. However, the elements and attributes are usually necessary to collect from the field include water level, wind speed and direction, bathymetry, current velocity, wave height and direction, salinity, grain size distribution, bed forms, suspended sediment concentration (SSC), and bed and suspended load transport. Some of these parameters are employed for the simulation purpose and some for the model calibration and validation (see Chapter 3).

Monitoring and data collection in the field of hydrodynamics in the coastal area are reasonably well developed and the water level, wave height and current velocity can be recorded with high resolution. Long-term monitoring of water level and archiving of the resulting data are activities, that provide the basis for predictive modelling. The coastal currents of interest include nearshore currents seaward of the surf zone and in channel entrances, as well as the alongshore current in the surf zone (Sorensen, 2006). Propeller and rotor current meters, electromagnetic current meters, ultrasonic current meter, and ADCP are typical instruments used commonly for measuring current velocities. The morphology can be measured by standard surveying techniques. However, owing to the dynamic nature of the coastal zone where large areas across the surf and nearshore zones must be rapidly measured, some unique techniques for hydrographic measurement have been developed. In addition, it is often desirable to measure the actual transport of sediment as well as the resulting hydrographic changes. This presents some significant problems that have not been completely mastered (Sorensen, 2006).

According to van Rijn (1993), accurate predictions require a detailed calibration of the model with precise field data. The most relevant parameters such as particle diameter, fall velocity, bed roughness, and sediment transport should be varied within their validity ranges to evaluate their effects on the morphological results (sensitivity computations). That is, to predict the consequences resulting from the morphological changes, it is of importance to have detailed knowledge of the local morphological variables such as the bed material size,

the settling velocities of the suspended solids and transport rates. Monitoring and field data collection for the morphological and sediment transport prediction is still in developing progress. Therefore, measurement and prediction of sediment fluxes are important goals in environmental and engineering coastal studies.

Errors in sediment transport estimates may be a result of a number of processes and factors including uncertainties in current measurements, vertical distributions of current velocity, sediment concentrations and instrument calibrations. Net sediment transport predictions will be particularly sensitive to any offsets or bias in the current or concentration estimates. The potential for error is compounded in a mixed sediment environment by the varying responses of different sediment size to the flow which implies the requirement for monitoring of both end members of the size spectrum. Field measurements of suspended sediment flux frequently do not take into account the wide variation of sediment size with time. The difficulty of measuring the full varying size spectrum of suspended sediment often leads to the measurement of only a portion of that spectrum and/or the assumption of a time-invariant sediment size distribution. In a mixed sediment environment such an assumption can lead to large errors in predictions of the magnitudes of concentrations and even flux directions (e.g. Ludwig & Hanes 1990; Bass 2000; Green *et al.* 2000; Jago & Bull 2000). Unlike coarser sandy material the behaviour of fine sediments is influenced by their cohesive nature, which allows particles to flocculate and affects their erodibility and settling velocity. In addition, their relatively slower settling velocity allows muddy sediments to remain in suspension much longer than sand and they may be easily advected into or away from a region of study (Bass, et.al., 2007).

Besides, as mentioned by van Rijn (1993), an important aspect of any morphological study is the field survey during which the samples to be analyzed are collected. It is important to be aware of the fact that the quality of the local study can only be as good as the quality of the information gained through sampling. Thus, any errors incurred during sampling will manifest themselves by limiting the accuracy of the study. The selected sites should be well disturbed over the area under the investigation and be representative of the (mean annual) prevailing hydraulic and morphological conditions. He classified the errors related to the measurements as systematic errors and random errors, and pointed out that a typical systematic error is the sediment discharge in the unmeasured zones below the lowest sampling errors accumulate with increasing number of measurements. According to his investigations the factors influencing the accuracy include 1) measuring method, 2) instruments available, 3) natural fluctuations of concentration, velocity, and transport, and 4) calculation method (extrapolation to unmeasured zones).

1.4 Sensitivity Analysis, calibration, and validation

Sensitivity analysis is an important step in model validation. The goal of performing sensitivity analysis of a simulation is to determine the effect of input variation and the effect of input uncertainty on the output values (Furbringer and Roulet, 1999). In any coastal simulation, sensitivity analysis will involve changing the model's input by a small amount and checking the corresponding effect on the model's output. If the output varies greatly for a small change in an input parameter that input parameter may require reevaluation (Law and Kelton, 1982). It is best to run the model several times by varying the parameter values. The desired goal is to determine if the basic pattern of the results is sensitive to changes in the uncertain parameters. In the execution of the model with different input parameters, it is necessary to check whether the reference mode is obtained with each sensitivity test. If the

simulation results are in agreement with the reference mode then the model can be considered robust.

The robustness of the simulation results can be tested by performing additional simulations with different initialization parameters. This comprehensive sensitivity analysis can provide insights into whether the obtained simulation results conform to reality. To interpret the simulation outputs and make inferences on how the coast or any type of system operates, it is necessary to have both theoretical and practical knowledge of the statistical aspects of simulation experimentation (initial conditions, data translation, replications, run length, etc.) and data outputs. The same principles that apply to the analysis of empirical data also apply to the analysis of simulated data (LaValle and Lakhan, 1993). Statistical tests will vary depending on whether the model is stochastic or deterministic. Lakhan (1986) and Lakhan and LaValle (1987) found that a stochastic simulation model on nearshore profile development will produce output data which are subject not only to random characteristics, but also to various degrees of correlation. Interpreting these results requires the utilization of a statistical methodology which will highlight the stochastic and other properties of the simulation outputs.

On the basis of the literature review by Popper (1968), he stressed that validating computer simulation models is difficult because simulation models contain both simplifications and abstractions of the real-world system. Zeigler et.al. (2000) also mentioned that for practical purposes, it makes sense to require that the model faithfully captures the system behavior only to the extent demanded by the objectives of the simulation study. According to them an experimental frame of interest is first determined, and replicated validity can be affirmed if, for all the experiments possible within the experimental frame, the behaviour of the model and system agree within acceptable tolerance.

The coastal simulation expertise can only develop a valid model by making certain that there is very close correspondence between the model and the coastal system. This is done by building a model that has high face validity. The model will be valid if it accurately predicts the performance of the coastal system. If this is not achieved then it is necessary to examine, and change if necessary, the structural and data assumptions of the model (Schwartz, 2005).

1.5 Objectives of this study

The consensus among the scholars and researchers is that 3D approach in solving coastal processes is a natural progression of research. The on going progress in computing allows the visualization of the flow characteristics and sediment suspension in three dimensions. On the other hand the 3D modelling like any kind of reliable modelling requires correct definition of all the input parameters such as water level for flow simulation and settling velocity, bed roughness, and critical bed shear stress for sediment dynamic simulation, which are preferably derived from the site specific field data. Also, it requires sufficiently precise field data on the flow characteristics and suspended sediment concentrations (SSC) for the calibration and validation proposes. A comprehensive knowledge of the processes involved is required to analyse and interpret the results. At the moment, still the challenging issue to apply 3D models is that they require large amount of computational memory and considerable time compared to the 2DH model. It is to be noted that the procedure of depth averaging in the 2DH model necessitates using depth-averaged field data which can result in some loss of information along the depth. But, the use of 3D model produces values at a number of layers along the depth, which can be matched to the field data at the same

locations and at their corresponding times. Therefore, a 3D model can be more useful when sufficient field data are available.

Palacio (2002) used a 2DH model of the Delft3D package for the hydrodynamic study of the area under this investigation. Since then, this model has been calibrated and validated by various investigators including Palacio (2002), Toro (2003), Palacio et.al. (2005), Mayerle et.al. (2005), Wilkens et.al. (2005) and Winter et.al. (2005). The sediment module of the package was then included in the simulations and the appraisal of the performance of the model were reported by Winter et.al. (2005) and Poerbandono and Mayerle (2005). Winter, et.al. (2005) pointed out that even though the model is capable to reproduce the main characteristics of suspended sediment transport across the tidal channels it contains some discrepancies. According to them discrepancy between the values of SSC derived from the model and those from the field specifically during slack-water times. On the basis of their simulation results the average percentage of data within a factor of 2 was of about 35%. As the predictive ability of the model in regard to sediment dynamics was relatively low they proposed some further investigations. It is therefore the aim of this study to investigate the performance of the model with the main interest in the prediction of SSC in order to find the reason or reasons for the weak correlation existed between the model results and the field data. The 2DH and 3D flow model incorporation with sediment module were used for this investigation. The model results were compared with the field data. The use of 3D model of the bight for this study was considered necessary on the basis of the following reasons. The first was to compare the 3D model results with those of the 2DH model to investigate whether any significant variation of the SSC along the depth exist, which cannot be detected using 2DH model. The second reason was to compare the 3D model results with the field data for the evaluation of the model performance as well as measuring devices. Specific objectives of this research can be summarized as follow:

i. To determine the predictive ability of two-dimensional modelling of the hydrodynamics and sediment processes in the Piep tidal channel system (see Figure 1.1),
ii. To examine the effect of waves on SSC under 1) moderate, and 2) stormy conditions,
iii. To explore the performance of the model regarding current velocities and SSC when tidal ranges vary, i.e. from neap to spring tide,
iv. To establish a three dimensional (3D) model of the bight,
v. To compare the current velocity and the SSC results of 3D simulation with those of the 2DH,
vi. To evaluate the predictive ability of the three-dimensional modelling of the hydrodynamics and sediment dynamics of the area incorporating field data,
vii. To identify spatial and temporal conditions which result in poor correlation between the model results and field data,
viii. To identify parameters and/or factors responsible for the deficiency in the model results, and
ix. To provide information for further development of the model.

1.6 Subject and Methods

The subject of the study is to evaluate the predictive ability of the Delft3D package for the hydrodynamics and sediment processes in the central Dithmarschen Bight. The Piep tidal channel system shown in Figure 1.1 was used for the evaluation of the model in view of the availability of field data covering the area temporally as well as spatially.

Field data: To obtain reliable results from models, a comprehensive knowledge of the processes involved is necessary but not sufficient. Precise values of parameters and variables derived on the basis of adequate field measurements are also needed to establish the model and also for the purpose of model calibration and validation. The need for 3D model approximations specifically can be justified on the basis of availability of the field data. The source of the required field data for this study was the "Prediction of Medium Term Coastal Morphodynamics", known as the PROMORPH project. This project was executed during the period May 1999 to June 2002, when the Dithmarschen Bight was surveyed comprehensively exploring morphology and hydrodynamic processes. This research project was sponsored by Germany's Federal Ministry of Education and Research (BMBF) (PROMORPH (2002) and Mayerle and Zielke (2005)).

The data collection was a combined effort of **Coastal Research Laboratory** at the Institute of Geosciences and the **Research and Technology Center Westcoast of** the University of Kiel, the **Institute of Fluid Mechanics** and the **Institute of Meteorology and Climatology of** the University of Hannover and **Institute of Coastal Research of** the GKSS Research Center (PROMORPH (2002) and Mayerle and Zielke (2005)).

The field data used in this study cover three cross sections in the three channels, namely Norderpiep, Süderpiep, and Piep channel (see Figure 3.1). The measurements were curried out at several stations along the width of each cross section and at various depths at these stations. These data made it possible to evaluate the results of the 3D model at every spatial position and temporal situation of the area under investigation. Some parts of these data were used to establish the model including water level, bathymetry, grain size, and wind velocity and direction. Current velocity and SSC measured data for the five measuring periods, including neap to spring tidal ranges, were used for the model calibration and some other five measuring periods were used for the model validation. More detail about the measured data can be found in Chapter 3.

Selection of numerical models: For the modelling purpose the Delft3D package of the Delft Hydraulics has been considered because 1) it has been developed specifically to apply for the shallow water regions and coastal water, 2) its application has been evaluated in different coastal areas among them the North Sea and specifically Dithmarschen Bight, and 3) the package had been employed for the area of interest by previous researchers including Palacio (2002), Toro (2003), Mayerle et.al. (2005), and Winter (2005) in two dimensions and their results and conclusions can be compared with the results of this study. Of the Delft3D Package the Flow and Wave modules were selected for the study. The Flow module can model the flow in two- and three-dimensions and are referred to as 2DH and 3D models hereafter in this study. They have the facility for the parallel simulation of the sediment dynamics. The wave module of the package has also been employed to study the effect of wave-induced currents on the sediment movement, which allows estimating the effect of wind on sediments besides the astronomical tides.

2DH modelling: The 2DH model of the Bight had been established and improved to some extent by researchers in Kiel University prior to this investigation. This model

was reproduced and employed for this study (see for instance Toro (2003), Mayerle et.al. (2005), and Winter (2005)). The model results for the flow characteristic was reported to be acceptable with the mean absolute error of less than 0.2 m/s (Palacio et.al., 2005). As the model results for the SSC showed some disagreements with the field data (Winter, 2005), it was found necessary to recalibrate the model. Chapter 5 of this study therefore, deals with the details of the simulations, calibrations, and validation of the 2DH model for the area under investigation. The wave module of the Delft3D package was also included in the simulations, in order to study the effect of wave-induced sediment transport in the area for moderate and stormy conditions. The results have been analyzed using scatter graphs and statistical analyses. As the improvement in the results after the recalibrations were not convincing for all the points and at all the cross sections, it was therefore, decided to examine the prediction capability of the 3D model.

3D modelling: The three dimensional model of the Delft3D package is developed by expanding the calibrated and validated 2DH model of the package. The sensitivity of the model for predicting SSC using different numbers of layers along the depth was examined. Following the establishment of the model with proper numbers of layers simulations were carried out for the periods where field data was collected. The 3D model results were compared with those of the 2DH model in order to find whether the distribution of the current velocity and SSC along the depth follow a uniform trend or not. The 3D simulated results were also compared with the field data employing statistical error techniques, scatter graphs, and analyzing the graphical distribution of the current velocity and SSC. It was found that the 3D model results like the 2DH ones show some dissimilarity with the field data in regards to the SSC prediction. On the basis of the data analysis it was found that the dissimilarity observed is partly due to the technical error in regards to measuring devices and data conversion equations, and partly due to the model deficiency. The model deficiency itself was probably the resultant of two factors: one of them is the simplification associated with the modelling and by the existing version of the Delft3d cannot be omitted, and the second one is the imprecise input parameters to the model. The latter one is in regard with the parameters like settling velocity, and critical bed shear stresses (see Chapter 2 for more information) which cannot easily be measured in the field. Due to the lack of the available field data these parameters are defined to the model on the basis of the literature suggestions and/or through calibration processes, which seems to result in deficiency in the model performance. The performance of the 3D model with the relevant discussions and some suggestions for improving the model results are presented in Chapter 6 of this study.

Chapter 2. Literature Review

2.1 Introduction

Solutions to coastal hydrodynamic and sediment transport problems can be achieved principally by using the four primary methods including field observations and measurements, analytical solutions, physical models, and numerical models. Any of these four, or a combination of them, may be the best approach for solving a particular problem. Field measurements can only be performed in a small area and for limited time periods as the cost resulting from making simultaneous measurements throughout an entire coastal zone is usually high. Field data collection and their analysis alone, will only demonstrate the coastal water behaviour under the set of conditions that existed during the time of measurements. Field data however, are an indispensable element in setting up, calibration, and verification of numerical and physical models.

Fully analytical methods are not available for complex flow existing in coastal waters, such as geometry, and sediment transport processes (Coastal Engineering Manual, 2008). Physical models have been used by engineers to study the behaviour of a coastal system visually (see for instance Chakarabati (1989), Denner (1989), and Sunamura (1989)). During the past three decades however, with the rapidly developing computer technology, computer modeling is becoming an indispensable tool for simulation, replacing or complimenting physical modelling.

As the aim of this investigation is to evaluate the performance of a numerical model, a survey of literature concerning hydraulic and sediment transport modelling was found essential. In this chapter at the beginning a brief introduction about available models and the selection of them for the area of interest regarding the aim and the cost are presented. Advantages and disadvantages of each of them are discussed. It is followed by the application of sediment specifically of cohesive type in the models which is the main concern in this thesis due to the nature of the area under the investigation. As a result of literature researches the key parameters of the cohesive sediment transport are defined and introduced.

2.1.1 Physical models

Physical models are scaled versions of the prototype. These scale models are constructed in the laboratory. Experiments are carried out with flows in the model and the results are scaled to values in the prototype. Scale models have been very popular in hydraulics over a number of years for the solution of complicated cases of fluid flow. Physical models however, are expensive and time consuming to operate. Furthermore, it is not always easy to modify a physical model, for the further testing.

Models should satisfy the geometric, kinematic and dynamic similarities. Geometric similarity applies to the shape. Distances in one system are in constant ratio of the corresponding distances in the other system. Dynamic similarity is assured if each of all the forces in a particular point in one system bears the same ratio of the corresponding force in the other system. If geometric and dynamic similarities are satisfied, kinematic similarity is automatically satisfied. Strict geometric similarity however, may not always be satisfied, for example, with roughness. Complete dynamic similarity between two systems also is not possible and usually only one dominant force is considered for model testing. According to Denner (1989) in many cases, the directional spread of waves in the physical models is omitted. The lack of full similarity introduces scale effects that introduce errors in the evaluation of values of the prototype. Mingham (2003) mentioned that physical scale models contain intrinsic scaling errors and are difficult to adapt to even slightly different situations. For further information on physical models, reference is made to Owen (1980), Novak and Cabelka (1981), Goda (1985), Allsop et al. (1995; 1996), and Besley et al. (1998).

2.1.2 Numerical Models

According to Lakhan and Trenhaile (1989) mathematical models are concerned with symbolic or formal assertions of a verbal or mathematical kind in logical terms. They have varying degree of complexity. A mathematical model may not represent all aspects of the actual environment but attempts to incorporate those features of the problem that are relevant, based on the fundamental physical, chemical, and biological principles. The parameters of the model can be adjusted so that the model can almost realistically represent certain characteristics of a particular coastal system. Both physical and mathematical models are site related and thus involving parameters have to be adjusted to suit the local circumstances. Conventional techniques of mathematical modeling and analysis are inadequate for understanding the coast, which can be viewed as a complex, dynamic large-scale system or super- system with an integrated arrangement of separate units or component systems, which vary in morphological form, pattern and configuration (Lakhan, 1989).

Numerical models are categorized within the mathematical models and are capable of simulating some processes that cannot be handled satisfactorily in any other way. They provide much more detailed results than mathematical methods and may be substantially more accurate. Given appropriate data, the execution of the computer model yields an approximate solution to the mathematical model (Ji, 2008). In many cases this computational approach is quicker and cheaper than the physical model. Furthermore numerical simulation is unaffected by scaling errors and can be flexible. Geometry, wave height, bathymetry, and other physical properties relevant to sediments and water can be changed easily. The numerical simulations can be repeated without imposing high costs.

According to Mingham (2003) numerical models with all of their advantages still contain some weaknesses and problems. There are two main problems with numerical simulation: 1) the underlying physics must be understood in such detail to capture the essential features of the flow. A complete description of the flow, even if this were possible, would yield a system of equations which would be so complex that they could not be solved in a reasonable time. In reality, a complete description is not possible because terms such as turbulent shear stresses and bed stresses are not sufficiently well understood and have to be approximated or modelled empirically. 2) The second problem with numerical simulation concerns the algorithms used to approximate the solution of the flow model. Solvers that are constructed only on the basis of mathematics do not always respect the underlying physics. These solvers may fail to conserve mass or momentum which can lead to large errors in the solution. One of the troublesome aspects of numerical modelling is also to determine open boundaries for the model and to make sure that the boundary conditions employed at the open boundaries are compatible with physical processes being simulated within the interior of the model domain (Denner, 1989). There is one further issue concerning the numerical simulation method that relates to the gridding of the computational domain. Problems in coastal hydrodynamics often deal with complicated geometries with highly irregular coastlines, the presence of islands and complex harbour and breakwater configurations. Classical finite difference approaches based on Cartesian grids use crude saw-tooth approximations to the boundaries of the domain which lead to unnecessary solution errors (Abbot et al., 1973; Falconer, 1980). Employing curvilinear coordinates (see Chapter 4) helped to overcome this problem with producing a boundary fitted grid (Borthwick and Barber, 1992; Barber and Pearson, 1996).

According to Ji (2008) numerical models in terms of model representations of space and time can be categorized as: (1) steady state or time dependent (dynamic) and (2) zero, one, two, or three dimensional. The temporal characteristics includes whether the model is a steady state or time dependent depending on the treatment of the time derivative in the governing equations. Nevertheless, as pointed out by Francisco et. al. (2006), in order to derive reasonable results from the numerical models, understanding the field and data collection constitute is the first and most important step. More details about numerical and mathematical modelling can be found in Abbot et al. (1973), Falconer (1980), Fennema and Chaudhry (1990), Dodd (1998), Mingham and Causon (1998), and Mingham (2003).

2.2 Spatial dimensions of a numerical model

Numerical models are classified by the number of spatial dimensions over which variables are permitted to change. Thus in a one-dimensional flow model, currents are averaged over two dimensions (usually width and depth) and vary only in one direction (usually longitudinally). Two-dimensional models average variables over one spatial dimension, either over depth (a horizontal model) or width (a vertical model). Three-dimensional models solve equations accounting for variation of the variables in all three spatial dimensions. Even though coastal processes are always 3D in nature, it may be described by a model of 1D, 2D, or 3D. If the system's variation in one dimension can be considered insignificant or can be represented by averaged values, this spatial dimension can be eliminated from the modeling study. It should be considered however that, averaging always leads to a loss in information. This cannot be completely avoided because averaging is essentially a filtering technique (Ji, 2008). Nix (1990) has also pointed out that comprehensive models should (but not always) have better mathematical, physical,

chemical, and biological representations of water systems than simple models do. Comprehensive models can be applied at various levels of detail. Van Rijn (1993) suggested that to select a model, the quality of the input data is of special importance and there is no point in selecting a sophisticated numerical model when the input data are of poor quality. He emphasised that predictions require a detailed calibration of the model aimed at reproducing the morphological development in the existing situation. Obviously the use of the upgraded models demands more field data.

With an increasing availability of computational power, there is a general shift occurring in sediment transport and morphological prediction from the use of 2D to 3D hydrodynamic simulations. However, it is not always necessary to make use of the vertical resolution in models. Leybourne (2002) studied the performance of a 2DH model with its companion 3D model for a shallow water having flat bathymetry and claimed that the 3D model offered no great improvement over the 2DH model. In an experiment concerning the sedimentation of a breakwater, Lesser et al. (2004) obtained approximately the same results using a 3D morphological model as did Nicholson et al. (1997) using a simpler 2D model. 3D models, sometimes include complex 3D effects automatically to the model that may not necessarily increase understanding of a morphological situation. Neill, et.al. (2007) wisely advised that the additional computing power available may be of more use in many situations in improving the horizontal rather than the vertical resolution.

2.2.1 One-Dimensional Models

One-dimensional models solve the unsteady, cross-sectionally averaged equation for the hydrodynamic and the mass balance of suspended sediment in the streamwise direction without solving the details over the cross-section. Most 1D models are mainly for non-cohesive sediment transport with the capacities to simulate simple processes of cohesive sediment transport (Huang et. al., 2006). This models are suited for rivers as sediment transport model especially for long-term simulation of a long river reach, where the lateral variations of hydraulic and sediment conditions can be ignored. One-dimensional models generally require the least amount of field data for calibration and testing. The numerical solutions are more stable and require the least amount of computer time and capacity. One-dimensional models are not suitable, however, for simulating truly two- or three-dimensional phenomena. An example of this approach can be found in, Ji et al. (2002) who used a 1D model to simulate the Blackstone River in Massachusetts. QUAL2E is an example of 1D industry-standard models.

2.2.2 Two-dimensional models

For computations at wide horizontal scales (estuaries, coastal zones, seas), usually a depth averaged flow model in combination with a simple equilibrium sediment transport formula is used. Two-dimensional models can be classified into two-dimensional horizontally averaged (2DH) and two dimensional vertically averaged (2DV) models. 2DH scheme is used where depth-averaged velocity and/or other parameters relevant to hydraulic and transport can adequately describe the variation of the parameters across a channel (Francisco et. al., 2006). That is where the flow field shows no significant variations in vertical direction and the fluid density is constant. Examples are tidal flow in well-mixed coasts and estuaries. 2DV simulations are of particular interest where width-averaged hydraulic and transport parameters can adequately describe the condition in the vertical direction (Francisco et. al., 2006). That is where the flow is uniform in one horizontal (lateral) direction, but with

significant variations in vertical direction. Examples are the flow across a trench or navigation channel, wind- driven circulation perpendicular to the coast, and flow over long-crested sand dunes. Most two-dimensional sediment transport models are depth-averaged models. Two-dimensional horizontal sediment transport and bed-evolution models are based on the depth-integrated equations of motions in combination with a wave model and a sediment transport model.

A basic depth-integrated approach was proposed by Galappatti and Vreugdenhil (1985). It was based on the convection-diffusion equation including boundary conditions at the bed and at the surface. It is assumed that the velocity and concentration profiles have a distribution similar to that of the equilibrium profiles, which restricts the application of the model to gradually varying flow conditions. According to Thomas (2000) 2DH models can usefully represent the shape of coastal waters and adjacent sea areas. The adjacent sea area generally forms the offshore boundary which is often an important source of sediment in the coastal water. 2DH models are capable of handling many features of coastal waters such as Coriolis effect, transverse components of flow, realistic friction and non-linearity via the distribution of flow through an arbitrary cross-section. 2DH models cannot however, represent secondary circulation, whether transverse and vertically sheared as at bends, or driven by lateral differences in salinity due to differential ebb or flood currents. Nor can 2DH models represent coastal water circulation (Thomas, 2000).

Ever since the usage of the numerical modelling become widespread, there are researchers including Wang (1989), van Rijn (1993), Leybourne (2002) who claimed the suitability of the 2DH models. However, there are researchers like Nix (1990), Noda (2003), and Huthance (2007) who emphasised that the depth-averaging procedure used in the 2DH modelling caused uncertainty in the results. Considerable studies have been carried out using depth-averaged two dimensional (2DH) models (see for example Ariathurai and Krone (1976), Cole and Miles (1983), and Struiksma (1985)). Delft3D from Delft Hydraulic, DIVAST from Cardiff University, and MIKE 21 from DHI water and environment are three examples of 2D industry-standard models.

2.2.3 Three dimensional models

In order to consider the hydrodynamic and transport processes more realistically and more accurately, three-dimensional (3D) models are necessary. Flow phenomena in nature are three dimensional. Turbulence is an essentially three-dimensional phenomenon, and three-dimensional models are particularly useful for the simulation of turbulent heat and mass transport. These models are usually based on the Reynolds-averaged form of the Navier-Stokes equations, using additional equations of various degree of complexity for the turbulence closure. Three-dimensional modeling is a very powerful tool in coastal engineering, but it also has high computational demands. In addition, it requires vast amounts of data for proper model setup, which takes time and is expensive to obtain. These requirements have, until recently, limited their use, but newer, faster, and more affordable computers, together with new instrumentation for data collection, may overcome these limitations in the near future (Francisco et. al., 2006).

To overcome the practical issue of high demand on computational resources many quasi-3D models have been developed by extending a 2DH model with an additional one dimensional vertical profile model (1DV), that allows for inclusion of spiral flows, (see for example Briand and Kamphuis (1993), Elfrink et al. (1996) and Rakha (1998)). In these models, the mean flow is determined by the 2DH model, but the flow and sediment transport profile

across the water column in the vertical direction are resolved by using a 1DV model. Such an approach has been proved to be particularly efficient in medium and long term morphological predictions (Li, et.al., 2007). Development of the quasi-3D models began with De Vriend and Stive (1987). The primary advantage of the quasi-3D models is that they solve for the vertical variation of the currents and include the leading order effect of the depth-varying currents on the depth averaged flow field all on a two-dimensional grid, preserving the computational speed of a 2DH model (Haas and Warner, 2009).

Some researchers such as Cheviet et. al. (2002), and de Vriend et al. (1993) suggested that in the coastal area, a 3D model is required especially when the sediment movement is in the cross-shore direction, at or near a bend, local expansion and contraction, or a hydraulic structure. That is as well of particular interest in situations where the flow field shows significant variations in vertical direction (Van Rijn, 1993). For instance, a helical secondary flow induced in a curved channel by the flow curvature leads to a bed load transport of material towards the inner bank of the curve. Erosion occurs on the outer banks and deposition occurs on the inner bank. The 3D models account for this effect by solving the vertical profile of secondary velocity in the river cross-section (Neill, et.al., 2007). According to Van Rijn (1993) a major problem encountered in 3D modelling is the determination of suitable and, realistic initial and boundary conditions. This often implies the necessity of a very extensive and expensive field-measurement program. Based on his experiments, he concluded that 3D-models are among the most sensitive and least successful of all numerical models.

In addition, the suitability of the use of 3D models is related to the number of the grids applied in the vertical coordinate. When the vertical grids are not defined accurately, the desirable results cannot be derived from the 3D model. In other words efficient and accurate results require refined grids. Van Rijn (1993) tested the influence of the number of vertical grid points applying a logarithmic vertical scale on the accuracy of the numerically computed concentrations and transport rates in comparison to analytically computed results for 5, 10 and 20 number of layers. He claimed that the maximum error does occur in the water surface region, where the vertical grid size is maximum. The errors in the depth-integrated transport rate are much smaller because most of the material is transported in the near bed region where the errors in the concentrations are small. Based on his experiments, he also concluded that in a sandy environment the number of grid points should be about 10, while in an environment with cohesive structure about 5 grid points may be sufficient.

A good example for the very first 3D development is the *full unsteady three-dimensional model for fluid velocities and sediment concentrations* of Wang and Adeff (1986) and McAnally et al (1986). Nowadays a number of 3D, time-dependent, free-surface hydrodynamic models are available for surface water and sediment transport modelling including Sheng and Butler (1982), Blumberg and Mellor (1987), Van Rijn and Meijer (1988), O'Connor and Nicholson (1988), Hamrick (1992), Casulli and Cheng (1992), Katopodi and Ribberink (1992), Cancino and Neves (1999), and others. Although these models all solve the same 3D Navier-Stokes equation, they can be significantly differed in terms of turbulence schemes, numerical methods, grid types, and/or solution algorithms (Ji, 2008). Delft3D (Delft Hydraulic), TRIVAST (Cardiff University), ECOMSED (HydroQual), and MIKE3 (DHI) are some examples of 3D industry-standard models.

2.3 Flow, Sediment transport and morphological models

The basis for the evaluation of sediment transport and the study of morphodynamics of a coast is an accurate knowledge of the flow field. Numerical models solve the mass transport equation for suspended sediment and the mass conservation equation for bed sediment after the hydraulic field is solved (Huang et. al., 2006). As pointed out by Black, (2003) the sediment flux prediction or forecast is at the bottom end of the "numerical chain". Therefore to obtain a good forecast all flow parameters governing the sediment transport including current velocity, waves, bottom shear stress and turbulence should be compute as accurately as possible. It is however, obvious that modelling always implies simplification. For instance, in the coastal shallow water for simplifying the equations of the flow, it is assumed that the pressure distribution follows the hydrostatic law. This restricts the range of applications of the model because it cannot be used to compute the flow in the vertical direction (Van Rijn, 1993).

When a reliable flow model is achieved the performance of the sediment module can be adjusted. The sedimentary processes in the coastal zone are controlled not only under the influence of flow but also by the sediment supply from the adjacent land drainage basins. Thus, natural precipitation, river discharge changes (Tsimplis et al. 2004) and/or anthropogenic changes in sediment supply (Poulos & Collins 2002) from the surrounding drainage basin areas might result in significant sedimentary and morphological changes in the coastal area (Velegrakis, et. al. 2007). The sediment transport models are useful tools for identifying locations of likely scour and deposition. This, in turn, can be used to predict the resultant long-term changes to the bathymetry and shape of the coastal zones.

To model sediment transport the most relevant parameters such as the particle diameter, the fall velocity, the bed roughness, and the shear stresses of the model should be varied within their validity ranges to evaluate their effects on the morphological results and computations of sensitivity (van Rijn, 1993). Velegrakis, et. al. (2007) emphasized the need for sufficient calibration and validation of these models using field data, in order to be able to investigate patterns of sediment movement, under different sets of prevailing hydrodynamic conditions and obtain successful predictions from such models. Even if better measurements have led to better theory and better computer simulations, sediment transport remains challenging, and its complexity cannot be underestimated (Black, 2003). According to Violeau et.al. (2002) inaccurate spatial description of the bathymetry, numerical schemes, incomplete and simplified modelling of a number of processes are some inconsistencies in the numerical models. On the basis of several case studies on sediment modelling, Black (2003) concluded that Lagrangian sediment transport modelling has systematically evolved to a high level of confidence, when the model is able to accept multiple inputs describing the natural system. He however, emphasized that the sediment model also relies on accurate modelling of waves and hydrodynamics.

Obviously, all the numerical models still have many limitations, and their results should always be interpreted with great care. Despite this deficiency, modelling enables researchers to better understand the physics of the area and the sediment behaviour in real coastal waters. Sediment predictions by the models are usually divided into two categories of non-cohesive and cohesive sediments. These are briefly discussed in the following subsections.

2.3.1 Non cohesive sediment model

Non-cohesive sediments are considered to be transported as two modes of bed load and suspended load. Bed load transport in non-uniform and non-steady conditions can be modelled by a formula-type of approach because the adjustment of the transport process to the new hydraulic conditions proceeds rapidly. On this basis, a two-dimensional horizontal or a one-dimensional approach is the most efficient approach, provided that the magnitude and direction of the bed-shear stress can be predicted with sufficient accuracy. If necessary, a (quasi-) three-dimensional flow model can be applied to compute the bed-shear stress in complicated situations such as the flow in bends; tide, wind and wave-induced flow in coastal seas (Van Rijn, 1993). Suspended load transport does not adjust rapidly to the new hydraulic conditions because it takes time and space to transport the particles upward and downward over the depth, which makes it necessary to model the convective and diffusive processes. These types of models are also called continuum models. The modelling of the small-scale and short-term processes requires a (quasi-) three-dimensional or a two-dimensional vertical approach; for example, scour and deposition near structures and harbours (Van Rijn, 1993).

2.3.2 Cohesive sediment models

In the subject of sediment transport, studying cohesive sediment is more complicated than non-cohesive and sand sediments. That is, cohesive sediments by the nature are composed primarily of clay-sized material, which have strong interparticle forces due to their surface ionic charges (Huang, et.al., 2006). Therefore, cohesive sediment transport involves the interaction of many known and unknown physical and chemical processes, forces, and fluxes. It is practically impossible to reproduce these processes in the laboratory due to scaling problems and the high costs. According to Toorman (2001) fieldwork to obtain comprehensive data sets is even more expensive. These complex problems can only be studied with the help of mathematical models, complemented by field data for calibration and validation. Therefore, an appropriate mathematical description of all these forces and fluxes in the three dimensions is needed to be developed, and, in principle, the features that occur in nature should be reproducible.
According to Odd (1988), the first cohesive sediment transport model, in which the complete cycle of mud transport and siltation was simulated, was the model developed at HR Wallingford in 1968 for the *Thames barrier investigation* (Owen and Odd, 1972; Odd and Owen, 1972). Since then a large number of models have emerged including 2DH (Torfs et al., 1996), sometimes multi-layered, 2DV (Winterwerp, 1998) and recently Quasi-3D and 3D (Lesser, et.al, 2004). Toorman (2001) pointed out that full 3D modelling for engineering applications is still very limited, as no computer is powerful enough to do the task within a reasonable time. According to him, some simplifications are necessary, i.e., vertical momentum exchange is neglected, and often no coupling between sediment transport and hydrodynamics is taken into account.

Due to the simplifications involved, models approximate the reality and fail to reproduce some phenomena occurring in the field. The simplifications arise from the limitations in computer capacity and the impossibility to account for the complexity of the very non-homogeneous and variable composition of natural cohesive sediments. Models, however, have the advantage over measurements in that they can cover much larger areas and provide data at many more points. Complementary measurements are required for calibration, validation and verification of the model. The collected data however, either in

the field or in the laboratory, are often incomplete, and do not allow calibration or validation of the models without making unverifiable additional assumptions, which contribute to a great deal to the inaccuracy of model predictions (Toorman, 2001).

In the simulation of cohesive sediment processes, a number of model parameters should be pre-evaluated, such as the bed roughness, critical shear stress for erosion/deposition, erosion rate, settling velocity, eddy viscosity, etc. If possible, these parameters should be investigated in situ or through laboratory experiments, but in practice they are usually unavailable. As a result, the processes of calibration and verification are always mandatory for validating the numerical simulations (see Mehta and Parchure (2000), and Xie et.al. (2010)).

In modelling sediment transport, the critical bed shear stress for erosion, τ_{ce}, the erosion rate, E, the settling velocity, w_s, and critical bed shear stress for deposition, τ_{cd}, of deposited sediments are the major processes that need to be understood before a successful modelling is possible.

2.3.3 Mixture of mud and sand

Fine sediments in coastal waters are mixtures of non-cohesive and cohesive materials including inorganic minerals, organic materials, and biochemicals (McAnally and Mehta, 2003). The behavior of the sand-mud mixtures and long-term morphodynamics are still pioneering areas where little progress has been made and which have received much less attention than desired. Because the interaction between sand and mud is very complex (Toorman, 2001). The characterizing feature of the cohesive sediments is that the individual primary grains are too small to settle under their own weight when suspended in water, since any disturbance, even Brownian motion, will tend to keep them suspended (McAnally and Mehta, 2003). According to Armanini (1995) the interaction between sand and mud is complex because the mixing within the bed can have a physical and biological origin. According to him physical mixing depends on the mud content within the bed and decreases with increasing mud content. According to Boudreau (1997) biological mixing can be categorized as local and non-local mixing. Local mixing is caused by organisms which move through the bed and therefore mix the sediment particles. Non-local mixing is caused by organisms that transport a specific sediment fraction from one level to another in the bed. Thus due to the complexity involved a few 2DH models have been developed in which the influence of the mud/sand ratio on the erosion characteristics is included; the Delft3D package for instance is one in which the effect of mixture of mud and sand has been included since 1998.

In addition to erosion and deposition processes, other processes such as consolidation, flocculation, and physical and biological mixing within the bed may also affect the bed composition. In an ideal process based model, all these processes should be taken into account for predicting the bed composition in time and space. However, the present knowledge of these processes for mixtures of non-cohesive and cohesive sediments is limited and constructing a process-based sand-mud model, that incorporates all processes is beyond the present state-of-the-art. Simplifications are therefore inevitable and consequently, the validity of the present sand-mud model herein is limited. Moreover, the limited availability of data is another problem for verification of the model results (van Ledden, 2002).

Dyer (1986), Raudkivi (1990), Torfs (1995) and Panagiotopoulos et al. (1997), all stressed the role of clay particles in the erosional behaviour of mixed beds. Torfs (1995) claimed that when a mixture of sand-mud was employed the non-cohesive behaviour of the bed was increasingly suppressed and that the critical mud content was not the same for different sand-mud mixtures. The observations of the transition between non-cohesive and cohesive behaviour as well as the critical erosion shear stress suggest that the erosion process is dominated by the clay content and not the mud content itself. From the modelling point of view, the traditional erosion formulae for sand and mud alone must be adapted because of this behaviour. Depending on the clay content in the bed, two regimes must be distinguished: a non-cohesive and a cohesive regime. The transition between both regimes according to Dyer (1986) should be given by clay content of 5 - 10%. A critical mud content can also be used, because bed composition measurements suggest a strong correlation between the clay content and silt content (% 0.002 - 0.063 mm) within the bed (Van Ledden, 2000). However, it must be kept in mind that a critical mud content seems to be a site specific value, depending on the clay/silt ratio.

Van Ledden (2002) offered an equilibrium mud content within the exchange layer when both deposition and erosion occur during the tidal period.

$$P_{m,eq} = \frac{w_s c}{M_{er}} \qquad (2.1)$$

In this equation, the settling velocity for mud *(* w_s *),* the mud concentration *(c)* and the erosion rate (M_{er}) form an important dimensionless parameter *(* $P_{m,eq}$ *).* This parameter expresses the ratio between the deposition and erosion flux capacity. His model results suggest that the sharp transition between areas with a very low mud content and other areas depends on the aforementioned dimensionless parameter. For low values ($P_{m,eq} < 10$) the transition is sharp, while for higher values the transition becomes more and more gradual. Based on the model results he also suggested that a local hydrodynamic parameter (e.g. maximum bed shear stress) for predicting the mud content at a certain location is not very useful for areas exposed to a relatively low bed shear stress. Apart from the local hydrodynamics, the local mud concentration, the settling velocity, the mixing properties within the bed and the sample depth are parameters which determine the local mud content.

Erosion of mixtures of sand-mud sediments with sand is also investigated by Torfs et. al. (2001) relying on laboratory flume experiments under steady flows. They found a highly non-linear relationship between critical shear stress and sand-mud weight fraction and concluded that this non-linear dependency is indicative of the interactive role of the mixture components in controlling erosion, and suggests a potential route for improvement in modelling erosion by accounting for these interactions.

2.4 Erosion

The assessment of the ability of the prevailing hydrodynamic conditions to suspend and transport the bed sediments is of paramount importance in investigations of sediment dynamics. These potentials can be assessed in terms of the percentage of time during which the prevailing currents and/or waves are capable of suspending the seabed sediments within the investigated area (Velegrakis et.al., 2007). Modeling the erosion of sediment beds continues to pose problems due to a lack of clear understanding of the way in which the

bed-water interface responds to a flow-induced stress. For steady or quasi-steady (e.g., tidal) flows, the formula relating the rate of erosion to the bed shear stress is generally stress-based. According to Mehta and Parchure (2000) such formulae are empirical approximations of very complex flow particle interactions which ultimately cause bed particles and aggregates to dislodge and entrain. According to Toorman (2001) and Winterwerp (2002) the bed exchange module is the weakest part in cohesive sediment transport modelling. One of the fundamental problems they pointed out regarding their statement was the lack of a general relationship between erosion strength and bed shear strength. They reckoned that even if the fundamental questions regarding the modelling of sediment exchange between water column and bed were resolved, the fact remains that the bed properties vary in time and space (both horizontally and in depth), for instance due to variations in sediment composition and biological activity.

Van Rijn (1993) introduced parameters that influence the erodibility of the cohesive sediment. He proposed five different categories which could influence the erosion rate including flow, wave, geological, chemical and biological features. Many attempts have been made to calculate the effect of these parameters indirectly and to relate the critical shear stress to parameters such as plasticity, voids ratio, water content, yield stress and others. However generally accepted relationships are still not available (van Rijn, 1989). Therefore, determination of critical bed shear stress (τ_{ce}) and erosion rate (*E*) should be based on field measurements, laboratory tests using natural mud, or through calibration of the numerical model.

On the basis of an extensive investigation, Parchure (1984) and Parchure and Mehta (1985) quantified the decrease in time of the erosion rate when a constant bottom shear stress was applied on a deposited bed. Piedra-Cueva and Mory (2001) continued the research and noted that interpreting the variation of erosion rate in terms of excess shear stress variation is not straightforward. They classified the Erosion laws published in the literature in two classes. The first type of erosion law estimates erosion rate as a power function of the excess shear stress:

$$E = M_{er}(\tau_b - \tau_{ce})^n \qquad \text{for} \quad \tau_b > \tau_{ce} \tag{2.2}$$

where

τ_b and τ_{ce} are bed shear stress and critical surface erosion shear stress respectively and M_{er} is mass erosion rate constant. This equation implies that the erosion rate is constant for a constant bottom shear stress. Although the well known linear erosion law (with *n*=l) is often attributed to Partheniades (1965), Ariathurai et al. (1977) actually introduced this law by fitting a linear equation to Partheniades' data. With this definition suspended sediment concentration in the water increases linearly with time which can only be true for homogeneous sediment beds with a constant shear strength with depth, occurring rarely in nature. The erosion rate decreases to zero when $\tau_b - \tau_{ce}$ decreases to zero. The second type of erosion law for deposited beds offered by Piedra-Cueva and Mory (2001) is written in the form

$$E = E_f \exp\left[\alpha_{er}(\tau_b - \tau_{ce})^n\right] \tag{2.3}$$

This type of erosion is called floc erosion and E_f is the residual floc erosion rate. Parchure and Mehta (1985) analyzed their results in terms of such an erosion law, for which they obtained *n=1/2.* It is important to point out that the two types of laws differ significantly at

the asymptotic condition $\tau_b - \tau_{ce} = 0$. Piedra-Cueva and Mory (2001) in their experiments found out that the erosion rate decreases exponentially with time while the excess shear stress decreases toward zero. They emphasized that the excess shear stress is the main parameter governing erosion. It was moreover shown by their data that the gradient of the bed shear strength enters the scaling of erosion. Erosion decreases when the gradient of the bed shear strength increases.

MacIntyre (1990) also carried out some investigations on erosion rate and found out that even with the sophisticated layer model used, the erosion rate of the layers cannot be assigned values in a physically based manner. Thus he concluded that the erosion rate is not a fundamental coefficient, but merely an apparent property of the bed. Andersen et.al (2002) claimed that the erosion rate of the sediments is highly influenced by the applied bed shear stress. The dependence on bed shear stress was also found by Winterwerp et al. (1992) who concluded that the erosion threshold of the bed material is mainly governed by physical properties of the sediment which are a product of sediment and hydraulic properties.

In his studies, Partheiades (2009) found that erosion may eventually stop which could be counted as indicative of an increase of the erosive resistance of the bed with depth and, possibly, with time. He also claimed that none of the previous research work addressed the initiation of erosion and the erosion rates after a critical shear stress has been exceeded. Based on the evidence from Sanford and Maa (2001), Maa and Kim (2002), and Maa et al. (2008) reasoned that the assumption of a constant critical erosion shear stress is also not true. They pointed to the experiments by Maa and Kim (2002) who carried out in situ erosion experiments at the York River, and found that critical bed shear stress for erosion increases with sediment depth (downward). Mahatma (2004) carried out an investigation in the North Sea coast. He observed negative correlation between erosion rate and critical erosion shear stress and claimed that this negative correlation is due to the fact that as the surface of the sediment becomes more resistant to erosion, the rate of erosion also is influenced. He also came to the conclusion that the variation of sediment erodibility at the area was more correlated with biological processes than other measured sediment parameters.

In Delft3D for modelling cohesive sediment equation 2.2 is employed with the power of one (see Section 4-3-4-1). Setting n as one in equation 2.2, two other parameters of the equation should be specified by the user including erosion parameter (M_{er}) and critical bed shear stress for erosion (τ_{ce}).

2.4.1 Erosion parameter

The value of erosion parameter (M_{er}) is considered as a calibration parameter. Reported values for M_{er} are in the range of 0.00001-0.0005 kg/m²/s (Partheniades, 1965). Some literature based values for erosion parameters are summarized in Table 2.1. M_{er} is generally assumed to be a constant material parameter, but it often varies with depth and time because of consolidation and physico-chemical effects. Figure 2.1 shows the presentation of M_{er} (presented as M_1 and M_2) together with a typical graph of erosion rate versus shear stress (Hwang and Mehta, 1989). Two straight lines in the Figure represent the surface erosion of bed at low shear stress and mass erosion at relatively high shear stresses. Looking at the Figure, the point in which bed surface erosion line meets the shear stress axes is the critical bed shear stress point for surface erosion.

Maa and Kim (2002) carried out an experiment in a tidal dominated area of *York River* in order to study erosion rate. Based on their experiments, they concluded that the M_{er} in eq. 2.2 can be selected as a constant in the acceleration phase of a tidal dominant field and as zero for the other phases. They also emphasized that this constant value for the erosion rate is different from spring to neap tide because of the change in the rates of erosion and deposition. Partheiades (2009) mentioned that cohesive materials with the same classification and very similar grain size distribution might display widely different resistance to erosion. This can be considered as the additional effect of mechanical composition that controls erosion of cohesive soils.

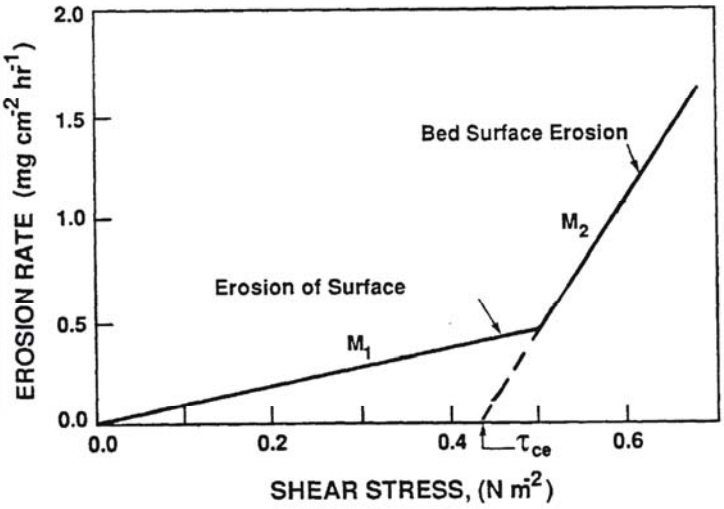

Figure 2.1 A typical Composite Erosion Rate Variation with Bed Shear Stress at a Mean Density of 1.1 gcm^{-3} for Okeechobee Lake in Florida Experiments (Hwang and Mehta, 1989)

2.4.2 Critical Bed Shear Stress for Erosion

The strength of cohesive sediment beds is commonly expressed as a function of the critical bed shear stress for erosion. The main problem however, is that there is still no common agreement about the parameters involved in defining critical bed shear stress for erosion. Parchure and Mehta (1985) stated that the value of critical bed shear stress for erosion depends on physico-chemical properties of the mud, chemical properties of the eroding fluid, flow characteristics, and bed structure. They also reported that the deposition and consolidation history play a role in the value of critical bed shear stress for erosion. Houwing (1999) carried out an investigation on the Dutch Wadden Sea Coast. He reported that there is no meaningful relation between the critical bed shear stress for erosion and bulk density, biotic factors, sediment concentration and biological activity. He concluded that the critical bed shear stress for erosion is not a good parameter to characterize erodibility of the bed. Krone (1999) also mentioned that time-averaged shear stress is not a useful tool for determining bed strength as a function of depth.

Experiments by Partheiades (2009) have shown that the critical stress for erosion is three to four orders of magnitude smaller than the strength of the soil. He therefore concluded, that the shear strength of the soil cannot be used as a unique criterion of soil resistance to erosion. Maa and Kim (2002) reported that critical shear stress for erosion is not constant and increases with depth, and that erosion is a relatively rapid process and with a constant bed

shear stress, erosion rate approaches zero very fast. They also mentioned that erosion in most coastal waters could only occur when the tide is in acceleration phases. In another words, suspended sediment concentration starts to increase immediately after the tidal acceleration phases and starts to decrease soon after bed shear stress starts to decrease.

Schweim et. al. (2002) carried out an extensive investigation on the erosion equations proposed by Partheniades (1965) and Parchure and Mehta (1985) and deposition equation proposed by Krone (1962). They came to the conclusion of certain limitation for the applied equations. They pointed out that in some simulations, a satisfactory agreement concerning the order of magnitude of concentrations between experiments and simulations was reached. According to them however, the agreement was rather due to the use of parameters fitted directly to the experimental database than to the accurate interpretation of physical phenomena involved.

In spite of the difficulty of determining critical bed shear stress, this parameter is still one of the main variables that is specified for modeling sediment transport. Table 2.1 is prepared as a guide to specify this value and to calibrate the sediment transport models. It contains the values of critical bed shear stresses for erosion and erosion parameters published in the literature. Some are derived through calibration processes and others through field or laboratory measurements.

Table 2.1 Range of Critical Bed Shear Stresses and erosion parameter based on literature Review

Area of investigation	critical erosion shear stress (N/m^2)	Erosion parameter ($kg/m^2/s$)	Proposed by
Bay mud	0.5	3.0×10^{-5}	Partheniades (1962),
Fraser River Delta (Canada)	0.11 to 0.50	-	Amos et.al (1997)
Baltimore Harbour (Maryland-USA)	0.05 to 0.10	-	Maa et.al. (1998)
Estuarial mud	0.4	71.0×10^{-5}	Mulder and Udink (1991)
Typical intertidal zone	3>	-	Riethmüller et al. (2000) Austen et al. (1999)
Typical intertidal zone	0.2 to 0.5	-	Andersen (2001)
Gironde estuary, France	0.8	0.01	Sottolichio et. al. (2001)
Hollandsch Diep freshwater, The Netherland	0.16 to 0.70	-	Andersen et. al. (2002)
Amazon Shelf	0.42	0.02	Vinzon and Paiva (2002)
Chesapeake Bay	0.026 to 0.1	-	Maa and Kim (2002)
Tamar Estuary	0.2 to 0.5	5.0×10^{-5} to 1.0×10^{-4}	Petersen et. al. (2002)
Tamar Estuary	0.1 to 0.4	0.2×10^{-3} to 1.3×10^{-3}	Petersen and Vested, (2002)
Lake mud	0.2	3.48×10^{-5}	Schweim et. al. (2002)
South western Baltic Sea (Germany)	0.04	-	Ziervogel et.al. (2003)
Experimental study on uniform dense bed	0.11 to 1.33	0.8×10^{-5} to 4.7×10^{-4}	Partheiades (2009)

2.5 Settling velocity

Settling velocity is specifically significant and sensitive for the cohesive sediments, as it depends on the state of flocculation of the suspension. It may vary largely over space and in time (e.g. Dyer, 1989). It is also known to vary with the sediment concentration itself. Van Rijn (1989) observed relationship of settling velocity of the fine particles to the salinity, the suspended sediment concentration, the water depth, and the flow velocity. He later (Van Rijn 1993) employed the data collected from field and laboratory studies for saline water conditions from extensive data and presented a plot of the settling velocity versus sediment concentration which is shown in Figure 2.2. Referring to the Figure, an increase of the settling velocity with concentrations up to about 1 kg/m^3 (1000 mg/l), in saline water, is attributed to the flocculation effect. The settling velocity decreases with increasing concentrations when the sediment concentrations are larger than 10 kg/m3 (10000 mg/l). The settling velocity of the flocs is reduced due to an upward flow of fluid displaced by the flocs.

Hwang et al (1989) pointed out that very fine particles tend to be transported as flocs rather than individual particles, and their settling velocity as flocs is supposed to be smaller than those of individual, because of their water contaminant. However, their shape and size become more spherical and larger with correspondingly reduced drag. Since the reduction in drag and increased size are much more significant than the decrease in density, the settling velocities of the flocs are substantially higher than those of individual particles.

Winterwerp (1999) also carried out an intensive investigation on the parameters affecting the settling velocity of the fine particles and introduced some more processes that can affect the settling velocity of individual particles in a suspension, including return flow, particle-particle collisions and interaction, and viscosity. Vinzon and Paiva (2002) noted that the settling velocity of cohesive sediments is influenced by flocculation, which in turn is affected by turbulence. They mentioned that turbulence could enhance the coagulation process, bringing particles together, or can breakup the already formed flocs, due to the shear stresses. They came to the conclusion that the settling velocities determined in laboratory conditions underestimated those determined from field observations as a result of absence of turbulence in the laboratory experiments.

Andersen (2001) calculated settling velocity with suspended sediment concentration for the *Danish Wadden Sea* area. The resulting graphs he derived from regression analyses are shown in Figure 2.3. His observations, as reported, is that there is a marked difference between the settling velocities found in the tidal channels and those for tidal flats, with generally higher settling velocities in the channels. He reasoned that the difference was due to the inclusion of sand in the suspended sediment in the channels, because sands tend to have much higher settling velocities than the fine materials.

The above observations, including Figures 2.2 and 2.3, revealed that a general relationship to determine the settling velocity of the fine particles at a particular location is not available. This suggests that the best approach to estimate this variable is to carry out field measurements. Since the settling and deposition process is most effective during the slack water period of the tidal flow; van Rijn (1993) proposed that the measurement of this parameter should be concentrated during this period of a tidal cycle.

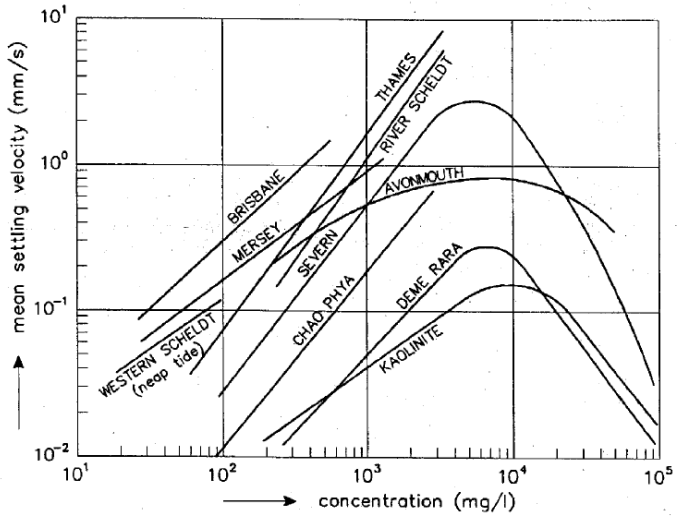

Figure 2.2 The influence of sediment concentration on the settling velocity (Brisbane in Australia; Severn, Avonmouth, Thames, and Mersey in England; Western Scheldt in The Netherlands; River Scheldt in Belgium; Chao Paya in Thailand; Demerara in South America) (Source: Van Rijn, 1993)

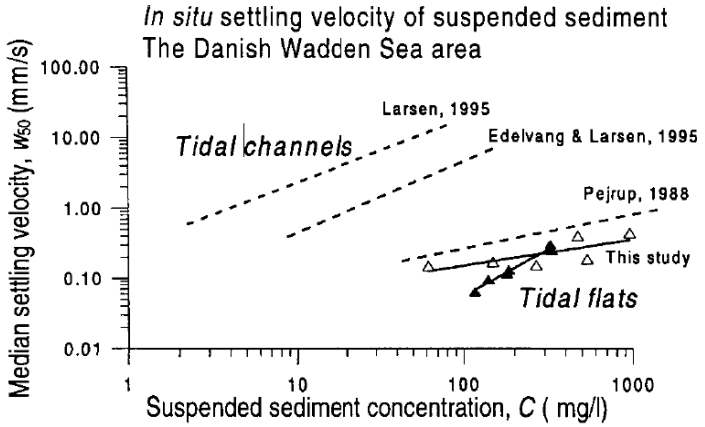

Figure 2.3 Correlation between suspended sediment concentration and median settling velocity from the Danish Wadden Sea (Andersen (2001)

During the last decades many attempts have been made to formulate the settling velocity of the cohesive particles. In view of the effect of the concentration of suspended sediment (c) on the settling velocity of the particles (w_s), a relationship between these two parameters was derived (see Mehta (1986) and van Rijn (1989)). The general formula is suggested as

$$w_s = k_1 c^m \qquad (2.4)$$

where both k_1 and m (= 1 to 2) are coefficients. This equation is valid for suspensions less than 0.01 to 10 kg/m^3. Shi et. al. (2003) used in situ measurements to derive the parameters k_1 and m of equation (2.4) from the Rouse number ($P_r = w_s / ku_*'$) of the equation (Rouse, 1937):

$$\frac{c}{c_a} = \left[\frac{z_b (h - z_a)}{z_a (h - z_b)} \right]^{w_s / k u_*} \qquad (2.5)$$

where, c and c_a are sediment concentrations at z_b (elevation above the bed) and at a (reference height) and h is water depth. Their final equation in the form of eq. (2.4) was:

$$w_s = 2.37 c^{0.84} \qquad (2.6)$$

More complicated equations have also suggested for defining the settling velocity, one of which is offered by Winterwerp (2002). He claimed that in dynamic environments, such as coastal waters, the settling velocity of cohesive sediment might vary in time and space by flocculation effects. Thus, for a single floc settling in a still, homogeneous fluid with viscosity μ, the settling velocity $\omega_{s,r}$ of such a floc can be assessed as follows (Winterwerp, 2002):

$$w_s = \frac{\alpha}{18\beta} \frac{(\rho_s - \rho_w)}{\mu} D_P^{3-n_f} \frac{D_{floc}^{n_f - 1}}{1 + 0.15 \mathrm{Re}_P^{0.687}} \qquad (2.7)$$

In which

ρ_s is sediment (primary particles in the floc) density, ρ_w is water density, D_{floc} is the diameter of the floc, D_P is the diameter of the primary particles, $\mathrm{Re}_P = w_s D / \nu$ is the particle Reynolds number, α and β are the shape parameters, and n_f is the fractal dimension, a representative of the number and the linear size of the primary particles. Typical values of n_f for flocs of cohesive sediment in coastal water columns are between 1.7 and 2.2, with an average value of 2 (Winterwerp, 1998). For spherical $(\alpha = \beta = 1)$, massive $(n_f = 3)$ particles in the Stokes regime $(\mathrm{Re}_P \le 1)$, the well-known Stokes' formula for a single, stationary falling particle is recovered as follows:

$$w_s = \frac{(\rho_s - \rho_w) g D_{floc}^2}{18 \mu} \qquad (2.8)$$

In an analysis of the results of some 200 samples collected during a period of several years in the Thames estuary, Burt (1984) reported that there was no influence of the tidal range (neap-spring cycle) on the settling velocity. His analysis has also shown that the flocs are mainly affected by eddy scales comparable to the floc size scales. These smaller eddy scales will be present during nearly all tidal conditions with the exception of the slack water periods. On the other hand Winterwerp et. al. (2002) , on the basis of field measurement and modelling investigation on *Tamar estuary* reported the observation of considerable variation in floc size, hence settling velocity over the tide, and over the spring-neap tide cycle. Their measurements also revealed the existence of a pronounced distribution in floc size, which varies over time. That is, at the beginning of a flood period hardly any macroflocs were observed in the field, whereas later in the tide, the fraction of macroflocs increased to about 45 to 80%. They concluded that at present, the effects of such a floc size distribution cannot be accounted for in available models, and more research would be required for a proper description of size distribution.

In view of the above reported observations, it seems that there is no algorithm for defining settling velocity of various particles and for including the flocculation effect into the

modelling. Winterwerp et.al. (2002) emphasized that whatever accurate the implemented mathematical-physical descriptions may have been, the accuracy of the results still largely depends on the values of the sediment parameters fed to the model, one of which is the settling velocity of the sediment. Therefore the best way to determine settling velocity in a particular place is site-specific measurements. If such measured data were not available from the field, the settling velocity values should be considered as one of the calibration parameters in the modelling.

By implementing a literature search on settling velocity, some values which were derived from field and laboratory measurements are presented in Table 2.2. The reported values were derived from field and laboratory measurements using various methods and instruments. These included the Owen tube, in situ video camera, settling tube, analysis of sediment concentration and laser-assisted particle sizing. An inspection of the values given in the Table shows that the values of settling velocity vary in the order of one magnitude amongst different coastal waters, bays and estuaries. The same variation can even be seen for a single area such as the Elbe Estuary, Germany (more than 28 times from 0.17 to 4.9mm/s) or Changjiang Estuary, China (10 times from 0.4 to 4.1mm/s). The content of the Table reveal the need for the site specific values and distribution of the settling velocity, that can only be derived through field measurements, employing upgraded, calibrated instruments.

Table 2.2 Settling velocities w_s of fine suspended particles reported in the literature

References	Locality	Measured/calculated	w_s (mm/s)
Puls & Kuehl (1989)	Elbe and Weser Estuaries, Germany	In situ Owen tube	0.01–3.50
Kineke and Sternberg (1989)	San Francisco Bay, USA	In situ settling tube	0.5-2.5
Van Leussen & Cornelisse (1993)	Ems Estuary, The Netherlands	In situ settling tube	0.56–2.82
Sanford and Halka (1993)	Chesapeake Bay, UK	Equation	0.8-0.14
Ten Brinke (1994)	Oosterschelde Estuary, The Netherlands	In situ settling tube	1.54
Pejrup & Edelvang (1996)	Elbe Estuaries, Germany	In situ Owen tube	0.17-4.9
Valeur et al. (1996)	The Sound, Denmark and Sweden	Sediment traps	0.04
Hill et al. (1998)	Glacier Bay, Alaska, USA	In situ settling tube	2.21
Hill et al. (2000)	Eel River Estuary, USA	Fitting method	0.06–0.10
van der Lee (2000)	Dollard Estuary, The Netherlands	Video in situ (VIS)	2.70
Le Hir, et al. (2001)	Gironde estuary, France	Through model calibration	0.5-2.0
Wijngaarden & Roberti (2002)	Hollandsch Diep and Haringvliet, The Netherlands	LISST-ST*	0.005-0.3
Dyer et al. (2002)	Tamar Estuary, UK	Video system	1-6
Petersen et al. (2002)	Tamar Estuary, UK	Through model calibration	5
Andersen et al. (2002)	Hollandsch Diep freshwater, The Netherlands	In situ settling tube	1.1
Vinzon and Paiva (2002)	Amazon Shelf, USA	Stokes' equation	0.02 to 2.8
Shi et. al. (2003)	Changjiang Estuary, China	Rouse equation	0.4–4.1

*The Laser In Situ Scattering and Transmissiometry-Settling Tube

2.6 Deposition

Many laboratory studies have shown that there is a shear stress threshold below which erosion does not occur, known as critical bed shear stress for erosion, and a lower threshold above which deposition does not occur, known as critical bed shear stress for deposition. Based on a laboratory study of Mehta and Partheniades (1973) the parameters that control deposition are: bed shear stress, turbulence process near the bed, settling velocity, sediment type, depth of flow, ionic affection and suspended sediment concentration. In contrast, some researchers have modelled erosion and deposition of mud without a deposition threshold.

This distinction can have important implications for prediction of suspended sediment transport and for data interpretation (Sanford and Halka, 1993).

Considering the existence of a threshold for deposition, it occurs only when the fluid shear stress exerted on the bed (bed shear stress, τ_b) is below a critical value for deposition (τ_{cd}). The deposition rate (D) is proportional to the difference of shear stress below that critical value and also depends on suspended sediment concentrations. It should be mentioned that these critical shear stresses vary with mud type, e.g. particle size distribution, and sediment concentrations (Mehta and Partheniades, 1973). In the context of tidal currents in coastal water the process can be described as follows: During high current velocities only those flocs with high density will be deposited. Then with decreasing velocities (near slack water) the light flocs will be deposited on the deposited dense flocs. At increasing velocities in the next tidal cycle, this floc can be eroded rather easily at low velocities.

Krone (1962), who carried out an intensive investigation on the deposition process of cohesive material, suggested the following equations to describe the deposition rate for low sediment concentrations (C < 0.3 kg/m^3):

$$\begin{aligned} &\text{No Deposition:} \quad D = 0 && \text{for} \quad \tau_b \geq \tau_{cd} \\ &\text{Full Deposition:} \quad D = \left(1 - \tau_b / \tau_{cd}\right) w_s c && \text{for} \quad \tau_b < \tau_{cd} \end{aligned} \tag{2.10}$$

in which

D is the deposition rate, τ_b and τ_{cd} are bed shear stress and critical value for deposition, respectively, w_s is settling velocity of particles or flocs at $\tau_b = 0$ (zero flow), as originally defined by Krone (1962), and C is suspended sediment concentration.

As published by van Rijn (1993) the complexity of defining a critical bed shear stress for initiation of deposition is mainly caused by the stochastical character of the driving fluid forces and the stabilizing resisting forces and by the lack of an unambiguous definition of motion. There are however, some estimations based on laboratory and field investigations proposed in the literature among them Whithouse et.al. (2000). they suggested under the certain conditions, including 1) the bed type dominated by mud and 2) the turbulence of flow assumed smooth, the shear stress is independent of the grain size. They concluded that under such a condition the critical bed shear stress for deposition could be taken as 0.08 N/m^2. Sanford and Halka (1993) however, suggested that the critical stress for deposition should be smaller than or equal to the critical stress for erosion, such that an intermediate range of bottom shear stresses can exist for which neither erosion nor deposition occur.

For most of the numerical modelling, critical bed shear stresses for erosion and deposition are two important parameters required for the bottom boundary condition of the model. As stated by Maa et. al. (2008) the existence of critical shear stress for erosion (τ_{ce}) is widely accepted, but the existence of critical shear stress for deposition (τ_{cd}) is still being debated. For instance, Sanford and Halka (1993) in their field investigations in Chesapeake Bay observed that the total resuspended sediment load increases in conjunction with increasing bottom shear stress, but deposition is initiated soon after the shear stress begins to decrease and long before the stress falls below the value at which erosion had previously begun. They therefore, concluded that for practical modelling purposes, allowing continuous deposition of a single resuspended particle class might often give quite satisfying results. Figure 2.4 is the reproduction of the Figure given by Sanford and Halka (1993) that shows the conceptual difference between the cohesive sediment paradigm of mutually exclusive erosion and

deposition and the alternative of stress dependent erosion with continuous deposition possible. In this Figure the upper panel shows the time history of bottom shear stress (τ_b) over a hypothetical tidal cycle where the τ_{ce} is the critical stress for erosion and τ_{cd} is the critical stress for deposition. The lower panel shows the expected response of the total suspended sediment load (SSC) with the solid line representing mutually exclusive erosion and deposition and the dashed line representing stress dependent erosion with continuous deposition. The effect of assuming continuous deposition in the concentration of suspended sediment is evident.

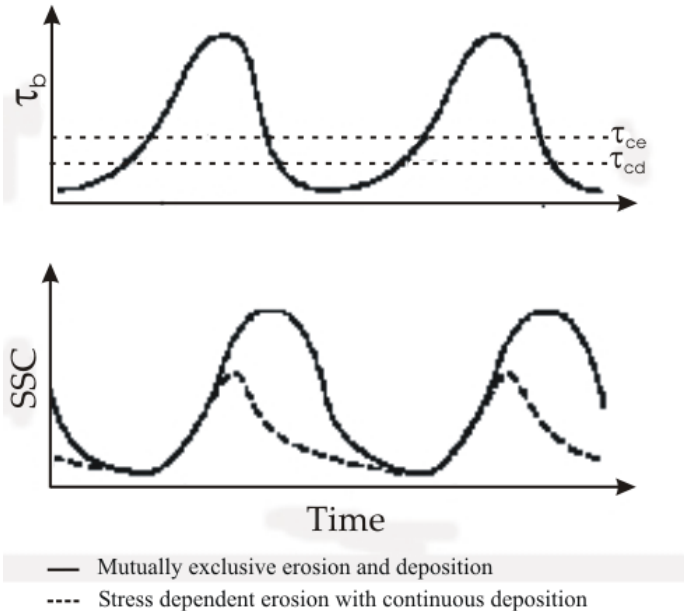

Figure 2.4 Illustration of the conceptual difference between the cohesive sediment paradigm of mutually exclusive erosion and deposition and the alternative of stress dependent erosion with continuous deposition possible (Sanford and Halka, 1993)

In another experiment Sanford and Halka (1993) compared total suspended load of two models; one with the assumption of exclusive erosion and deposition and the other with the assumption of continuous deposition; with the in situ measured data of Chesapeake Bay. They reported the failure of the exclusive erosion and deposition model and relatively success of the continuous deposition model to predict the total suspended load. They offered two different explanations for their observations: 1) fine sediments do maintain a constant exchange with the sediment bed; i.e., that deposition can always occur independent of any critical stress, and 2) the sediments behave as an admixture of particle classes with a sequence of increasing critical erosion and deposition stresses, such that the last class which is eroded, will deposited very soon after the shear stress begins to decrease.

Later on, Maa, et.al. (2002) and Winterwerp, et.al. (2004) on the basis of experimental studies, came to the conclusion that the so-called probability of deposition (hence the critical shear stress for deposition) did not exist, but that this phenomenon was to be interpreted as a probability of resuspension.

Based on research reviews, Teeter (2005) concluded that single grain sediment models which allow simultaneous erosion and deposition (Luettich et al. (1990), Hawley and Lesht (1992), and Lick et al. (1994)) can predict resuspension more accurately than single grain models with mutually exclusive erosion and deposition, despite considerable laboratory experimental evidence supporting the latter assumption. He reasoned that failure of single grain models with mutually exclusive erosion and deposition is that natural sediments with silt and clay have multiple thresholds. He also concluded that the reason for the success of the models that allow simultaneous erosion and deposition is that concentration-dependent depositional flux acts as a compensation to limit erosion, similar to a decrease in sediment bed erodibility with erosion depth observed in laboratory experiments (Teeter, 2003).

Nevertheless in the review of the research done on deposition processes; including the reports by Le Hir et. al. (1993), Ariathurai and Krone (1976), O'Connor and Nicholson (1988), Odd (1988), Lang et al. (1989), Perillo and Sequeira (1989), and Uncles and Stephens (1989); it can be concluded that the empirical constants that determine deposition like threshold for deposition and also deposition rate are specifically site specific and depend on the sediment history as well as its composition. Some reported values for the critical bed shear stress for deposition are presented in Table 2.3. It was demonstrated that a cohesive bed is very sensitive to minor changes of environmental parameters, such as water quality and temperature.

Table 2.3 Critical bed shear stress for deposition reported in the literature

References	Locality	Critical bed shear stress for deposition (N/m^2)
Van Rijn (1993)	Hollands Diep (lake)	0.08-0.1
Van Rijn (1993)	Maas River	0.06
Van Rijn (1993)	Breskens Harbour (estuary)	0.06
Van Rijn (1993)	Delfzijl Harbour (estuary)	0.03
Van Rijn (1993)	San Fransisco Bay	0.1-1.7
Van Rijn (1993)	Maracaibo estuary	0.08-1.6
Petersen et al. (2002)	Tamar Estuary, UK	0.5
Schweim et al. (2002)	Lake mud	0.615
Petersen et. al., (2002)	Tamar Estuary	0.5
Petersen and Vested, (2002)	Tamar Estuary	0.6-1.0

Chapter 3. Introducing the area and Available field data

3.1 Introduction

The area under this investigation is the central Dithmarschen Bight. This area has been the subject of many studies in the recent decades. In this chapter a brief summary of the characteristics of the area relevant to this investigation including the meteorological, hydraulic, geomorphologic and sediment dynamics of the area are presented. The field data that have been employed in this study for the model evaluations are also presented with a brief introduction to the devices in which the measurements were carried out.

3.2 Location of Dithmarschen Bight

The central part of the Dithmarschen Bight is located in the southeastern part of the North Sea (Figure 3.1). The area is confined from the north by the Eider estuary and from the south by the River Elbe. The most dominant morphological features of the area are tidal flats, tidal channels and sand banks over the outer region. Under moderate conditions the maximum mean water depth in the tidal channels is about 18m, and approximately 50 % of the domain falls dry at low tide. The tidal flats and sandbanks are exposed at low water (Mayerle and Zielke, 2005). The most dynamic morphological units are found at the western boundary of the tidal flats where wave action interferes with strong tidal and wind driven currents. The banks and shoals in this region exhibit the highest migration rates.

The Norderpiep channel in the northwest and the Süderpiep channel in the southwest are the two main branches that drive out from the North Sea into the Dithmarschen Bight. Crossing through tidal flats eastward, the two channels merge to form the Piep channel. Further eastward the Piep splits up into three second-order channels and finally into several tidal creeks which are scattered across the tidal flat area of the Meldorf Bay (see Figure 3.1). The three channels together form the Piep tidal channel system, which has the shape of a lying Y. The width of the channels and their rivulets (ending the tidal flats or the shore) varies spatially and temporally from a few meters to about 4 km. The water depths of the main channels vary from 5 to 25m. This channel system was specifically selected for the modelling investigations because some long-term monitoring data, collected under PROMORPH project, were available. These data together with some information from previously measured- and model-based investigations were used for this study. The data used in this study cover three cross sections in the Piep tidal channel system. These are: T1 in

the Norderpiep channel, T2 in the Süderpiep channel, and T3 in the Piep channel (see Figure 3.1). The width of the channel at cross section T1 is about 770m and the water depth varies from 2.8 to 16.1m, at cross section T2 the width is about 2040m and the depth varies from 7.3 to 15.6m and, at cross section T3 the width is about 1200m and the depth is from 6.2 to 17.9m.

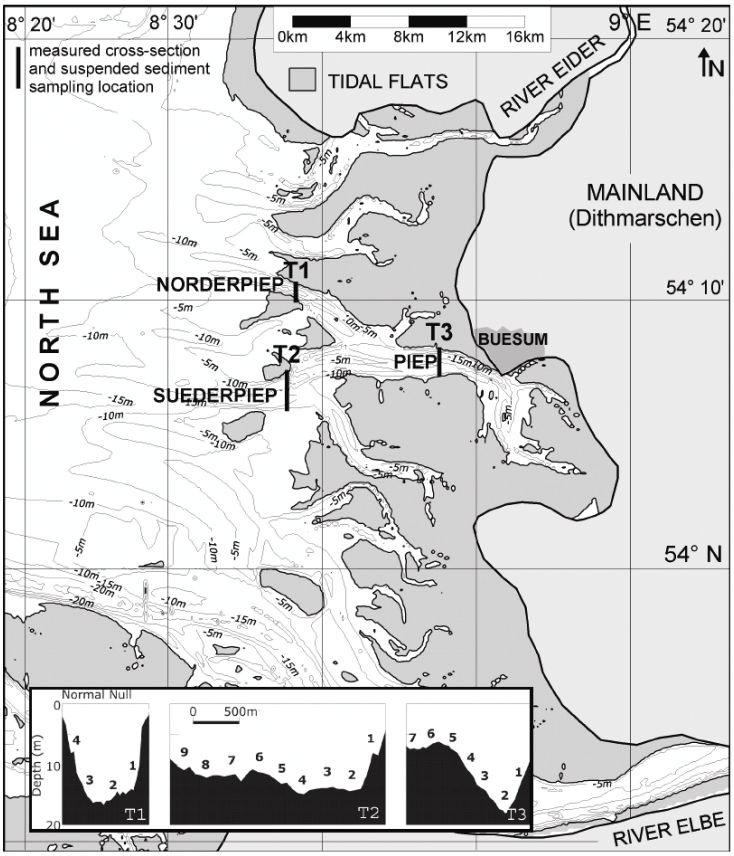

Figure 3.1 Area under the investigation showing the locations of the cross section T1, T2 and T3 (Winter et.al., 2005)

3.3 Geological, Morphological and Morphodynamic Features of the Area

Based on Dittmer's (1938) study, Pleistocene sands form the innermost layer of the bottom area and showed that the surface of the Pleistocene sediments dips down from east to west (more rapidly in the south) to a depth of approximately 30 m below sea-level. This basic layer is covered by a layer, known as Dithmarscher Klei, which consists of cohesive silty clay deposits. Dithmarscher Klei layer can reach a thickness of up to 10 m. the outmost layer of the bottom are non-cohesive sandy sediments and can be as thick as 20m especially at tidal flats (see Figure 3.2). However, the absence of this layer in some locations causes an exposure of the under layer consolidated cohesive sediment, which can potentially hinder further erosion. This layer is known as Early Holocene layer (EHL) that causes restrictions in

the morphological development of the channel. As shown in Figure 3.3 the EHL is mainly exposed in the deeper parts of the channel where continual erosion has removed all the outer-layer of non-consolidate sediment (Mayerle et al., 2002). These parts of the channels behave like a natural basement that hinders erosion processes.

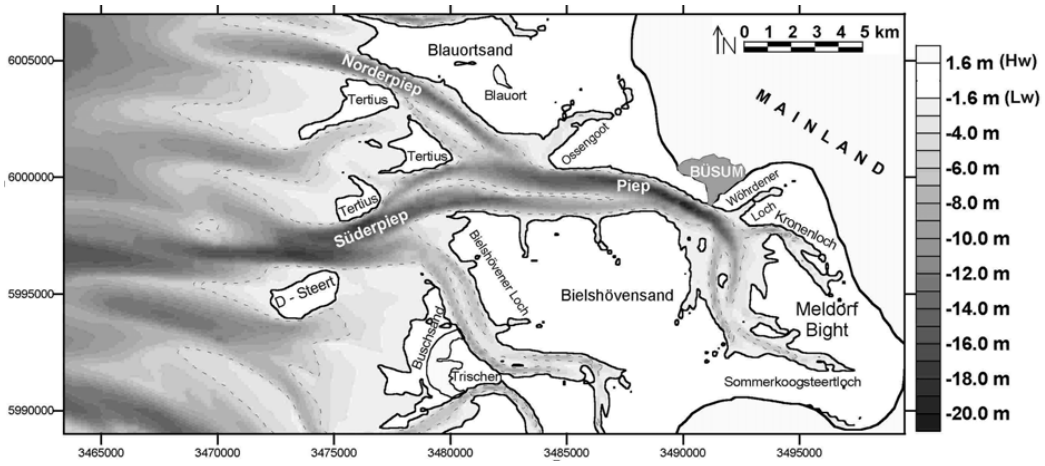

Figure 3.2 Morphology of the area (Wilkens, 2004)

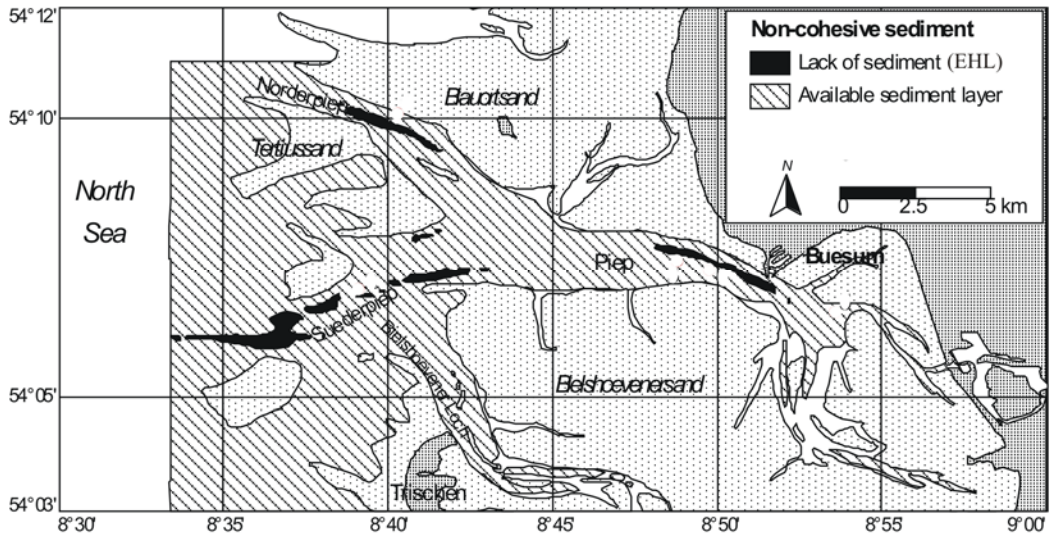

Figure 3.3 Availability of sediment and EHL positions in the tidal channel (Mayerle et al., 2002)

Poerbandono and Mayerle (2005) reported that the seabed in the tidal channels was essentially composed of sandy sediments and mud as well as consolidated deposits. They claimed that in the tidal flat the spatial distribution of the sediment doesn't follow any regular trend. They reported that plane bed, mega ripples and sand dunes are observed in the tidal channels. In the deeper area where consolidated mud exists, generally no bedforms are reported. The bedform types and lengths obtained on the basis of SSS (side scan sonar) during PROMORPH project surveys are shown in Figure 3.4. On the basis of analysing measuring surveys, Mayerle et al. (2005) reported that bed forms develop primarily in the

most exposed areas of the Süderpiep, and along the sides of the channels, especially in the Norderpiep and Piep. According to them, Megaripples with lengths varying from about 3m to 22m were mainly observed and that the average bed-form lengths varied between 7m and 10m in the Süderpiep and Piep tidal channels and between about 3m and 6m along the Norderpiep channel.

On the basis of morphological investigations of the area carried out by Wilkens and Mayerle (2005), they prepared Figure 3.5 which shows the morphological changes from 1977 to 1999. In the Figure the migration of channels, flats and shoals can be observed (changes in depth of up to 8 m). The expansion of the tidal flat towards the south and northeast causes changes to the Norderpiep and Suederpiep channels. Wilkens and Mayerle (2005) reasoned that Norderpiep and to some extent Suederpiep migrate towards the north, as evidenced by parallel stretches of sedimentation and erosion. They also studied in detail the morphological changes in two cross sections in Süderpiep and Piep channel (shown as 1 and 2 in the Figure 3.6). The migration of both channels during a period of about 22 years is clearly shown in the Figure. By the further study of the changes of the profiles for these cross sections, as shown in Figure 3.6, they concluded that the presence of a shoal just south of the Süderpiep channel prevents this channel from migrating southwards. As a result they concluded that the area is fairly dynamic.

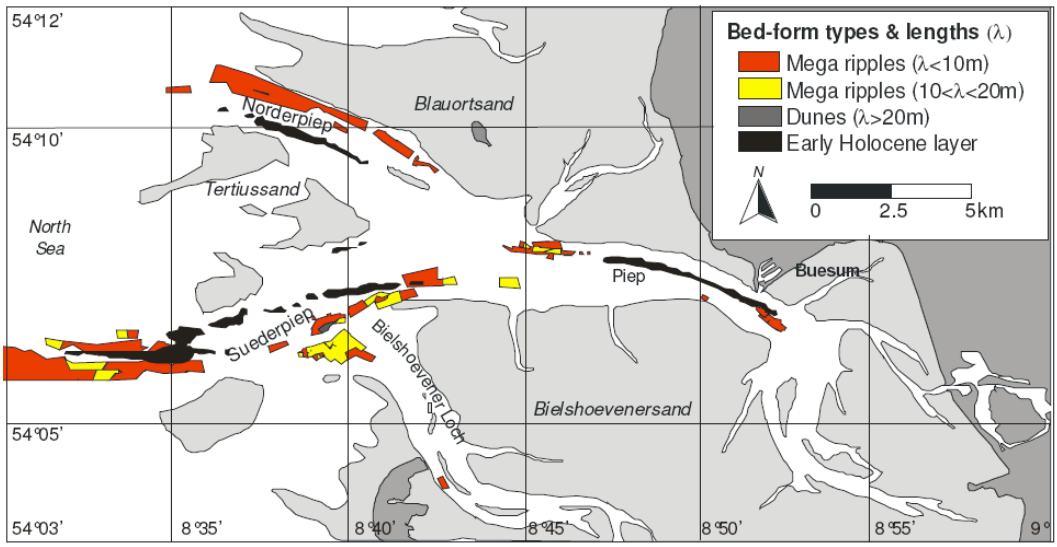

Figure 3.4 Spatial variation of bedforms (Mayerle et al., 2005)

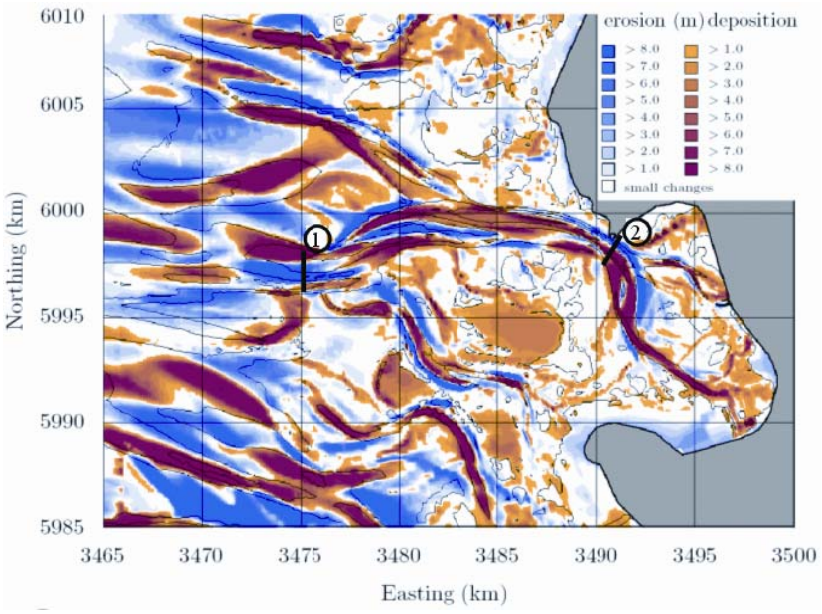

Figure 3.5 Sedimentation and erosion in the Dithmarschen Bight between 1977 and 1999. Isobaths shown for 1977 bathymetry (Wilkens and Mayerle, 2005)

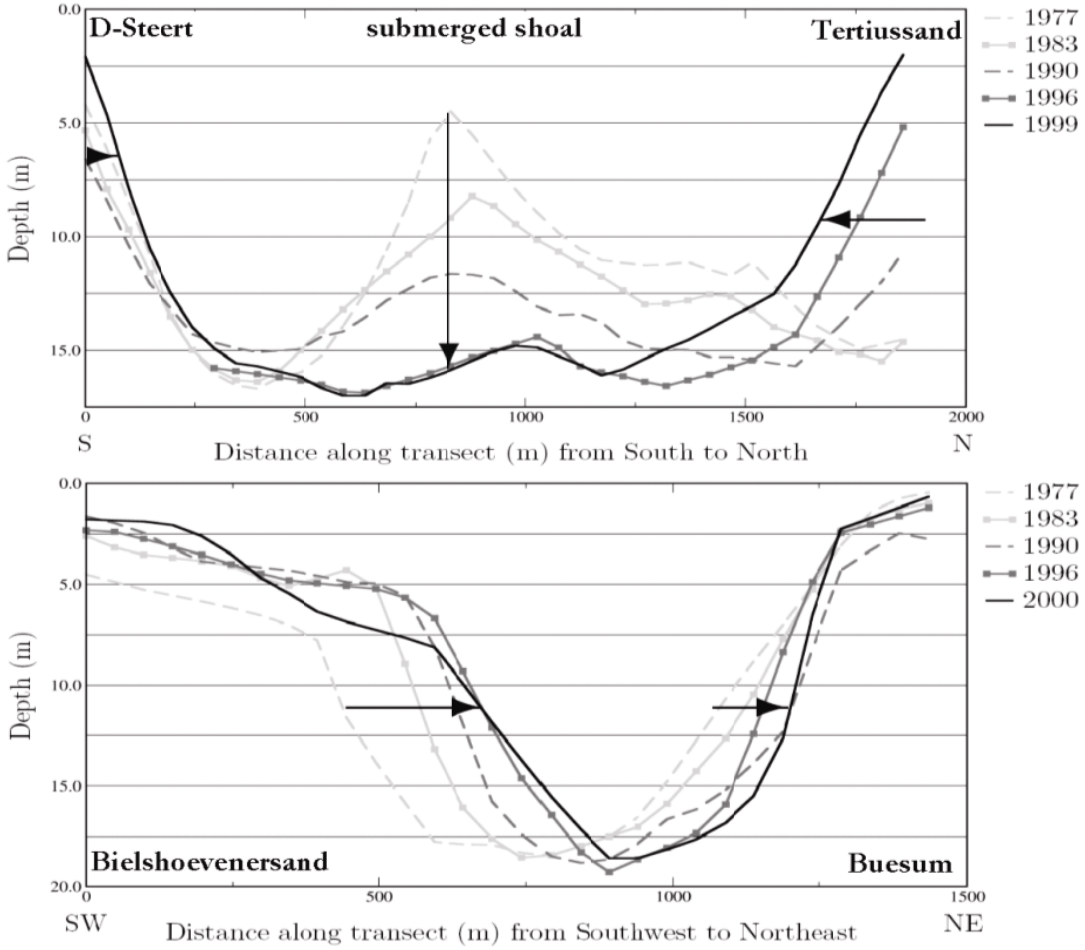

Figure 3.6 Long term morphological changes of two cross sections in Süderpiep and Piep channel

3.4 Meteorology and wave characteristic of the area

The average monthly temperature in the Dithmarschen Bight is reported 9.1°C with the minimum of –15.6°C and maximum of 31.6°C. The mean precipitation is approximately 708 mm/year (Müller, 1996). With regard to the wave and wind climate, the bight is classified as a storm wave environment with prevailing westerly winds (SW-W) significant wave heights up to 4m. The wave heights in the outer region attain 3 to 4 m, they however break along the edge of the tidal flats (margins) of the central Dithmarschen Bight (Palacio, et.al., 2005). Despite the absence of barrier islands, intertidal and supratidal sandbanks in the outer regions prevent the penetration of waves into the tidal flat area. Small wind-generated waves of up to about 0.5 m in height are observed in the study area (Mayerle and Zielke, 2005 and Toro, et. al, 2005). However, the wave height of up to 5m are also reported from meteorological records in Büsum, which was the resultant of severe storms likes those in 1967 and 1999.

The representative local wind data used in this investigation is based on a twelve-year data set derived from the synoptic PRISMA model (Luthardt, 1987). PRISMA data consist of observed wind fields, modulated and interpolated over a grid with a regular mesh spacing of 42 km and a time resolution of 3 hours. In addition to measured wind velocities, the observed surface pressure data are used to generate a synoptic scale wind field by means of the geostrophic wind equation. A detailed description of the generation of PRISMA datasets from measurements is given by Luthardt (1987). Figure 3.7 is the wind rose for the Dithmarschen Bight, showing the probability of occurrence of each combination of wind speed and direction. The graph is prepared by Wilkens (2004) using the PRISMA database of 1989 to 2000. According to this Figure, the mean wind speed is about 6.1 m/s and the most frequent directions range from 210° to 300°, which are in relatively good agreement with measurements carried out at the Büsum station (Wilkens, 2004).

The wave conditions in the area depend on the swell waves approaching from the open North Sea as well as on the locally generated wind waves. Most of the swell waves approach through the western part of the area. The distribution of the wave over the area depends strongly on the local bathymetry. The influence of local waves on currents is moderate over the tidal flats and negligible in the tidal channels. Storm surges may produce water level set-ups of up to 5 m, favouring the propagation of waves into shallow regions. Even under such conditions, however, wave effects are mostly confined to the outer sandbanks (Palacio, et.al., 2005).

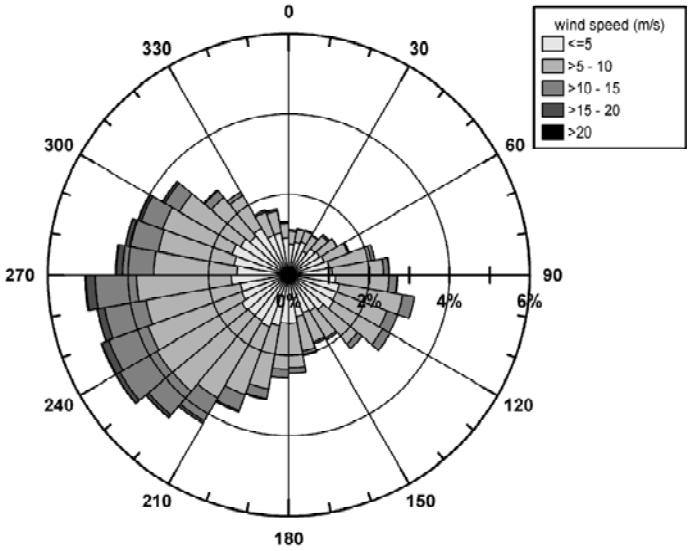

Figure 3.7 Wind rose for the study area, based on data extracted from the synoptic PRISMA meteorological model (Luthardt, 1987). Nautical convention for the direction; the radial axis shows the probability of occurrence per wind speed interval (Wilkens, 2004)

3.5 The Hydrodynamics of the area

The hydrodynamic characteristics of the area are known to be dominated by semidiurnal tides in the type of M2 constituent and a tidal period of approximately 12 hours and 24 minutes (Aspe, 2004). The area is characterized by a meso-tidal regime with a mean tidal range of about 3.1m in the southern and 3.4m in the northern part (Wilkens, 2004). The recorded neap and spring tidal range in the area is about 2.8m and 3.5m respectively (Wilkens, 2004).

In the tidal channels unlike tidal flats water always flows during a full tidal cycle. The maximum mean velocities are about 1.2 to 1.5m/s in the tidal channels and 0.3 to 0.7m/s on the tidal flats (Reimers, 1999). The temporal and spatial variations of the currents are strongly influenced by the complex bathymetry. Extreme velocities may reach up to 2 m/s in tidal channels and up to 1 m/s on the tidal flats (Wilkens, 2004). The maximum depth-averaged current velocity approximately doubles from neap to spring tide (Mayerle and Zielke, 2005).

According to Dronkers (1986) the specific topographical feature of the area leads to a longer slack water period before flood than before ebb, resulting in a shortened flood phase and a lengthened ebb phase. From an analysis of water level measurements in the Norderpiep and Suederpiep, he reported the existence of a slight asymmetry between the duration of flood and ebb phases. The average flood phase duration is 6 hours while the average ebb phase duration is 6 hours and 20 minutes. The time it takes from slack water to maximum ebb current is about 22% of the tidal period, whereas the time needed from slack water to maximum flood current is 27% of the tidal period. Dronkers (1986) asserted that such a situation could count as "ebb-dominated".

Over fifteen tidal gauges are settled in the German Bight (red dotes in Figure 3.8), three are located in the area under investigation. These gauges are *Blauort* in Norderpiep channel, *Tertius* in Süderpiep channel, and *Büsum* around the Piep channel. The collected water level

data from these three stations were used for the evaluation of the hydrodynamics of the model. Their locations are shown in Figure 3.8, and the corresponding water level variations in Figure 3.9. Referring to this Figure a time lag of about 20 minutes exists between the Tertius and Büsum stations.

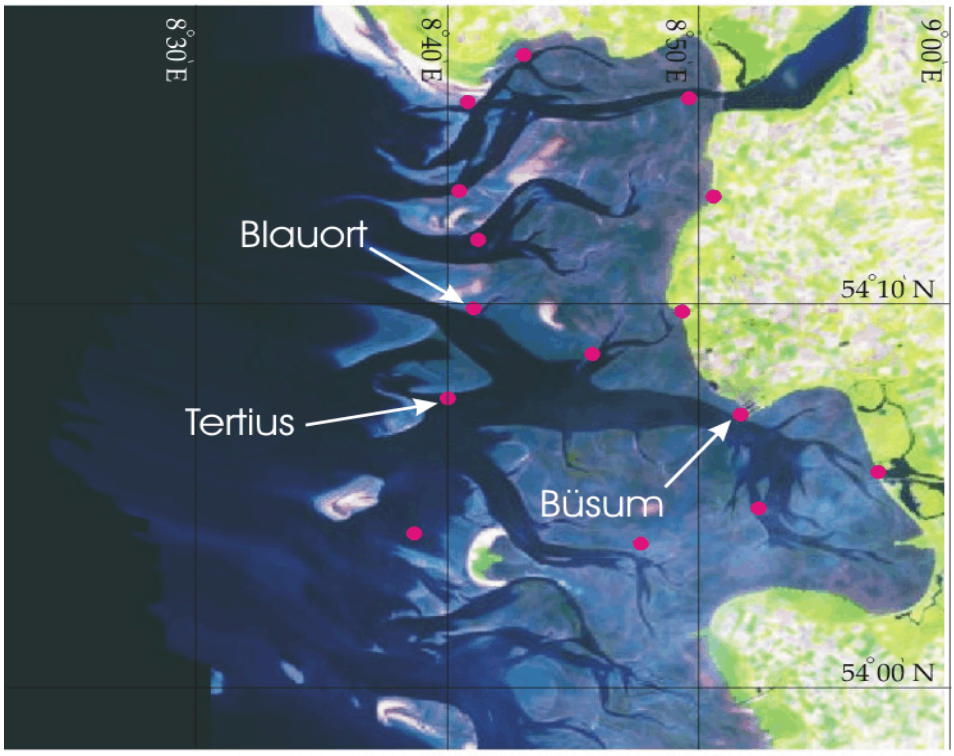

Figure 3.8 Locations of water level gauges

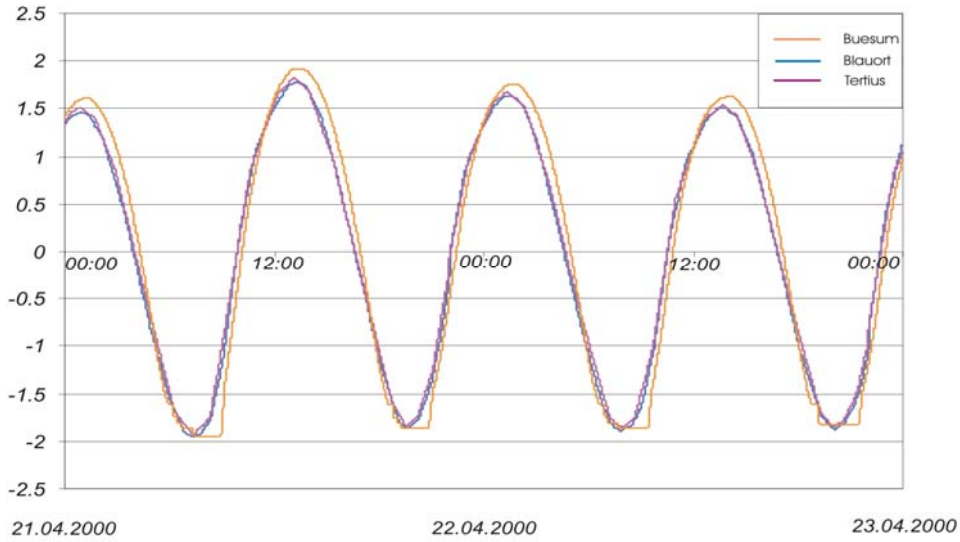

Figure 3.9 Water level time series in Blauort, Tertius and Büsum stations

3.6 Water Temperature, Density, and Salinity

The water temperature in the area varies between values close to 0°C and up to 18°C, depending on the season (Wilkens, 2004). On the basis of the field investigations Mayerle and Zielke, (2005) and Toro et.al., (2005) reported that the variation in temperature and salinity is fairly uniform over the water column. Toro et.al. (2005) reported that the spatial variations of water temperature in the area are insignificant and the seasonal variation is from about 6-7 °C in March to about 16-17 °C in September. According to Poerbandono (2003) the salinity varies from 20 to 29ppt in winter and from 25 to 33ppt in summer and no significant salinity gradients over the vertical and across the channels can be observed. Figures 3.10 and 3.11 shows the variation of temperature and salinity along the relative depth over complete tidal periods at cross-sections T2 and T3. These cover the periods 21-23 March 2000 (tidal ranges between 3.9 and 4.1 m), 5-6 June 2000 (tidal range of about 3.7m), 5-6 September 2000 (tidal ranges between 2.9 and 3.1m) and 5-6 December 2000 (tidal ranges between 2.3 and 2.5m). As a result of the uniform profiles of salinity and temperature, the flow in this area is considered to be quite homogeneous.

The density of water in the Wadden Sea vary usually between 1024 kg/m^3 in the Wadden Sea area and 1000 kg/m^3 in the sandy soil and peat districts. According to Burchard et al. (2008) the water in the inner regions of the Wadden Sea is typically about 0.5–1.0 kg/m^3 less dense than the North Sea water. During the winter this occurs mostly because of freshwater runoff from the Elbe and Eider River and net precipitation; and during the summer it occurs mostly due to differential heating caused by the surface warming. Burchard et al (2007) argued that the interaction of even such a small horizontal density gradients with tidal currents may generate net onshore fluxes of suspended particle matter in the area.

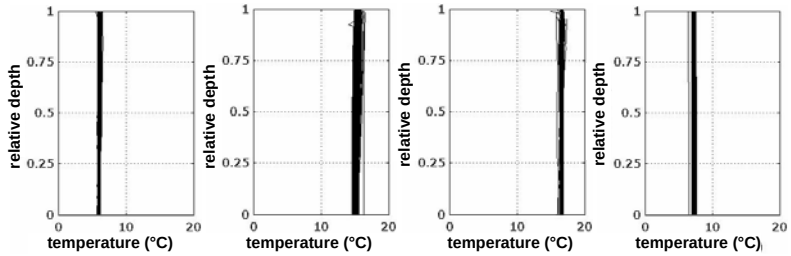

March 21, 2000 June 5, 2000 September 5, 2000 December 5, 2000

a) Cross-section T2

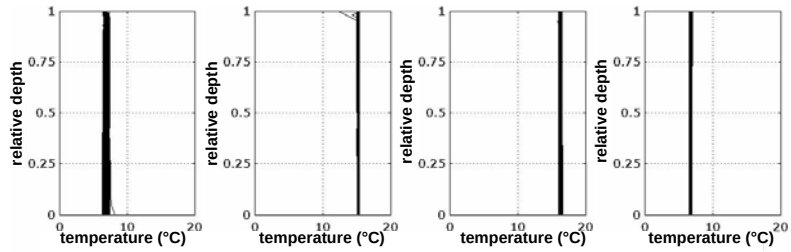

March 23, 2000 June 6, 2000 September 6, 2000 December 6, 2000

b) Cross-section T3

Figure 3.10 Seasonal variation of vertical temperature profiles in cross-sections T2 and T3 (Toro, et.al. 2005)

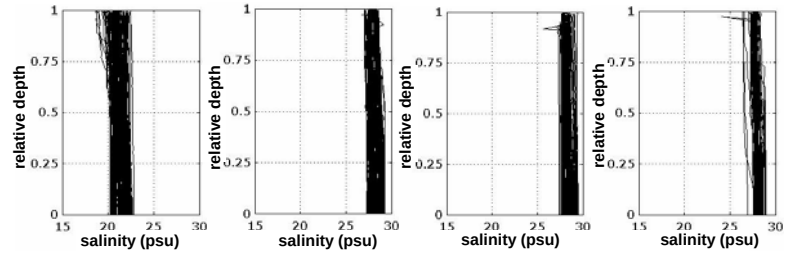

March 21, 2000 June 5, 2000 September 5, 2000 December 5, 2000

a) Cross-section T2

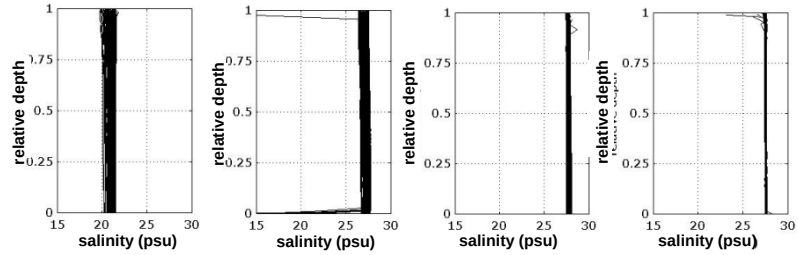

March 23, 2000 June 6, 2000 September 6, 2000 December 6, 2000

b) Cross-section T3

Figure 3.11 Seasonal variation of vertical salinity profiles in cross-sections T2 and T3 (Toro, et.al. 2005)

3.7 Sediment Distribution and Sediment Dynamics of the Area

The surface of the tidal flats is mostly composed of sandy sediments with median particle diameter of more than 63 μm. Down to a depth of 30 cm the deposits in most cases are not macroscopically layered. Ricklefs, K., & Asp Neto, (2005) studied the distribution of the sediment particles specifically on the tidal flat areas. Figure 3.12 show the distribution of the grain size in the tidal flat area according to their findings. From the Figure they concluded that the median grain sizes of the particles increase from the wave dominated western regions to the sheltered eastern areas.

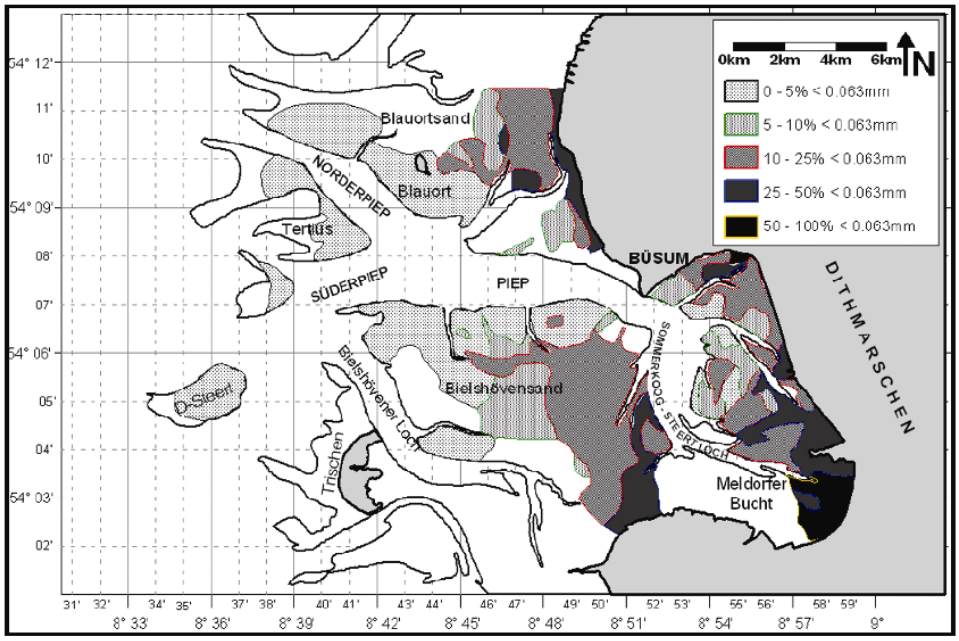

Figure 3.12 Map of grain size characteristics in the tidal flat area (Ricklefs, K., & Asp Neto, 2005)

According to Figge (1980) more than half of the sand fraction in the bight has a diameter between 63 to 250 μm and about 40% between 250 to 500 μm. He characterized the main part of the tidal flat as muddy tidal flat with the mud contents more than 50%. Reimers (2003) reported a trend of grain size reduction in the tidal flats from outer areas towards the coast, which can also be seen in Figure 3.12. This particular characteristic of the tidal flat can cause deceleration in the hydrodynamic energy towards the shore.

Vela Diez (2001) studied the distribution of the median grain size specifically in the tidal channel system. On the basis of his findings the distribution of the bed sediments along the channels is represented in Figure 3.13. The spatial distribution of the median grain size of the bed sediment in the tidal channels varies from consolidate mud and sand to fine sand. Even though the characteristic of bed sediment is a mixture of different grain sizes from silt to sand, the material transported in suspension in the area is essentially silt with the grain sizes up to 5 times smaller than those of mobile sediments on the bottom. Mayerle et al. (2002) reported that the sediment size transported in suspension reduced drastically to the values of 6 to 86 μm.

The transport of sandy material in the area is restricted to the near-bed layers. Schrottke and Abegg (2005) reported the existence of suspended sand in the area due to turbulent mixing processes. They mentioned that the total amount of suspended sand depends on the hydrodynamical energy, and the particle size, type, and shape. They also emphasized that suspended sand transport even close to the seabed under tidal flows is very low and insignificant. Poerbandono (2003) reported fairly uniform distributions of suspended sediment concentration and transport over the depth. He reasoned that this is due to the small grain sizes of sediment in suspension and the strong levels of turbulence maintained by the tidal currents. High turbulence sustained by tidal currents in combination with the small settling velocities of the fine material prevent sediment deposition during slack water. According to Poerbandono (2003), Background concentration of suspended material ranging from 0.04 to 0.14kg/m^3 are reported in the area. As a result, large amounts of fine material are always in motion, thus restricting the entrainment of seabed sediments to short periods of high current velocities during the ebb and flood phases.

On the basis of model results, Poerbandono and Mayerle (2005) claimed that the contribution of the bed load to the total amount of transported material is far less significant. They reasoned that this finding confirms the importance of suspended sediment concentration as the primary mode of material transport in the investigation area. The average contribution of bed load transport to the total load transport amounts to only about 2%. In the main tidal channels it is found that the suspended sediment transport contribution is equal to or greater than 99%, compared to about 96 to 98% on the tidal flats.

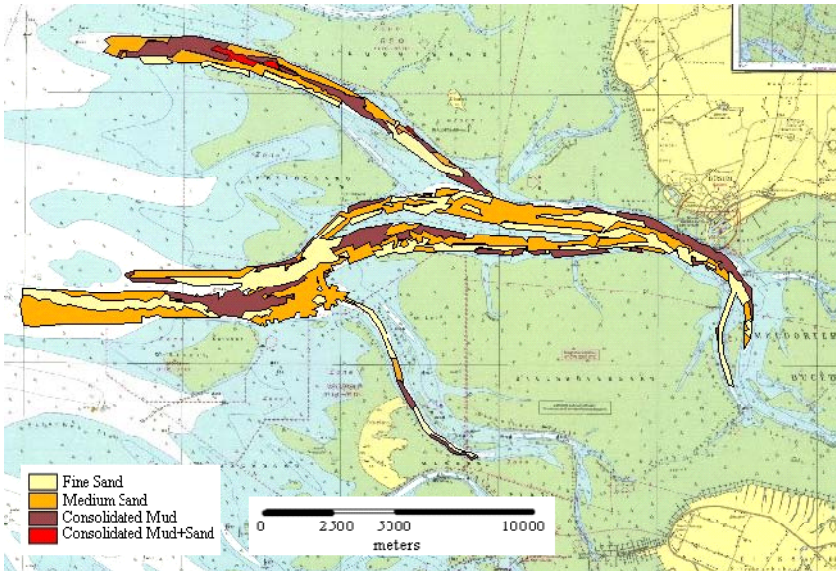

Figure 3.13 Distribution of sediment types, after Vela Diez (2001)

Poerbandono and Mayerle (2005) studied the flow and the sediment dynamics of the area, focusing mainly at the processes at cross sections T1, T2, and T3 (shown in Figure 3.1). As the field data and their model results have been used in this study, it seems relevant to present a summary of their observation and concluding remarks here.

Depth-averaged suspended sediment concentrations at cross-sections T1, T2 and T3 varied from 0.04 to 0.10, 0.06 to 0.14 and 0.06 to 0.14kg/m^3, respectively. The range of approximate ebb to flood ratios of tidally-integrated transport at cross- sections T1, T2 and T2 are 0.61 to 0.95, 0.82 to 1.09 and 0.79 to 1.30, respectively. A tendency towards flood domination is reported for cross-section T1, and T2. At all of the cross-sections a balance between the total amount of suspended material transported onshore and offshore during the consecutive flood and ebb phases exist. Up to 105,000 metric tons of suspended material are transported through the two cross sections T2 and T3 during one tidal cycle. Of this amount, more than 80% is transported through cross-section T2. The southern banks of cross-sections T3 and T2, where potentially mobile sediment is available, are subjected to an intensive erosion and sediment transportation specifically during maximum ebb and flood currents. Therefore, intensive morphological activity is observed at these cross sections. The flow discharges and sediment transport rates at cross-section T2 are 5 and 2.5 times higher than those at cross-sections T1 and T3 respectively.

3.8 Measurements and devices

The field data employed in this investigation can be divided into two types: 1) input data for setting up and running the model, and, 2) the data used for analysing the model results, and for model calibration and validation. The model input data in this study included bathymetry, sediment grain size distribution, bed roughness, variations of water level, astronomical tides, and the wind data. The data required for the analysis of the model results, calibration and validation consisted of the current velocity and the suspended sediment concentration. The input data required for setting up the model are explained to some extent further in the context of the Delft3D model set up in Chapter 4. Measuring techniques and devices used to record the current velocity and the suspended sediment concentration are briefly discussed in the following sub sections.

The data used in this study were those collected during the PROMORPH project (see Section 1-6). They were collected using equipped cruising vessels under calm weather conditions. That is, because the rough conditions, with high waves, storm and strong currents might result in failing devices or inaccuracies in the measurements. The cruises were carried out across several cross sections including T1, T2, and T3 (see Figure 3.1) during a full tidal cycle. In each measuring campaign the data were collected for the whole depth at several specified stations across the cross sections.

3.8.1 Current velocity

Acoustic Doppler Current Profiler (ADCP) had been used to measure current velocities. The working principle of this instrument is based on the transmission of sound pulses of known frequency from its transducers into the water column. Application of ADCP for measuring current velocity is restrained by several limitations and sources of error. The limitations arise mainly from the design and technology used for the device and the nature of acoustic wave propagation in the water. Errors may appear from the uncertainty of the calculation due to presence of noise from transmitted echo and pulse, frequency of sound wave and beam angle and inappropriate handling of the device. Statistical treatment to the data may reduce the uncertainty due to random error, whereas, measuring procedures, e.g. measurement under calm weather condition, accurate estimate of transducer depth, etc, make it possible to handle bias errors which may occur from the application of ADCP measurements in field

condition (Simpson, 2001). Van Rijn (2002) reported an accuracy of ± 5 cm/s for 30 seconds averaging in ship-mounted ADCP.

The two ADCP devices used in the PROORPH project were the 1200 KHz Broadband Direct Reading (manufactured by RD Instruments). Their accuracy for point measurements under laboratory conditions is given as ±0.25% of the measured value ±0.0025m/s by the manufacturer. The instruments were mounted at the bow of the vessels pointing downward. Measurements covered the water column from about 1.6m below the free surface, due to transducer draught and blanking distance, down to the seabed. The bin sizes during the measurements were set to 0.5m (Jiménez-González, et.al., 2005). The vertical measurements covered the water column from a level about 0.5m above the seabed. The vessel moved forward and backward along the transect during a full tidal cycle collecting ADCP data along the route. Vertical profiles of the current velocity thus were collected for the whole period of the tidal cycle. Figure 3.14 shows the procedure schematically.

According to Jimenez-Gonzalez et. al, (2005) the accuracy of the ADCPs for measurements in the tidal channels of the central Dithmarschen Bight on the basis of the standard deviations for point measurements are approximately constant. They evaluated the accuracy of the device with values of about 0.06 m/s and 0.14 m/s for distances above and below 1m from the seabed, respectively. They also mentioned that the accuracy of the devices for measuring depth-averaged velocities was about 0.015 m/s.

3.8.2 Suspended sediment concentration (SSC)

Obtaining measurements of suspended sediment concentration (SSC) is a key element in morphodynamic experiments in the coastal zone. There are a large number of instruments available and a variety of approaches have been taken, but much work remains to be done to obtain reliable measurements over a reasonable spatial and temporal scale (White, 1998). The SSC measurement techniques can be categorized as direct and indirect measuring device. Direct measurement techniques include various traps and acoustic doppler instruments that measure SSC and velocity simultaneously through some portion of the water column. Indirect techniques for measuring SSC include optical and conductivity devices. To obtain SSC during the cruises of PROMORPH project Niskin bottle as trap sampler, and transmissometer as optical device were employed. Later on the echo intensity (EI) data derived from the ADCP device was also used to estimate the SSC of the area. As the SSC derived from these devices were the main source of model evaluation in this study, their accuracies play an important role in model assessment. Toro (2003) mentioned that measurements with which numerical outputs are compared are associated with some uncertainties. Thus he concluded that there is no justification to calibrate the device for differences smaller than measurements accuracy. According to him, one should be aware of the uncertainty in the results and also of the source of error to look for a way to improve the accuracy, if required. In the following a brief explanation about the devices used and their accuracy are presented.

3.8.2.1 Niskin bottle

A number of devices have been used in attempts to trap sediment suspended in the water column of the net transport in coastal zone, but the oscillatory motion associated with wave action makes this task much more difficult than, for example, under unidirectional flow in a river. Pump samplers have been used with varying degrees of success and various bottles for capturing the suspended sediment load including Niskin bottle. These all require

considerable effort and the logistical difficulties coupled with doubts as to the accuracy of the sampling process have limited their further use (Schwartz, 2005).

Niskin bottle is a mechanical sampler, used to collect water samples. It has stoppers on both ends, which at desired depth are released capturing a sample of the water from that depth. The principle of this method is simply based on collecting specific amount of water-suspended sediment over a certain period. In overall 233 water samples were collected at three cross-sections in the main tidal channels. They were taken at 1m above the seabed using a Niskin bottle sampler in water depths ranging from 5m to 26m. Depth-averaged current velocities of up to 1.6m/s and point sediment concentrations ranging from 0.04kg/m^3 to 1.1kg/m^3 were measured at the sampling stations (Poebandono and Mayerle, 2005). The SSC values derived from the Niskin bottle have been used for calibrating transmissometer (see Section 3-8-2-2).

3.8.2.2 Transmissometer

Optical devices emit light and give a measure of the SSC in the water column at a point either through the degree of attenuation of the light beam or through the amount of light reflected from particles in suspension. They therefore do not provide a direct measure of SSC and thus must be collocated with another device for the sake of calibration. The light transmitted is generally in a narrow wave band in the infrared range in order to minimize the effects of natural light in the water.

Transmissometer measures the degree of attenuation of the light over a fixed distance separating the emitter from the receiver. They are best suited for work some distance seaward in depths greater than 10 m where SSC are relatively low (Schwartz, 2005). Bunt et.al. (1999) carried out an intensive investigation on the accuracy of optical devices. They emphasized the significance of calibration for deriving reliable SSC. They however mentioned that there is insufficient information on the effect of a series of grain-related factors upon transmissometer device. According to their results, following parameters could affect transmissometer response: grain size changes (by over hundred times), shape and surface roughness (by about ten times), particle flocculation (by about two times), existence of plankton (by about four times), and air bubbles (by about two times). They pointed out that these factors vary in importance depending upon the environmental setting, so that it is important to have a broad understanding of the hydrodynamic, sedimentary and biological regimes at a study site. One of the advantages of the transmissometer is that it can provide a continuous, time-resolved SSC monitoring system and enables the study of distribution of SSC in detail.

An optical beam transmissometer device, which employs visible light with a wavelength of 660±12nm and a 2cm travel distance, has been employed during the cruises of PROMORPH project to collect SSC. The vertical resolution of the device was set to 0.2m. For collecting the SSC at different levels along the depth, the transmissometer together with one CTD (Conductivity, Temperature, and Depth) device and one Niskin bottle sampler were mounted on a frame. In each cruise the frame was lowered at specified positions from the surface to near the bottom across each cross section (see Figure 3.14). The CTD device in the frame provided the height at which the beam scatter data are collected.

According to Poerbandno and Mayerle (2005), to convert the optical transmission data to SSC, those SSC determined from about 200 Niskin bottle samples according to the method described by Ohm (1985) and Ricklefs (1989) were employed. The proposed equation for this conversion, through statistical analyses is:

$$c = (7A + 33)10^{-3} \qquad (3\text{-}1)$$

Where, c is concentration of sediment, and $A = -L^{-1}\ln(I)$ is the attenuation coefficient, in which L is the transmissometer path length in cm, and I is the optical transmission as a decimal fraction.

Using RMAE method, Poerbandono (2003) reported that the accuracy of optical measurements was about 30% on the basis of agreement with concentrations determined from physical samples. This low accuracy has been claimed to be due to an insufficient sensitivity of the optical beam transmissometer with a path length of only 2 cm for detecting low concentrations (Poerbandono and Mayerle, 2005).

The suspended sediment concentration data used in this study for the model analysis are mainly those converted from the transmissometer device on the basis of equation 3-1, unless the use of other data source is mentioned.

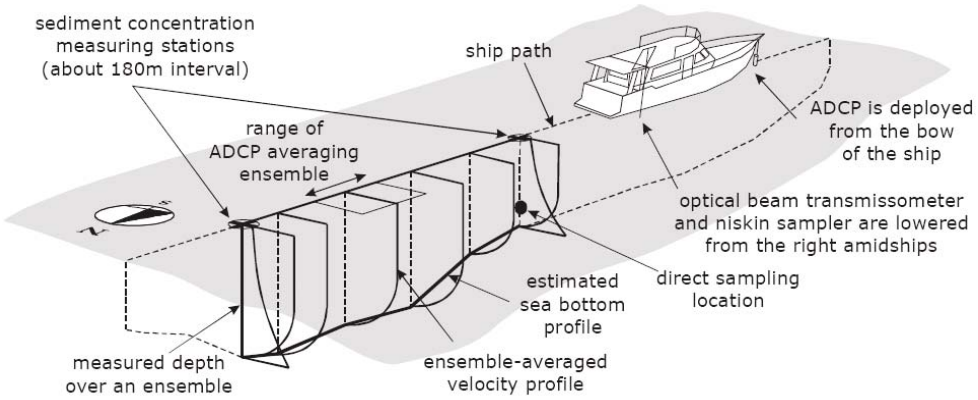

Figure 3.14 Measuring technique along a cross section

3.8.2.3 ADCP

ADCP devices provide echo strength data from the water layers being measured which are referred as echo intensity (EI). Poerbandono and Mayerle (2005) on the basis of the methods proposed by Deines (1999) and SonTek (2002) investigated the possibility of converting the EI data to the SSC. They proposed to convert the proportionality of the echo intensity increment between two depths in the water column, into the concentration of suspended sediment. They used EI records and corresponding transmissometer data to derive a conversion equation on the basis of the empirical equation proposed by Gartner (2001), which is a linear relationship between logarithm of concentration and echo intensity (equation 3-2):

$$10\log_{10}(c) = a_i.EI + b_i \qquad (3\text{-}2)$$

where a_i and b_i are constants, c is suspended sediment concentration, and EI is an echo intensity value. Using the data from the area under investigation and a regression analysis as calibration procedure, equation 3-3 was obtained:

$$c = 10^{(0.038EI - 4.357)} \qquad (3\text{-}3)$$

The concentrations derived by applying this equation were in good agreement with those obtained from the transmissometer with the average relative error of about 31%. They also reported that the values of the suspended sediment concentration derived from the ADCP were generally lower than those from the transmissometer device.

Poerbandono and Mayerle (2005) concluded that the concentration from converted acoustic *EI* are within a good agreement with respect to those obtained from the optical beam transmissometer. About 93% of data pairs are within a factor of 2. Accordingly, the average relative error is about 31% and the average absolute error is 0.03 kg/m^3. A tendency of underestimation and increasing of discrepancy with the increase of depth-integrated concentration magnitude are identified. However, the approach is independent to the location of measurements, current velocity and water depth. These results encourage the use of acoustical profiling for monitoring fine suspended sediment transport.

Here it should be pointed out that the suspended sediment concentrations (SSC) derived from the equation 3-3 are of the third level accuracy. That is, the back scatter data derived from the transmissometer device were converted to the SSC using the SSC samples from the Niskin bottle. These converted SSC data then, used for the calibration of equation 3-3, to convert echo intensity data to the SSC. Taking into account that the number of the collected samples with Niskin bottles were limited to 233 samples, the accuracy of equations 3-1 and 3-3 are associated with uncertainties including the error device and error in accumulation and conversions.

3.9 Measured data at Cross Sections

The measuring campaigns used in this study was part of the PROMORPH project (2000-2002) and consisted of seven surveys over cross section T1, eight surveys over cross section T2, and nine surveys over cross section T3. The date of the surveys, corresponding tidal range, period of measuring cruises, and the number of stations where the measurements were carried out are summarized in Table 3.1. As previously mentioned these cruises were carried out with two instrumented ships. During each cruise the ship was sailing bidirectionally across the cross section to collect the data. The ADCP was always submerged during the cruise, while the transmissometer attached to the CTD was lowered in the specific positions in each cross section. These stations were separated from one another by a distance of about 180m, hence the number of measuring stations in the cross-sections and for the different campaigns in each transect was not the same. The number of measuring stations in cross sections T1, T2 and T3 were 4, 9 to 12 and 6 to 7 respectively. The locations of these stations, for the measuring campaign in March 2000, were shown previously in the Figure 3-1.

These measured data were employed in this study for calibrating, validating and also analysing the model results. From the measuring campaigns those which covered a whole tidal cycle were employed for calibrating the model. These include five fallowing tidal periods: 21 to 23 March 2000, 05 to 06 June 2000, 05 to 06 September 2000, 12 to 13 September 2000, and 05 to 06 December 2000. For these periods measurement are available for all three cross sections. For validating purposes also five tidal period were considered including: 14 to 16 March 2000, 13 to 14 June 2000, 12 December 2000, 22 June 2001, and 28 June 2001.

Table 3.1 Number of ADCP transects, transmissometer profiles and water samples are collected during Measurement surveys at cross sections T1, T2, and T3 under the PROMORPH project

Channel	Date of Measurement	Tidal Range (m)	Nr. Of Stations	Measuring duration	Nr. Of ADCP transect	Nr. Of Trans. profiles	Nr. Of water samples
Norderpiep Channel (T1)	March 16th 2000	3.2	4	From: 8:06 To: 20:14	64	123	7
	March 22nd 2000	4.0	4	From: 8:04 To: 20:02	65	126	5
	June 5th 2000	3.8	4	From: 9:23 To: 20:59	61	32	14
	September 5th 2000	3.1	4	From: 4:13 To: 16:57	59	105	28
	September 12th 2000	3.2	4	From: 4:59 To: 17:09	67	131	8
	December 5th 2000	2.3	4	From: 5:57 To: 18:08	73	44	11
	December 12th 2000	3.8	4	From: 7:21 To: 11:05	15	27	6
Süderpiep Channel (T2)	May 19th 1999	3.6	-	From: 7:21:14 To: 10:30:16	9	16	0
	March 21st 2000	4.1	9	From: 6:52 To: 19:45	30	132	9
	June 5th 2000	3.8	12	From: 9:31 To: 21:10	33	116	9
	June 13th 2000	-	-	From: 9:19 To: 10:54	6	15	1
	September 5th 2000	3.1	12	From: 3:52 To: 10:23	21	84	9
	September 12th 2000	3.2	11	From: 4:57 To: 16:57	22	102	21
	December 5th 2000	2.3	10	From: 5:45 To: 17:56	23	86	8
	December 12th 2000	-	-	From: 6:31 To: 11:21	9	28	3
Piep Channel (T3)	March 14th 2000	-	-	From: 6:54 To: 16:31	29	125	8
	March 23rd 2000	4.2	7	From: 7:33 To: 21:14	50	163	7
	June 6th 2000	3.7	7	From: 7:36 To: 16:24	37	90	15
	June 14th 2000	-	-	From: 3:28 To: 15:57	38	129	26
	September 6th 2000	2.5	7	From: 4:32 To: 15:50	27	91	24
	September 13th 2000	3.4	7	From: 5:32 To: 10:38	17	55	5
	December 6th 2000	2.4	6	From: 6:40 To: 19:11	44	130	8
	June 22nd 2001	-	7	From: 6:07 To: 12:35	18	76	9
	June 28th 2001	-	7	From: 5:43 To: 17:52	40	90	9

Chapter 4. Delft3D Package relevant to present application

4.1 Introduction to Delft3D package

Delft3D Package developed by WL Delft Hydraulics simulates unsteady two- and three-dimensional flows, sediment transport and, morphological changes in rivers and coastal areas. It is composed of several modules that can be executed independently or in combination with other modules. A so-called communication file provides the information exchange between the modules automatically. The modules used in this research are: Delft3D-FLOW in combination with the online sediment version of the package, and Delft3D-WAVE. The content of this study is consistent with the version 3.27.01 of the Delft3D-FLOW and -WAVE software (WL | Delft Hydraulics).

Objectives of this chapter are:

1. an overview of hydrodynamic and transport equations employed in Delft3D package,
2. an overview of the parameters and variables used for the setting up of the models, and
3. a brief review of the 2DH model set up by previous researchers such as Palacio (2002), Mayerle and Palacio (2002), Mayerle et. al. (2005), Poerbandono and Mayerle (2005), and Escobar (2007).

It should be noted that the information presented in the section 4-2 to 4-4 of this chapter is mostly extracted from the Delft3D manual.

4.2 Delft3D-FLOW

Delft3D-FLOW is a multi-dimensional (2D or 3D) simulation program which computes non-steady flow and transport phenomena that result from tidal and meteorological forcing on a rectilinear or a curvilinear, boundary fitted grid. The flow field is solved on a rectangular grid in 3D simulations; the vertical grid is defined following the sigma co-ordinate approach

(see Section 4-3-2). The hydrodynamic conditions such as current velocity, water elevations, density, salinity, and eddy viscosity and diffusivity computed in this module could be used as inputs for other modules.

Delft3D-flow is structured to perform hydrodynamic computations and simultaneous computation of salinity, transport, and heat transfer. Sediment transport and morphological changes within the Delft3D-FLOW module can also be computed simultaneously, which is called as online in the Delft3D manual. This part of the package simulates morphological changes due to the bed-flow interactivity. It includes transportation, erosion and deposition for both, cohesive and non-cohesive sediment for up to five fractions of sediment. Simultaneous computation of hydrodynamic and sediment transport has following features:

1. three-dimensional hydrodynamic processes and the adaptation of nonequilibrium sediment concentration profiles are automatically accounted for in the suspended sediment calculations,
2. the density effects of sediment in suspension (which may cause density currents and/or turbulence damping) are automatically included in the hydrodynamic calculations, and
3. sediment transport and morphological simulations are simple to perform and do not require a large data file to communicate results between the hydrodynamic, sediment transport, and bed updating modules.

Computation of morphological changes resulting from the transport, erosion, and deposition of sediment is possible using the online sediment module of Delft3D, which makes the sediment version of Delft3D-FLOW especially useful for investigating sedimentation and erosion problems in complex hydrodynamic situations.

The accuracy of the computed results for flow characteristics and sediment dynamics is strongly dependent on the chosen physical and numerical parameters in the model set up. Physical parameters are those parameters related to the nature of the area and can be measured directly in the field or calculated indirectly concerning other field parameters; they include bottom roughness, settling velocity, bed shear stresses and other flow, sediment and morphological characteristics of the area. Numerical parameters are those parameters which are employed as a matter of modelling, including grid resolution, time step, smoothing time, and marginal depth.

4.3 Model structure

The system of equations in Delft3d contains momentum equations, the continuity equation, the transport equation, and turbulence closure model. The user may choose to solve the hydrodynamic equations on a Cartesian rectangular, orthogonal curvilinear (boundary fitted) or spherical grid. The boundaries of coastal waters are in general curved and are not smoothly represented on a rectangular grid. Therefore the use of rectangular grids causes irregularity at boundaries which may introduce significant discretization errors. To reduce these errors boundary fitted orthogonal curvilinear co-ordinates are used. In the following sections a brief review of these equations are presented.

4.3.1 Model Grids

In Delft3D finite difference method is used for solution of the partial difference equations. To discretize the 3D shallow water equations in space, the model area is covered by rectangular, curvilinear, or spherical grids. It is assumed that the grid is orthogonal and well structured. The variables are arranged in a pattern called the Arakawa C-grid (a staggered grid). In this arrangement, the water levels (pressure points) are defined at the centre of a cell; the velocity components are perpendicular to the grid cell faces where they are situated (see Figure 4.1).

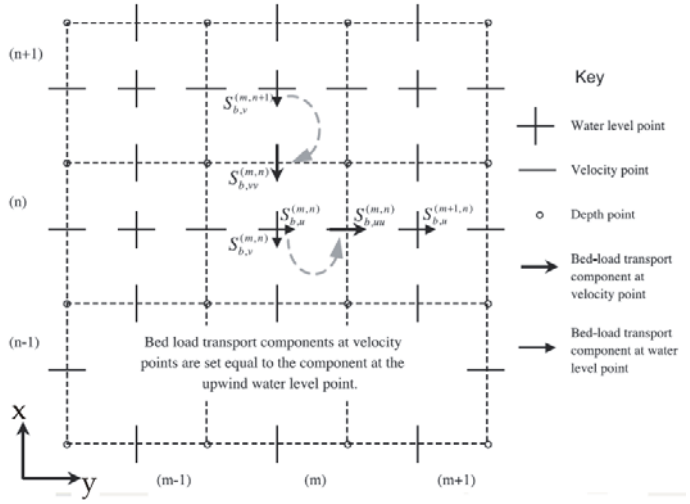

Figure 4.1 Setting of bed-load transport components at velocity points (DELFT3D-FLOW, user manual)

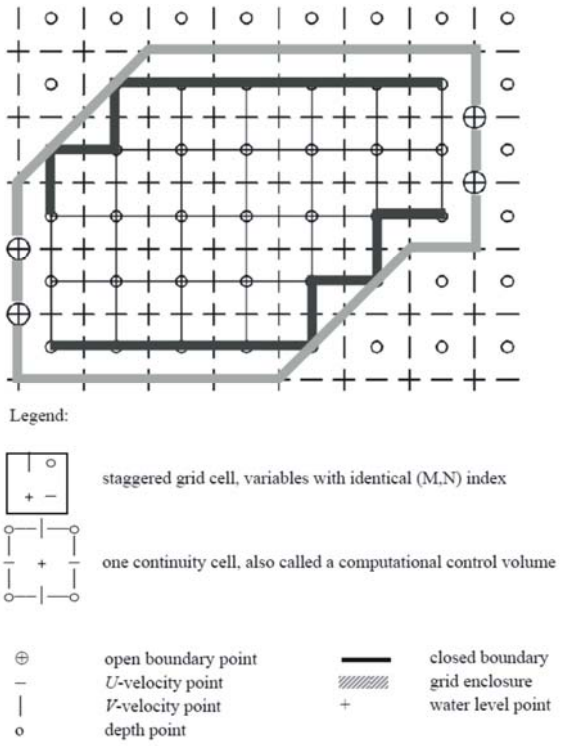

Figure 4.2 An Example of Delft3d-Flow Model Area (DELFT3D-FLOW, user manual)

To compute water level and velocity in each grid point, a so-called computational grid enclosure is applied. This grid enclosure consists of one or more closed polygons which specify the boundary of the model area. The boundaries could be defined as close, along water-land line, or open, across the flow field (Figure 4.2).

4.3.2 Vertical Coordinate System

The vertical non-dimensional σ-coordinate system was first introduced by Phillips (1957) for atmospheric models. The flow field is considered as consisting of a number of layers in the vertical direction. Each layer is bounded by two sigma planes, which are not strictly horizontal but follow the bottom topography and the free surface. It is scaled between 0 and –1 in which the zero value relates to the surface and minus one to the bed. In this system, the layer interfaces are chosen following planes of constant σ. Thus, the number of layers over the entire flow field is constant, irrespective of the local water depth; in another words the thicknesses of layers vary with the depth. Therefore the distribution of the relative layer thickness is usually non-uniform (Figure 4.3). This allows for more resolution in the zones of interest such as the near surface area (for instance wind-driven flows) and the near bed area (for like sediment transport).The governing equation reads as:

$$\sigma = \frac{z - \xi}{h} \qquad (4\text{-}1)$$

where z is the vertical co-ordinate, ξ is the free surface elevation above the reference plane (at z =0), and h is the total water depth (Figure 4.3).

Computationally, each layer is a flow channel above a horizontal grid at reference level with open and closed (land) boundaries bounded with σ-interface planes above and below the cell. For each layer the system of equations is solved.

Osinski (2007) stated that the amount of suspended sediment concentration predicted by the model depends directly on the distance of the closest grid point from the bed. According to Lesser et. al. (2000) the computed suspended sediment concentration profile is virtually independent of the number of layers used. They however, mentioned that the choice of layer spacing could have a significant effect on the accuracy of the predicted concentration. A logarithmic distribution of layer thickness is necessary to achieve accurate current velocity and sediment concentration (see Section 2-2-3). In a simulation with few layers, the thickness of the bottom layer should be chosen carefully to avoid some of the layers being neglected from the suspended sediment transport calculations.

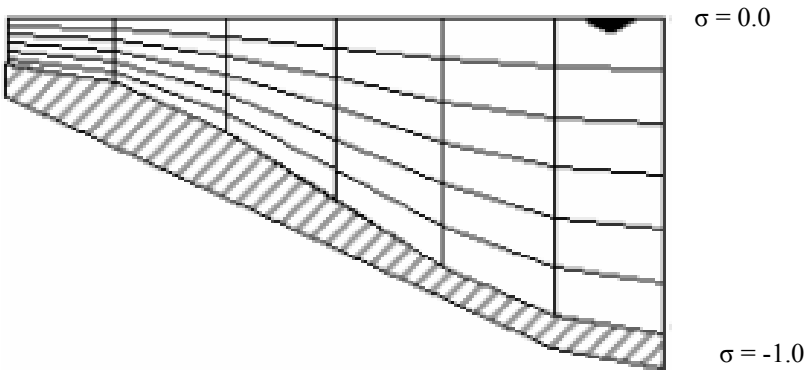

Figure 4.3 Typical Vertical Grid Consisting Of Six Equal Thickness σ-Layers (DELFT3D-FLOW, user manual)

4.3.3 Hydrodynamic equations

The hydrodynamic module calculates non-steady flow and transport phenomena resulting from tidal and meteorological forcing on a curvilinear, boundary-fitted grid. It is based on the full Navier-Stokes equations with the shallow water approximation applied.

4.3.3.1 Continuity Equation

The continuity equation in Delft3D is calculated as depth-averaged disregard to the dimensions (in both 2D and 3D versions). It is given by:

$$\frac{\partial \zeta}{\partial t} + \frac{1}{\sqrt{G_{\xi\xi}}\sqrt{G_{\eta\eta}}} \frac{\partial \left[(d+\zeta) U \sqrt{G_{\eta\eta}} \right]}{\partial \xi} + \frac{1}{\sqrt{G_{\xi\xi}}\sqrt{G_{\eta\eta}}} \frac{\partial \left[(d+\zeta) V \sqrt{G_{\xi\xi}} \right]}{\partial \eta} = Q \qquad (4\text{-}2)$$

where t is time, ζ is free surface elevation above the reference, ζ and η are horizontal curvilinear coordinates, G is a coefficient used to transform curvilinear to rectangular coordinates, U is flow velocity in ζ direction, V is flow velocity in η direction, and Q is discharge source or sink per unit area.

4.3.3.2 Momentum Equation

In the approach of Delft3D the vertical momentum equation is reduced to the hydrostatic pressure relation using the assumption of the shallow water. Vertical accelerations are assumed to be small compared to the gravitational acceleration and are not taken into account. Horizontal momentum equations therefore for both 2DH and 3D simulations are the same. In 3D models however, the vertical velocities are computed from the continuity equation (see section 4-3-2-4). Momentum equations in Delft3D read as:

$$\frac{\partial U}{\partial t}+U\frac{\partial U}{\partial x}+V\frac{\partial U}{\partial y}+\frac{\omega}{h}\frac{\partial U}{\partial \sigma}-fV=-\frac{1}{\rho_0}P_x+F_x+M_x+\frac{1}{h^2}\frac{\partial}{\partial \sigma}\left(v_V\frac{\partial U}{\partial \sigma}\right)$$
$$\frac{\partial V}{\partial t}+U\frac{\partial V}{\partial x}+V\frac{\partial V}{\partial y}+\frac{\omega}{h}\frac{\partial V}{\partial \sigma}-fU=-\frac{1}{\rho_0}P_y+F_y+M_y+\frac{1}{h^2}\frac{\partial}{\partial \sigma}\left(v_V\frac{\partial V}{\partial \sigma}\right) \quad (4\text{-}3)$$

where ω is velocity in the σ direction, f is Coriolis parameter, v_V is vertical eddy viscosity for momentum, subscripts x and y represent the direction, *P* is horizontal pressure term and is approximated by, Boussinesq' equations, *F* is horizontal Reynolds stress and is determined using eddy viscosity, and *M* is presenting the external momentum due to sources and sinks.

4.3.3.3 Hydrostatic pressure assumption

With the "shallow water assumption" the vertical momentum equation reduces to a hydrostatic pressure equation. The vertical accelerations are assumed to be small in comparison with gravitational acceleration in the shallow water system such as coastal areas, estuaries, lagoons, rivers, and lakes and therefore are not taken into account. The equation is therefore simplified to:

$$\frac{\partial P}{\partial \sigma}=-\rho_w g h \quad (4\text{-}4)$$

where ρ_w is density of water in kg/m^3, and g is gravity in m/s^2.

4.3.3.4 Vertical Velocity

The vertical velocity in the σ coordinate (ω) is computed from the continuity equation:

$$\frac{\partial \omega}{\partial \sigma}=-\frac{\partial \zeta}{\partial t}-\frac{\partial [hU]}{\partial x}-\frac{\partial [hV]}{\partial y} \quad (4\text{-}5)$$

In the 3D simulation the vertical velocity w is calculated considering horizontal velocities, water depths, water levels, and vertical velocities according to σ coordinates:

$$w=\omega+U\left(\sigma\frac{\partial h}{\partial x}+\frac{\partial \zeta}{\partial x}\right)+V\left(\sigma\frac{\partial h}{\partial y}+\frac{\partial \zeta}{\partial y}\right)+\left(\sigma\frac{\partial h}{\partial t}+\frac{\partial \zeta}{\partial t}\right) \quad (4\text{-}6)$$

4.3.4 Transport equation

Transport of suspended sediment is calculated by solving the three-dimensional advection-diffusion (mass-balance) equation as follows:

$$\frac{\partial[hc]}{\partial t}+\frac{\partial[hUc]}{\partial x}+\frac{\partial[hVc]}{\partial y}+\frac{\partial[\omega c]}{\partial \sigma}=$$
$$h\left[\frac{\partial}{\partial x}\left(D_H\frac{\partial c}{\partial x}\right)+\frac{\partial}{\partial y}\left(D_H\frac{\partial c}{\partial y}\right)\right]+\frac{1}{h}\frac{\partial}{\partial \sigma}\left[D_V\frac{\partial c}{\partial \sigma}\right]+hS \qquad (4\text{-}7)$$

where c is mass concentration of sediment in kg/m^3, D_H, D_V are eddy diffusivities of sediment fraction m^2/s, and S represents source or sink terms per unit area.

In a 3D simulation "3D turbulence" is computed by one of the turbulence closure modules incorporated in the package. In the 2DH simulation the 2D turbulence is a measure of the horizontal mixing that is not resolved by advection on the horizontal computational grid. The values for 2D turbulence may either be specified by the user as a constant or space-varying parameter, or can be computed using a sub-grid model for horizontal large eddy simulation (HLES).

The transport equation in Delft3D is also formulated in a conservative form in orthogonal curvilinear coordinates in the horizontal direction and σ coordinates in the vertical. In order to solve equations 4-2 to 4-7 the horizontal and vertical eddy viscosity (ν_H and ν_V) and diffusivity (D_H and D_V) need to be prescribed. The horizontal eddy viscosity and diffusivity are assumed to be a superposition of three parts including molecular viscosity of the fluid (water), "3D turbulence" computed by a selected turbulence closure model (see Section 4-3-4-3 below), and "2D turbulence". The relationship between the vertical eddy diffusivity and vertical eddy viscosity may be written as:

$$D_V=\frac{\nu_V}{\sigma_c} \qquad (4\text{-}8)$$

in which σ_c is the Prandtl-Schmidt number which varies between 0.5 and 1. It is about 0.9 in near wall flows, 0.5 in plane jet and mixing layer, and 0.7 in round jets. The value of Prandtl-Schmidt number for the shallow water is between 0.5 and 1 (Launder, 1991).

4.3.4.1 Exchange with the Bed

The exchange of sediment with the bed is accounted for by means of sediment sources and sinks placed near the bottom of the flow. Separate pairs of sediment source and sink terms are required for each sediment fraction. These are calculated and located for mud sediment fractions different from sand sediment fractions.

For sand sediment fractions, the van Rijn (1993) approach is followed. A reference height is calculated based on the bed roughness. The sediment source and sink terms are located in the first computational cell that is entirely above the reference height (the reference cell). Cells that fall below the reference cell are assumed to respond rapidly to changes in the bed shear stress, and have a concentration equal to the concentration of the reference cell. The sediment concentration at the reference height is calculated using a formula derived by van Rijn (1984) that includes the presence of multiple sediment fractions:

$$c_a = 0.015\rho_s \frac{d_{50}}{a} \frac{T_a^{1.5}}{D_*^{0.3}} \qquad (4\text{-}9)$$

in which *a* is reference level above the mean bed, c_a is the mass concentration of the sediment at the reference height *a*, T_a is the dimensionless bed shear stress (eq. 4-10), and D_* *is* dimensionless particle diameter (eq. 4-11).

$$T_a = \frac{\tau_b - \tau_{ce}}{\tau_{ce}} \qquad (4\text{-}10)$$

$$D_* = \left[\frac{(s-1)g}{\nu^2}\right]^{1/3} d_{50} \qquad (4\text{-}11)$$

where $\tau_b = \rho g \left(\frac{\bar{u}}{C'}\right)^2$ is grain related or effective bed shear stress, τ_{ce} is critical bed shear stress for erosion, *s* is relative density of sediment ($= \rho_s / \rho_w$), ν is eddy viscosity, and d_{50} is median particle size of sediment.

For mud sediment fractions the source and sink terms are always located in the bottom computational cell. Therefore the definition of erosion and deposition plays an important role in cohesive sediment calculation. The fluxes between the water and the bed (erosion and deposition) for cohesive sediment fractions are calculated using Partheniades-Krone formulations (Partheniades, 1965):

$$E^{(\ell)} = M^{(\ell)} S\left(\tau_{cw}, \tau_{cr,\varepsilon}^{(\ell)}\right) \qquad (4\text{-}12)$$

$$D^{(\ell)} = w_s^{(\ell)} c_b^{(\ell)} S\left(\tau_{cw}, \tau_{cr,d}^{(\ell)}\right) \qquad (4\text{-}13)$$

$$c_b^{(\ell)} = c^{(\ell)}\left(z = \frac{\Delta_{zb}}{2}, t\right) \qquad (4\text{-}14)$$

where ℓ represents the fractions of the sediment, E is the erosion flux (kg/m²/s), M_{er} is the user defined erosion parameter (kg/m²/s), D is deposition flux (kg/m²/s), w_s is hindered settling velocity (m/s), c_b is average sediment concentration in the near bottom computational layer, and $S\left(\tau_{cw}, \tau_{ce}^{(\ell)}\right)$ and $S\left(\tau_{cw}, \tau_{cr,d}^{(\ell)}\right)$ are the erosion and deposition step functions respectively. These functions are defined as:

$$\begin{aligned} S\left(\tau_{cw}, \tau_{ce}^{(\ell)}\right) &= \left(\frac{\tau_{cw}}{\tau_{ce}^{(\ell)}} - 1\right), \quad \text{when } \tau_{cw} > \tau_{ce}^{(\ell)} \\ &= 0 \quad \text{when } \tau_{cw} \le \tau_{ce}^{(\ell)} \end{aligned} \qquad (4\text{-}15)$$

$$S\left(\tau_{cw},\tau_{cd}^{(\ell)}\right)=\left(1-\frac{\tau_{cw}}{\tau_{cd}^{(\ell)}}\right), \quad \text{when } \tau_{cw}<\tau_{cd}^{(\ell)}$$
$$=0 \quad \text{when } \tau_{cw}\geq\tau_{cd}^{(\ell)} \tag{4-16}$$

In these functions, τ_{cw} is maximum bed shear stress (N/m²), $\tau_{ce}^{(l)}$ is a user-defined critical erosion shear stress (N/m²) for erosion, and $\tau_{cd}^{(l)}$ is a user-defined critical deposition shear stress (N/m²) for deposition.

The above mentioned formulas are valid for each sediment fraction (ℓ). For cases where several fractions are involved, the erosion rate will be affected. To solve this complexity, in the Delft3D package, it is considered that the erosion rate is proportional to the sediment fraction in the top-most layer of the bed. That is, the cohesive sediment fraction is supposed to form a layer covering the top most layer of the bed.

4.3.4.2 Bed Load Sediment Transport

In the package bed load sediment transport is calculated for the sand sediment fractions employing Van Rijn's (1993) approach. It is applied to the near bed sediment particles specifically below the reference height, *a*. The basic formulation of the bed load transport without the consideration of the wave reads as:

$$\left|S_b\right| = f_{BED}\eta_{re}0.5\rho_S d_{50}u_*'D_*^{-0.3}T_a \tag{4-17}$$

where the $\left|S_b\right|$ is the bed load transport rate (kg/m/s), f_{BED} is a user-specified calibration factor, η_{re} is the relative availability of the sediment fraction in the mixing layer, and u_*' is effective bed shear velocity.

The direction of the bed load transport is taken to be parallel with the flow in the bottom computational layer.

4.3.4.3 Turbulence Closure Model

Turbulence is responsible for most of the vertical transport within the near bed region and is considered to be diffusive because it exhibits the ability to transport and mix momentum, energy and contaminants at a rate that far exceeds that associated with molecular processes. The main problem to model the turbulence structure is that the scale of eddies is too small compared with the grid sizes. To handle this problem in the Delft3D package the turbulent processes are carried out using a sub-grid method. Such a procedure does not simulate the details of the turbulent motion but only simulate the effect of turbulence on the mean-flow behaviour.

In Delft3D-FLOW package the contribution of 3D turbulent eddies to the vertical exchange of horizontal momentum and mass is modeled through a vertical eddy viscosity and eddy diffusivity coefficient. The coefficients are assumed to be proportional to a velocity scale and a length scale. The coefficients may be specified as a constant or computed by means of an algebraic, k-l or k-ε turbulence model, where k is the turbulent kinetic energy, l is the mixing length and ε is the dissipation rate of turbulent kinetic energy.

It should be noted that the most universal turbulence model is not necessarily the most suitable one for a particular problem. In particular, it is important to find out how well the various models can cope with the complications present in hydraulic problems, such as irregular geometries, buoyancy and free-surface effects. Following suggestions are recommended in the Delft3D manual to employ an appropriate closure module:

1. the use of k-l or algebraic closure model for areas where the condition of the flow is well mixed. This was considered to be the case for the area under the investigation,
2. the use of k-l or k-ε module for areas where vertical circulation exists, and
3. the use of k-ε module for cases where at least 20 layers are used for simulation.

4.3.5 Boundary Conditions

Well-defined boundary conditions for the model are very important to obtain acceptable results from the model. For this reason hydrodynamic and sediment transport condition must be specified correctly at the open boundaries. To solve the equations two types of boundary conditions consisting of vertical and lateral boundaries are to be specified.

4.3.5.1 Vertical Boundary Conditions

In the σ-coordinate system, the bed and the free surface correspond with σ-planes. Therefore, the vertical velocities at these boundaries are simply:

$$\omega(-1) = 0 \text{ and } \omega(0) = 0 \qquad (4\text{-}18)$$

where ω is velocity in the σ direction. Exchange of sediment with the bed is described in Section 4-3-4-1.

4.3.5.2 Lateral Boundary Conditions

For the lateral boundary, open and closed boundaries are usually considered. The contour of the model domain consists of parts along "land-water" lines (river banks, coast lines) which are called closed boundaries and parts across the flow field which are called open boundaries. Closed boundaries are natural boundaries and the current velocities normal to them are set to zero. Open boundaries are always "water-water" boundaries. In a numerical model open boundaries are introduced to restrict the computational area and so the computational effort. They should be defined as far away as possible from the area of interest to avoid the effect of open boundary conditions on the area under the study. Open boundary conditions that can be defined in the DELFT3D package include the water level, the current velocity, and the flow discharge. The selection of boundary conditions depends on the type of flow to be simulated and the availability of measured data.

4.4 Wave module

Wave forcing can be included into the hydrodynamic module by an interrelated module named Delft3D-WAVE. It simulates the evolution of wind-generated waves in coastal waters. The wave module computes wave propagation, wave generation by wind, non-linear wave-wave interactions and dissipation, for a given bottom topography, wind field, water level and current field in waters of different depths. Delft3D-WAVE supports, a third

generation wave model; SWAN. This wave model computes the full (directional and frequency) spectrum on a rectilinear or curvilinear grid with many processes formulated in detail (Delft3D-WAVE User Manual).

One option to simulate the current and wave together is to use Online Delft3D-WAVE. Using this option, the simulations are carried out considering direct coupling between Delft3D-FLOW and Delft3D-WAVE. Every time the communication file is written, subsequently a WAVE simulation is performed. Afterwards FLOW resumes, using the latest WAVE results. For this reason prior to starting the FLOW simulation with online Delft3D-WAVE, the WAVE input file also should be prepared.

In simulations including waves, the hydrodynamic equations are solved in a Generalized Lagrangian Mean (GLM) reference frame. In GLM formulation, the 2DH and 3D flow equations are very similar to the standard Eulerian equations; however, the wave-induced driving forces averaged over the wave period are more accurately expressed. The relationship between the GLM velocity and the Eulerian velocity is given by

$$\begin{aligned} U_{GLM} &= u + u_s \\ V_{GLM} &= v + v_s \end{aligned} \qquad (4\text{-}19)$$

where U_{GLM} and V_{GLM} are GLM velocity components, u and v are Eulerian velocity components, and u_s and v_s are the Stokes' drift components (Walstra et al., 2000).

4.5 An overview on the 2DH set up of the model for central Dithmarschen Bight

The Delft3D package was employed by Palacio (2002), Mayerle and Palacio (2002), and Mayerle et al. (2005) to study the hydrodynamics of the bight in two dimensions (2DH). They calibrated and validated the hydrodynamic setup of the model using field data. Winter and Mayerle (2003), Mayerle and Poerbandono (2005), and Escobar (2007), later added the sediment transport module for the study of the sediment transport in the area. Simultaneously, by developing roughness maps for the area and further improvement of these maps, the performance of the model was improved considerably (Pramano, 2005; Mayerle et al., 2005 and Escobar, 2007). In this section a brief overview of the model set up used in those studies is reviewed.

4.5.1 Model Border and Grid

The boundaries of the model have been chosen far from the area of interest, namely the Piep tidal system. This has ensured that the boundary conditions will not affect the hydrodynamics and sediment transport at the monitoring points. The border of the model is as shown by red line in Figure 4.4. The model consists of a closed land boundary at the east, and three open boundaries in the north, west, and south.

The model grid adapted by Palacio (2002), Mayerle and Palacio (2002) has been employed in this research. It contains approximately 36,000 grid cells covering the domain. The size of the grid cells is approximately 90 m (in north-south direction) by 150 m (in west-east direction) for the tidal channels, and 250 m by 250 m for the tidal flats. Grid lines preferably follow the tidal channel axes which reduce the magnitude of the convective accelerations and therefore the associated non-linearity.

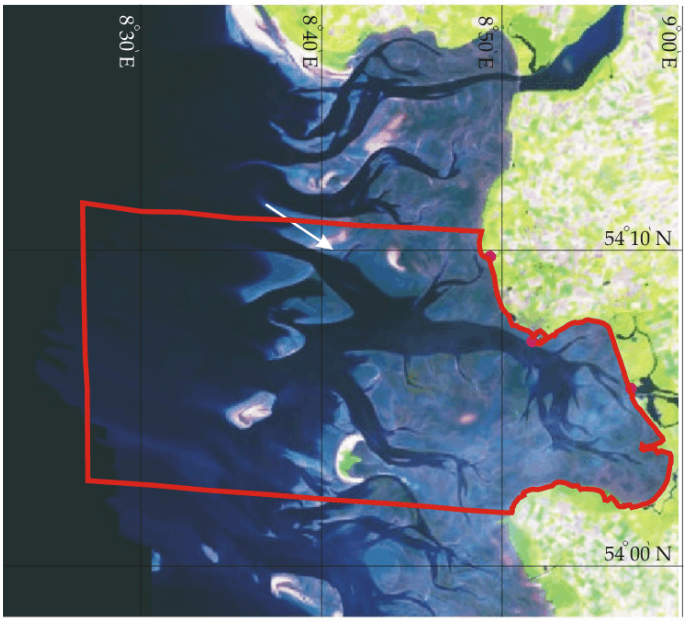

Figure 4.4 Boundaries of the Model

4.5.2 Bathymetry

The data for the bathymetry of the model were a combined set of data from the Federal Maritime and Hydrographic Agency (BSH) in Hamburg for the channels and those from the Office of Rural Areas (ALR) in Husum for the tidal flat and shallow regions. Figure 4.5 shows the model bathymetry of the area.

Model simulations performed in the present investigations covered only short periods ranging from 3 to 5 days, and due to the relative stability of the main tidal channels, bathymetry changes were neglected as was assessed by Escobar (2007).

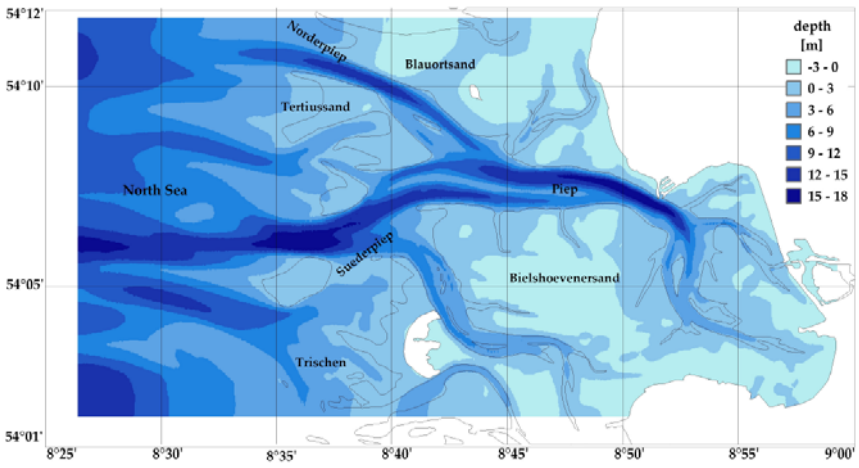

Figure 4.5 Model bathymetry (Escobar 2007)

4.5.3 Determination of the Condition along the Boundaries

As stated in Section 4.6.1, the eastern boundary is a closed boundary. The northern and southern boundaries are located mainly in tidal flat areas and fall dry during low tide. According to Palacio (2002) they do not affect the hydrodynamics of the area significantly. For the open boundary input data in terms of water levels were considered, because of the availability of long time data collected for the entire North Sea. The nested procedure provided by the package was used to prepare the astronomic water level data for the Dithmarschen Bight model.

When boundary conditions of a model are generated by a larger (overall) model it is called a nested model. The use of a nesting procedure here allows the determination of water levels at the boundaries through incorporation of water level data of the entire North Sea, for which a time series data, having been collected over a long time, were available. The procedure takes into account the effect of wind, wave and astronomical tide. For large area models the amplitudes and phases can be interpolated from nearby ports.

To derive water level values for the open boundaries of the Dithmarschen Bight model the following procedure is carried out. The model of a larger (overall) area consisting of the entire North Sea called the Continental Shelf Model was already established by Verboom et al. (1992), as shown in Figure 4.6(a). At the open boundaries of the Continental Shelf Model astronomical components for the water levels were imposed. Water level results of the Continental Shelf Model in the monitoring points were imposed onto the open boundaries of the German Bight Model (Figure 4.6(b)), which is an adapted version of the model developed by Hartsuiker (1997). Similar procedure is executed to impose water level data from the German Bight Model onto the open boundaries of the central Dithmarschen Bight model (Figure 4.6(c)). The nesting procedure for the area under the investigation had been tested and qualified by Mayerle et. al. (2005).

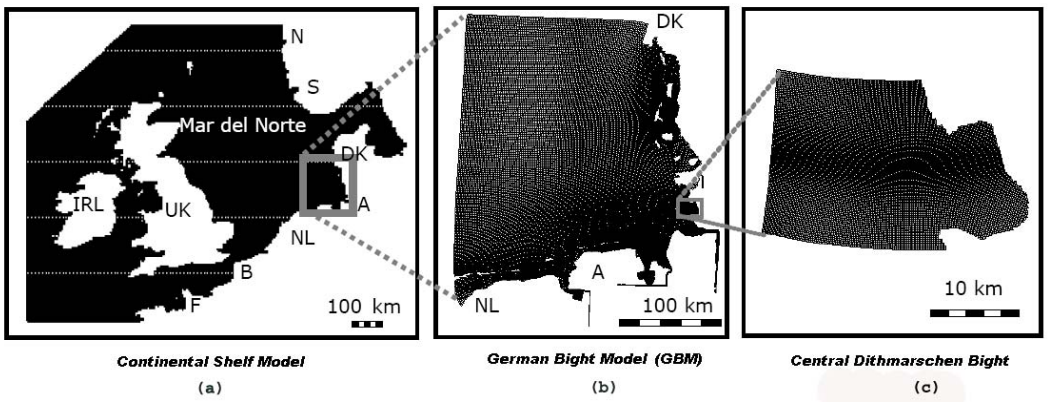

Figure 4.6 Nesting sequence for the generation of open boundary conditions

4.5.4 Monitoring Points

In order to verify the results of the model output in comparison with the measured data, observation points and cross sections should be set in the model at the same geographical positions of the points and cross sections where measurements were carried out. The

number and positions of monitoring points in the model should be matched with the number and geographical positions of measuring points. Figure 4.7 shows the cross sections used for measurement in Norderpiep (T1), Süderpiep (T2) and Piep (T3) channels. The monitoring points at each cross section are also presented in the Figure. Dates and the number of monitoring points for each campaign are summarized and given in Table 3.1 in Chapter 3.

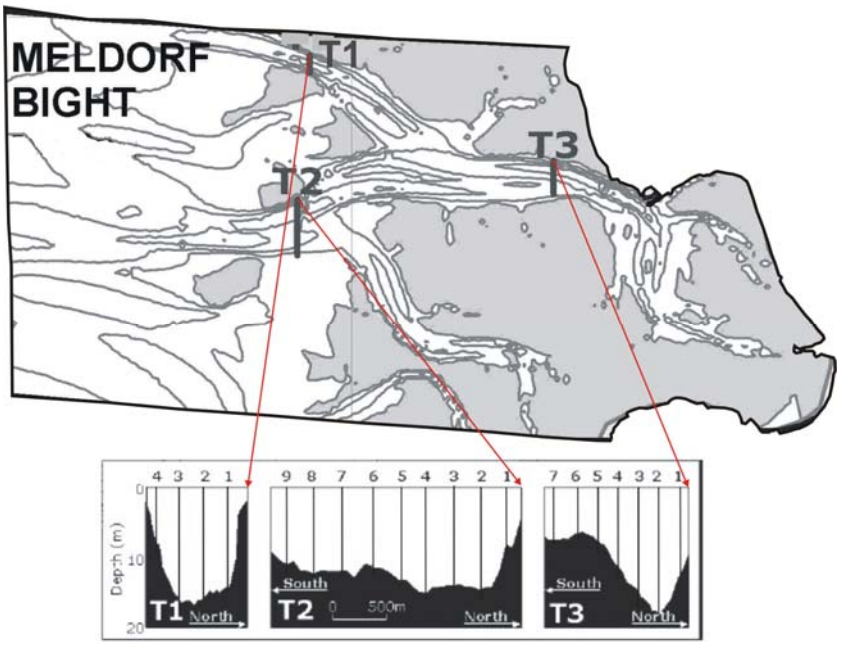

Figure 4.7 Location of Cross Sections and Monitoring Points in the Model

4.6 Sediment and morphological Data Input

4.6.1 Grain Size Map

Asp et al. (2001), Wilkens (2004), and Wilkens and Mayerle (2005) carried out extensive research on the morphodynamics of the central Dithmarschen Bight. Wilkens (2004) used a combination of measurements and mathematical modelling to study the morphodynamics of the tidal channel system in the bight. He chose a uniform distribution of the sediment grain size for the model. He concluded that the performance of the model could be improved if the spatial distribution of grain sizes, similar as possible to that in the field, was considered in the model.

To develop a function capable of producing a high-resolution sediment map of the study area with the limited grain size measurements available Escobar and Mayerle (2006) and Escobar (2007) carried out an intensive experiment. They investigated the possible correlation between the hydrodynamic patterns and the grain size distribution. Escobar (2007) determined a functional relationship between flow-wave characteristic and grain size, and concluded that the most important properties to create the distribution of the grain size in the area were the wave characteristics. Based on this conclusion he prepared a grain size map for the area. About 200 surface sediment samples gathered in the Dithmarschen Bight

for a range of flow-wave conditions were considered as a proof. The temporal variation of grain sizes was neglected. The grain size map prepared by Escobar and Mayerle (2006) and Escobar (2007) is shown as Figure 4.8 below.

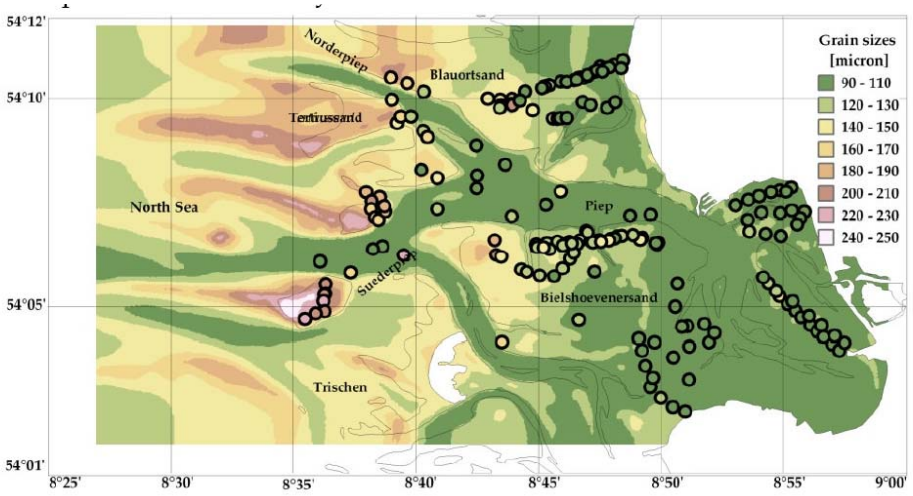

Figure 4.8 Predicted (background) and measured (circles) grain sizes in the study area (Escobar 2007)

4.6.2 Bed Roughness Map

The bed form and equivalent roughness size in the area were investigated by Pramono (2005). According to him, the study area has bedform heights that vary from 0.10m to 0.50m and bedform lengths that vary from 4m to 22m. He concluded that on the basis of bedforms classifications the area consists of megaripples and dunes. He also attempted to estimate equivalent roughness sizes of the area using the current velocity data in the tidal channels. employing both empirical equations and numerical simulations, he produced a bedform map for the area on the basis of velocity characteristics. He also stated that the bedform dimensions and equivalent roughness sizes in shallow areas derived by the empirical equations were in good agreement with those from field observations.

Mayerle et. al. (2005) and Escobar (2007) carried out investigations to represent more realistic bedform patterns applicable to the model. They also employed empirical equations in combination with numerical simulations. The empirical equations they used were those propsed by Van Rijn (1993) to estimate bed form dimensions and roughness size at low flow regime.

Escobar (2007) considered a steady flow with constant values of depth, velocity and shear stress were superimposed on an unsteady flow by taking into account three following assumptions:

1. the short tidal period to guarantee small or gradual bedform readjustments (i.e. the critical shear stress is exceeded during short periods),
2. a constant amplitude of the cyclic flow, and
3. no sedimentation during the tidal cycle.

He concluded that if a representative flow was defined for unsteady flow both the steady and unsteady flows would cause similar bedform dimensions. Thus steady flow theories might be applicable in determining bedform sizes in unsteady cyclic flows. By using this methodology together with the empirical equations of Van Rijn (1993) and application of 2DH flow simulation, bed roughness values for entire area of Dithmarschen Bight were calculated and a roughness map were prepared for the area. Figure 4.9 is a typical roughness map which had been developed using the methodology proposed by Escobar (2007).

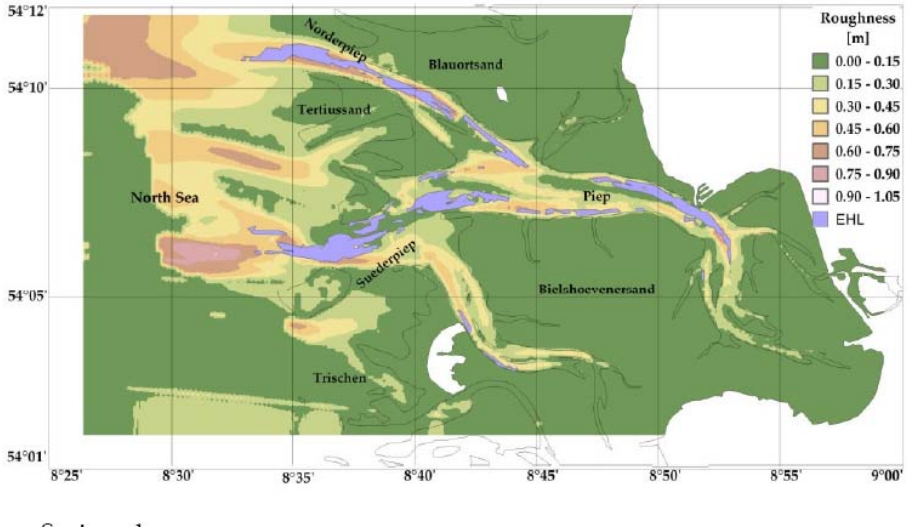

Figure 4.9 Bedform Roughness Map for Dithmarschen Bight (Escobar 2007)

4.7 Sediment Transport Model of the Bight

From the year 2000 to the year 2007, several 2DH sediment transport models were used, assessed and improved to some degree for the area under this investigation by Poerbandono, 2004, Winter et al., 2005, Mayerle et al.,2005, Escobar, 2007. In almost all these studies the 2DH simulations had been executed using the flow, and sediment transport modules. In the majority of the simulations carried out so far, the effect of waves was disregarded. The 2DH sediment transport model covers the same area and implements the same grid as the flow and wave models (see Fig. 5.1).

Winter et.al., (2005), Mayerle et.al., (2005), and Escobar (2007) reported that the developed models were sufficiently accurate to provide values of the suspended material concentration comparable with those of the field data to a certain extend. Winter, et.al. (2005) pointed out that even though the model is capable to reproduce the main characteristics of suspended sediment transport across the tidal channels it contains some discrepancies. As the predictive ability of the model in regard to sediment dynamics was relatively low they proposed more detailed investigations. The relevance of several factors affecting the performance of the sediment transport model was identified and strategies for its improvement were proposed. The results of investigations carried out by Mayerle et.al., (2005) clearly indicated the relevance of bed roughness, particularly with regard to sediment transport predictions. They emphasized the importance of employing spatial variability of bed roughness in the model based on field data. In addition, the inclusion of cohesive

properties of sediment, sediment grain sizes, and also the incorporation of conditions below the loose sediment layer proved to be most relevant.

As a result, improvements to the 2DH sediment transport model were made by considering spatial variable bed roughness and sediment sizes as well as accounting for the effect of non-cohesive and cohesive sediments (Escobar, 2007, Mayerle and Escobar, 2008). The strategies proposed for improving the performance of the model were the use of the maps of sediment sizes and the bed roughness, which were prepared by these investigators. The map presented as Figure 4.8, covers the spatial variability of the sediment sizes for non-cohesive sediments as well as the bed forms, and that as Figure 4-9 covers the spatial variability of the bed roughness. Comparisons of field measurements and model simulations at several cross-sections were employed to assess the efficacy of the proposed methodology. It was found that the incorporation of cohesive properties of sediments, the variability of bed roughness and the conditions of the seabed resulted in improvements in accuracy of about 25%, 15% and 10% respectively. The results showed that despite the high accuracy achieved in terms of statistical parameters there were still some discrepancies, in particular regarding the phase lags, between the model results and the field data (Mayerle and Escobar, 2008).

Chapter 5. Performance of the 2DH Sediment Transport Model

5.1 Introduction

In this chapter, results of investigations concerning the ability of the two-dimensional depth-averaged (2DH) process based model for simulation of sediment transport are summarised. The model comprises of modules for simulation of flow, waves, and sediment transport. A detailed assessment of the existing model, sensitivity analysis, calibration and validation were carried out using the data, described in Chapter 3. Initially the accuracy of the existing model was checked. This was followed by several sensitivity studies to assess the importance of the open sea boundary conditions and, the effect of waves on flow and sediment transport. The results of calibration and validation of the model covering a wide range of tidal conditions are presented. The ability of the 2DH sediment transport model in predicting the suspended material concentration for the prevailing tidal conditions of the study area is demonstrated.

5.2 2DH Flow Model

The 2DH flow model used in this study was the one that had been developed by Palacio et al. (2005), Mayerle et al (2005), and others for the prediction of water levels and current velocities (see Chapter 4). The model domain shown in Figure 5.1, used in those studies was also employed here. A curvilinear grid with the grid spacing that ranged from 90m to 230m was discretized the 640km^2 area of the domain for modelling in all these investigations**.** Several approaches for prescribing conditions along the open sea boundaries were proposed and tested against field measurements. The report by Mayerle et al. (2005), indicates that the condition at the western open sea boundary is the most relevant one to adequately describe the water levels in the model. The required wind data for the adjacent area, as stated in Chapter 3, were obtained from the PRISMA interpolation model developed by the Max Planck Institute of Meteorology in Hamburg (Luthardt, 1987). The PRISMA wind data is generated every three hours with an area resolution of 42km.

The 2DH flow model has been calibrated and validated using measurements of water levels at several tidal gauges and current velocities at several cross-sections by Toro et al. (2005). The locations of the tidal gauges (G1 to G6) and cross-sections (T1, T2 and T3) used for the calibration and validation of the models are shown in Figure 5.1. Adequate performance of

the model for predicting water levels and current velocities have been reported by Toro et al. (2005), Palacio (2002), Palacio et al. (2005) and Mayerle et al. (2005).

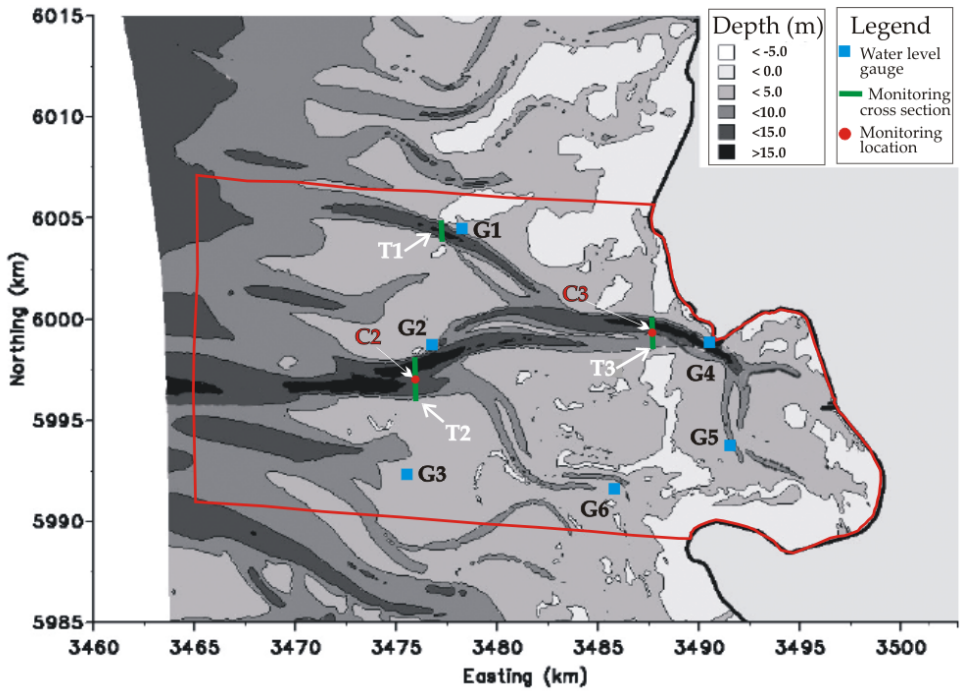

Figure 5.1 Model domain

5.2.1 Water level discrepancies

To verify the flow model, the whole range of tidal conditions prevailing in the area was considered for the comparison of water level values from the model and the field data. Water levels specified along open sea boundaries of the model were obtained from a nesting sequence covering the north-west European North Sea Continental Shelf Model and German Bight Model (see Chapter 4). For the same period of model simulations, water level data records from the tidal gauges located near the western open sea boundary (G1 and G2 in Figure 5.1) are used for the comparison. Figure 5.2 shows a comparison of measured and computed water levels at cross-section T1 in the Norderpiep tidal channel. The graph show very similar trend of variations for computed and measured water level. It can be seen that although the model is able to describe the tidal variations, some discrepancies exist between the model results and the field data. In the Figure the computed values show a phase lag of up to about one hour from the measured values. It can also be seen that in addition to the phase lags the model is unable to reproduce low water levels accurately.

Further investigations were carried out to determine the possible sources for these discrepancies. These included the re-examination of the model bathymetry, the verification of the effect of waves on the water levels, and the accuracy of the open sea boundary conditions assigned to the model.

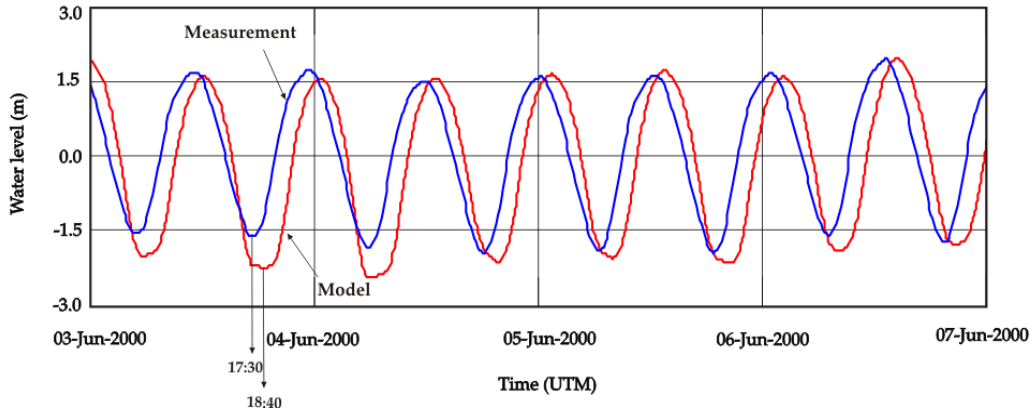

Figure 5.2 Comparison of measured and computed water levels at cross-section T1 in the Norderpiep tidal channel - June 3 to 7, 2000

5.2.1.1 Examination of the model bathymetry

Bathymetric surveys comprise of sample depths with a variable spatial resolution. As the measuring locations usually do not coincide with the coordinates of the model grid, interpolations are needed. The interpolation procedure sometimes results in deviation between the actual hydrographic surveys and the interpolated results. As stated in Chapter 3, the bathymetry data used in the model were a combined data from the Federal Maritime and Hydrographic Agency (BSH) in Hamburg for the channels and the Office of Rural Areas (ALR) in Husum for the tidal flat and shallow regions, both from the year 2000.

In order to check the accuracy of the model bathymetry, comparisons of the model and measured bed elevations covering the entire domain were carried out. Figure 5.3 shows the differences in bed elevations between the two bathymetries obtained from all the available measurements and the ones obtained by interpolation of the measurements on the model grid. In general the agreement on the tidal flats and channels is reasonable. The differences are on the average in the order of a few cm. But along the margins of the Piep tidal channel system (Norderpiep, Suederpiep and Piep) discrepancies of up to about 2m can be seen. A more detailed analysis at these locations revealed that the differences are probably associated with the grid resolution which is unable to describe the slopes of the tidal channels adequately. Further comparisons of the measured and model bathymetries were carried out at three cross-sections along the main tidal channels at which measurements were carried out. There are the cross-sections T1 on the Norderpiep, T2 on the Süderpiep and T3 on the Piep (Chapter 3). Referring to Figure 5.4, it can be seen that the profiles used in the model are in good agreement with those from the measurements.

Despite the differences in the bed elevations along the margins of the tidal channels it was concluded that the actual bathymetry is well represented in the model and thus is not the source for the discrepancies in the simulated water levels.

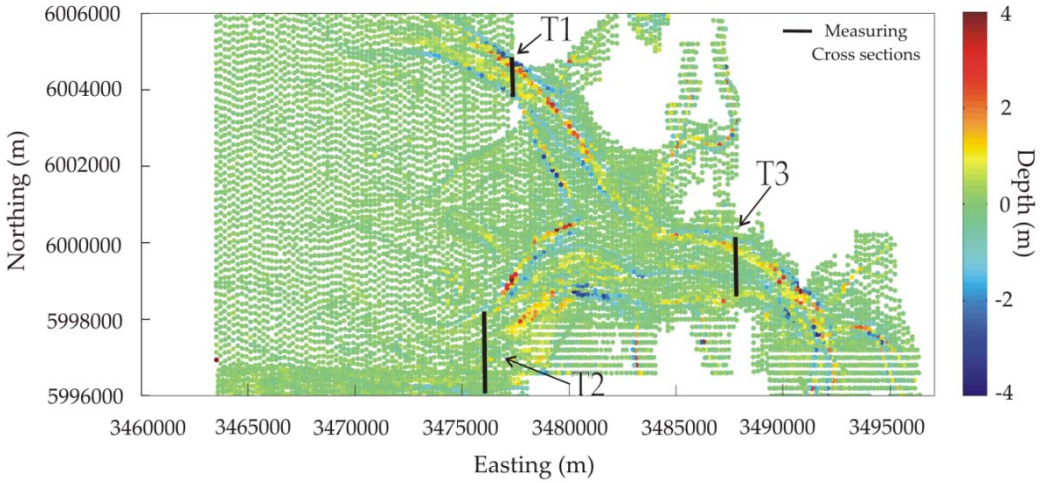

Figure 5.3 Difference between bathymetries in m (measurements– model)

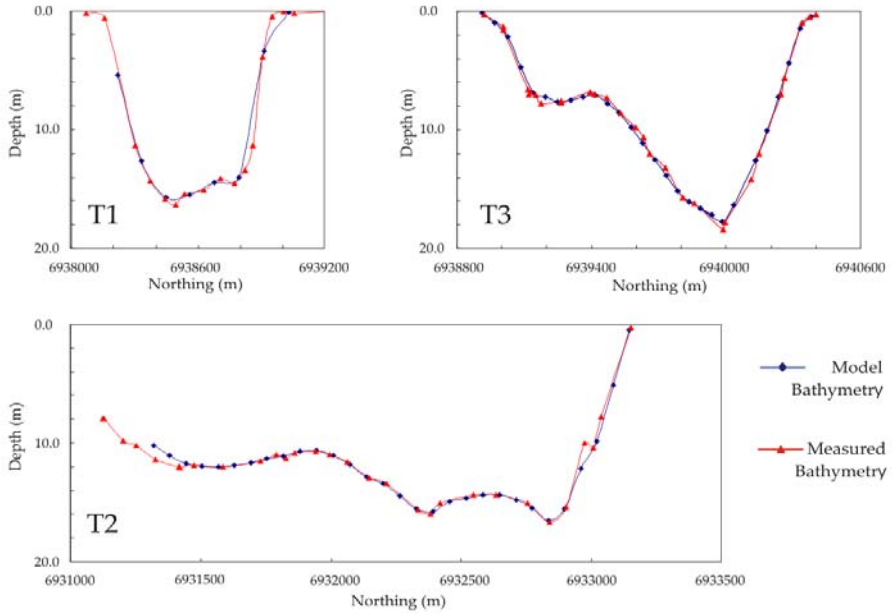

Figure 5.4 Comparisons of the bed elevation at selected cross sections

5.2.1.2 Waves superimposed on water levels

The phase-averaged wave model SWAN, developed at the Delft Hydraulic (Booij et al., 1999 and Ris et al., 1999) coupled with the flow model (see Section 5-2) was used in this study. SWAN is a third generation model, capable of simulating waves propagation, refraction, shoaling, wind-induced generation and dissipation due to white-capping, depth-induced wave breaking, bottom friction and wave-wave interactions. The model is fully spectral,

meaning that solves the spectral action balance for a specified number of directional sectors and frequency intervals.

In the investigations carried out up to now, attention was given primarily to the ability of the model in simulating waves under moderate winds and waves generated by local winds. It was found that the effect of moderate waves on the water levels and currents is negligible and therefore disregarded (Wilkens, 2004, Mayerle and Zielke, 2005 and Wilkens et al., 2005). Thus far in the majority of the flow model simulations covering conditions with relatively low winds, the wave effects were not taken into account (Palacio, 2002, Palacio et al., 2005, Mayerle et al., 2005).

To advance the understanding of the effect of waves on water levels, additional model runs implementing the coupled flow and wave models, were carried out both for moderate and more adverse wind conditions. Simulations were carried out initially for the period from 3rd to 8th of June 2000, with moderate wind condition. This period is characterised by tidal ranges of about 3.7m and wind velocities up to 11 m/s**.** Figure 5.5 shows comparisons of the measured and computed water levels at Büsum Gauge G4 (see Figure 5.1). It can be seen that except during short intervals, there are almost no differences between the modelled water levels with and without the wave model inclusion. This confirms the previous findings (see Mayerle et al., 2005) that under moderate wind conditions the inclusion of waves on the flow modelling is not required.

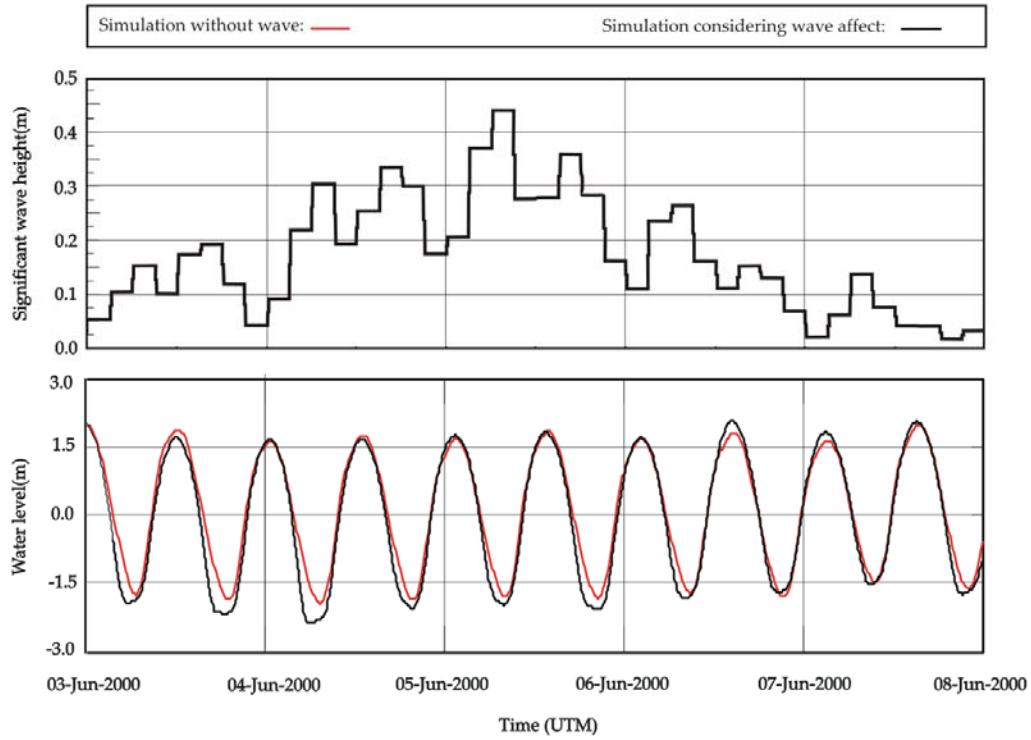

Figure 5.5 Comparison of measured and computed water levels from simulations with and without waves - Station G4- Period June 3 to 8, 2000 - Moderate wind conditions

Following the investigations for moderate wind conditions, sensitivity studies covering more adverse weather conditions were undertaken. The simulations covered the period

November 2nd to December 7th, 1999, during Storm Anatol. This period is characterised by tidal ranges of about 5.0m and wind velocities of up to 30m/s. Figure 5.6 shows the resulting water levels obtained from the simulations with and without the wave model inclusion. Due to the extreme winds, increases in water levels has been observed after the peak storm. The differences in water levels between the simulations using just the flow model and the coupled flow and waves resulted reaches to more than 1 m for the high and low water during the 6th of December 1999. (see Figure 5.6). During periods of lower waves these differences gradually vanished. As no measured data for this period are available the certainty of the results cannot be assured. In view of the above mentioned observations, it seems necessary to include the wave module to the flow simulations in stormy conditions.

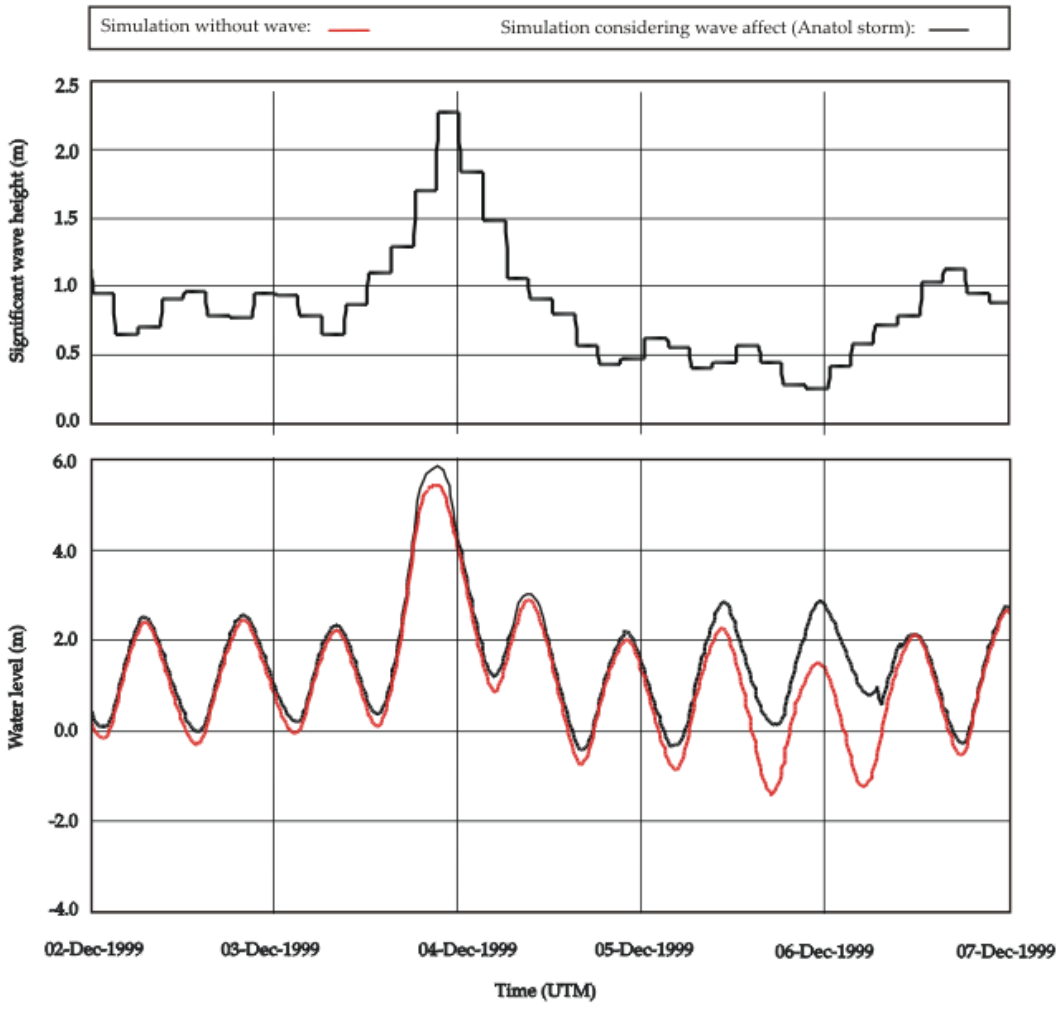

Figure 5.6 Comparison of the computed water levels at Gauge G4, from simulations with and without the wave model inclusion, for the period from the 2nd to the 7th of December 1999, during which the Storm Anatol had occurred

5.2.1.3 Water levels along the open sea boundaries

It was reported by Mayerle et al. (2005) that the precise specification of the conditions along the western open sea boundary is important in the accuracy of results from the flow model. As measured water levels are not available over the open sea boundaries of the model, values obtained from simulations using a nesting sequence covering the adjacent North Sea were used (see Figure 4.6). Echeverrie (2004) reported that the water levels and phases derived from the nesting sequence were not always in good agreement with the observed values. He proposed the following adjustments to the amplitudes and phases of the water levels on the grid points located along the open sea boundaries of the model as:

$$H_{adj} = \frac{1}{\overline{\Delta A}} H_{nest} - \overline{\Delta H} \qquad (5\text{-}1)$$

$$t_{adj} = t_{nest} - \overline{\Delta t} \qquad (5\text{-}2)$$

in which H_{adj} is the corrected water level, $\overline{\Delta A} = A_{nest} / A_{meas}$ is the average amplitude ratio, H_{nest} is the water level obtained from the nesting sequence, $\overline{\Delta H} = H_{nest} - H_{meas}$ is the average difference in the peak water levels, t_{adj} is the adjusted peak occurrence time, t_{nest} is the peak occurrence time derived from nesting sequence, and $\overline{\Delta t} = t_{nest} - t_{meas}$ is the average difference in the peak occurrence time.

In this study the procedure proposed by Echeverrie (2004) was adopted to adjust the phases and amplitudes of the nested water level. To test the effectiveness of these corrections, simulations for a wide range of tidal conditions were carried out. Table 5.1 presents the results of the simulations covering five periods with tidal ranges between 2.3m and 4.0m. Referring to the Table, corrections required to the phase vary from 30 to 52 minutes for the tidal ranges of 2.3 to 4 respectively. The results of corrected amplitude also show a clear dependency with the tidal range. Adjustments of up to -17cm and +16cm are required respectively for the spring (4.0 m) and neap (2.3 m) tidal cycles. The comparisons of the measured and the computed water levels at cross-section T1 with and without applying the corrections are shown in Figures 5.7 and 5.8. These are respectively for the spring and the neap tidal cycles. It can be seen that as a result of the corrections there is a significant improvement in the agreement between measured and computed water levels.

Table 5.1 Correction factors applied to the water levels along the open sea boundaries

Date	Tidal range (m)	Correction to the phase (min)	Correction to the amplitude (m)
March 21 to 23, 2000	4.0	$t_{nest} - 52$	$H_{nest} - 0.17$
June 5 to 6, 2000	3.7	$t_{nest} - 41$	$H_{nest} - 0.13$
September 5 to 6, 2000	3.2	$t_{nest} - 40$	$0.98 H_{nest}$
September 12 to 13, 2000	3.0	$t_{nest} - 40$	$0.98 H_{nest}$
December 5 to 6, 2000	2.3	$t_{nest} - 30$	$0.9 H_{nest} + 0.16$

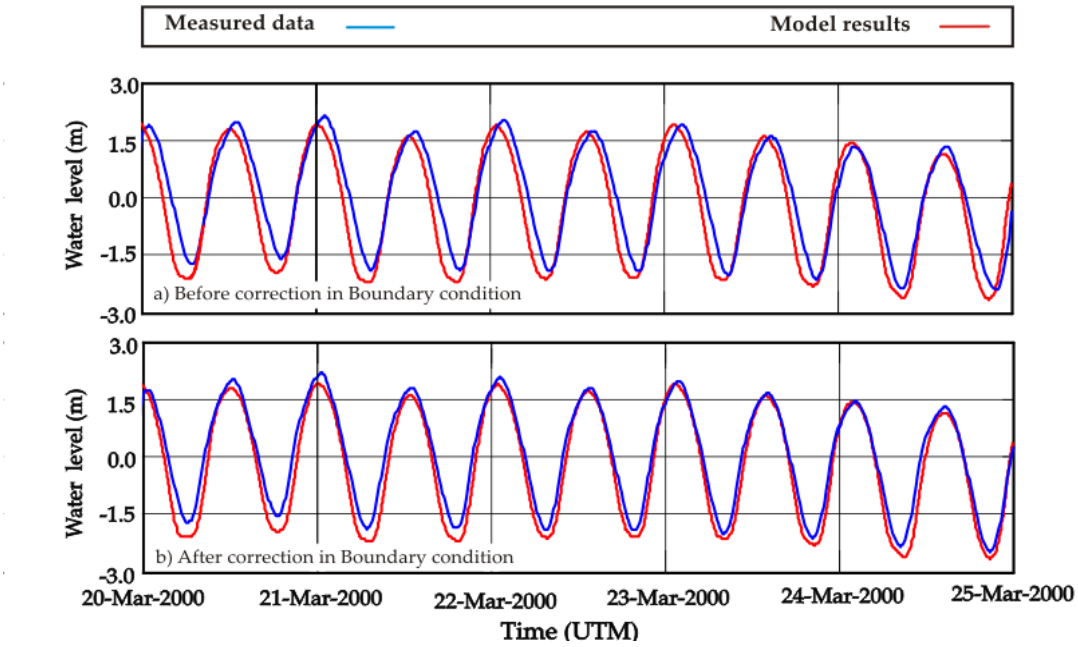

Figure 5.7 Comparison of measured and computed water levels at the centre of cross-section T1 before (a) and after (b) applying the corrections to the open sea boundary conditions–Spring tide, March 20-25, 2000

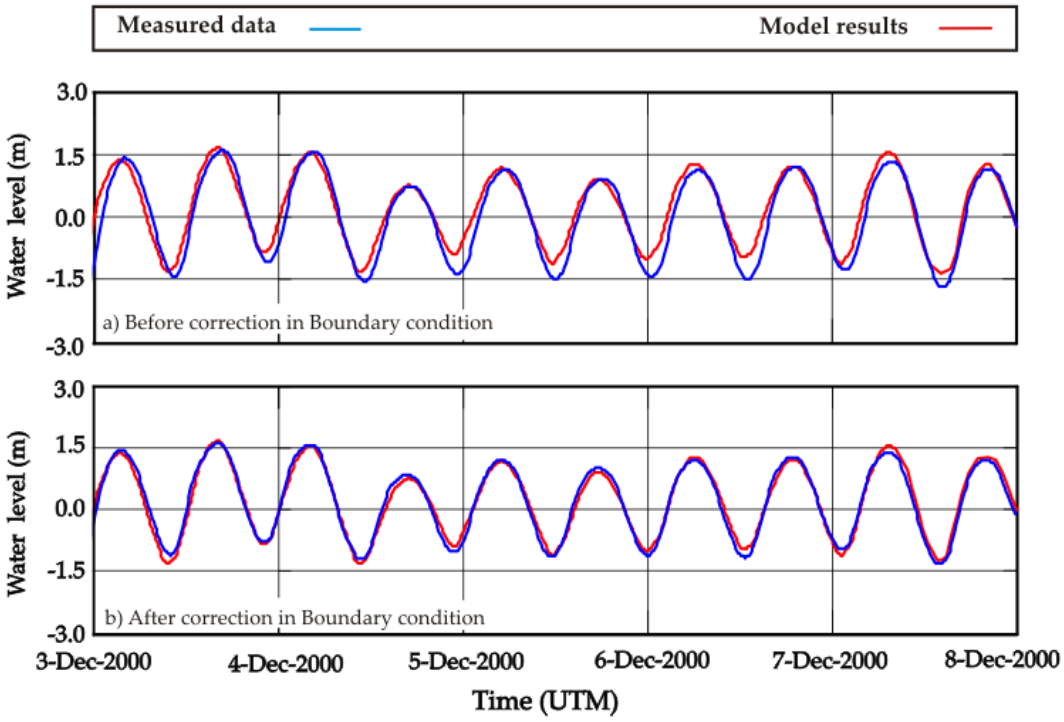

Figure 5.8 Comparison of measured and computed water levels at the centre of cross-section T2 before (a) and after (b) applying corrections to the open sea boundary conditions – Neap tide, Dec 3 to 8, 2000

5.3 2DH Sediment Transport Model

In this section the performance of the 2DH sediment transport model is explained and presented in four steps. 1) First the performance of the sediment transport model that was used and calibrated through previous studies, referred to in this study as the ”existing model” (see Section 4.7), is assessed. 2) This is followed by sensitivity studies of the model for the conditions along the open sea boundary and the presence of waves. 3) Stage three cover a discussion of the results obtained from the sediment transport model after incorporating all the improvements envisaged and calibrating for the whole range of tidal conditions. 4) Finally the model is validated using the set of data that was not employed in the calibration. The predictive ability of the 2DH sediment transport model was assessed to identify the need for three dimensional model simulations.

5.3.1 Existing model

In this section the performance of the model available at the beginning of the present study is assessed. Simulations were carried out using the same grid configuration and maps of grain sizes and bedform roughness as described in Chapter 4. An assessment was carried out on the basis of comparison of measured and computed depth-averaged suspended material concentrations at the cross-sections T1, T2 and T3 (see Figure 5.1). The field data used for comparisons were those measured at the cross-sections by means of optical beam transmissometers mounted in CTD sensors and equipped with a Niskin bottle sampler. Details of the device, measurements and conversion procedure reported by Toro et al. (2005) was described briefly in Chapter 3. In order to investigate the variation of suspended sediment concentration and transport during a tidal period, measurements of current velocity and optical transmission profiles from moving vessels were carried out at the selected cross-sections. The vessel moves back and fourth in a cross-section during the entire period. The resolution of the optical beam transmissometer was set to 0.2m. After conversion of the transmissivity into suspended material concentration the vertical profiles were averaged over the depth. This enabled direct comparisons with the results of the 2DH sediment transport model. The number of monitoring points and the distance between them depend on the shape and dimensions of the cross-section, which are presented in Table 5.2 for all the measurements used for the model performance. Cross section T1 consists of the least number of monitoring points (4) due to its narrowness, and cross section T2 consists of the largest number, with the number varying from 9 to 12, depending on the measuring season. The locations of these stations, for the measuring campaign in March 2000, are shown in the Figure 3-1.

Regarding the sediment properties, altogether five sediment fractions were used, of which four describe the non-cohesive sediments and one represents the mud fraction. The mud content and properties of the non-cohesive sediment fraction were those derived from sediment samples taken at several locations as reported by Poerbandono and Mayerle (2005). The characteristics of the non-cohesive fractions accounting for 75% of the sediment mixture are listed in Table 5.3. The main properties of the mud fraction (about 25% of the mixture) including settling velocities, critical shear stresses for erosion and sedimentations as well as the erosion parameters were obtained through calibration using field measurements of suspended material at several cross-sections. The measurements used in the investigations covered the entire range of tidal conditions (from 2.3 to 4.0m) typical of the study area.

Table 5.2 lists the variation of the calibrated mud properties with the tidal ranges. The Table shows a clear distinction among the mud properties. That is, for tidal ranges higher than 3.0m the values resulted for the settling velocity are between 1.6 and 2mm/s and for the tidal range equal to 2.3m, it is 1.3mm/s. it can also be seen that the critical shear stress equal to 0.65N/m² and between 0.8 and 1.0N/m² resulted for tidal ranges equal to 2.3m and higher than 3m respectively.

Table 5.2 Properties of the mud fraction as proposed by Escobar (2007)

Period	Tidal range (m)	Nr. of measuring stations	Settling velocity (mm/s)	Critical bed shear stress for sedimentation (N/m²)	Critical bed shear stress for erosion (N/m²)	Erosion parameter (kg/m²/s)
Mar. 21-23, 2000	**4.0**	**20**	**1.60**	**2.88**	**0.89**	**5.10e-004**
June 5-6, 2000	**3.7**	**23**	**2.00**	**3.24**	**1.00**	**4.70e-004**
Sept. 5-6, 2000	**3.2**	**23**	**1.60**	**3.02**	**0.79**	**5.70e-004**
Sept. 12-13, 2000	**3.0**	**21**	**1.76**	**3.12**	**0.88**	**5.20e-004**
Dec. 5-6, 2000	**2.3**	**20**	**1.30**	**2.90**	**0.65**	**1.57e-004**

Table 5.3 Sand fractions used by Escobar (2007)

Sand Fraction	Range of grain sizes (μm)	Adapted d_{50} (μm)
1	D_{50}<110	100
2	110<d_{50}<120	115
3	120<d_{50}<150	135
4	D_{50}>150	180

All the measuring stations in cross sections T1, T2 and T3 for the entire range of tidal conditions have been used for the statistical error analyses. The Relative Mean Absolute Error (RMAE) was considered for the purpose of error analyses. Altogether 434, 520, and 510 values were used respectively at cross-sections T1, T2 and T3 to calculate RMAE. The resulting RMAE between measured and computed depth-averaged suspended sediment concentration along cross-sections T1, T2 and T3 (see Fig. 5.1) are listed in Table 5.4. Referring to the Table, the ranges of RMAE values vary between 0.39 and 0.91, which are considered quite good for the ability of the model in predicting suspended material concentration. The agreement was found to be better for mean and spring (RMAE values from 0.39 to 0.73) than for neap tides (RMAE values from 0.75 to 0.91).

In Figure 5.9 scatter plots of the measured versus computed suspended material concentrations covering all the simulated conditions are shown separately for the three cross-sections for the different executed simulations. The first column of plots (Figure 5.9a) are those for the existing model and are discussed in this section, the other columns represent the proceeding simulation results and are discussed in the following Sections. The

black dashed lines in the plots represent the factor of 2 and the central solid line represents perfect agreement between the measured and predicted suspended sediment concentrations. The best-fit equations and correlation coefficient were calculated for these data and given on the top left corner of each plot. The red line in the Figures represent the best-fit equation of the data. It can be seen that for all the simulations and at all the cross sections a high proportion of values were within the factor of 2, which according to Van Rijn, (2002) is considered as quite high quality for predicting suspended sediment concentration. However, in the plots considerable numbers of points are also located outside the factor of 2. The scatter of the points outside the factor of 2 is more evident at cross-sections T2, and T3. With regard to the best fit lines and correlation coefficient it can be seen that very poor correlation between the model and field data are suggested. The reason for the weak correlation at this point is supposed to be due to the unadjusted boundary conditions (see Section 5.2.1).

Figures 5.10a to 5.12a show scatter plots of measured versus predicted suspended material concentrations respectively at cross-sections T1, T2 and T3 separately for the five simulated periods. The corresponding best fit lines and correlation coefficients are also given in the Figure. Referring to the figures, it can be seen that the observed values are above the domain of factor of 2, i.e. the observed values are larger than those predicted by the model. This is more evident in the scattergrams for the period of the low tidal range for the 5th to the 6th of December 2000, where almost no values are within the factor of 2. It can also be seen that the scatters are more pronounced for the values at cross-section T2, and T3, i.e. discrepancies are more significant at these cross-sections (see Figure 5.11a and 5.12a).

Table 5.4 RMAE between modeled and measured suspended material concentrations

Period/ tidal range	Existing model, as also used by Escobar (2007)			With improvements to the open sea boundary conditions for flow			Calibrated Model		
	T1	T2	T3	T1	T2	T3	T1	T2	T3
Mar. 21-23, 2000 (4.0 m)	0.44	0.39	0.42	0.40	0.35	0.42	0.31	0.40	0.48
June 5-6, 2000 (3.7m)	0.57	0.55	0.48	0.46	0.50	0.49	0.49	0.50	0.50
September 5-6, 2000 (3.2m)	0.47	0.46	0.51	0.40	0.66	0.42	0.52	0.45	0.62
September 12-13, 2000 (3.0m)	0.73	0.45	0.56	0.68	0.51	0.71	0.47	0.47	1.00
Dec. 5-6, 2000 (2.3m)	0.91	0.75	0.76	0.71	0.40	0.49	0.73	0.60	0.51

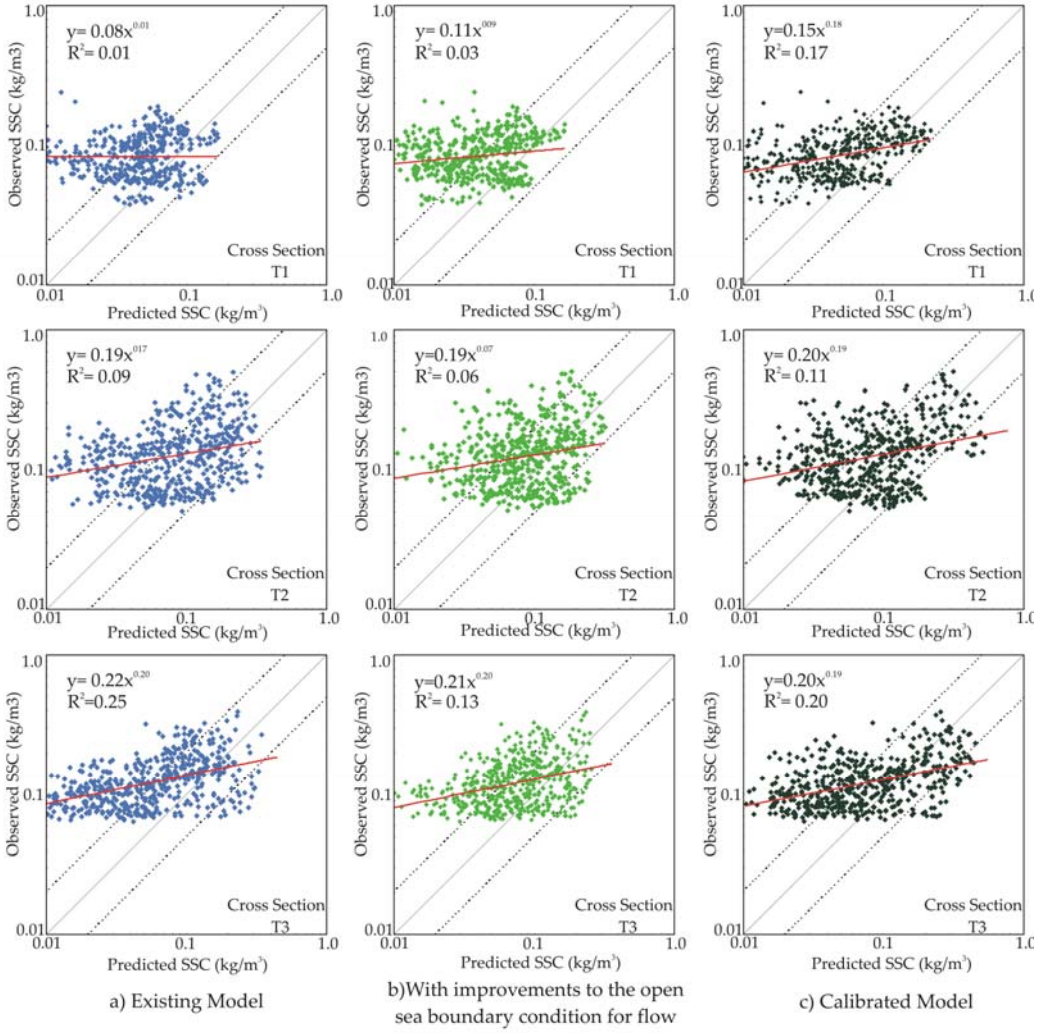

Figure 5.9 Performance of the 2DH Sediment Transport Model for prediction of Suspended Material Concentration at cross-sections T1, T2 and T3

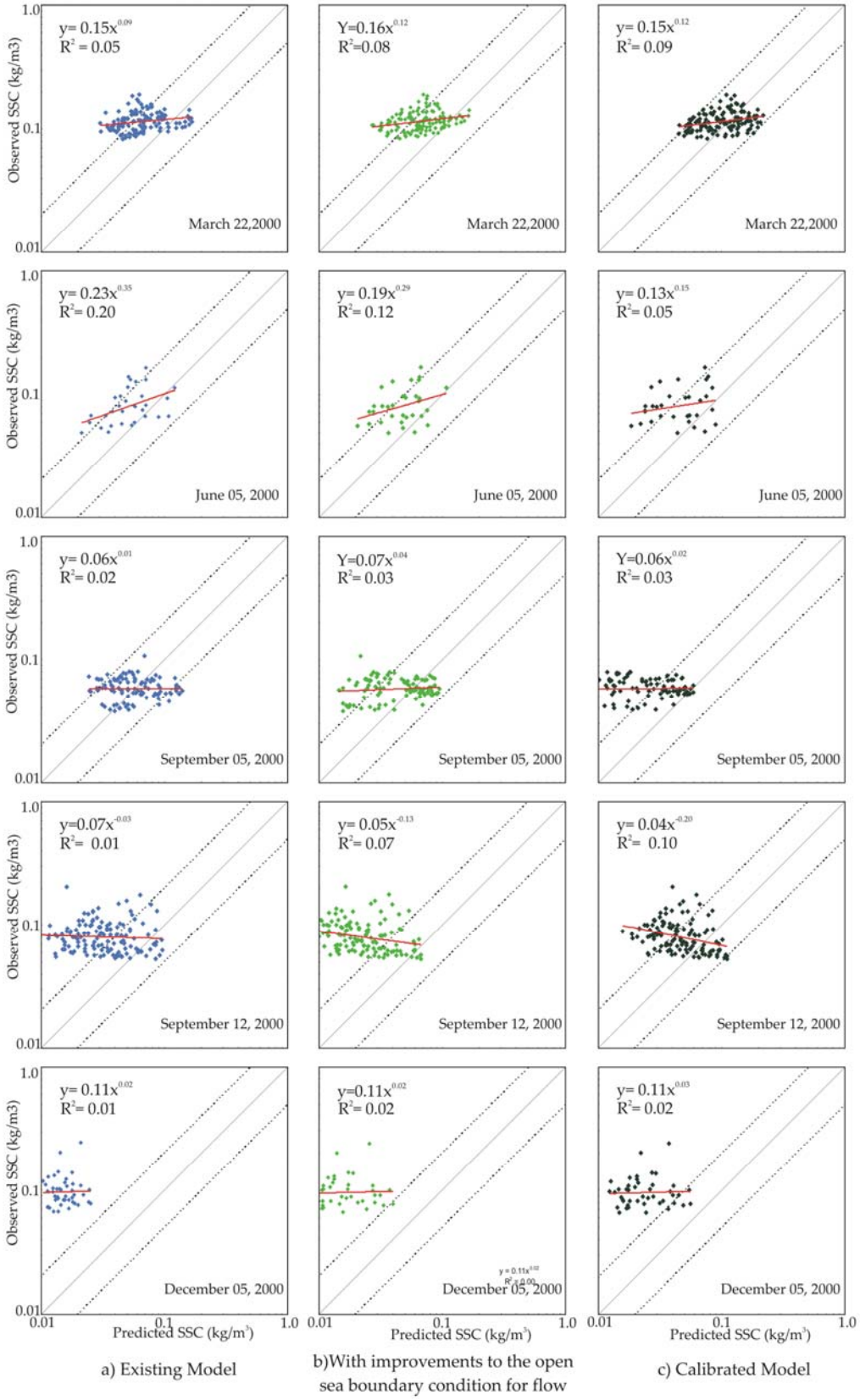

Figure 5.10 Performance of the 2DH Sediment Transport Model for prediction of Suspended Material Concentration at cross-section T1

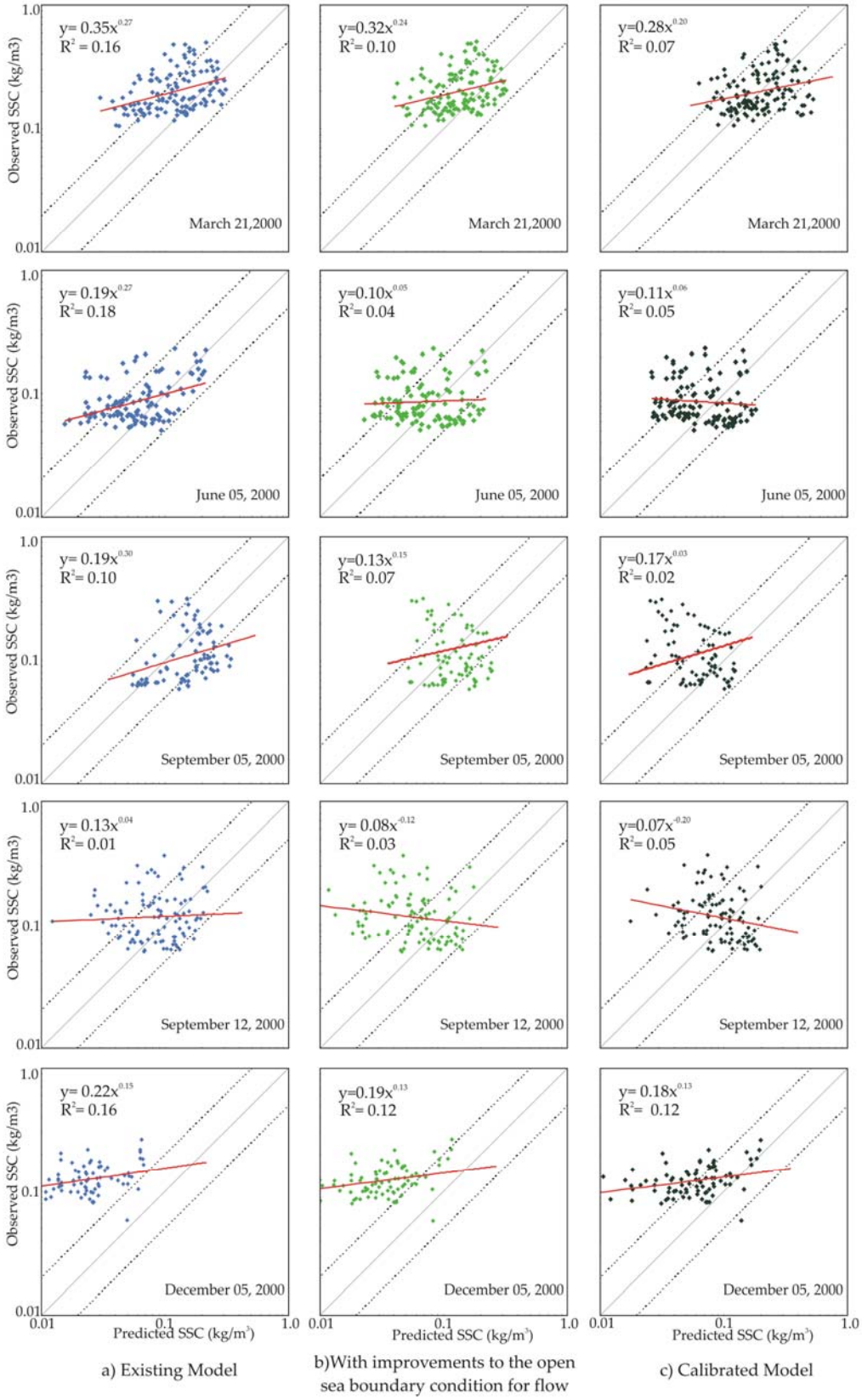

Figure 5.11 Performance of the 2DH Sediment Transport Model for prediction of Suspended Material Concentration at cross-section T2

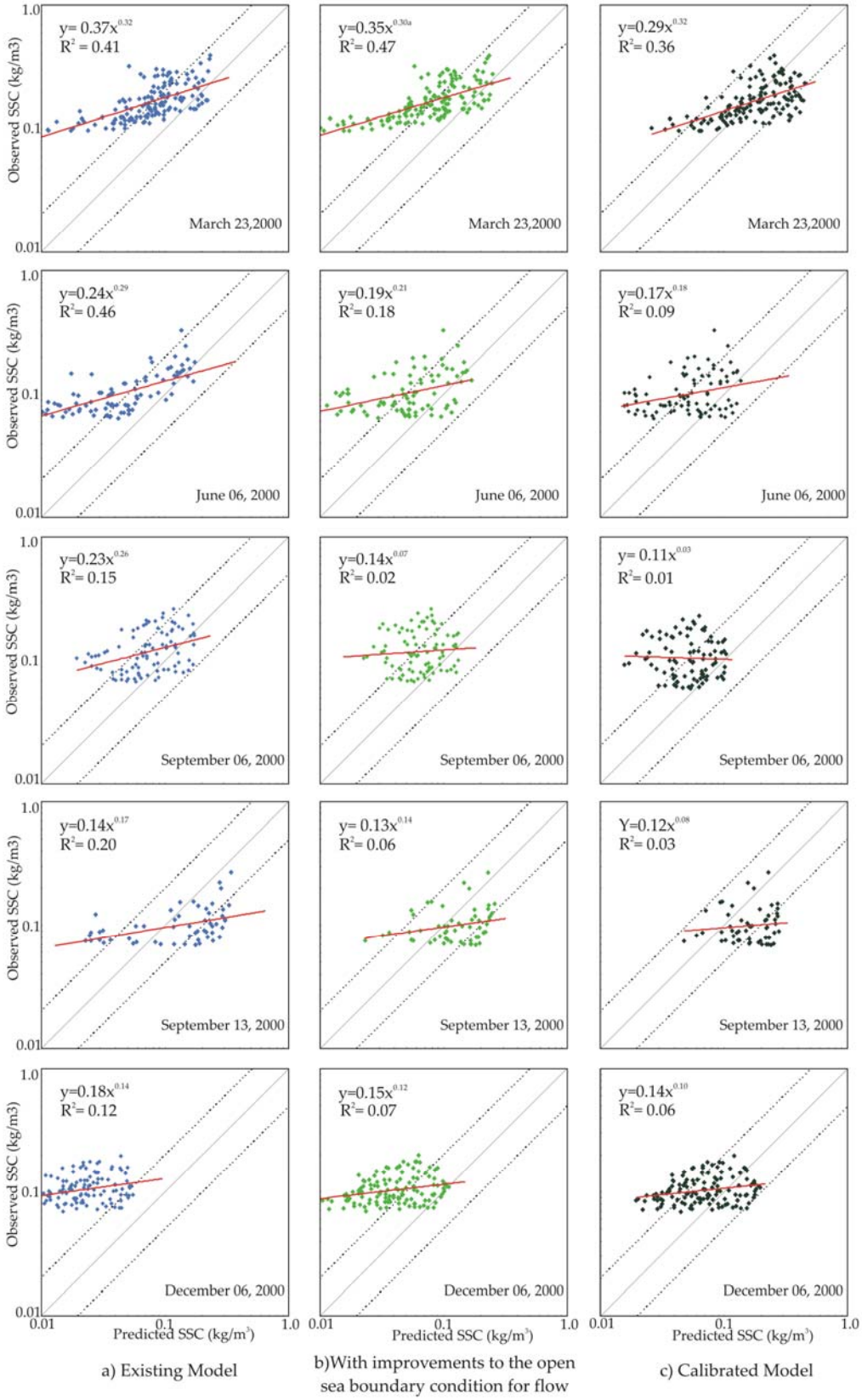

Figure 5.12 Performance of the 2DH Sediment Transport Model for prediction of Suspended Material Concentration at cross-section T3

5.3.2 Sensitivity studies

In this section two aspects that may affect the predictive ability of the sediment transport model were studied in detail. This includes: a) the assessment of the effect of the conditions specified along the open sea boundaries of the flow model (see Section 5.2.1.3) and b) the need to account for waves in the sediment transport simulations.

5.3.2.1 Relevance of the open sea boundary conditions for flow

In order to verify the influence of the conditions imposed along the open sea boundaries of the flow model on the sediment transport rates, additional simulations covering the whole range of tidal conditions were carried out (see Section 5.2.1.3). The same model settings adopted for the existing model were employed for these simulations (see Tables 5.2 and 5.3). For the water level variations at the open sea boundaries, the phase and amplitude corrections given in Table 5.1 were applied.

The resulting RMAE between measured and computed suspended sediment concentration at the cross-sections T1, T2, and T3 (Figure 5.1) are given in Table 5.4. On the basis of the RMAE values the open sea boundary conditions has a certain effect on the suspended sediment concentration. RMAE values for these simulations range between 0.35 and 0.71, while as stated previously for those from the existing model are between 0.39 and 0.91. Comparing RMAE values of the simulations with improvements to the open sea boundary conditions and those of the existing model, it can be seen that the predicting ability of the model has been improved at the most of the cross sections and particularly for the higher tidal ranges.

Scatter plots of the measured versus computed suspended material concentrations covering all the simulated conditions are shown separately for the three cross-sections at Figure 5.9b, ie. Improved boundary. The results are quite similar to those obtained from the existing model. It can be seen however, that the number of values that are within the factor of two has increased particularly for cross sections T2 and T3. The correlation coefficient between the computed and measured data however, is decreased from 0,09 to 0.06 for T2 and from 0.25 to 0.13 for T3, i.e. lower correlation between the predicted and the measured values, after applying the corrections at boundary conditions.

Figures 5.10b to 5.12b show scatter plots of measured versus predicted suspended material concentrations for the simulations with consideration of boundary corrections respectively at cross-sections T1, T2 and T3 separately for the five simulated periods. The corresponding best fit lines and correlation coefficients are also given. It can be seen while the corrections applied to the boundaries resulted that more points of the plots, specifically at cross section T2 (Figure 5.11b), being positioned within the factor of 2, the correlation between the predicted and observed values has been mostly decreased. The results revealed that the model needs further calibration (Section 5-3-3).

5.3.2.2 Relevance of waves

The relevance of waves in the sediment transport simulations was investigated. Simulations covering both moderate and extreme wind conditions were carried out. The effect of waves on the sediment transport was estimated on the basis of comparisons of the simulated suspended material concentrations with and without the presumption of wave effect. The assessment of the effect of waves on the suspended material concentration for moderate conditions covered the period from June 3 to 8, 2000. The period from November 29 to

December 5, 1999, during the Storm Anatol, was also selected for verifying the effect of the waves under more intense wind conditions.

Figure 5.13 shows the variations in water levels, significant wave heights, and suspended sediment concentrations with and without the effect of waves for the period of moderate wind conditions at a monitoring point C3 located at the middle of the cross-section T3 in the Piep tidal channel (see Figure 5.1). The tidal range during this period was about 3.7m and wind velocities were up to about 11m/s**.** During this period the significant wave heights at the observation point were up to about 0.45m. The effect of the waves on the suspended material concentration is considerable for significant wave heights higher than about 0.4m. The maximum discrepancy between the simulations with and without wave affect during the simulated period resulted approximately equal to 0.03kg/m^3. For predicting suspended material concentrations, it is necessary to couple wave and flow models when the significant wave heights exceeds approximately 0.4m.

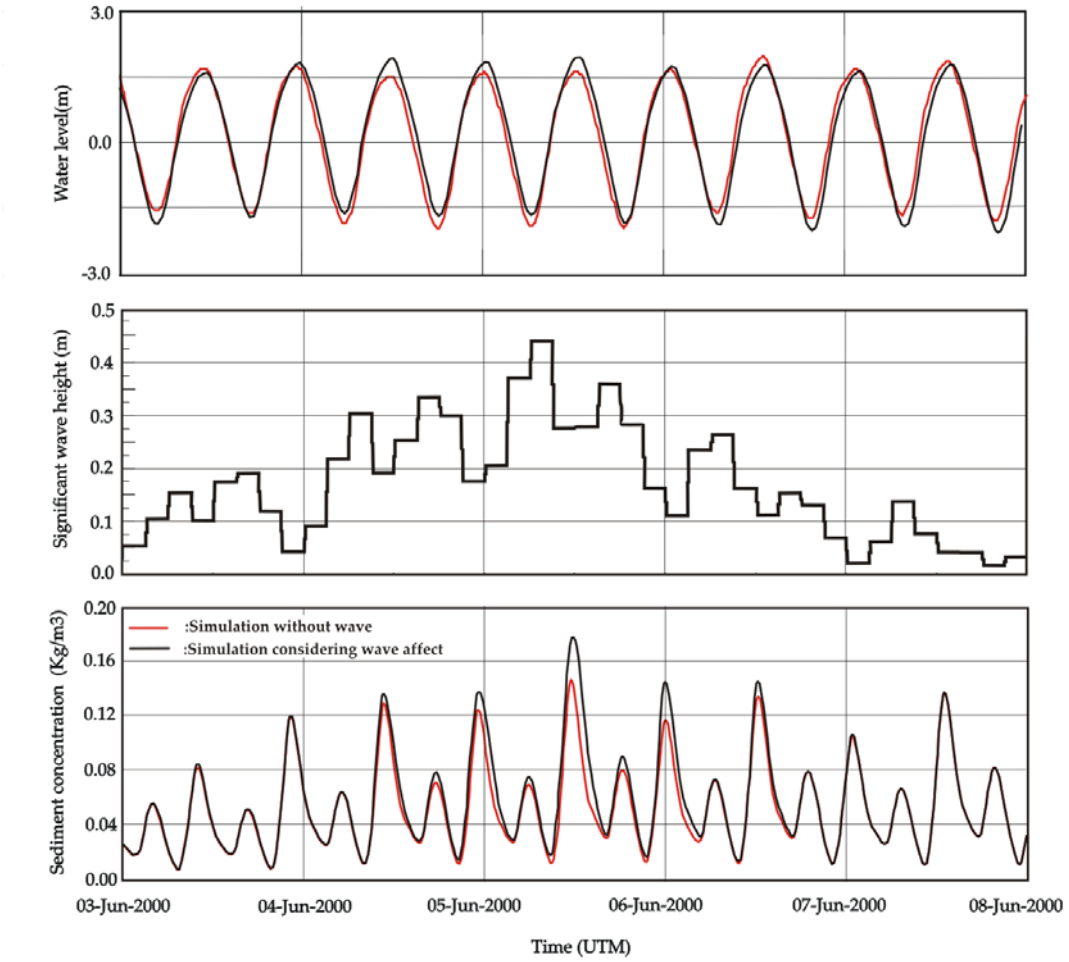

Figure 5.13 Effect of waves on the sediment transport for moderate wind conditions June 3 to 8, 2000

Figure 5.14 shows the variation in water levels, significant wave heights, and suspended sediment concentrations during the Storm Anatol. This period is characterised by a tidal range of about 6.0m and significant wave heights up to 2.2m. Comparisons of the results of the simulations with and without the effect of waves at the same monitoring point at cross-

section T3 were carried out. It can be seen clearly from the Figure that the effect of the waves on sediment transport cannot be ignored for stormy conditions. The maximum suspended material concentrations values derived from the model with waves (coupled flow and wave models) resulted up to 20 times higher than those from the simulation without the waves. Maximum suspended material concentrations of up to 0.2-0.3 kg/m^3 and up to 6kg/m^3 resulted respectively in the simulations without (flow only) and with the wave model (coupled flow and wave models). As mentioned before measured data for this period were not available for the comparison. However, the model results shown in Figure 5.14 are in agreement with the findings obtained on the basis of moderate wind conditions. That is, for the period in question the effect of waves on sediment transport becomes important for significant wave heights higher than about 0.4m. Thus it is again confirmed that whenever the significant wave heights exceed approximately 0.4m the effect of waves must be considered.

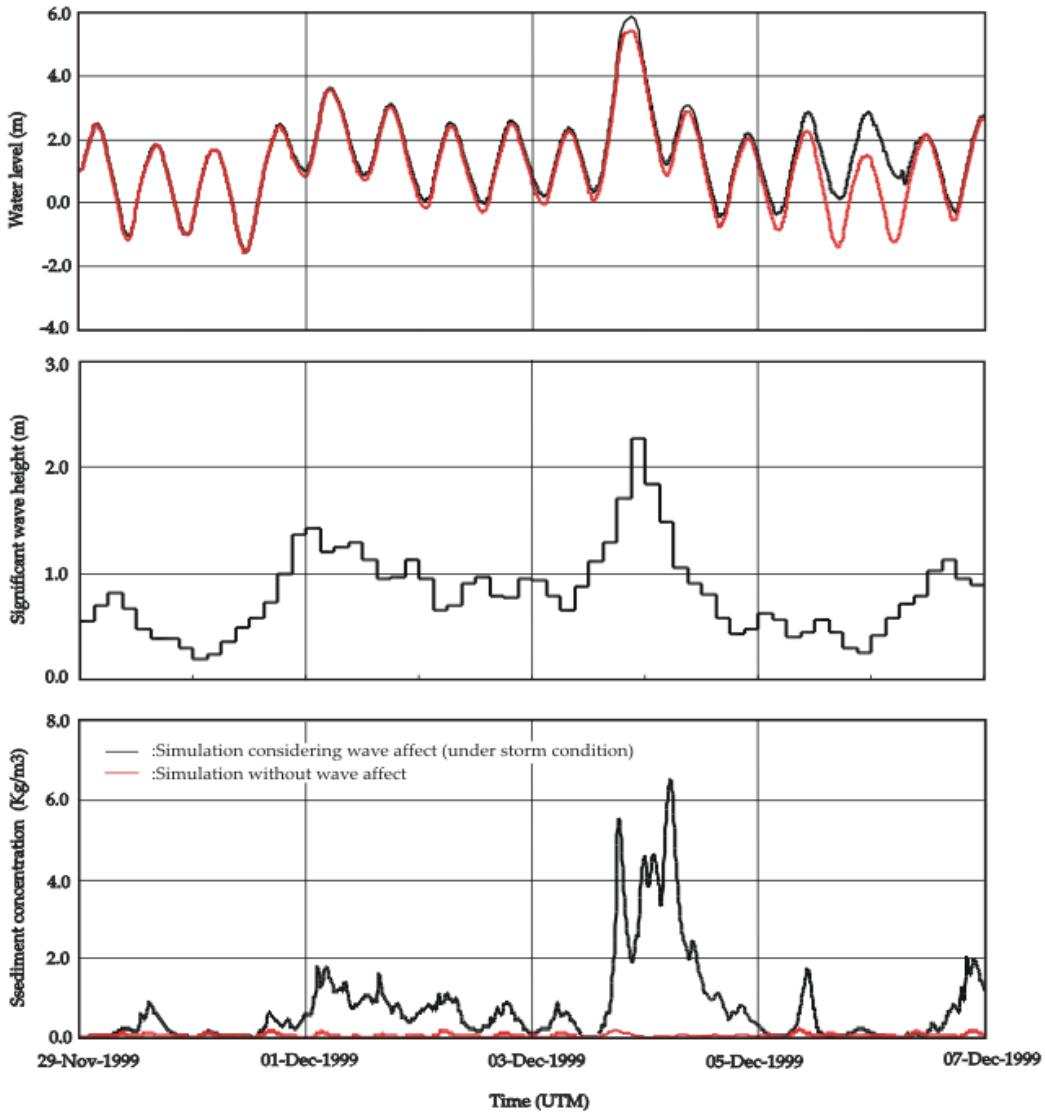

Figure 5.14 Effect of waves on the sediment transport for extreme wind conditions Storm Anatol

5.3.3 Model calibration

In this section the calibration of the 2DH sediment transport model and its output results are presented. Simulations were carried out with improved conditions along the open sea boundaries of the flow model. The calibration focused primarily on the adjustment of the properties of the mud fraction. The same field data used to check the performance of the existing model, were also employed for calibration. In this study it was aimed to derive more general model settings in terms of sediment properties for the mud fraction applicable to high tide (between 3.2 and 4.0 m) and low tide (between 2.0 to 3.0 m). The five sets of measuring conditions covering tidal ranges between 2.3 to 4m were split into periods with tidal ranges higher and lower than about 3m. Table 5.5 shows the sets of properties of the cohesive sediment fractions obtained as a result of the calibration.

All the measuring stations in cross sections T1, T2 and T3 and the entire range of tidal conditions have been considered for the statistical error analyses. The resulting RMAE between measured and computed suspended sediment concentration at the cross-sections T1, T2 and T3 are listed in Table 5.4. Except for the results at cross-section T3 corresponding to the tidal range of about 3m (RMAE=1), the RMAE values are slightly better and/or comparable to those obtained with the earlier model settings (see Table 5.3).

Table 5.5 Properties of the cohesive sediments used in the calibration

Parameters / Tidal conditions	Tidal range (m)	Settling velocity (mm/s)	Critical bed shear stress for sedimentation (N/m^2)	Critical bed shear stress for erosion (N/m^2)	Erosion parameter ($kg/m^2/s$)
High tides	**3.2 to 4.0**	**1.6**	**0.80**	**0.80**	**5.10×10^{-4}**
Low tides	**2.0 to 3.0**	**1.3**	**0.65**	**0.65**	**5.10×10^{-4}**

Figure 5.9c (Calibrated model) shows scatter pltos of the observed versus predicted suspended material concentrations at cross-sections T1, T2 and T3. With regard to the correlation coefficient it can be seen that the performance of the models after the calibration has been improved specifically at cross sections T1 and T2; i.e. from R^2=0.01 to R^2=0.17 at T1 and from R^2=0.09 to R^2=0.11 at T2, but from R^2=0.25 to R^2=0.20 at T3. The plots also reveal that more computed values are positioned within the factor of 2 of the measured data at all cross sections.

Figures 5.10c to 5.12c show scatter plots of measured versus predicted suspended material concentrations respectively at cross-sections T1, T2 and T3 separately for the five simulated tidal periods. The corresponding best fit lines and correlation coefficients are also given in the plots. Although no certain improvement in the correlation coefficients of the data observed, it can be seen that more predicted data are within the factor of 2 of field data for the majority of the plots. The discrepancies between the predicted and observed SSC are more significant at cross-section T2 (Figure 5.11c) with regard to cross-sections, and for the period December 5 to 6 with regard to the tidal range.

In general poor correlation between the model results and field data are observed. The reason for this weak correlation at this stage is not clear and is to be discussed in the next chapter. However, it should be pointed out that most of the sediment samples used for defining the sediment properties are from locations near cross-section T3. Therefore to improve the model performance, further sediment samples covering the entire model domain should be taken to enable a better description of the spatial variability of the sediment properties.

5.3.4 Model validation

In this section the results of the validation of the sediment transport model are summarised. Five sets of measurements, not used in the calibration, were employed for the validation. The data covers tidal conditions ranging between about 2.7 and 3.5m. The wind velocities during the measurements were up to about 10m/s. The same measuring strategy, devices and cross-sections, as described in Chapter 3, were employed to these sets of field data. Table 5.6 lists the measuring periods, number of stations across the cross-sections and the tidal ranges. It can be seen that most of the measurements were taken at cross-sections T3.

The model settings used in the calibration (Table 5.5) were used for the validation. The resulting RMAE between measured and computed suspended sediment concentrations at the cross-sections T1, T2 and T3 are listed in Table 5.6. The RMAE values vary between 0.51 and 0.62. These values are very much comparable to the results obtained from the calibrating simulations (Table 5.4).

Table 5.6 Model validation
RMAE values between modeled and measured suspended material concentrations

Tidal cycle	Nr. of measuring stations	Tidal range (m)	RMAE		
			T1	T2	T3
Mar. 14 to16, 2000	12	3.0-3.5	0.62	NM	0.55
June 13-14, 2000	14	3.0-3.3	NM	0.48	0.55
Dec. 12, 2000	4	3.2	0.42	NM	NM
June 22, 2001	9	3.6	NM	NM	0.51
June 28, 2001	7	2.7	NM	NM	0.51

NM: no measurements available

Figure 5.15 shows plots of the observed versus predicted suspended material concentrations at cross-sections T1, T2 and T3 for the five periods. The corresponding best fit lines and correlation coefficients are also given in the plots. Similar to the calibration, the predictive ability of the model resulted within a factor of two of field data for major points. The weak correlation between the model and field data also can be observed which is comparable to those of calibration.

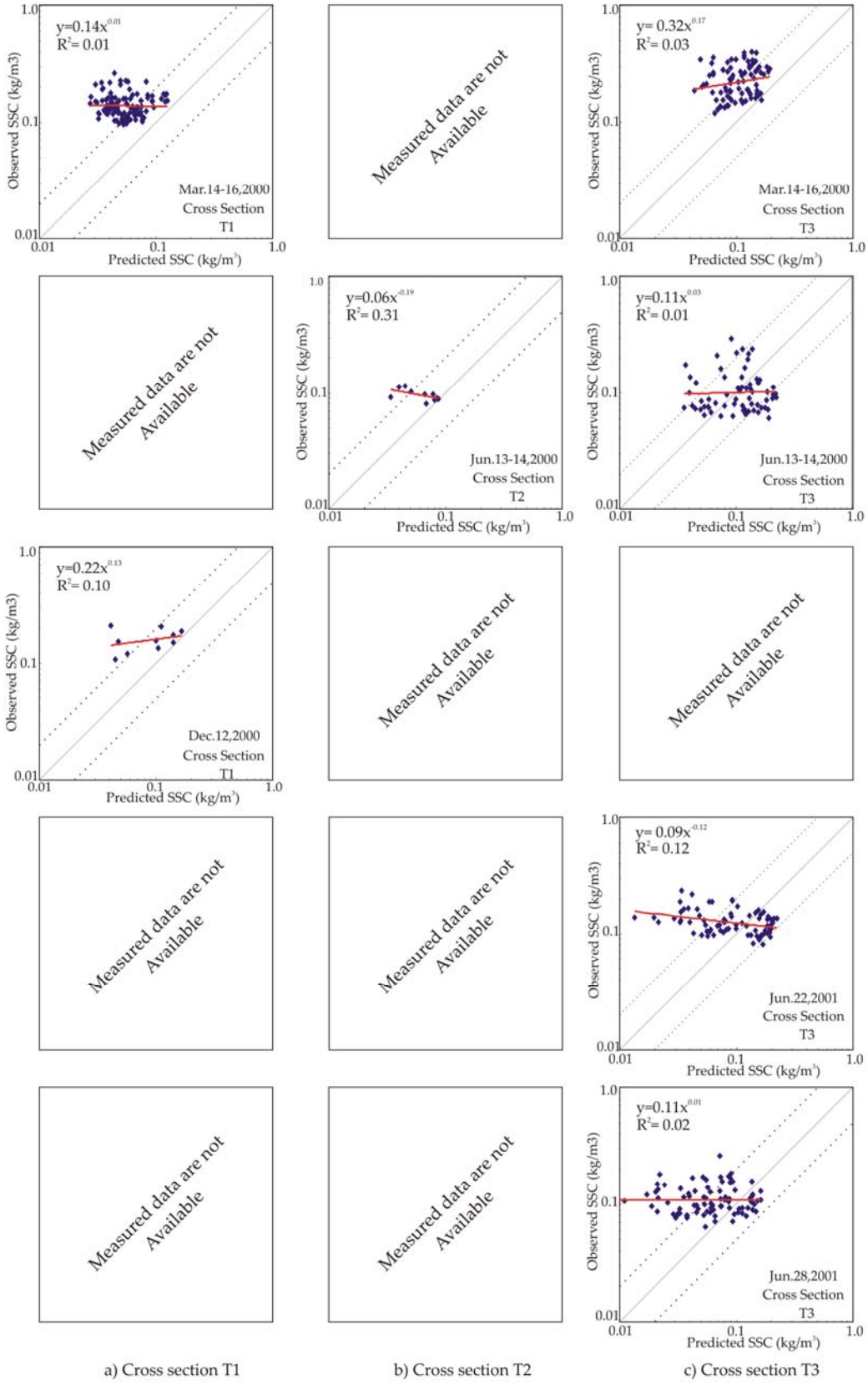

Figure 5.15 Validation of the performance of the calibrated 2DH sediment transport model for prediction of suspended material concentration at cross-sections T1, T2 and T3

5.3.5 Prediction of current velocity and suspended sediment concentration according to the tidal range

In this section the sensitivity of the predictive ability of the model to the varying tidal ranges are evaluated. The aim was on one hand to demonstrate the model ability in predicting current velocity and suspended sediment concentration (SSC) for the whole range of conditions and on the other hand to identify those tidal conditions for which some further improvements in the model are necessary. Thus a comparison of the measured data and the model results covering the whole tidal ranges were carried out. The investigations covered tidal ranges from 2.3 to 4.0m as listed in Tables 5.3 and 5.6. A detailed analysis of the measurements is summarised in Poerbandono and Mayerle (2005). The calibrated and validated 2DH flow and sediment transport model was used for this analysis.

Figure 5-16 shows the dependency of maximum depth averaged current velocities (left) and SSC (right) with tidal range separately for the cross-sections T1, T2 and T3. All the results derived from the calibrated model (red dots), and validated model (blue dots) in combination with the field data (black dots) are used for this analysis. In order to divide the results derived during the flood phase from those of the ebb phase the negative sign for both current velocity and SSC is used for the data derived during ebb condition.

The modelled and measured values of maximum depth-averaged current velocities are in good agreement with each other and approximately similar values resulted at each cross section for a given tidal range for both the model and field data. The best agreement between the modelled and measured results with regard to the current velocity is achieved in ebb conditions, which is more evident in cross sections T1 and T3. Slight underprediction however, is observed in model results for flood condition for all cross sections and in ebb condition for cross section T2. It can be seen that underprediction is more pronounced for the high tidal ranges.

With regard to SSC, underprdiction by the model can be seen in both ebb and flood phase for almost the whole tidal range. The variation of SSC along the tidal range for all the cross sections however, is not similar. The slightest variation SSC over the full tidal ranges was observed in cross section T1 for model and measured results. At the lower tidal range the model tends to underpredict SSC, however in the higher tidal range the model predictions are in good agreement with measured data. This is true for both ebb and flood conditions. In cross section T2 model tends to underpredict values of SSC for the whole tidal range in both ebb and flood conditions with respect to the available measured data. For the highest tidal range however (about 4m), some overprediction is observed in the flood condition (see cross section T2 in Figure 5.16). Underprediction of SSC by the model is also observed in cross section T3 for low and mean tidal range particularly during the ebb phase. However, the modelled and measured data at this cross section show good agreement in the high tidal ranges. The further assessment of the modelled SSC in regard to the underpredictions observed in this Chapter is discussed in Chapter 6.

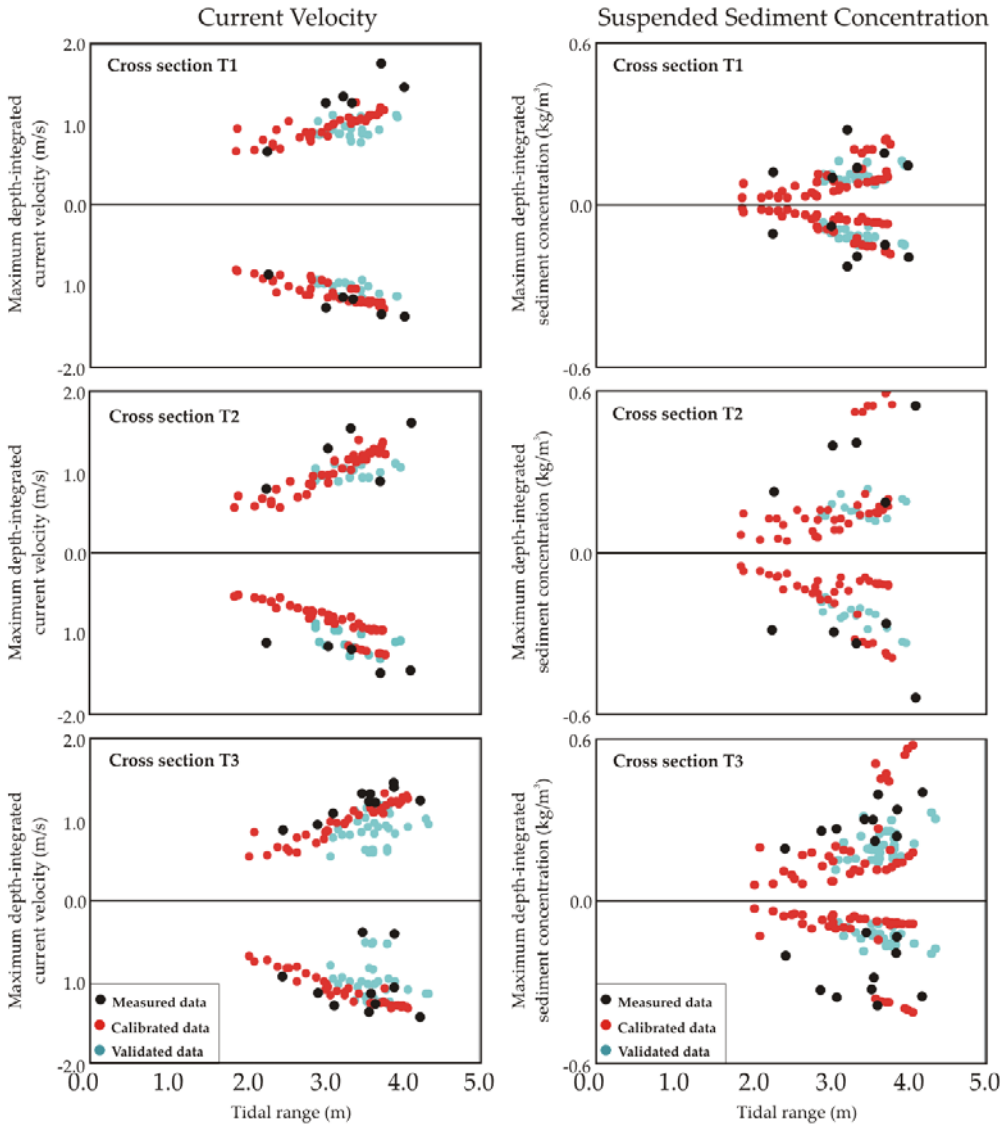

Figure 5.16 Comparison of measured and modelled variations of the max. depth averaged current velocities (left) and max. suspended sediment concentration (right) with tidal ranges at cross-sections T1, T2 and T3

5.4 Summary

In this chapter the results of the investigation on the performance of the existing 2DH flow and sediment transport model were presented and discussed. This involved the use and assessment of the model available at the beginning of this research. Scatter plots and Sensitivity analysis showed relatively poor correlation between the model results and the field data. Sensitivity analysis to identify the reasons for the discrepancies observed in water level performed by model and those from the field data model were also carried out.

The hypothesis that the conditions specified along the open sea boundaries may affect the performance of the model was tested. That is the water level variations at these boundaries as derived from the nesting procedure were evaluated by the 2DH model and the field data. The effect of subsequent corrections made to the amplitude and the phase of the water level

at these boundaries was also tested by the model results and the field data. It was found that the specification of water levels measured in the near vicinity of the western open sea boundaries and also employing corrections to the water levels predicted by the nesting sequence covering the adjacent coastal area provided good predictions of the water levels within the study area.

Calibration of the model was carried out with the aim to achieve general model settings in terms of sediment properties for the mud fraction applicable to high tide (between 3.2 and 4.0 m) and low tide (between 2.0 to 3.0 m). As far as the accuracy of the suspended sediment transport model is concerned, it was found that none of the models, including the existing model (Section 5-3-1), model with improvement to the open boundaries (Section 5-3-2-1), and calibrated model (5-3-3) could not predict the suspended sediment concentrations within a factor of two of the measured data for all the values. The correlation between the model results and the field data was quite poor in all the models. The range of the correlation varied between 0.11 (cross section T2) and 0.20 (cross section T3) for calibrated model. The reason for the poor correlation between the modelled and measured data is not quite clear at this stage, and is to be discussed in more detail in next Chapter. It looks as though that the predictive ability is very much dependent on the sediment characteristics in the area. As there is a strong gradient between the sediment data from the outer to the inner parts, further measurements covering the entire domain are recommended. This would provide the description of the spatial variability of the input data.

The effect of waves on values of the water level and the suspended material concentrations was also examined by coupling wave and flow model. It is shown that the effect of waves on the flow and to a certain extent on the sediment transport is negligible for moderate winds and waves. However, the effect of waves on suspended sediment concentration becomes important for significant wave heights equal or higher than about 0.4m. Furthermore the suspended sediment concentrations during extreme winds were found to be affected extremely by waves. The model suggests that the significant wave height of about 2.2m increases the peak SSC by about 20 times. The field data for this condition however was not available to verify the model results.

It was understood that the predictive ability of the 2DH coupled flow, waves and sediment transport model for predicting hydrodynamic is reasonably good and to some extent for predicting suspended material concentrations is acceptable. In overall the results obtained indicate that the model tends to underpredict values of suspended sediment concentration at all cross sections.

Chapter 6. Performance of the 3D Sediment Transport Model

6.1 Introduction

In this chapter, the results of investigations for the current velocity and the suspended sediment concentration computed using the three-dimensional (3D) model are presented. The calibrated and validated 2DH model, described in Chapter 5, was extended to the 3D model. For the 3D simulation, the wind effects were considered by means of the Prisma wind data, as given in Chapter 3. Based on the conclusion in Chapter 5 the effect of the waves was disregarded for moderate conditions for which the significant wave height is less than 0.4 m.

The performance of the 3D model is assessed through comparisons of the outputs of the 3D and 2DH models with the data from the field measurements. Graphical and statistical analyses have been employed for these comparisons.

6.2 Selection of number of layers and Turbulence closure module (TCM)

It is known that the computational time for simulation depends on the number of grid points, including the points on the vertical grid. Thus the more the number of layers the more time is needed for the computation. On the other hand decreasing the number of layers along the depth may decrease the accuracy of the results. An optimum number of layers therefore, should be chosen to keep the computational time low with reasonable accuracy of the results. Several simulations were executed using different numbers of layers. These are: one simulation with 5 equal thicknesses of the layers, and four simulations with unequal thicknesses of 5, 7, 10, and 12 layers along the depth. For these unequal thickness layers the thicknesses varied logarithmically from the bed to the surface. This was used on the suggestion by the Delft3D manual and in consideration of the fact that in open channel flow vertical velocity profile is generally logarithmic.

The results of suspended sediment concentrations (SSC) obtained from these simulations and those from the 2DH model were employed for the sensitivity analyses. Figure 6.1 shows

SSC time series at the middle point of the cross section T3 (point C3 in Figure 5.1) for near bed and near surface layers derived from all above-mentioned simulations. As the values available for the 2DH simulations were depth averaged ones, the SSC time series from 2DH simulation are similar in both graphs of the Figure. From the Figure it can be observed that the sensitivity of the model to predict suspended sediment concentration depends highly on the numbers of layers employed. Table 6.1 represents in a compact form the averaged sensitivity of the above mentioned simulations to predict SSC for near surface layers (to the right of the yellow coloured cells) and for near bed layers (below the yellow coloured cells). The results show that by increasing the number of layers from 10 to 12 the sensitivity of the model for SSC is insignificant. In the context of the sensitivity they are about 2.0% in the near bed layer and about 1.5% in the near surface layer.

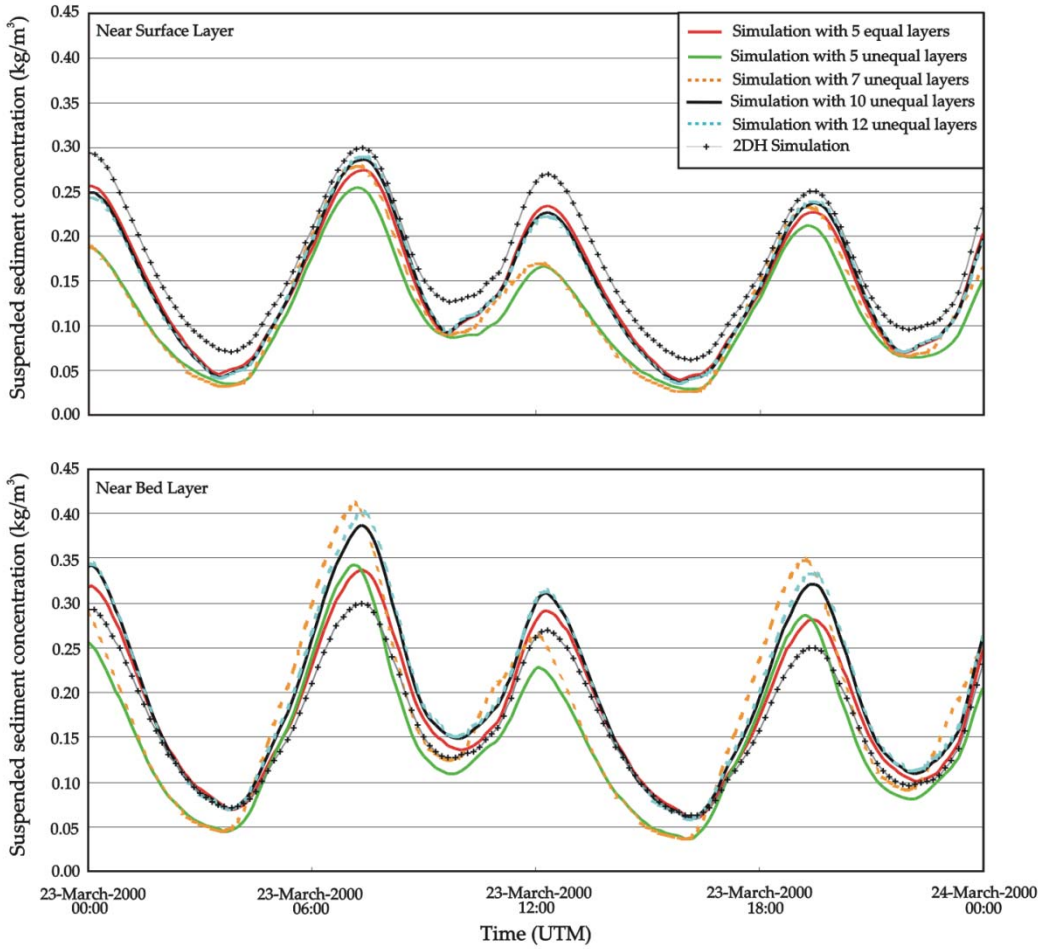

Figure 6.1 Time series of suspended sediment concentration for different number of layers across the depth for near surface (up) and near bed (down) layers

The SSC values from all the above mentioned 3D simulations and those from the 2DH model together with the field data were used to prepare profiles for four different tidal phases: flood, high slack water, ebb, and low slack water. Figure 6.2 shows the suspended sediment concentration profiles along middles of cross section T1, T2, and T3 (C1, C2, and C3 respectively in Figure 5.1). From the Figure, it can be observed that there is a large difference between the model results employing different numbers of layers especially at cross section T2 during high and low slack water. It can also be seen that none of the model results are in

perfect agreement with the field data at all the observations points presented in the Figure. However, a relatively good agreement between the model results and the field data can be observed for the cross section T1.

For the statistical analysis, the relative mean absolute error (RMAE) of the SSC from all simulations with different numbers of layers in comparison with the field data were calculated, and are presented in Table 6.2 for cross-sections T1, T2 and T3. The best results are achieved when 10 and 12 unequal layers, with logarithmic distribution, are employed. This achievement applies for individual cross section and for the average of all cross sections. Considering these results together with those from sensitivity tests, the 10 unequal layers of logarithmically distributed thicknesses along the depth of the flow were selected for subsequent investigations in this Chapter.

Table 6.1 Sensitivity analysis of the simulations employing different number of layers in regard to the SSC prediction

	2DH Simulation	Simulation with 5 equal layers	Simulation with 5 Unequal layers	Simulation with 7 layers	Simulation with 10 layers	Simulation with 12 layers
2DH Simulation	Sur. → / Bot. ↓	17.20%	33.52%	30.07%	17.45%	18.06%
Simulation with 5 equal layers	7.29%	Sur. → / Bot. ↓	27.24%	25.72%	3.86%	5.46%
Simulation with 5 Unequal layers	7.29%	28.90%	Sur. → / Bot. ↓	7.82%	19.86%	19.22%
Simulation with 7 layers	23.59%	27.56%	12.73%	Sur. → / Bot. ↓	16.87%	16.12%
Simulation with 10 layers	15.11%	7.24%	24.66%	19.35%	Sur. → / Bot. ↓	1.53%
Simulation with 12 layers	15.11%	8.95%	25.66%	18.77%	2.02%	

Bot: Bottom layer results

Sur: Surface layer resutls

Table 6.2 RMAE values for suspended sediment concentration derived from the field and those of simulated results employing different number of layer configurations

Simulation with different layers	RMAE				Rank
	T1	T2	T3	Average	
5 equal layers	0.47	0.48	0.43	0.46	3
5 layers	0.52	0.57	0.53	0.54	5
7 layers	0.31	0.59	0.58	0.49	4
10 layers	0.27	0.45	0.44	0.39	1
12 layers	0.29	0.45	0.43	0.39	2

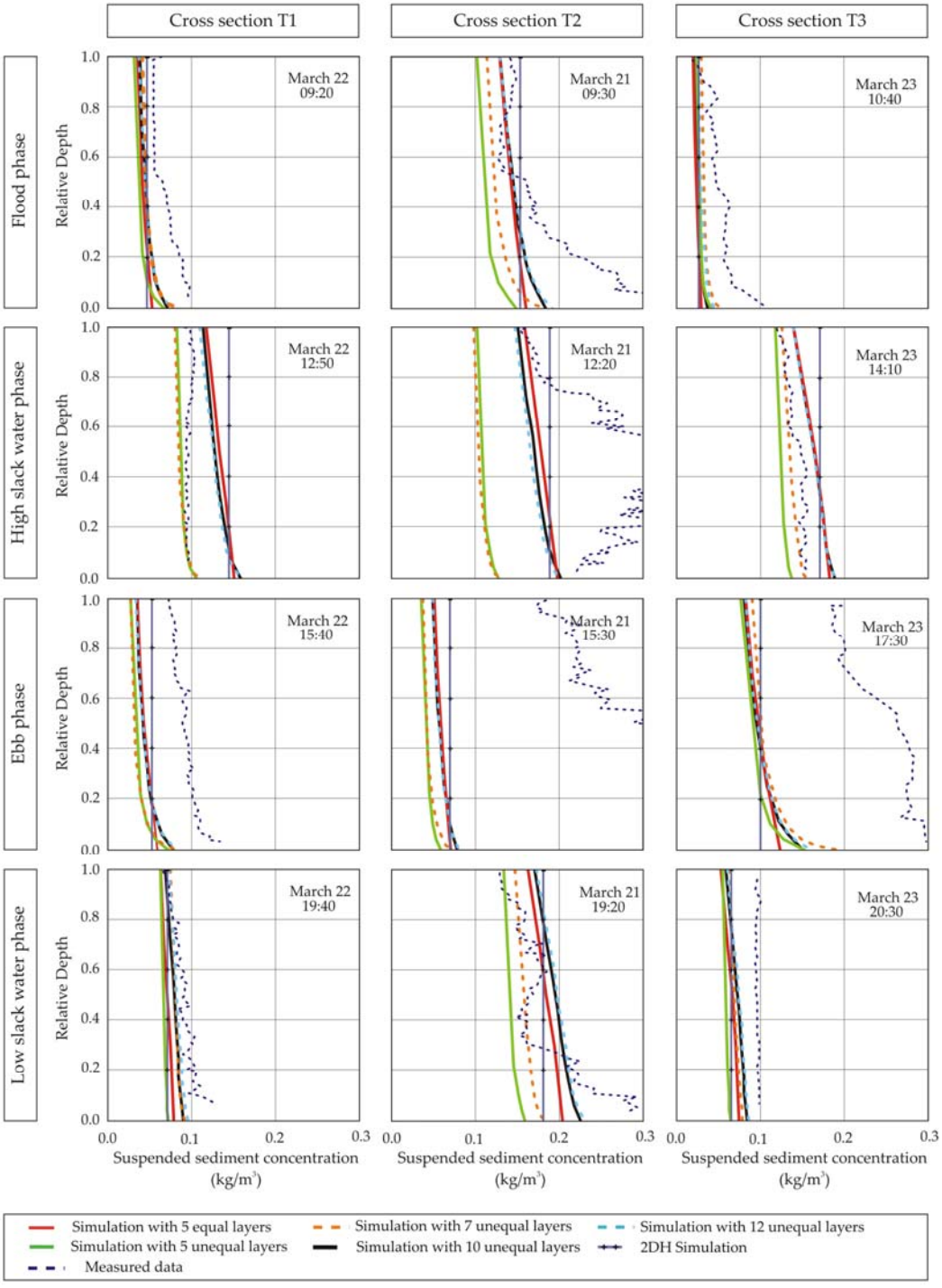

Figure 6.2 Suspended sediment concentration profiles from 3D simulations with equal thicknesses of 5 layers, unequal thicknesses for 5, 7, 10 and 12 layers, together with profiles from 2DH simulations and field data for cross sections T1, T2, and T3. From the left: Flood phase (first row), High slack water (second row), Ebb phase (third row), and Low slack water phase (forth row)

When the 2DH model is extended to 3D model, a turbulence closure module should also be defined to it. As mentioned in Section 4-3-4-3, four turbulence closure modules (TCM) are available to set up the 3D model. Three of them: the algebraic, k-l, and k-ε modules were

used and simulations carried out for sensitivity analysis. Comparison of the results of the suspended sediment concentration (SSC) derived from the simulations using different TCM showed only slight differences. The statistical error analysis, RMAE was employed, with the field data and the computed SSC values from the three simulations, at the cross-sections T1, T2 and T3 to evaluate the performance of each of the models. The RMAE vales presented in Table 6.3 prove that employing each of the three TCM modules does not significantly change the predicted values of the SSC. In view of the values of RMAE and taking into account the well-mixed nature of the flow and also the usage of 10 vertical layers, it is decided that the use of k-l module is appropriate for the area under the investigation (see section 4-3-4-3).

Table 6.3 RMAE for suspended sediment concentration derived from field and those of simulated results using different turbulent closure modules

Simulation with different TCMs	RMAE			
	T1	T2	T3	Average
k-l module	0.27	0.45	0.44	0.39
k-ε module	0.27	0.46	0.44	0.39
Algebraic module	0.27	0.45	0.44	0.39

At that stage of the investigation the suspended sediment concentration (SSC) outputs from 3D model, using 10 numbers of layers and k-l turbulence module, were compared with those from the corresponding 2DH model. Simulations in 3D were carried out with the same input data and for the same tidal periods as those used for the calibrated 2DH model (Section 5-3-3).

The values of the RMAE between the SSC results derived from 3D simulations and the measured data were calculated for the cross-sections T1, T2 and T3, and compared with the corresponding values from the 2DH simulations (from Table 5.5). The results are shown in Table 6.4. Referring to the Table it can be seen that in all the simulations for all tidal periods, the RMAE for 3D simulations, at cross section T1, are lower than those from 2DH simulations; but at both cross sections T2 and T3 only three out of five of values are lower. While the procedure to calculate RMAE for 3D and 2DH is different, it can be questioned whether the 3D simulations lead to any improvement in the results. However, it is seen that the range of the RMAE deviation between 3D and 2DH results is not excessive (up to about 35%).

Table 6.4 RMAE values between modeled and measured SSC for 2DH and 3D simulations

Period (tidal range)	RMAE for 2DH simulation			RMAE for 3D simulation		
	T1	T2	T3	T1	T2	T3
March 21-23, 2000 (4.0 m)	0.31	0.40	0.48	0.27	0.45	0.44
June 5-6, 2000 (3.7m)	0.49	0.50	0.50	0.39	0.44	0.54
September 5-6, 2000 (3.2m)	0.52	0.45	0.62	0.51	0.58	0.79
September 12-13, 2000 (3.0m)	0.47	0.47	1.00	0.42	0.40	0.66
December 5-6, 2000 (2.3m)	0.73	0.60	0.51	0.61	0.52	0.48

6.3 Comparison between 3D model results and field data

6.3.1 Performance of the model in regard to the current velocity

To assess the predictive ability of the 3D model with respect to the hydrodynamics of the area, the current velocities derived from the model were compared with those from the field. At each layer, the current velocities at all monitoring points of each cross section were interpolated across the width of the cross section for the duration of one full tidal cycle. For the purpose of comparison the results reported by Poerbandono and Mayerle (2005) were used. They used the field data and calculated the depth-averaged values for the current velocity to present the variations of the variable for the same tidal period. The variations of current velocities at each layer of the cross sections during the full tidal cycle are presented in colour-coded contours in Figures 6.3 to 6.5 for cross sections T1, T2, and T3 respectively. In these Figures from the top are the graphs of water level time series followed by the field data contours in shades of grey colour (Poerbandono and Mayerle, 2005), and the model results at three representative layers: near the surface, the mid-depth, and near the bed layers. The corresponding cross section profiles are presented on the left hand side of each graph. The red line in each profile is the position of the representative layer.

Referring to the model graphs, the gradual decrease of current velocities from the surface layers to the bed layers is seen in all the cross sections. The model graphs also show that the peak velocity values at the bed layers are specifically lower than those at the surface layers. The temporal and spatial positions of the peak velocities however, are similar at different layers. Comparisons between the field data and model results of the three cross sections showed similar patterns of spatial and temporal variations of current velocity in all cross sections. The peak current velocity of the field data and the model results exactly coincide spatially and temporally at all the cross sections. It can be seen, for instance, in Figure 6.5 that the model is able to reproduce two peak velocities northward and southward of the cross section T3 during flood phase which conforms with the field data plot. The results prove the capability of the 3D model to predict current velocity in reasonable agreement with the field data. The capability of the 2DH model regarding the hydrodynamics prediction is investigated by Palacio et.al. (2005). They reported that the mean absolute error of predicted current velocity by the model is less than 0.2 m/s.

As the peak velocity is higher in the flood phase than that in the ebb phase at all of the three cross sections, the channels can be considered as flood dominated. However, if the time durations between reversal of the peak velocities for the consecutive flood to ebb and ebb to flood tidal cycles are considered (Groen, 1967), the flood domination condition will apply only to the cross sections T1 and T2. With respect to measured data, Mayerle and Zielke (2005) and Toro et. al. (2005) also reported the domination of flood at these two cross sections. In cross section T3 however, the time durations between reversal of the maximum velocities for both the consecutive flood–ebb and ebb–flood tidal cycles are equal to about six hours. That is a no flood or ebb dominated condition can be suggested.

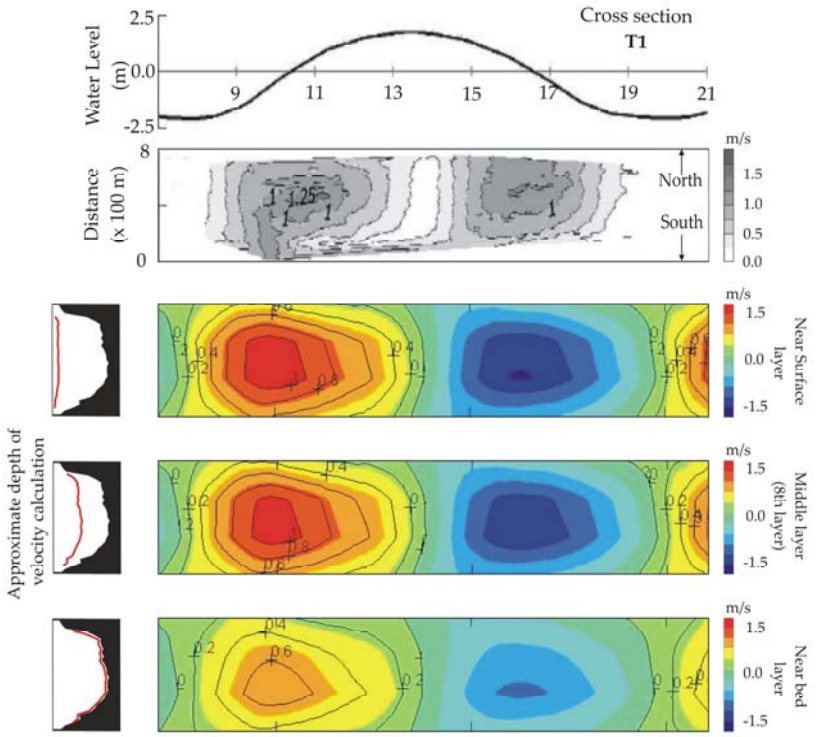

Figure 6.3 From the top: water level time series, the field data contours of depth averaged velocity (Poerbandono and Mayerle, 2005), Colour coded contours graphs of the velocity from the model for the near surface, at middle depth, and near bed layers for Cross section T1

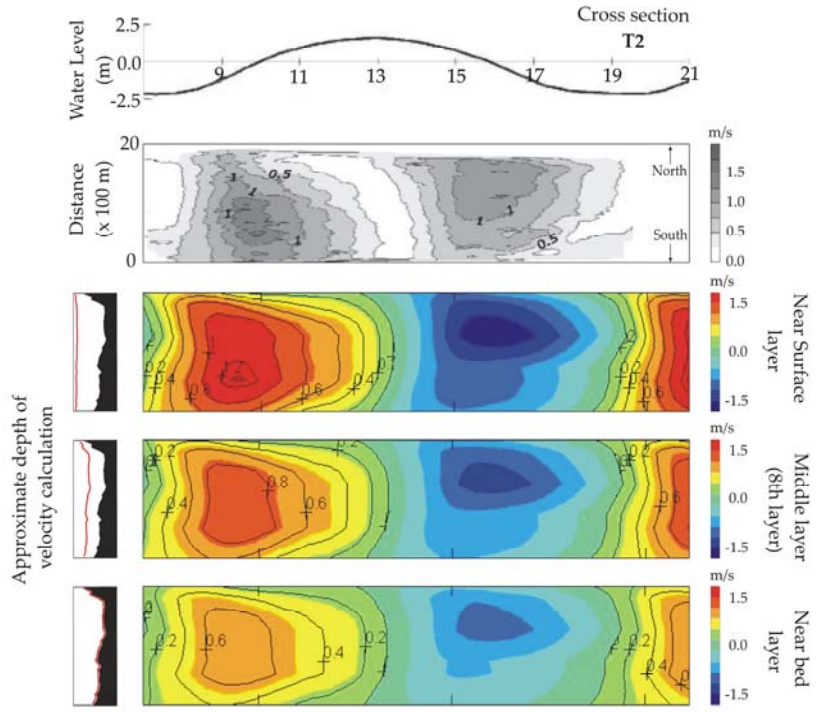

Figure 6.4 From the top: water level time series, the field data contours of depth averaged velocity (Poerbandono and Mayerle, 2005), Colour coded contours graphs of the velocity from the model for the near surface, at middle depth, and near bed layers for Cross section T2

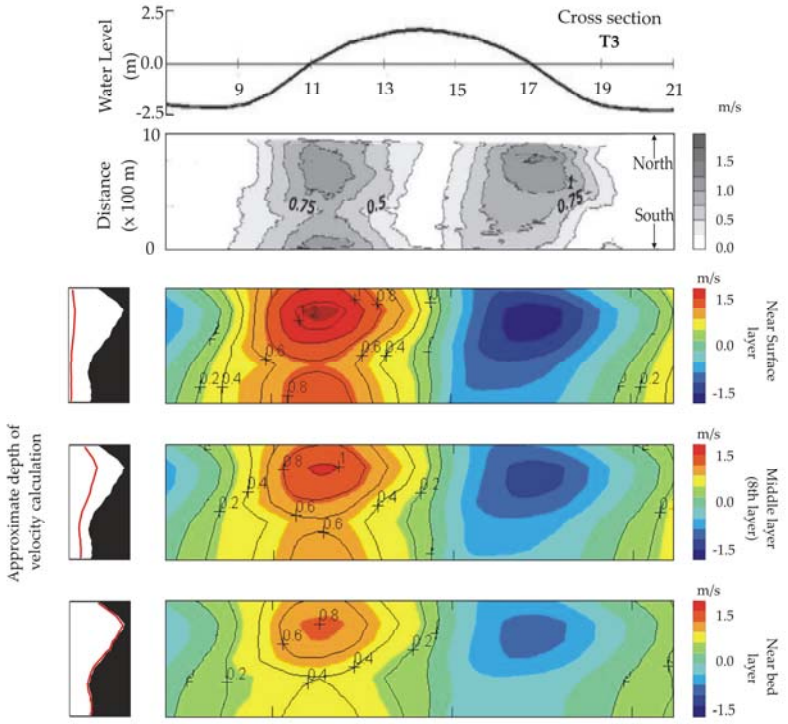

Figure 6.5 From the top: water level time series, the field data contours of depth averaged velocity (Poerbandono and Mayerle, 2005), Colour coded contours graphs of the velocity from the model for the near surface, at middle depth, and near bed layers for Cross section T3

6.3.2 Current Velocity and Sediment Concentration Profiles

In this section the variations of the current velocity and the suspended sediment concentration (SSC) along the depth obtained from the 3D and the 2DH simulations are compared with those of field data. As the data collection at various points relate to certain time, the model results had been extracted in such a way that their times and locations matched with the times and the locations of the field data. The time difference between the field data and the model results for comparison never exceeded 5 minutes, and the spatial difference of the points in the field data and the model did not exceed 50 meters. This was found reasonable in view of the grid length being 90m. Typical profiles of the current velocity and suspended sediment concentration for all monitoring points in cross-sections T1, T2 and T3 are presented in Figure 6.6 and Figure 6.7 for the high slack water and ebb phase, respectively. The sets of data are those collected on 21, 22 and 23 of March 2000, covering a sequence of spring tides with an average tidal range of about 4m.

From Figures 6.6 and 6.7 it can be seen that the current velocity profiles derived from the 3D and the 2DH simulations are in good agreement with each other. These profiles are also in good agreement with those of field data, with the exception of profiles 1 and 3 corresponding to cross section T1 in ebb phase (Figure 6.7). The disagreement in these profiles could possibly be due to measurement error, since the results from the models are in good agreement with the measurements in all the other monitoring points of the same cross section. Besides, the capability of the model to predict current velocity has been verified as presented in the previous section.

The SSC profiles derived from the 3D and 2DH simulations are also in quite good agreement with each other for the two tidal conditions, especially where the variation of SSC along the depth is negligible (cross section T1 in both Figures). For the positions where the variation of the SSC along the depth is not uniform, 2DH results are in agreement with 3D results at near surface (cross sections T2 and T3). Concerning the field data following observations for cross sections T1, T2, and T3 are made:

At the cross section T1 and during the high slack water (Figure 6.6) all the SSC profiles for all the monitoring points are in reasonable agreement with the model results. During the ebb phase (Figure 6.7) this reasonable agreement is specifically deserved for two out of four monitoring points (profiles 1 and 2). In the cross section T2, the SSC profiles derived from 3D model are generally in good agreement with the field data in monitoring points 1 to 4 especially during the ebb condition. Marked disagreement is evident between the model results and field data in profiles 7 to 9 during slack water (Figure 6.6) and in profiles 5 to 9 during the ebb condition (Figure 6.7) especially from the near bed layer to the middle of the depth. In the cross section T3, the SSC profiles derived from 3D model show overprediction during the high slack water phase in profiles 2 to 5 and underprediction in the near bed layers of profiles 6 and 7 (Figure 6.6). During the ebb condition underprediction is evident in all of the monitoring points except for profile 2. The degree of underprediction is larger in the shallow water regions of the cross section (profiles 4 to 7 in Figure 6.7). Comparisons between the SSC profiles derived from the model and those of the field data during the full tidal cycle revealed that certain dissimilarity exists between the model results and field data at shallow water regions of the cross sections specifically during the ebb phase. The shallow water regions of the cross sections consist of monitoring points 6 to 9 in cross section T2, and monitoring points 4 to 7 in cross section T3.

Variations of the suspended sediment concentration (SSC) predicted by the model in comparison with those of the field data along the depth for duration of the ebb and the flood phases are assessed. For this purpose the ratios of the observed (field data) to the predicted SSC along the depth were calculated at the cross sections T2 and T3. The plots of the variation of these ratios with respect to the depth of flow are shown in Figures 6.8 and 6.9, respectively for cross section T2 and T3. In each cross section two monitoring points, one in the shallow water region and the other in deep water region were used. In each Figure, the plots for the ebb phase are on the left and those for the flood phase on the right. The monitoring point in shallow water region and its corresponding results are shown in blue and those for the deep water are presented in red. It can be seen clearly that the ratio of observed to predicted SSC for the monitoring points in shallow water is larger than those in the deep water at both cross sections. It can also be seen that the ratio during the ebb condition are much higher than that during flood phase especially in near bed layers. Figures 6.8 and 6.9 confirm again that the model results during the ebb condition are not in a good agreement with those of the field data.

The dissimilarities between the SSCs predicted by the model and obtained from the field in the shallow water area can be explained in terms of deficiency in the model and existence of some error in measurements collected at shallow water regions. These subjectes are discussed to some extent below.

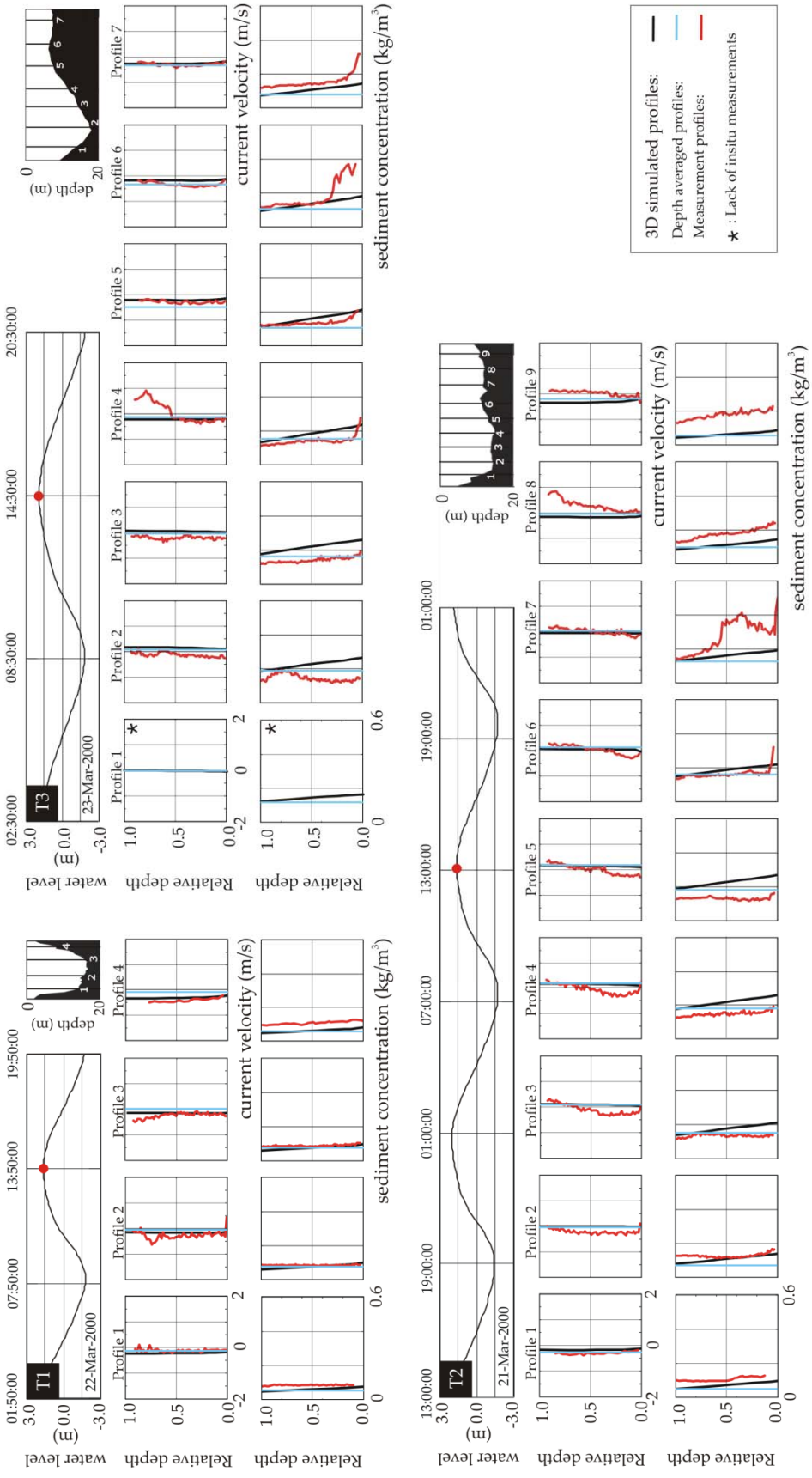

Figure 6.6 Current Velocity and Suspended Sediment Concentration Profile derived from 3D model, 2DH model and in situ measurements during the *high slack water* for cross sections T1 (in Norderpiep channel), T2 (in Süderpiep channel), and T3 (Piep channel)

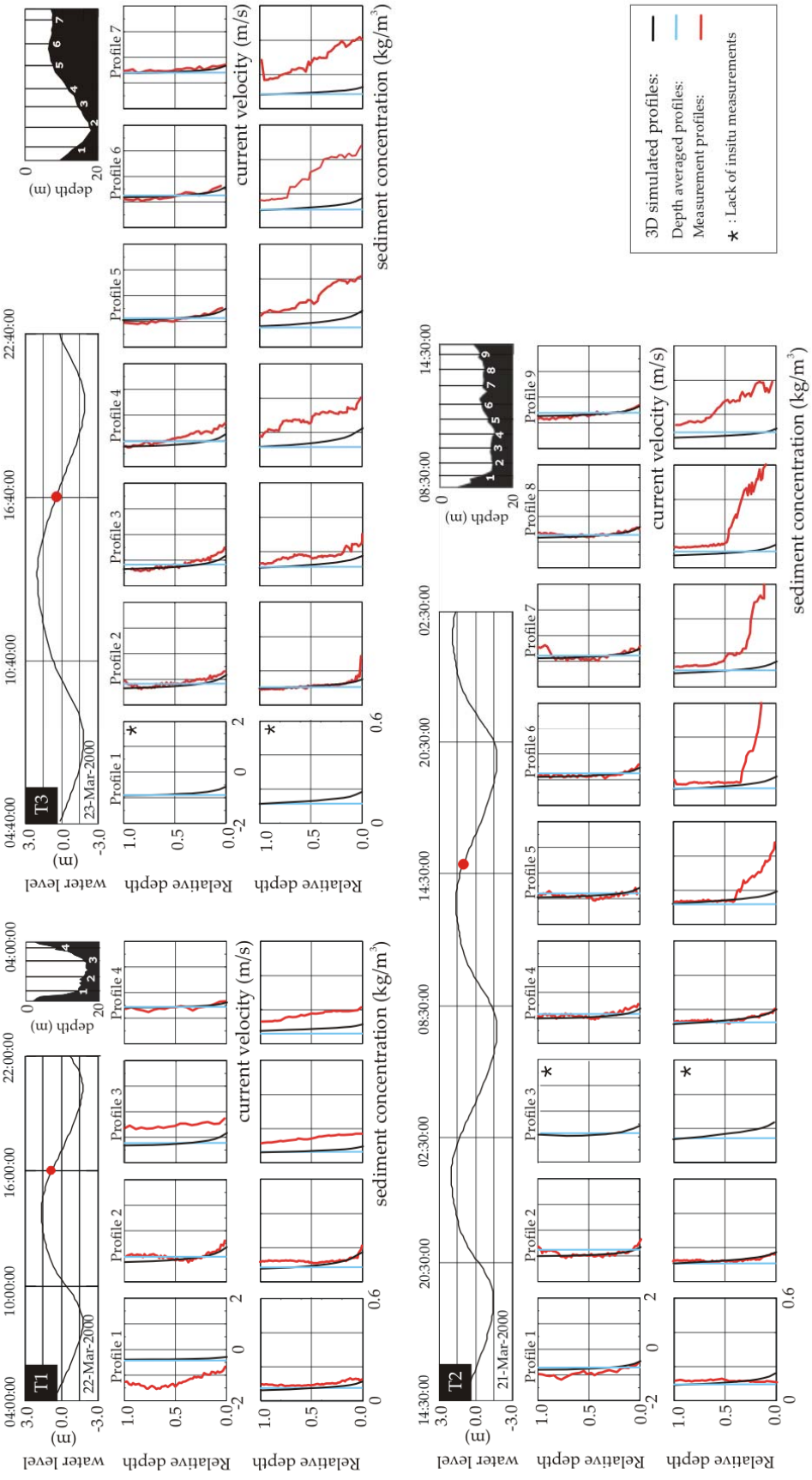

Figure 6.7 Current Velocity and Suspended Sediment Concentration Profile derived from 3D model, 2DH model and in situ measurements during the *ebb condition* for cross sections T1 (in Norderpiep channel), T2 (in Süderpiep channel), and T3 (Piep channel)

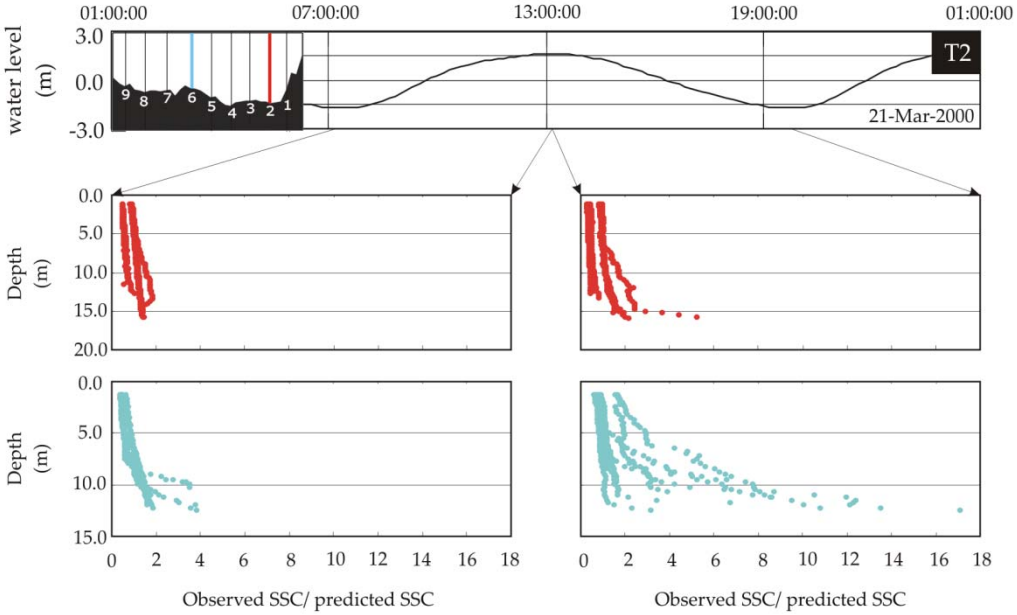

Figure 6.8 Variations of the ratio of observed to predicted SSC along the depth of flow for monitoring points in deep water (shown in red) and in shallow water (shown in blue) at the cross section T2 during one ebb phase (left plots) and one flood phase (right plots)

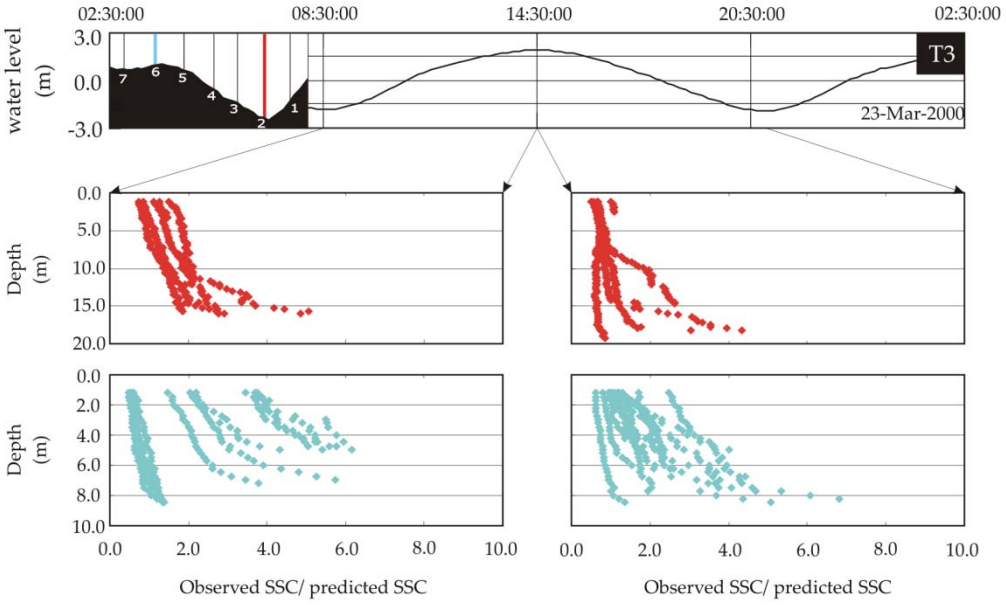

Figure 6.9 Variations of the ratio of observed to predicted SSC along the depth of flow for monitoring points in deep water (shown in red) and in shallow water (shown in blue) at the cross section T3 during one ebb phase (left plots) and one flood phase (right plots)

The simplifications associated with the modelling can be resulted in the poor correlation between the predicted and observed results. There might be some uncertainty in the input of bed roughness values in particular for the shallow water and tidal flat areas. As discussed in Chapter 3, the bed roughness used in the modelling was produced by Escobar (2007) who had employed empirical equations but limited field data. Another possible reason for the model deficiency can be the supply of sediment from the shallow water areas and more specifically the tidal flats. The model might not be able to properly simulate the amount of sediment washed out from the land and the tidal flat areas through the channel during the ebb conditions because of the insufficient supply of sediments. This may be applicable specifically to the cross section T3 due to its proximity to tidal flats and the water-land interactions. If this explanation is correct, the SSC values obtained from the model at this cross section for both the deep and shallow water regions should show underprediction. This feature can be observed in some extent in Figure 6.9.

As mentioned above the dissimilarity between the model and measured data in the shallow water area, can also be due to measurement errors in these areas. Considerable variation that exists in the particle size distribution in shallow water areas could be a source of errors in the measurements. Gordon, et. al. (1980), Kitchen & Zaneveld (1980), Bishop (1986), Moody et.al. (1987) and Bunt er.al. (1999) reported that the variation in particle size distribution is the most influential physical characteristic of the sediments on the response of optical devices. Zerull and Weiss (1974) and Bunt et.al. (1999) suggested that variations in floc size could double the variation in instrument response for similar mass concentrations (see Section 3.8.2.2). Existence of biological matter in shallow water area can also affect the recorded data by transmissometer. As pointed out by Walker (1981), biological matters such as chlorophyll-a and phytoplankton even though relatively insignificant by mass, their effect on the response of optical instruments is significant in the coastal zone. These organisms are known to be active in the shallow water area where light is sufficient. The sticky nature of these particles causes flocculation between the fine particles. Ebb conditions are favourable for their activities because of the decrease in the water level and increase in the transmitted light. In addition, lower current velocity during ebb phase compared with flood phase is an appropriate environment for these processes. Discrepancy in transmissometer results could also be due to air bubbles originated by water organisms (sea grass, sea weeds and algae). Bunt et.al. (1999), Puleo et.al., (2005) and Campbell et.al. (2005) reported the significance of air bubbles to the response of the optical backscatter devices. They reported that air bubbles can double the response of the device. It is known that the biological activity in the area under investigation causes air bubble release. As mentioned previously these bio particle activities are higher in the shallow water area.

In order to investigate whether the transmissometer data is one of the source of error, the values of the SSC derived from both the transmissometer and the ADCP devices were compared with the model results. As stated in Chapters 3, the echo intensity data recorded by the ADCP device were converted to the SSC. The procedure and the calibrated equation for conversion of the echo intensity data to the SSC values are briefly described in Chapter 3 (for more detail see Poerbandono and Mayerle, 2005). Figure 6.10 shows the SSC profiles derived from both instruments and also model results. Referring to the Figure, the graphs are for cross sections T1, T2, and T3 and cover the time of high slack water (first row in each cross section) and the ebb phase (second row in each cross section). Keeping in mind that the ADCP-based SSC values are likely to be underestimated (Poerbandono and Mayerle, 2005, and Bartholomä, et.al., 2009), it can be seen from the Figure that they do not show the same trend in the shallow water area as as the transmissometer -based SSC values.

The SSC profiles from the ADCP, in similarity with the model results have fairly uniform distribution over the depth. However, the SSC profiles derived from the transmissometer records in the shallow water area do not show uniform distribution of the SSC over the depth. It is stated in Chapter 3 that the area under investigation is categorized to be well-mixed which suggests the uniform distribution of SSC along the depth. It is also mentioned in Section 3-8-2-2 that the accuracy of the converted SSC from the transmissometer device is about 30% on the basis of agreement with concentrations determined from physical samples (Poerbandono and Mayerle, 2005). Taking into account these statements, together with the results presented above, it may be concluded that existence of error in the SSC data from the transmissometer in the shallow water regions can explain a part of the discrepancies observed between the field data and the model results.

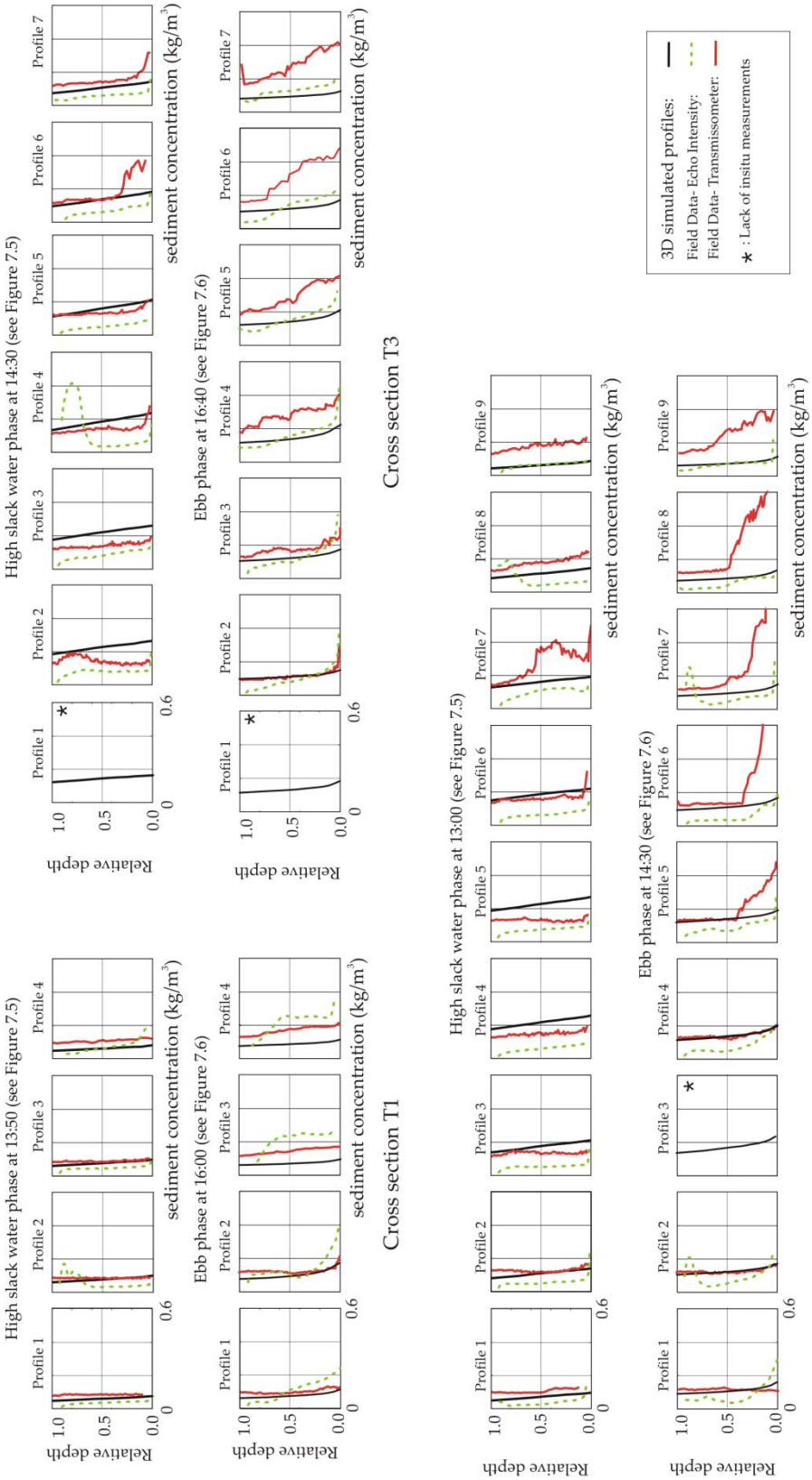

Figure 6.10 Suspended Sediment Concentration Profile derived from 3D model, and in situ measurements using two different devices; transmissometer and ADCP for cross sections T1, T2, and T3 during *high slack water* (first row for each cross section) *and ebb condition* (second row for each cross section)

6.3.2.1 Statistical analyses of results

To compare the range of the variations of the predicted and the observed values of the SSC statistically, box and whisker plots were prepared for the five tidal periods mentioned in Section 3-9. Figure 6.11 represents the plots separately for model and field data at the cross sections T1, T2, and T3. The same number of field data and model results were considered to assure the comparability. Only those values from the model results were considered where the corresponding measured data were available. In the plots the box represents the lower and upper quartile and red pluses are the values which has been distinguished to be out of the range statistically, have referred to as the outliers.

At the first glance, the plots show considerable outlier points in the field data compared with the model results. The plot for the cross section T2 shows the highest number of outliers, which is followed by the plot for the cross section T3. It can also be seen that the lowest value predicted by the model is always lower than its corresponding measured value. This behaviour of the model, which is observed in all plots for the cross sections and for the five tidal periods, suggests underprediction by the model when the sediment concentration is low. In overall a relatively good agreement can be seen for the tidal cycle of 21st to 23rd of March 2000.

As discussed in Section 6-5, the values of the SSC derived from the transmissometer in shallow water area may contain some error particularly at cross sections T2 and T3. Above-mentioned descriptive statistical analysis was employed to analyses the SSC values derived from the transmissometer in comparison with those derived from the ADCP. For this analysis, two sets of SSC data were selectively prepared for cross sections T2 and T3. These are SSCs derived from the ADCP in the shallow water area, monitoring points 5 to 9 of cross section T2 and 5 to 7 of cross section T3 (see Figure 6.5), together with those derived from the transmissometer for the deep water regions. These sets of data; called Exclusive sets in this study; are compared with the SSC values derived from the transmissometer device at all locations for both cross sections T2 and T3.

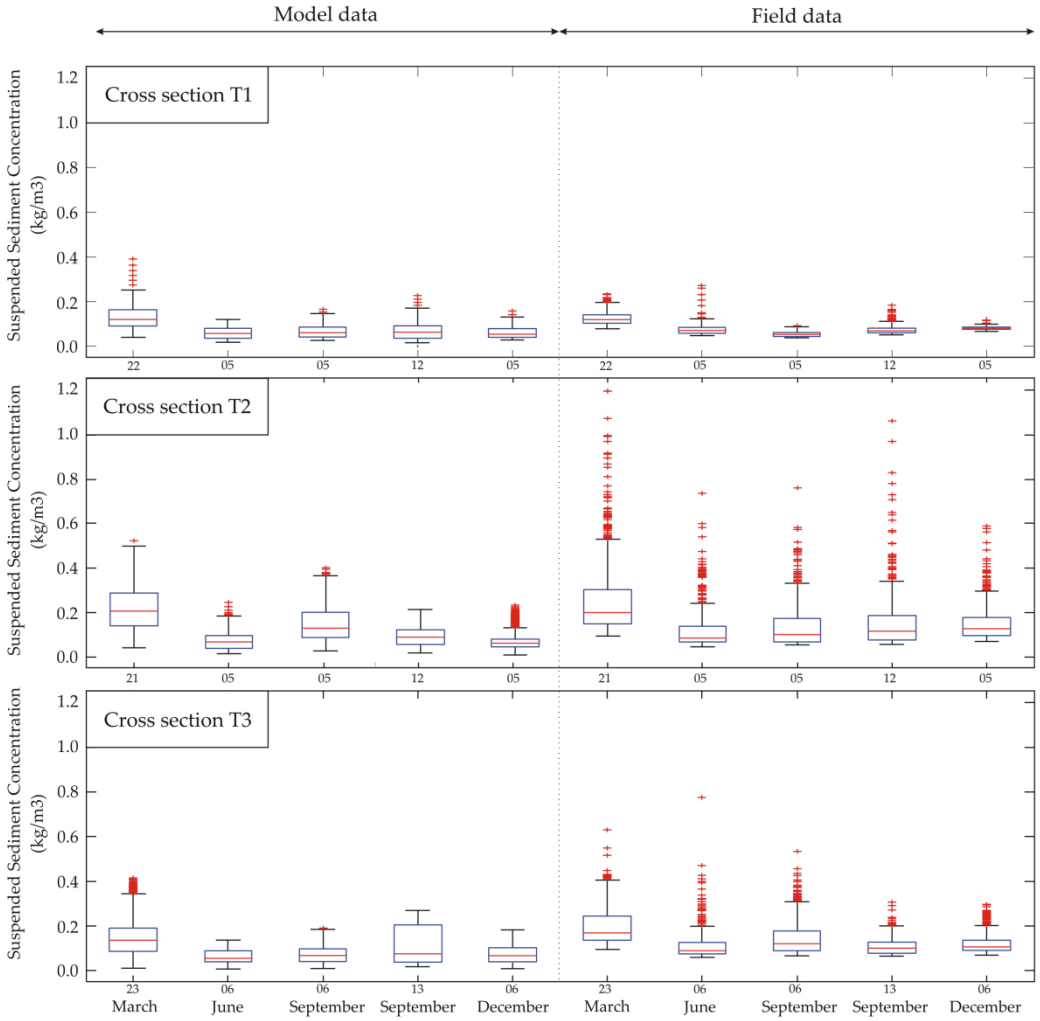

Figure 6.11 Box and Whisker plot of suspended sediment concentration derived from the model (left side plots) and from transmissometer (right side plots) for cross sections T1, T2, and T3 for five tidal periods

Figure 6.12 presents the box and whisker plots for the SSC data derived from the transmissometer records (on the left side) and Exclusive sets of SSCs data (on the right side). It can be seen from the plots that in the Exclusive sets of data, considerable decrease in the lowest value of SSC for all the tidal ranges achieved. These low values however, are still higher than those predicted by the model (Figure 6.11). This confirms the underprediction by the model when the suspended sediment concentration is low. It can also be seen that the lowest SSC values of the Exclusive data sets for all the tidal ranges and both cross sections are always similar. It can be concluded that the ADCP may not be the proper device to use when the SSC is very low. Employing Exclusive data sets resulted less outliers and considerable improvement to the values at the cross section T2. This conclusion however, is not applied to the values at the cross section T3.

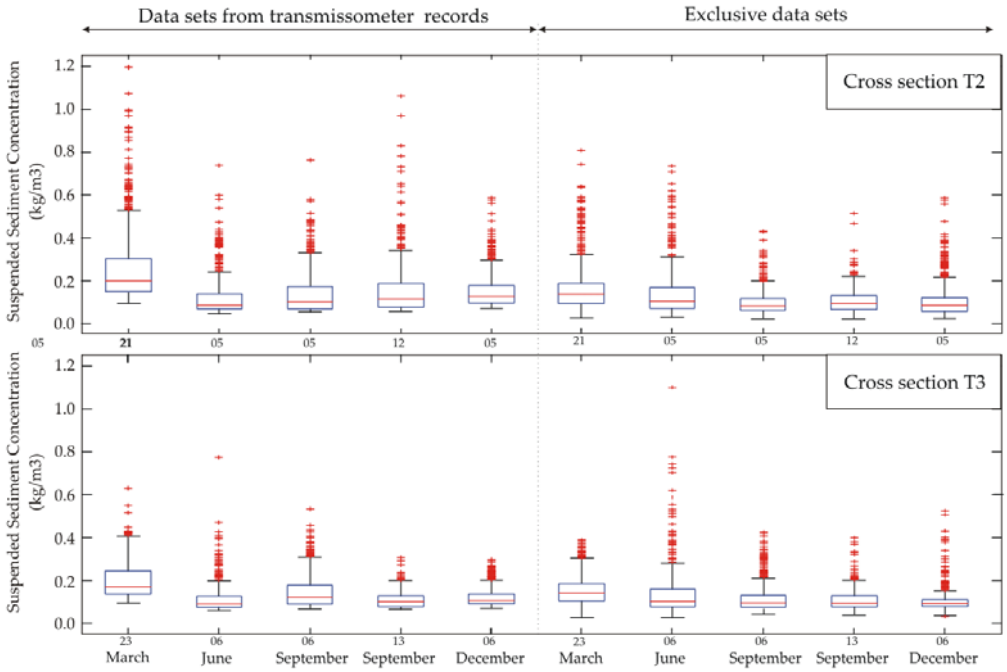

Figure 6.12 Box and Whisker plot for measured SSC data derived from transmissometer (left side plots) and from Exclusive data set; employing ADCP data in shallow water and transmissometer data in deep water (right side plots) for cross sections T2, and T3 for five tidal periods

6.3.3 Measured versus Predicted suspended Sediment Concentration (SSC)

To evaluate the predictive ability of the 3D model the results of the suspended sediment concentration (SSC) from the simulations, covering the three cross-sections T1, T2 and T3 and all the layers along the depth for the five tidal periods mentioned previously (see Section 3-9) were compared with the corresponding measured data, using scatter plots. Figure 6.13 shows individual scatter plots of measured versus computed SSC at each cross-section and for each tidal period. The representative lines of the factor of 2 of measured data, the corresponding best fitted lines and correlation coefficients are also given on the plots. While a large proportion of points are within the factor of 2, there are many points outside these lines in most of the plots. It can be seen that most of the points are positioned above the line of perfect correlation revealing underprediction by the model especially at cross sections T2 and T3. Previously in Section 6-3-2 underprediction by the model was observed and to some extent discussed. Comparisons of the plots in Figure 6.13 with those given for the calibrated 2DH model results in Figure 5.12c, 5.13c, and 5.14c respectively for cross section T1, T2, and T3, show relatively similar scatter of data. Comparing the correlation coefficients of the plots however, revealed considerable improvement. That is, for the 3D model results these are 0.11 to 0.34 at T1, 0.09 to 0.42 at T2, and 0.10 to 0.26 at T3, while for the 2DH model they are respectively 0.02 to 0.09, 0.02 to 0.12 and, 0.01 to 0.36. Due to increase of the number of the data in the 3D model in comparison with the 2DH model the agreement between the model results and field data has been increased significantly. This improvement is evident in the best-fit line and also correlation coefficient of each plot. The improvement is generally highest for cross section T1 and lowest for cross section T3. The trend of improvement in each cross section do not follow any logic, which is because of its dependency to the number of the data available and also the accuracy in the measured data.

In order to determine whether the discrepancy observed between the measured and predicted values of SSC in Figure 6.13 is depth dependent, following investigation were carried out. The SSC data along the depth from the model and measurements were divided into two sets. One set named as the "near bed set" consisting of the SSC values from the bed to a chosen level positioned at 25% of the depth above the bed and one named as the "far from bed set", consisting of the SSC values from this level to the surface. The scatter plots for these two sets are shown in Figure 6.14 individually for cross sections T1, T2 and T3. The plot of each cross section covers all available data for five measuring periods. In the Figure the data for "near bed set" and "far from bed set" are shown in blue and green respectively. Another set of data which covers the whole data from the bed to the surface is also plotted and shown in grey. The black dashed lines represent the domain of factor of two of measured data respectively. The best-fit equations and correlation coefficient were calculated for these data and given on the top left corner of each plot. Referring to the Figures, it is seen that the scatter of data outside the factor of 2 lines for the plots of the "far from bed set" is less than that for the full set and for the "near bed set". This is more pronounced for the values at cross sections T2 and T3. However, no significant improvement was achieved in the best-fitted equations and correlation coefficient in either of the two sets, "near bed set" and "far from bed set", in comparison with those of the total depth (the plot in grey). Another test was made by fitting the lines of factor of five of measured data to the plots in Figure 6.14, according to the suggestion made by Soulsby (1997) and by Davies and Villaret (2002). They stated that for cases when the modelled SSC are within the lines of the factor of five of measured SSC, the model results could be considered to be in an acceptable range. The lines of factor of five are shown in the Figure in dotted red. It can be seen that the number of the points being outside the factor of five are more considerable for the "near bed set" (blue points). The percentages of the predicted SSC points that are positioned within the factor of five of the field data are 98.11%, 93.17% and 84.03%, respectively for cross sections T1, T2, and T3.

As discussed in Section 6-3-2, the instrument error may affect the scatters of SSC, thus be responsible for the deviation observed between the model results and measured data specifically in shallow water regions of cross sections T2 and T3. Because, the observed deviations between the model results and the measured data were more pronounced at these cross sections. The possibility of this error and its effect on the results were investigated. The exclusive data sets prepared in Section 6-3-2 were considered for this investigation. The Exclusive sets of data together with the corresponding results from 3D model were used to prepare the scatter plots shown in Figures 6.15 and 6.16 for cross sections T2 and T3, respectively. In these Figures the plots on the left sides consist of the SSC derived from the transmissometer versus model data, and the plots on the right side consist of the SSC from Exclusive data set versus model data. The use of Exclusive data set for cross section T2 clearly resulted a positive shift of the data toward the limit represented the factor of two of field data. For the two out of five cases however, the results suggest overprediction by the model. This is in contrast with the behaviour of the model which showed underprediction in contrast with the transmissometer data (the corresponding plot in the left). For cross section T3 use of the Exclusive data set showed improvement in one out of five data sets. From the results it can be concluded that the error from transmissometer device in shallow water regions could possibly be a reason for the deviation observed between modelled and measured SSC in cross section T2. For cross section T3 however, error in transmissometer data only partly explains the differences observed between the model and measured SSCs.

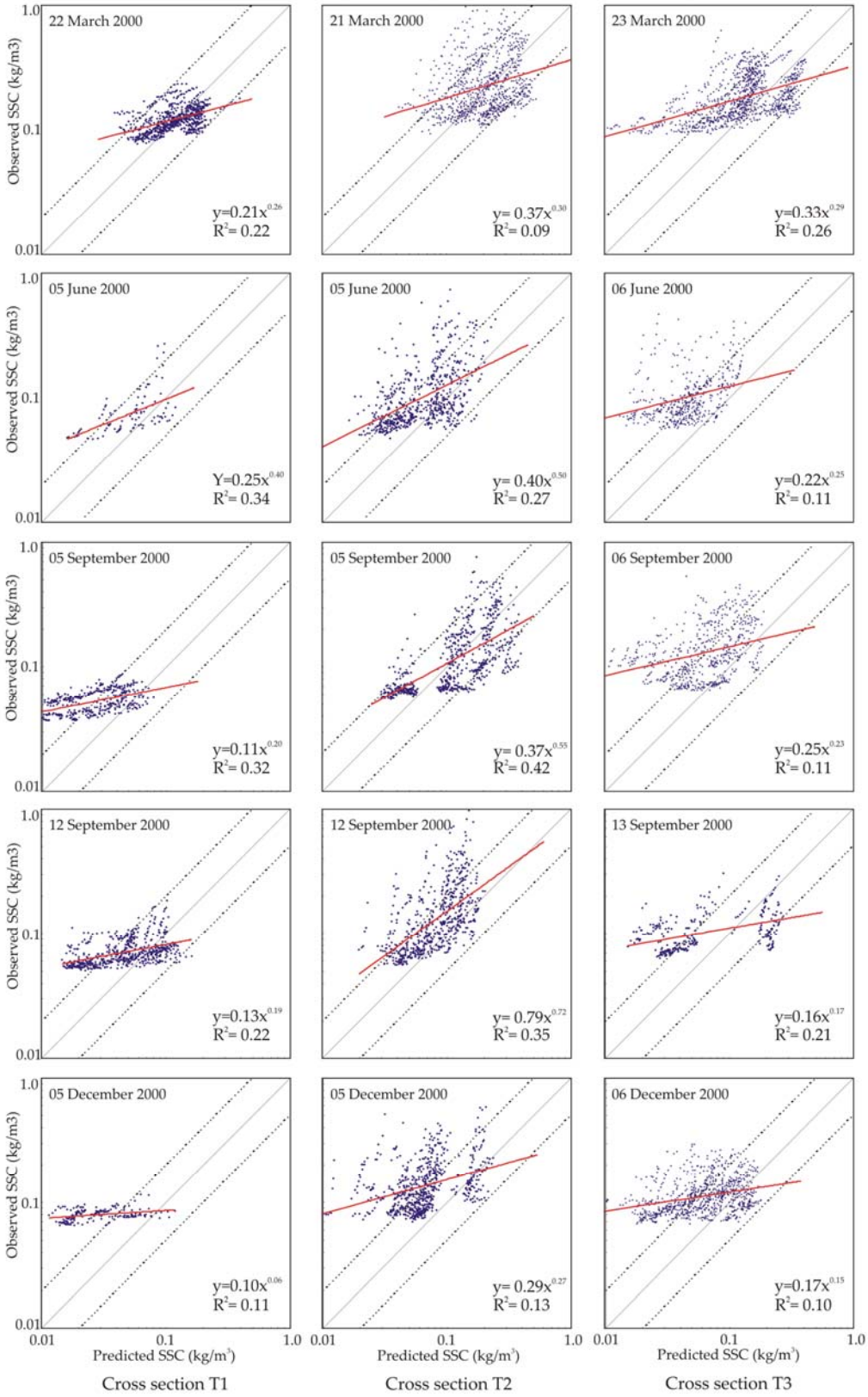

Figure 6.13 SSC predicted by 3D model versus SSC measured in the field at cross-sections T1, T2 and T3 for five different period of the year 2000

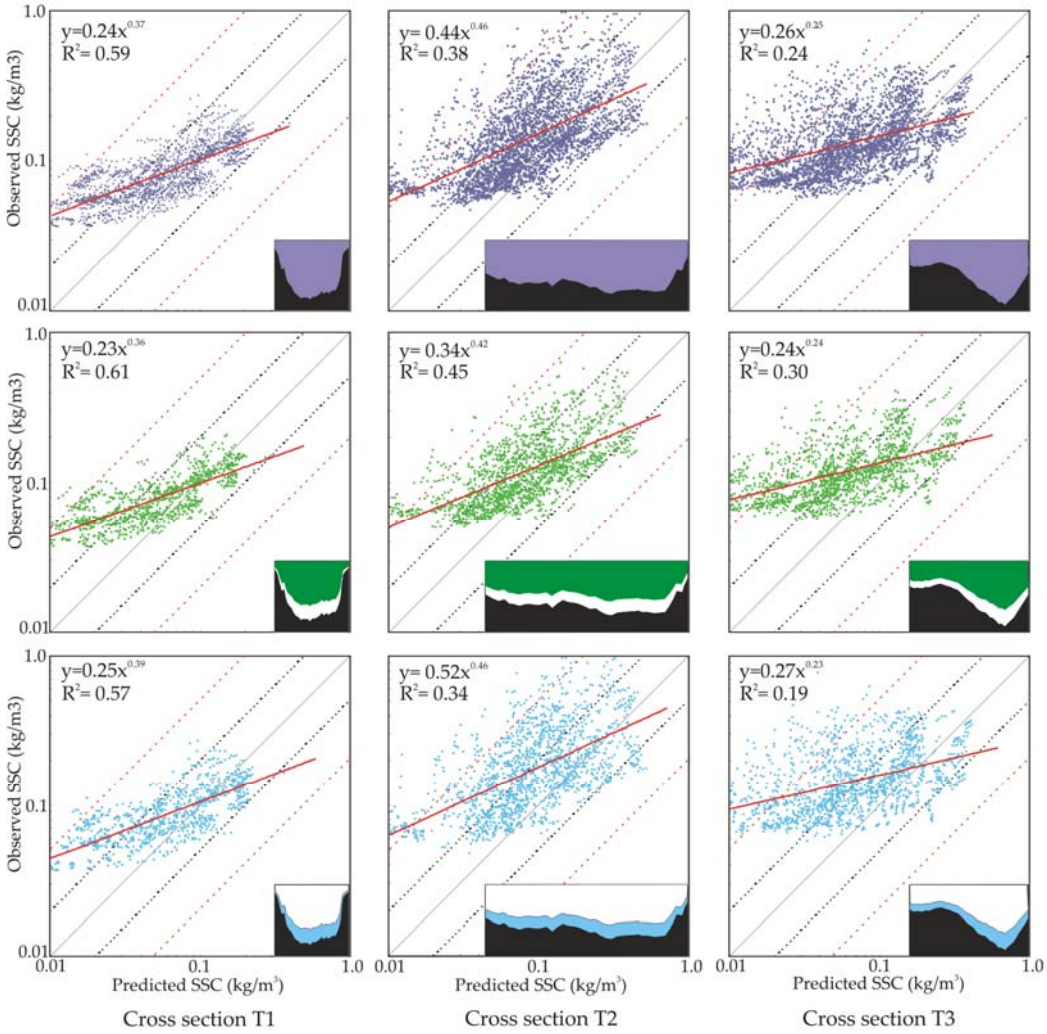

Figure 6.14 SSC predicted by 3D model versus SSC measured in the field at cross-sections T1, T2 and T3 for the total depth (shown in gray), for the layer above 25% of depth (Far From Bed Set, shown in green), and for the layer below 25% of depth (Near Bed Set, shown in blue)

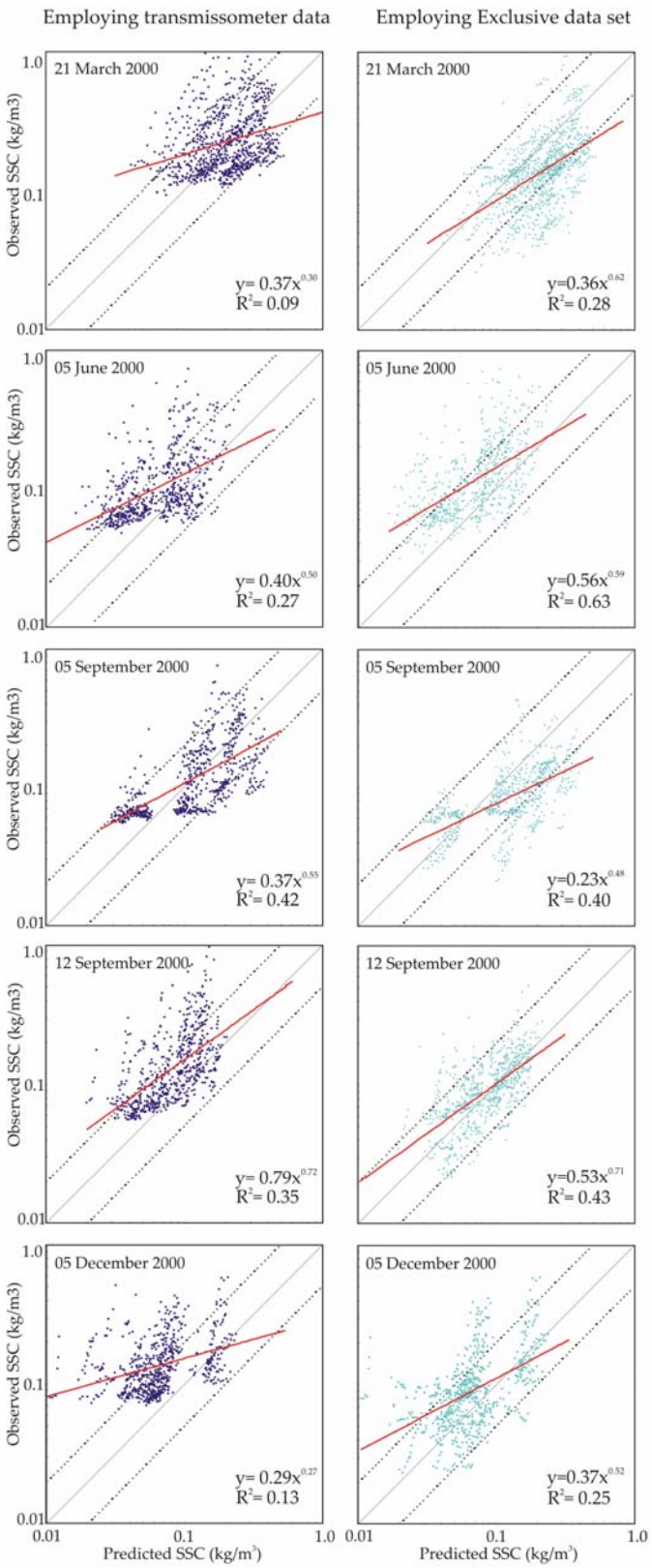

Figure 6.15 SSC values predicted by the 3D model versus SSC values from conversion of transmissometer data (the graphs on the left) and from the Exclusive data set (the graphs on the right) at cross-sections T2 for five different periods in year 2000

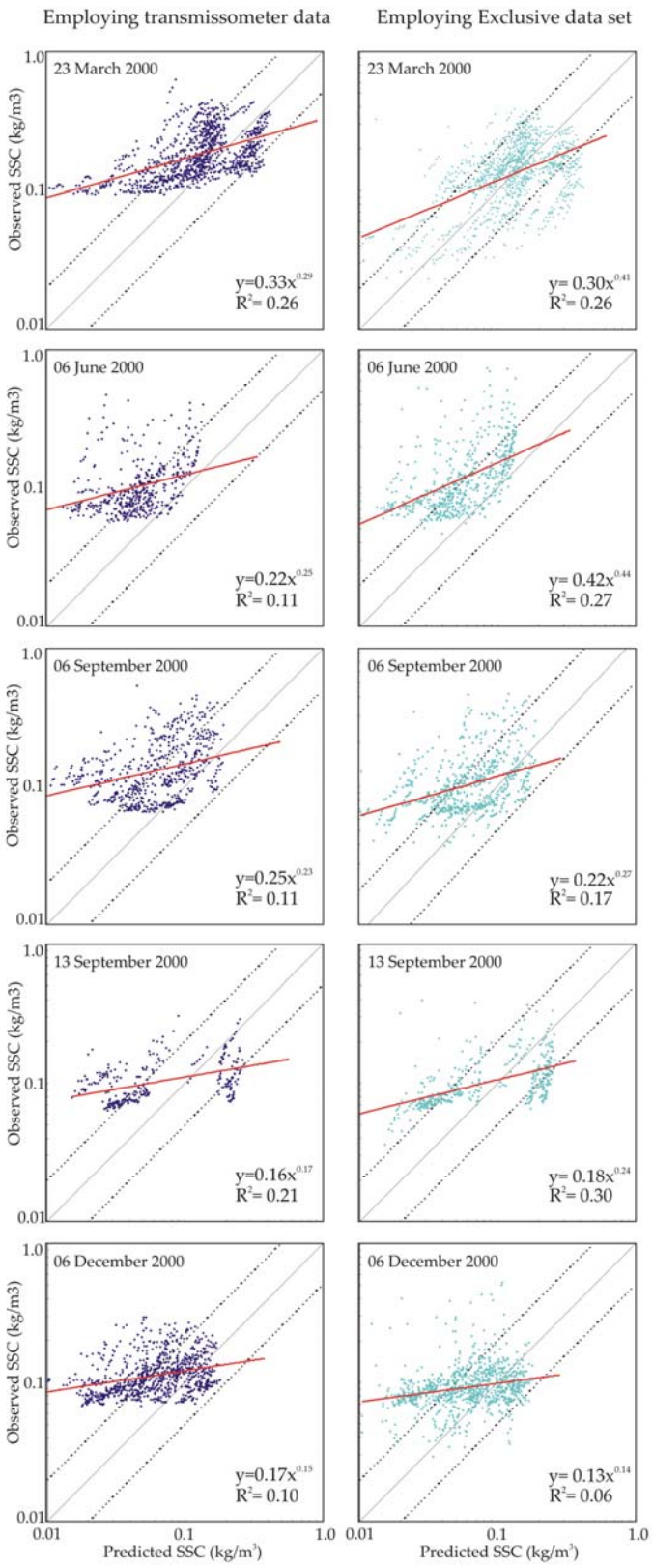

Figure 6.16 SSC values predicted by the 3D model versus SSC values from conversion of transmissometer data (the graphs on the left) and from the Exclusive data set (the graphs on the right) at cross-sections T3 for five different periods in year 2000

6.3.4 The effect of the Flow model performance on the distribution of the SSC

It is stated in Chapter 3 that Dithmarschen Bight is a tidally dominated area, thus currents in the area are essentially generated by the tide. Hence it is appropriate to test the correlation of suspended sediment concentration (SSC) computed from the model and those from the field during a tidal range by means of current velocity. As the current velocity of the model has been qualified with an error of less than 0.2 m/s (see Section 6-3-1 and Palacio et. al., 2005), this variable was found proper representative factor of the tidal range. To minimize the errors regarding hydrodynamic results (see profiles 1 and 3 in Figure 6.6) only those current velocities from the model were considered in which their differences with those of field data were less than 0.2 m/s. For each selected current velocity the corresponding temporal and spatial values of the SSC were obtained from the model and the field data. The ratio of computed to the observed SSC was calculated for each current velocity. Using semi-logarithmic coordinates the scatter plots of these ratios versus current velocities are shown in Figure 6.17. The resulting plots for all five tidal ranges are presented in the plots. The plots cover all the three cross sections; T1, T2, and T3, in each tidal period. Red lines in the Figures represent the factor of two of the field data.

Referring to the Figure, a relatively similar trend in all of the plots can be observed for the variation of the ratios of SSC (predicted to observed) with current velocities. That is, the lowest scatters can be seen during slack waters when the current velocity decreases to nearly zero, the ratios are approximately between 0.5 and 1. The scatter tends to increase with increasing current velocities during both conditions of ebb and flood phase. The scatter of the ratio SSC reaches its maximum at the current velocity of about 0.5 m/s (0.1<ratio of predicted to observed SSC <4). The scatter again decreases with increasing current velocities, during both ebb and flood conditions. At maximum current velocities during both ebb and flood conditions the predicted SSC values are once again in good agreement with the observed SSC. This is more evident in flood condition for all plots, where the range of the ratios is from 0.6 to 2. In the ebb condition however, good agreement is observed only in the first three scatter plots, during the high tidal ranges of 3.2 to 4 m (see Section 5-3-3).

The ratio of predicted to observed SSC versus current velocity for three cross sections T1, T2, and T3 separately are presented in Figure 6.18. The graph of each cross section consists of all five periods of tidal range. The graphs show that the scatter is the lowest during slack waters and at the maximum current velocities, and the highest at low current velocities of about 0.5 m/s. In this particular Figure however, it can be seen that the best performance of the model is at cross section T1, where the ratio of predicted to observed SSC varies between 0.7 and 3 at low current velocities. The weakest performance is observed at cross section T3, having large scatters at low current velocities (about 0.5 m/s) and a large number of points correspond to the ratio of 0.1. That is, the predicted value is ten times lower than the observed value. Winter et.al. (2005) also reported that the model tends to underpredict the SSC at low current velocities.

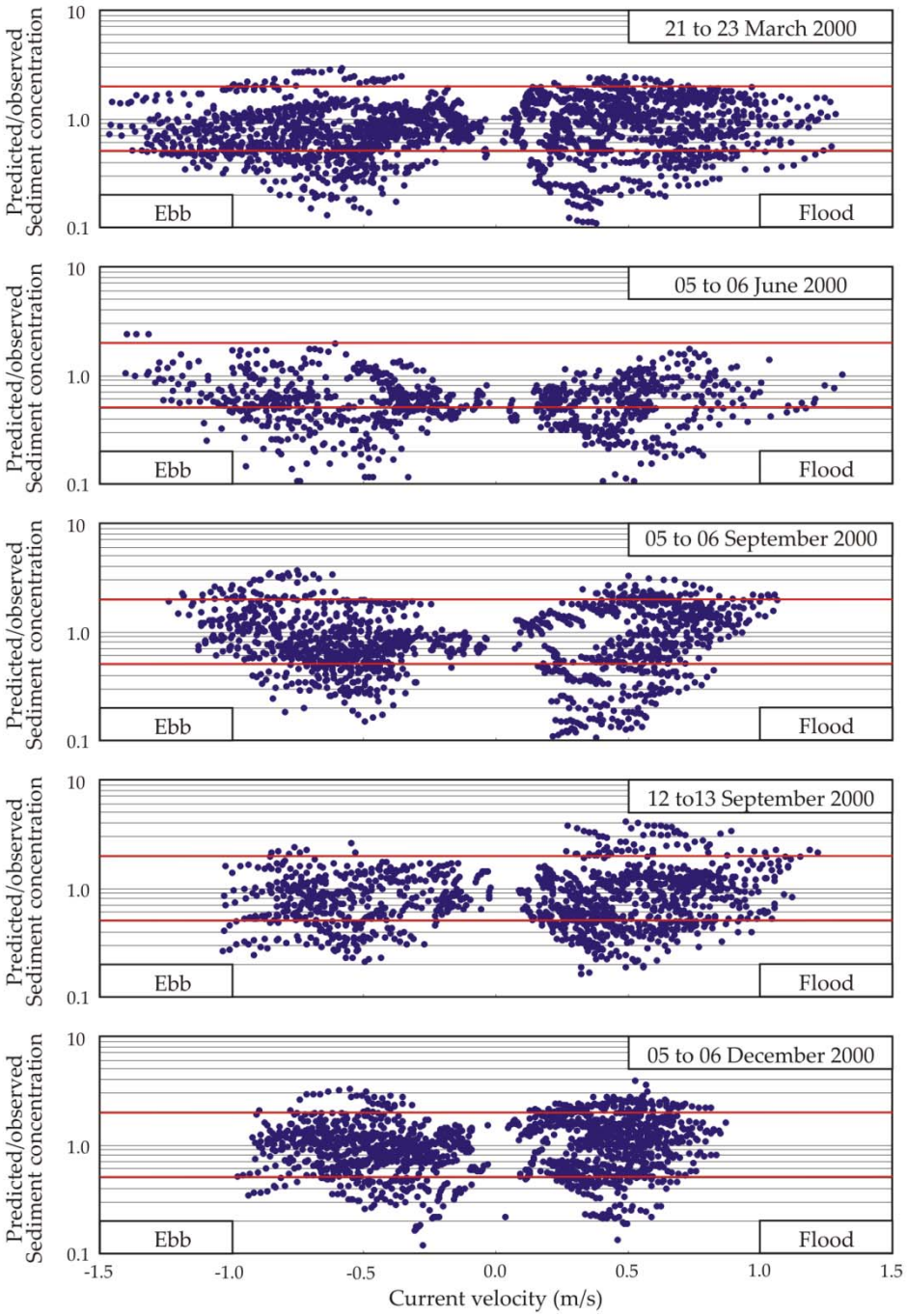

Figure 6.17 The ratio of predicted to measured (observed) suspended sediment concentration versus current velocity for five tidal conditions

In addition to the errors resulted from the field data, some model related factors can be considered for discrepancies that have been observed between the field data and the model results, specifically at conditions of low current velocities. The first and the most probable reason is the use of a constant settling velocity for the whole area and for the whole tidal cycle. According to Winterwerp (2001) there are large variations in the value of the settling velocity having the higher values around the slack water due to mainly flocculation of sediment. His conclusion is that flocculation is a factor that explains why it is not possible to

simulate the observed features in suspended sediment concentrations properly using constant settling velocity. On the basis of the suggestion by Winterwerp and van Kesteren (2004), the value of the settling velocity around slack water is controlled by several factors most importantly flocculation. Talke & Swart (2006) also emphasized the necessity of considering variation of the settling velocity during a tidal cycle in order to simulate the behavior of the suspended sediment. In their investigations they showed that biological matters and turbulence processes played an important role in the variation of the settling velocity during a tidal cycle.

Another factor that could affect the model performance during low current velocity is the use of a constant erosion rate for the whole area. Bilgili et al (2003) reported that the acceleration of flow near the slack water when current velocity levels were down (after slack water) could produce additional shear forces in the bed that caused an increase in the suspension of sediment particles. According to Davies et. al. (2002) and Werf (2003) the tendency of the model to underpredict suspended sediment concentrations after slack water in the low velocity condition can be due to a residual amount of suspended sediment in quiescent conditions, which is caused by turbulence. As the turbulence modules just simulate the effect of turbulence on the mean-flow, it might not be able to accurately reproduce this residual amount. Eisma and Li (1993) report that the deflocculating effect by which large flocs break up into smaller particles during or after the settling to the bottom (around the slack water) could increase the amount of SSC observed in the area.

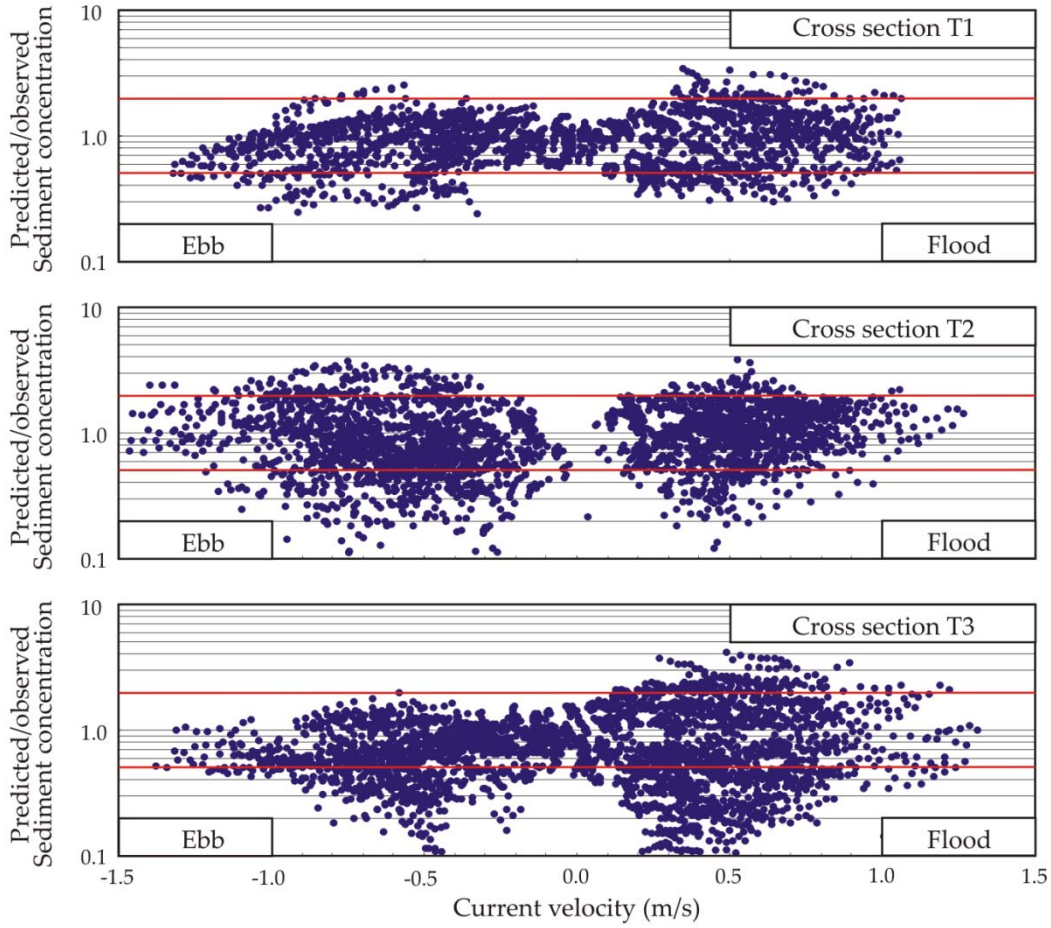

Figure 6.18 The ratio of predicted to measured (observed) suspended sediment concentration versus current velocity at cross section T1, T2, and T3

6.4 Further assessment of the performance of the 3D model

In this section the ability of the 3D model is demonstrated through the evaluation of the variation of the SSC results from the model through the following points of view. The time series of SSC distribution across the cross sections T1, T2, and T3 for a full tidal cycle are prepared for different layers along the depth and assessed in comparison with the corresponding field data. The developed pictures of the evolution of the vertical profiles of the SSC at the three cross sections during a tidal period are discussed. Instantaneous pictures of the SSC at each of these cross sections for different phases of a tidal cycle are prepared using the model results and the field data. For all of the presentations described in the following sub sections, the field data that have been employed are from 21st to 23rd of March 2000 during which the tidal range was approximately 4m. This selection was based on the following considerations:

1. The field data in this period are quite in close agreement with the model results in comparison with the other periods of measurements (see Figures 6.10, 6.11 and also Table 6.4).

The field data from the same period had been analysed by Poerbandono and Mayerle (2005) and their report is considered in the following evaluation of the model results.

6.4.1 Distribution of SSC time series across the cross section in various layers of depth

To reproduce the pattern of variation of SSC across the cross sections T1, T2, and T3, for a full tidal cycle, the suspended sediment concentration (SSC) computed from the model at each monitoring points were interpolated across the cross section at each specific time. This procedure was carried out for all the layers across the depth. Figures 6.19 to 6.21 show the distributions of the SSC for the duration of the full tidal cycle at cross sections T1, T2, and T3 respectively. In these Figures from the top are the graphs of water level time series followed by the depth-averaged SSC data from the field reported by Poerbandono and Mayerle (2005). The plots resulting from the 3D model are presented in colour-coded contours at three layers for the sake of brevity. These are the near surface, the mid-depth, and the near bed layers. The corresponding cross section profile and the layer position (with the red line) are also presented on the left hand side of each graph. The distribution of current velocity for the same tidal period and cross sections are presented in Figures 6.3 to 6.5. It can be seen that unlike the current velocity distribution, the distributions of the SSC across the cross sections during a full tidal cycle predicted by the model show some dissimilarity in comparison with those of the field data. The distribution of the SSC at each cross section is discussed to some extent below.

Referring to Figure 6.19, the patterns of variations of the SSC in cross section T1 according to the model results and the field data are more or less similar. However, there is a delay of about an hour between the time predicted by the model and that obtained from the field data for the occurrence of the peak SSC, during the ebb current. For both the model and the field data the concentration of suspended sediment reaches its highest value during the ebb phase and tends to happen in the region near the southern bank of the channel. In view of the current velocity distribution given in Figure 6.3, the maximum current velocity during the flood phase is higher than the maximum current velocity during the ebb phase, which suggests the higher peak of SSC during the flood phase. However, in regard to the modelled

and measured SSC of Figure 6.19 the higher maximum SSC occurs during the ebb phase. The only reason that can be offered is that there exists a higher supply of suspendable sediment in the area during the ebb phase. The reason for the increase in the values of the SSC in the region near the southern bank of the channel can be explained in terms of the energy level and bed characteristics at the cross section. Referring to Figure 3.7, at the bed northern bank of the cross section T1 is covered by mega ripples, while the southern bank of this cross section is dominated by Early Holocene layer (Mayerle et. al. 2002). As reported by Vela Diez (2001), the energy level due to the current and thus the erosion rate in the southern bank region of this channel should be higher than those in the northern bank region. The suspended sediment transported to this cross section with the returning ebb current cannot easily settle down in the southern regions due to the high energy level. Besides, the role of the tidal flat area near the southern bank of the cross section to supply suspendable sediment to the channel should not be ruled out. As reported by Reimers (2003), this area is covered with sediment grain sizes from 0.11 to 0.23 mm with cohesive sediment content of about 5%.

Figure 6.20 shows the distribution of the SSC at cross section T2. As seen form the Figure, the spatial and temporal patterns of the variation of the SSC, in the first period from the low to the high slack water, are roughly similar for the model results and the field data. That is, flood current causes an increase in the SSC in the vicinity of the southern bank (shallowest part of the cross section). In the following tidal period from high to low slack water however, the peak SSC recorded from the field data is close to the southern bank and that of the model is close to the northern bank. However, as reported by Mayerle et. al. (2002) the southern bank of this cross section is covered with early Holocene layer, where the sediment is not freely available due to a consolidated layer. This would explain that the SSC observed in the south bank region is not local, but is transported with the ebb current from the downstream and/or from the tidal flat around the channel. The maximum current velocity during the flood phase is higher than the maximum current velocity during the ebb phase at this cross section (Figure 6.4). Hence, the higher value of the peak SSC during the ebb phase in comparison with that in the flood phase, can be attributed again to some high supply of suspendable sediment during the ebb phase. The current velocity and the SSC graphs of the model, Figures 6.4 and 6.20 respectively, reveal that the peak SSC coincides spatially with the peak current velocity. It can also be seen that a second peak of SSC with very low values is computed by the model in the same spatial position as that of measured data at the near bed layer. It may be concluded that according to the configuration of the model the supply of sediment for transporting to this cross section by ebb current was not sufficient to reproduce the peak SSC at the same position as that observed in the field data. This subject is further discussed in the following sections. It should be added that at cross section T2 as for T1, the peak SSC predicted by model for the ebb tidal cycle shows a delay of about one hour in comparison with the field data.

Referring to Figure 6.21, for cross section T3, it can be seen that in the first tidal cycle from the low to the high slack water, the spatial pattern of SSC variations for the model results are relatively similar to the field data. In both the model and the field graphs the peak SSC due to current is close to the southern bank. However, there is a delay of about half an hour between the time predicted by the model and that obtained from the field for the occurrence of the peak SSC, during the flood phase. In the second phase of the tidal cycle, from high to low slack water, the peak of the SSC which can be observed in the field data in the proximity of the southern bank, is not reproduced by the model. The model results show continuous

reduction in the values of the SSC after the occurrence of the maximum flood current until the following low slack water.

In Figure 6.22 the time series variation of the SSC derived from the model results at the near bed layers of the three cross sections T1, T2, and T3 is presented. The temporal pattern of SSC variations shows the similar pattern of two peaks per tidal cycle at cross sections T1 and T2. At cross section T3 however, the model has reproduced only one peak SSC, occurred during the flood phase. An investigation into this behaviour of the model at this cross section was carried out which is described in the following section.

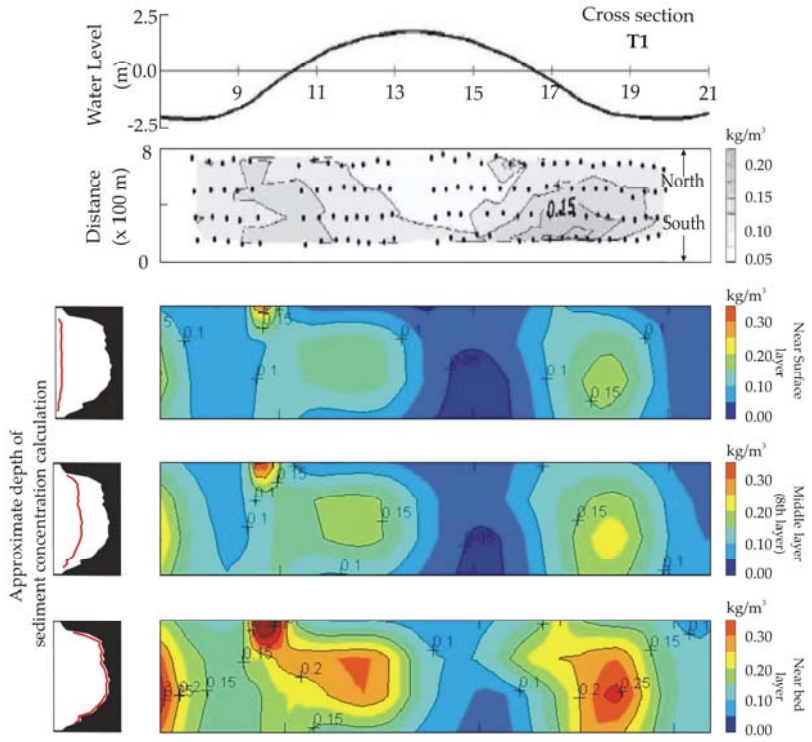

Figure 6.19 From the top: water level time series, the field data contours of depth averaged sediment concentration (Poerbandono and Mayerle, 2005), Colour coded contours graphs of the sediment concentration from the model for the near surface, at middle depth, and near bed layers for Cross section T1

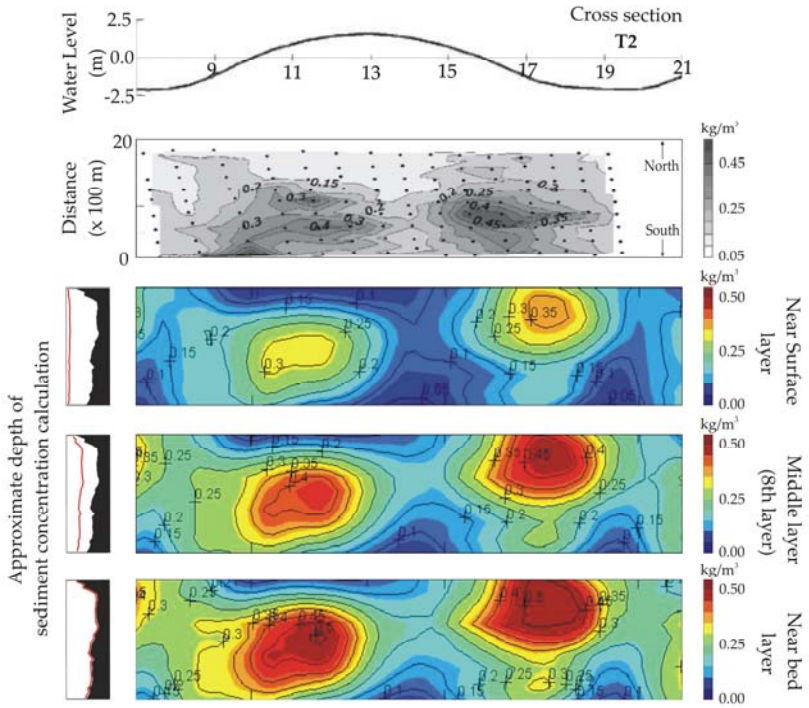

Figure 6.20 From the top: water level time series, the field data contours of depth averaged sediment concentration (Poerbandono and Mayerle, 2005), Colour coded contours graphs of the sediment concentration from the model for the near surface, at middle depth, and near bed layers for Cross section T2

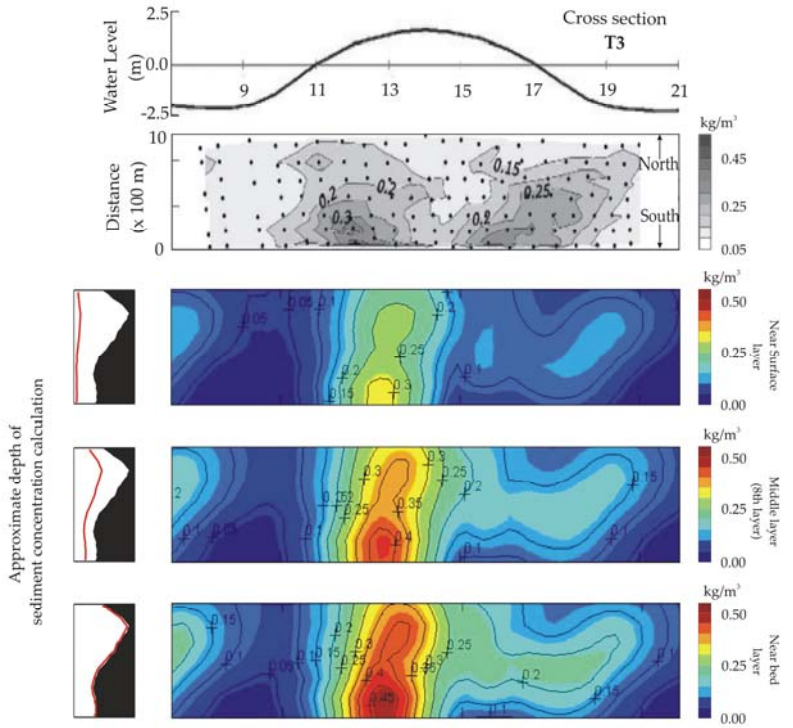

Figure 6.21 From the top: water level time series, the field data contours of depth averaged sediment concentration (Poerbandono and Mayerle, 2005), Colour coded contours graphs of the sediment concentration from the model for the near surface, at middle depth, and near bed layers for Cross section T3

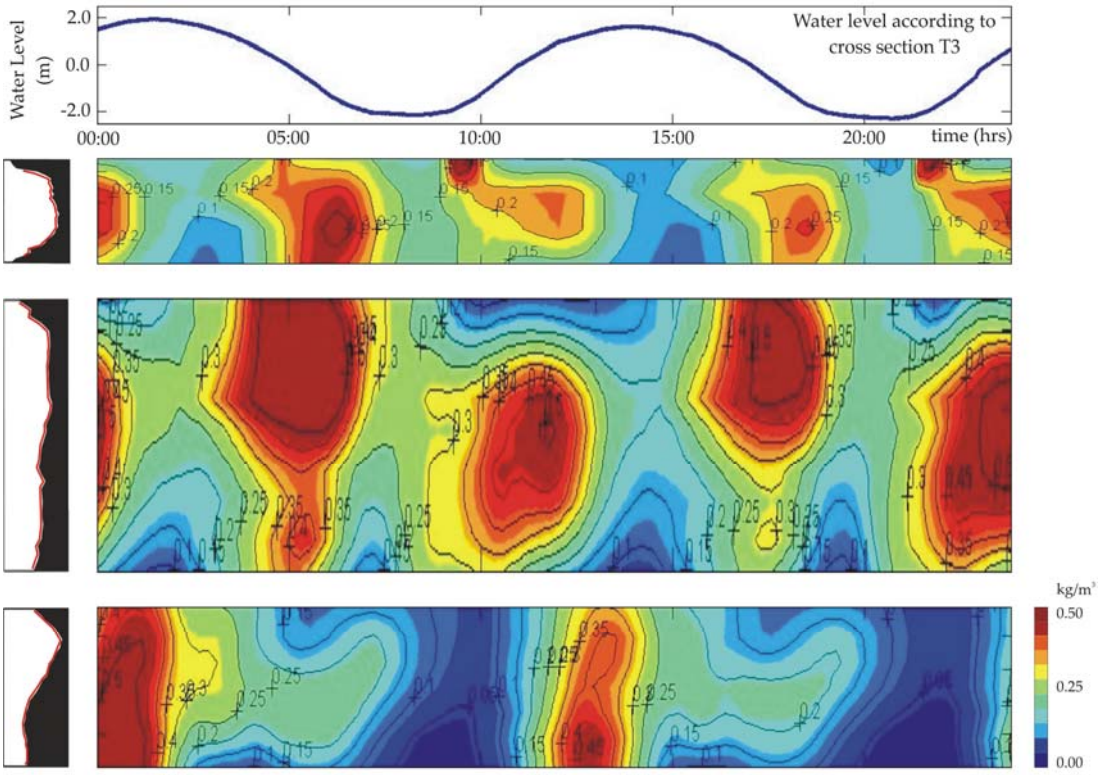

Figure 6.22 From the top: water level time series at cross section T3, colour coded contours for the variations of the SSC for the near bed layer at cross sections T1, T2, and T3 respectively

6.4.2 Evolution of the vertical profiles of suspended sediment concentration (SSC)

The SSC model results at the monitoring points C1, C2 and C3 in the middle of cross sections T1, T2, and T3 respectively (shown in Figure 6.1), covering the whole flow depth and the tidal period from 21st to 23rd of March 2000 were used to prepare the graphs of the evolution of the SSC, given in Figure 6.23. It can be observed from the plots that at all the monitoring points for duration of the flood phase, the SSC starts to increase from the near bed layer to the surface and reaches its peak before the high slack water time. The peak SSC is higher at the higher high water time in comparison with that at the lower high water time. For instance, see the peak SSC at 00:00 hour in comparison with that at 12:00 hour on the 22nd of March. During the ebb phase the same trend of variations of the SSC as that during flood phase can be observed at monitoring points C1 and C2. That is, the SSC value starts to increase from the bed with increasing the ebb current velocity and reaches its peak value just before the low slack water. The peak value of the SSC is higher at the time of lower low water in comparison with the peak at the time of higher low water.

For point C3 at cross section T3, the peak SSC value which is at the time of high slack water (for instance 00:00 hour on the 22nd of March) starts decreasing at the surface but not in deeper layers. The SSC decreases even during the following ebb tidal cycle and reaches its minimum value after the proceeding low slack water. In the near bed layer the concentration of suspended sediments shows high values until the proceeding low slack water. At this

monitoring point, as discussed previously, the peak SSC during the ebb current cannot be observed along the depth.

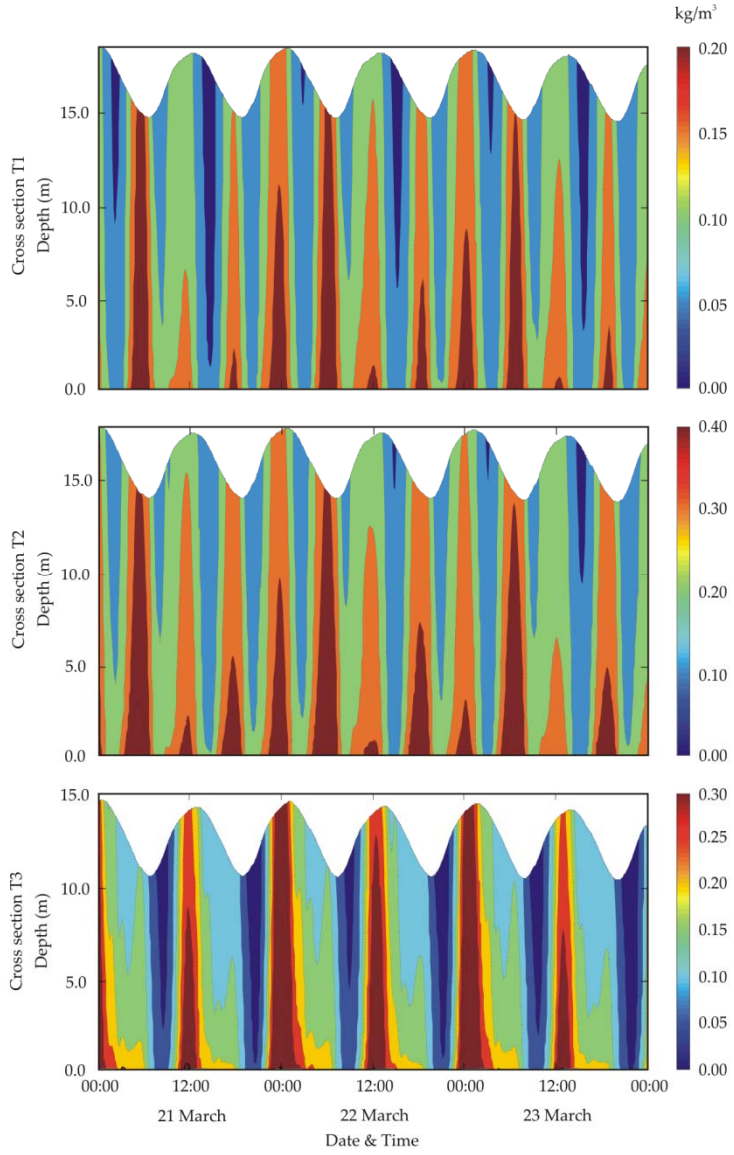

Figure 6.23 Graphs of the evolution of the vertical profiles of the SSCs respectively at middle point of cross section T1 (C1), T2 (C2), and T3 (C3)

For the tidal period where the field data were available (from 08:24 to 20:24 on 23rd of March 2000) these and the model results at the midpoint C3 of the cross section T3 were used to prepare the evolution of vertical profiles of the SSC. The resulting graphs are given in Figure 6.24. Referring to the graph for the field, two peaks of the SSC can be observed, one during the flood and one during the ebb tidal phase. It can also be seen that the two peaks are relatively close to each other (about 4 hours interval between the two peaks) and that in the near bed region the SSC remains high during the times between the two peaks (value of about 0.25 kg/m^3). This indicates that the sediments suspended during the flood phase did not get sufficient time to settle to the bed completely, thus during the returning ebb, the current caused further increase in the concentration of suspended sediment. Referring to the

graph for the model, as discussed in the previous section, it seems that the established model is incapable of reproducing the peak SSC during the ebb phase at this cross section.

From the results it can be concluded that this incapability of the model might be the main reason for the deviations observed between the model and measured data at this particular cross section (see for instance Figures 6.12 and 6.16). The insufficient supply of sediment from the tidal flat area on the eastern side of this cross section is responsible for this behaviour of the model. In another words, the modelled tidal flat areas do not supply sufficient sediment during the ebb current. There are several parameters and/or factors that might be responsible for this insufficient supply of sediments. One of those is grain size distribution of sediment particles in the tidal flats. It might be that the grain size distribution used as an input map of the model is not in agreement with the actual grain size distribution existing at the area during the data collection. As reported by Escobar (2007), the prepared map of the grain size distribution, presented in Section 3-7, was based on a limited number of measurements specifically on the tidal flat areas. He pointed out the existence of some localized discrepancies between the values in map and the actual values in the field. Precise information of the grain size distribution could improve the model results.

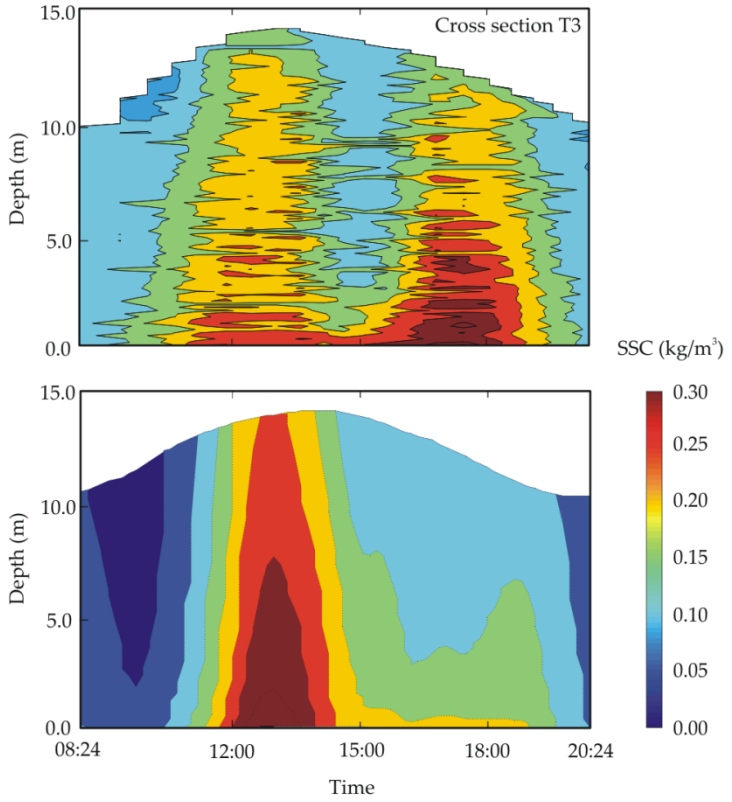

Figure 6.24 Graphs of the evolution of the vertical profiles of SSC from the field data (the top graph) and from the model results (the below graph) at the monitoring point C3 of the cross section T3

The second factor that might be responsible for the insufficient supply of sediment is the use of a constant settling velocity for the channels and the tidal flats. Distribution of different grain size in the area is necessitated using different settling velocities. Analysis of laboratory and field data has shown that the settling velocity of the flocs is related to the sediment concentration (van Rijn, 1993), the water depth (Owen, 1970), the flow velocity (Cornelisse, et al, 1990), flocculation and biological activities (Winterwerp et.al., 2002). Thus the settling

velocity for tidal channels cannot be the same as those for tidal flat area, because of flow depth and biological activity in the tidal flat. However, the use of variable settling velocities as a map is not yet incorporated in Delft3D model.

The third factor to consider for the observed model deficiency is the assignment of a constant erosion rate for the whole area, due to lack of the field data. The erosion rate is defined in the model via the critical bed shear stress for erosion (CBSSE) and the constant erosion parameter (see equation 2.2 of Chapter 2). The difficulties to measure this parameter in the field have prevented us to prepare a map of the distribution of CBSSE for the area. Therefore, this parameter is defined to the model as a single value for the whole area under investigation.

A combination of the above mentioned factors are probably involved for the deficiency observed in performance of the model specifically at cross section T3. As a trial a map has been prepared for the CBSSE, with the values for the tidal flat area being 50% less than those of the tidal channel. That is, to allow more sediment to be suspended and transported by the ebb current from the tidal flat area. The results which is presented in Figure 6.25 shows successive peaks of SSC due to the ebb current as well as flood current. It can however, be seen that this map of CBSSE resulted an increase in the SSC values for the whole period of tidal condition. Comparison of the model results of the Figure 6.24 and 6.25 also reveals that employing lower CBSSE for the tidal flat resulted in higher peak SSC values during ebb than during flood phase. This is in agreement with the field data qualitatively. The necessity for the production of a CBSSE map on the basis of the field data and model simulations is therefore suggested for the improvement of the model results.

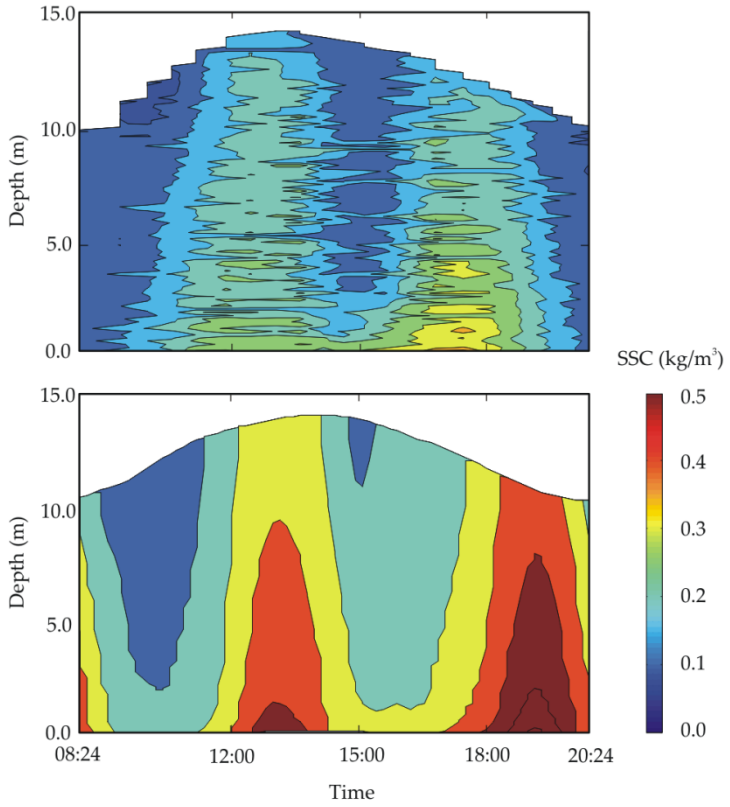

Figure 6.25Graphs of the evolution of the vertical profiles of SSC from the field data (the top graph) and from the model results using low value of critical bed shear stress for erosion for the tidal flat (the below graph) and high value for tidal channel

6.4.3 Snapshots of Suspended Sediment Concentrations in cross sections

Suspended sediment concentration (SSC) derived from the model and field data for cross sections T1, T2 and T3 were interpolated along the width and between the layers of the cross section to prepare instantaneous pictures of the SSC at different tidal stages. These pictures or snapshots at times of flood, high slack water, ebb and low slack water are given in Figures 6.26 to 6.28 for cross sections T1, T2 and T3 respectively. The top snapshot for each pair is from the model results and the one below from the field data. The observations and the deduction that can be made from these snapshots are described separately for each cross section. In descriptions the plots related to the model results and field data are defined as model and field plots correspondingly.

Cross section T1: During the flood phase there is a good agreement between the model and the field plots. The SSC is the maximum near the bed layer and decreases gradually toward the surface and the northern and southern banks (the right and the left sides of the snapshot respectively). At the high slack water, the model plot shows the same pattern of the SSC distribution as that during flood phase. The field plot however, shows some high SSC in the region close to the southern bank from the bed to the surface and the SSC decreases abruptly to remain the same elsewhere at the cross section. During the following ebb phase, the model plot shows a high concentration in the near bed layer with a tendency toward the northern bank. The SSC decreases gradually toward the surface and the southern bank. While, the field plot shows some high SSC in the region near the southern bank and nearly over the whole depth and the SSC decreases gradually toward the northern bank. In the low slack water, the field and model plots show relatively similar pattern of SSC distribution and the concentration decreases from the bed to the surface.

As can be seen during both the high slack water and ebb phase, the field plots show high SSC in the region near the southern bank and over the whole depth (uniform pattern along the depth), which decreases gradually toward the northern bank. This suggests the existence of a cross current from the southern bank to the northern bank, which transports the easily suspendable sediments of the southern region provided by the tidal flat area southward of the cross section toward the north. The migration of the channels toward the north which is reported by Wilkens and Mayerle (2005) supports this suggestion (Figure 3.6). Two main reasons that can be given for the model not predicting this cross flow are as follows. Either the grid cells of the model are too large (90 m) to simulate a cross current with low velocities, or the grain size distribution used by the model does not match the prototype distribution on the tidal flat areas. The latter was explained in the previous sections. No attempt was made to check the effect of various grid sizes and their configurations on the above mentioned behaviour of the model. This would require comprehensive grain size information from the field.

Cross section T2: During the flood phase in both model and field plots the suspension of sediment occurs at the same spatial position. The pattern of variation of SSC is not similar along the depth. In the model plot the SSC is the maximum in the small area around the midpoint of near the bed and decreases gradually toward the surface. In the field plot maximum SSC covers a larger area until the mid depth decreases rapidly toward the surface. During the high slack water, the model plot show the same pattern of SSC distribution as that observed in the model plot during flood phase, however with lower values for the SSC. This is an inconformity with the decrease in the current velocity in this tidal phase. The field plot at this tidal stage shows a localised high SSC in the region near to the southern bank extending to the mid cross section which decrease quickly from the mid cross section toward

the northern bank. During the following ebb phase, the model plot shows maximum SSC in the near bed layer of the northern bank with the gradual decrease towards the surface and the southern bank. While according to the field plot the high values of SSC are in the near bed layers of southern bank and decreasing gradually and in layers toward the surface and northern bank. This dissimilarity between the model result and field data has also been observed and discussed to some extent in section 6-4-1 (see Figure 6.20). During the low slack water, both model and field plots show the same pattern for SSC distribution as their corresponding plots during the ebb phase, but with some lower values for the SSC.

In cross section T2, like the cross section T1, the field plots for the tidal stages of high slack water and ebb phase indicate the transverse movement of SSC from the south bank toward the middle of cross section. This transverse movement again indicates the existence of a cross current, which transports sediments from the tidal flat area southward of the channel to the channel. The two reasons why the model did not show this cross flow, provided for cross sections T1 can be considered for this cross section. These are the large size of grid cells in the model and/or the imprecise grain size distribution used for the model.

Cross section T3: During the flood phase, both the model and the field plots show the same pattern of distribution of SSC across the cross section. That is, the concentration which is high in the bed to the middle layers of the southern bank region decreases gradually toward the surface and the northern bank region. The SSC values are higher for the model plot. At the following high slack water, the model plot shows high SSC at the deep region of the cross section near the northern bank, but the field plot shows high SSC in the shallow region of the cross section near the southern bank. This plot also shows that the SSC decreases abruptly toward the surface and the northern bank region, with the exception of an area of a high concentration in the middle of the cross section. During the following ebb phase the model plot show the same pattern as that during the flood phase with high SSC in the southern bank decreases gradually toward the northern bank. In the model plot it can be seen that the same process is started to develop in the near bed layer. The supply of sediment in the model is not sufficient for this process to be developed towards the surface (see below). At the low slack water, both the model and field plots show the same pattern of SSC distribution, with the maximum SSC at the deepest position of the cross section decreasing gradually towards the surface.

Referring to the model plots of this cross section for the four tidal phases, it is seen that the values of the SSC for the ebb phase and the low slack water are much lower in comparison with those for the flood phase and the high slack water. The reason for the low values of SSC during the ebb phase of this cross section is discussed in detail in Section 6-4-2. In that Section also is suggested that including the spatially variable critical bed shear stress for erosion (CBSSE) to some extent could solve the problem. Using the revised value suggested in that section the simulations were carried out, the results of this model was used to prepare the snapshot plots, which are given in Figure 6.29. Referring to this Figure successive performance of the model was achieved during the ebb phase. That is, the peak of SSC influenced by the ebb current is reproduced by the model. However, as it can be seen overprediction is imposed to SSC values computed by the model all over the cross section and for all tidal stages. In order to achieve the reliable results precise field measurements all over the area with the aim of estimating critical bed shear stress for erosion are needed to be carried out.

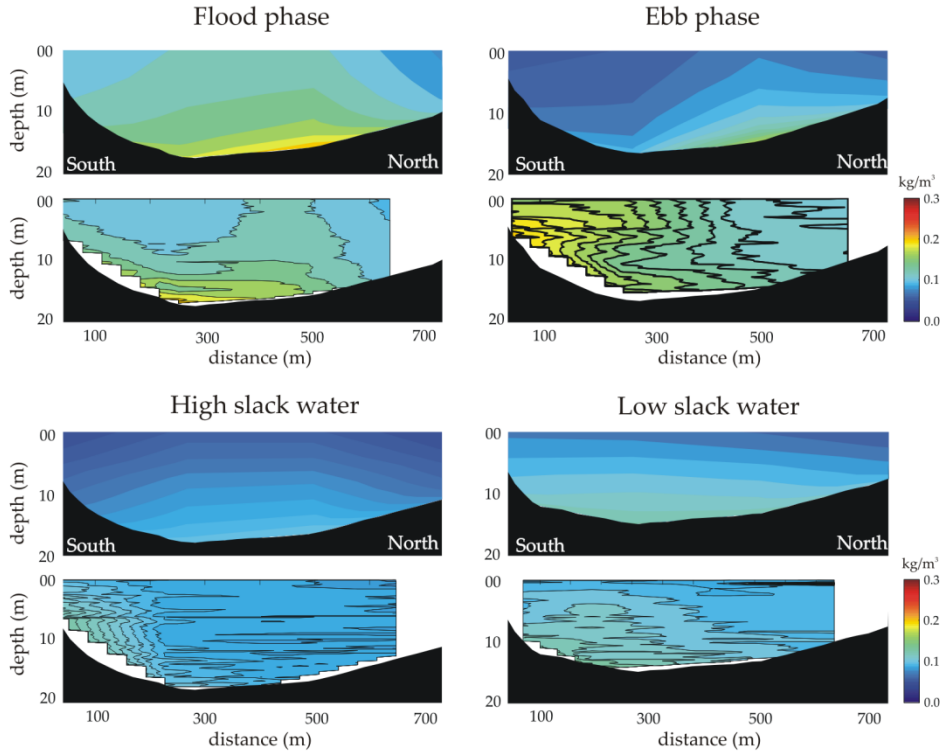

Figure 6.26 Snapshots of SSC distribution for flood, high slack water, ebb, and low slack water phase at cross-section T1. In each pair the top snapshot represents model results and the one below shows field data

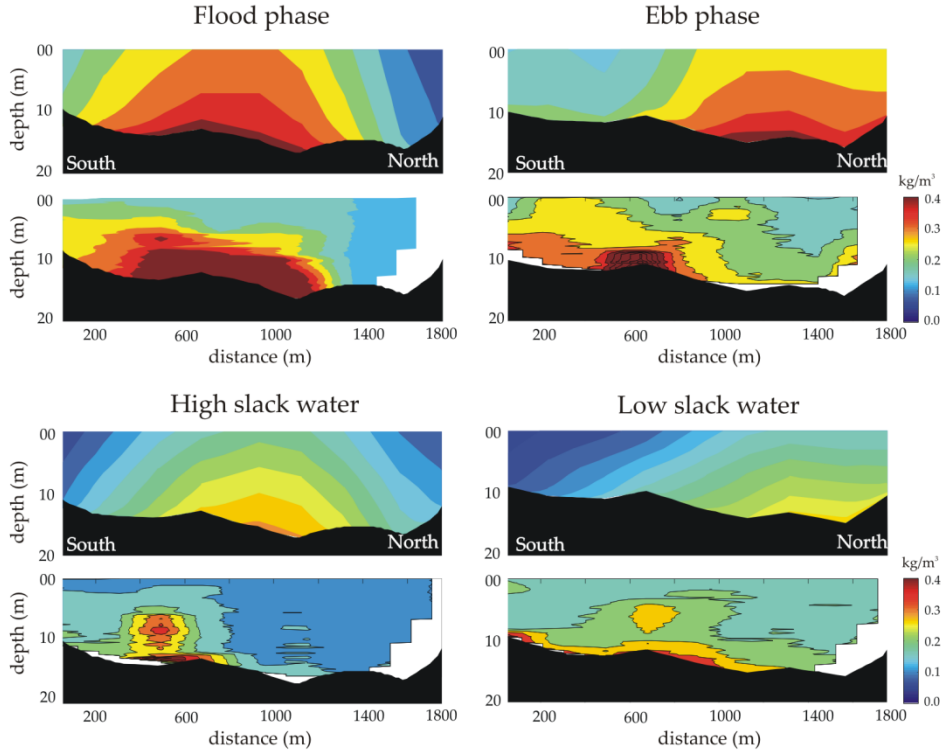

Figure 6.27 Snapshots of SSC distribution for flood, high slack water, ebb, and low slack water phase at cross-section T2. In each pair the top snapshot represents model results and the one below shows field data

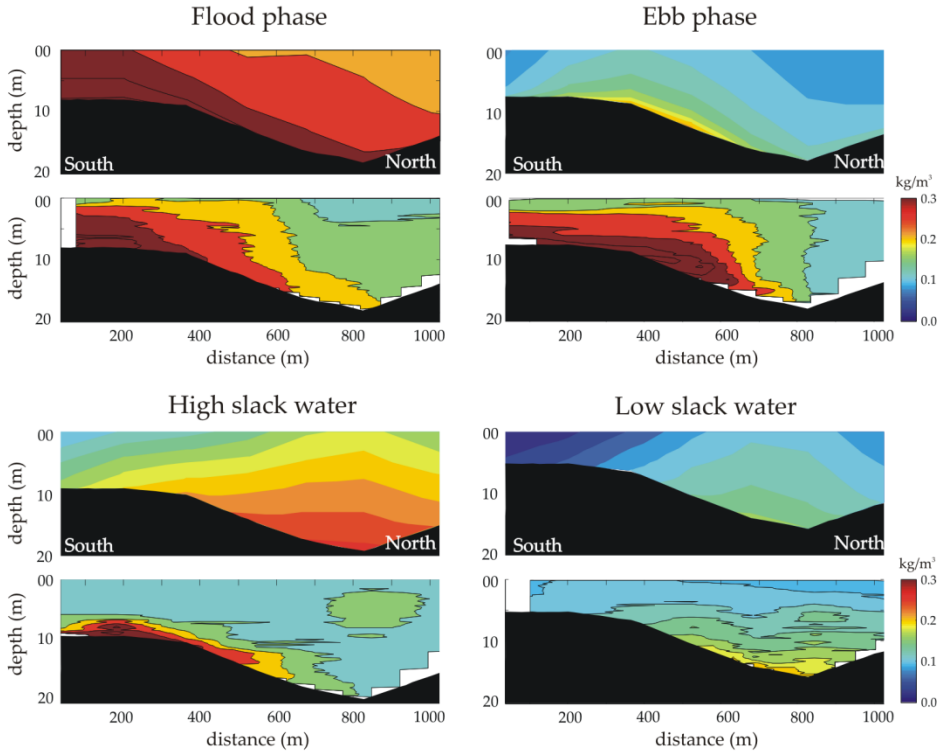

Figure 6.28 Snapshots of SSC distribution for flood, high slack water, ebb, and low slack water phase at cross-section T3. In each pair the top snapshot represents model results and the one below shows field data

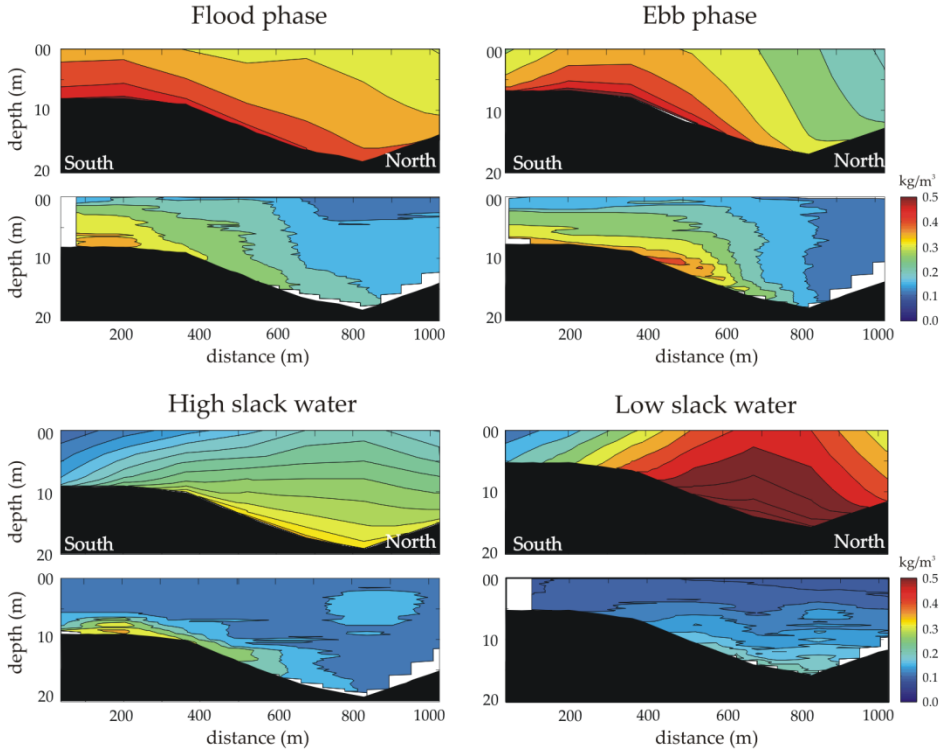

Figure 6.29Snapshots of SSC distribution for flood, high slack water, ebb, and low slack water phase at cross-section T3. In each pair the top snapshot represents the results from the simulation employing two different values of CBSSE for the tidal flat and tidal channel, and the below snapshot shows the field data

6.5 Summary

In this chapter the ability of the 3D model of the Delft3D package for the prediction of the suspended sediment transport has been investigated. The results from the 3D model were compared with the field data and also with the results from the 2DH model. It was found that the results from the 3D model do not show significant differences from those of the 2DH model. However, the 3D model results confirmed the well mixed water condition of the area, as the suspended sediment concentration (SSC) showed fairly uniform distribution over the depth. It was shown that the 3D model can provide very useful information about hydrodynamics and sediment dynamics and made it possible to find some weak points related to the measurement techniques and also some deficiencies in the modelling.

Current velocities derived from the model showed good agreement with the field data for the whole period of tidal cycle with the maximum difference of less than 0.2 m/s as observed by Palacio et. al. (2005) using the 2DH model. Regarding the module of the package for the sediment dynamics, some disagreements were observed between the 3D model results and the field data. It was found that the dissimilarities observed are partly due to some errors in the measuring devices and partly due to the model deficiency.

Studying the scatter of the SSC during a full tidal cycle showed that the larger dissimilarity between the modelled and the measured SSC values occurred during periods with low current velocities (less than 0.6 m/s). For these periods when the calculated ratios of the observed to the predicted values of the SSC were compared with the values of the current velocity showed that the observed SSC values were 0.1 to 4 times the predicted ones. Employing constant settling velocity in the simulations was suggested to be a passible factor responsible for the deficiencies observed.

The model is incapable to reproduce the peak SSC at cross section T3 during the ebb phase. The most probable cause identified was the insufficient supply of sediment from the tidal flat area located on the eastern side of cross section T3. This lack of sediment supply in the modelling, was attributed to one or a combination of the following factors:

1) The grain size distribution used as an input map to the model might not be in agreement with the actual grain size distribution in nature during the data collection,

2) Using one constant settling velocity for the whole tidal area including the tidal flat and tidal channel, and

3) Using a constant estimated erosion rate and/or critical bed shear stress for the area.

It was shown that when various values of critical bed shear stress for erosion were introduced for tidal flat and tidal channel the model results did improve qualitatively. To improve the results quantitatively however, precise measurement of the parameters involved is recomended.

Comparisons of the snapshots of SSC variations derived from to the field data, at cross sections T1 and T2, suggest the existence of a transverse current from the south bank toward north bank. This cross flow however, was not observed in SSC variations derived from the model results. It was reasoned that either the size of grid in the model might not be small enough to capture a cross current having a low velocity or the use of the grain size distribution provided for the model area in the south of the these cross sections is not in agreement with the actual field data.

Chapter 7. Conclusion

7.1 Predictive ability of two-dimensional modelling

7.1.1 Hydrodynamics domain

The ability of the model to calculate variation of the water level during various tidal cycles was evaluated. Even though the model was able to describe the trend of tidal variations reasonably well, some amplitude differences and phase lags of up to about 1 hour, in comparison with the field data were observed at several locations. The reason for this dissimilarity was attributed to the boundary conditions. Therefore, the water level variations imposed at the western boundary which was derived from the nesting procedure were adjusted. The adjustments to be made for tidal ranges of 2.3 and 4.0m were 30 and 50 min, for the phase shift and +16cm and -17cm for the tidal height, respectively. Applying these adjustments to the boundary conditions resulted in an improvement of 8% in the hydrodynamic results of the model.

The current velocities predicted by the model were in good agreement with the field data, i.e. the mean absolute error was less than 0.2 m/s. Some slight under-prediction of current velocity was observed during the flood phase. It was also observed that the effect of waves on water levels and current velocities was not significant for moderate winds having velocities less than 11m/s. Under stormy condition however, the effect of waves on water levels are significant. The coupled wave and flow modules for Anatol storm (with wind velocities of about 30m/s) resulted in water levels that were 2m higher than that derived from the model using only the flow module.

7.1.2 Sediment transport domain

To evaluate the ability of the model to predict suspended sediment concentration (SSC), three settings of the model were used, including existing model, the model with improvement to the open boundaries, and the calibrated model. It was found that none of these models could predict the SSCs within a factor of two of the measured data for all the values. Besides, the correlation between the model results from all the models and the field data was quite poor. The correlation coefficients for the results from the calibrated model were between 0.11 at cross section T2 and 0.20 at cross section T3.

Relative mean absolute error (RMAE) between the model results and the field data for the SSC showed that the best performance of the model was achieved for the tidal range of 4.0m, using the data of the measuring campaign between the 21st to the 23rd of March 2000. The error values were 0.31, 0.40, and 0.48, respectively for the SSC results at cross sections T1, T2, and T3. The results obtained indicate that the model tends to underpredict values of SSC at all cross sections.

The effect of waves on prediction of SSC was investigated. It was found that the waves having significant wave height of 4m increases the peak SSC of about 0.03 kg/m^3. The effect of wind generated waves on SSC during Anatol storm with significant wave height of up to 2.2m was extreme (6 kg/m^3). However, it should be mentioned that field data for these conditions were not available to evaluate the certainty of the results.

7.2 Predictive ability of three-dimensional modelling

7.2.1 Establishment

With respect to the computation needs and required accuracy the inclusion of ten vertical layers in non-dimensional σ-coordinate system was found appropriate through sensitivity and error analyses. Increasing the number of layers beyond the ten, the improvement in the prediction of the SSC was insignificant; i.e. increasing the number of layers from ten to twelve, the sensitivity analysis showed an improvement of about 2%. The trend of increasing the thicknesses of the layers was considered logarithmic from the bed to the surface. To include the effect of the turbulence in the model, the k-l module was considered sufficient through sensitivity and error analyses.

7.2.2 Comparison between the performance of the 2DH and the 3D models

The RMAE values calculated between the SSCs derived from the 3D model and the field data did not show any significant differences with those calculated between the 2DH model and the field data.

The graphical analyses of the 3D model results show a uniform distribution of the current velocity and the SSC over the depth, comparable with those of depth-averaged results from the 2DH model. This observation confirmed the assumed well-mixed coastal water condition of the area. The correlation between the predicted and the observed SSC values was considerably increased by the use of the 3D model in comparison with the 2DH model results. This was especially significant for cross section T1, at which correlation coefficients resulted from the 2DH model were from 0.02 to 0.09 and those from the 3D model were from 0.11 to 0.34.

7.2.3 Comparison the performance of the 3D model with the actual results of the field

In the analyses of the SSC profiles derived from the 3D model with those derived from the field, some dissimilarities was observed relating to the ebb current and the shallow water regions of cross sections T2 and T3. For this tidal condition in these regions, the SSC values derived from the model were lower than the data, which were obtained from the conversion of transmissometer records to the SSC. Comparison of these SSC data and those derived

from the ADCP device, and considering the well-mixed condition of the area, it was concluded that the dissimilarity should be due to some errors in transmissometer records. That is, when transmissometer data for the shallow water regions were omitted from the set of field data particularly at cross section T2, the agreements between the model results and the data were improved significantly. Existence of biological matters in shallow water area especially during ebb condition was suggested to be responsible for overestimation of SSC records by the transmissometer. Besides, biological matters produce air bubbles which may also affect the transmissometer readings up to two times.

Through the functional relationship established between the current velocities and the ratio of the predicted to the measured SSC, a good agreement between the modeled and measured SSC was found at the slack water and at maximum current velocities. Large differences were observed during the condition of low current velocities, between 0.3 and 0.6 m/s, as the ratios of the predicted to the measured SSC varied between 0.1 and 4.0. This was attributed to the existence of some deficiencies in the model. It has been discussed that using a constant settling velocity and/or a constant critical bed shear stress in the model for the whole area and for the whole tidal cycle are likely cause of the observed disagreements.

Comparison of the modeled and measured time series of the SSC distribution across the cross sections showed a phase lag of about one hour during the ebb current at cross sections T1 and T2. At cross section T3 a time lag of about half an hour has been found during the flood phase. The phase lag during the ebb phase was suggested to be due to the insufficient supply of the sediment for the ebb current

Through the comparison of the modeled and measured SSC snapshots for each cross section at different tidal phases it was concluded that the predicted SSC values are in good agreement with the field data during the periods of flood phase and low slack water and at all of the cross sections. Spatial dissimilarities are observed in the distribution of the SSC, during the periods of high slack water and the ebb phase at cross sections T1 and T2. Consideration of hydrodynamics and the location of the cross sections led to the possible existence of a cross current from the southern bank region to the northern one.

It was also found that the model could not simulate the peak SSC during the ebb current at cross section T3. An insufficient supply of sediment from the tidal flat area eastward of the cross section was considered to be responsible. The input of different values of the critical bed shear stress for erosion for the tidal flat areas and the tidal channel eastward of this cross section did improve the model results qualitatively.

7.2.4 Parameters and/or factors responsible for the model deficiency

The comparisons of the model results and the field data showed that for some specific points at the cross sections and at some times during the tidal cycle the model did not result in accurate values of the SSC. Although some simplifications are always involved in modeling, causing some deviations from the reality, the aim is to minimize these deviations.

It is usual practice to combine some properties of the system into one parameter or assign fixed values for the parameters while in reality they may vary spatially and temporally. Therefore, it is imperative to carefully select these parameters before assigning them to the model. Following factors and/or parameters are considered to be responsible for the dissimilarity observed between the model results and field data:

i. dissimilarity between the grain size distributions that exist in the field and those are fed into the model, specifically on the tidal flat area;

ii. the use of one constant settling velocity for the whole tidal area, consisting of tidal flats and tidal channels, and for the whole tidal cycles;

iii. the use of one constant estimated critical bed shear stress for erosion for the area, due to the lack of the field data;

iv. not taking into account biological activity and flocculation processes; and

v. uncertainty in the roughness values assigned to the model, owing to the lack of the field data.

As stated in Section 7.2.3 the use of spatially variable critical bed shear stress for erosion for tidal channel and tidal flats improved the model performance. This suggests the need for the preparation of a map of the parameters involved, including critical bed shear stresses and settling velocity, for the area on the basis of field measurements. At present, while the Delft3D package allows the use of spatially variable of the critical bed shear stresses and erosion parameter of the area, by using the add-on file facility for these parameters, such facility however, does not exist for the settling velocity parameter. It may also be suggested the need for a further improvement of the existing grain size map of the area through a more extensive field measurements, considering that the existing map was prepared on the basis of limited field data.

7.2.5 The choice of the 2DH or the 3D model for the area under investigation

In this study both 2DH and 3D model were employed and predictive ability of both were investigated and discussed. Comparison of the current velocity and the SSC results from the 2DH and the 3D simulations showed their differences were not significant. It was shown that the values derived from the 3D models represented a fairly uniform distribution over the depth having a quite good agreement with the corresponding depth averaged values derived from the 2DH model.

At the current state of the available data, the use of the 3D model does not seem to be justified for the area under investigation, considering its demand for a larger memory allocation, longer time for the computations, and the similarity of the results with those of the 2DH model. However, it is shown that the use of the 3D model made it possible to find some weak points and deficiencies in the model and/or in the collected data from the field through the prepared graphs and snap shot of the SSC, which provided very useful information about the flow and sediment dynamics in the area.

References

Abbott, M.B., Damsgaard A., and Rodenhuis, G.S., 1973. *System 21, Jupiter, A design system for two-dimensional nearly-horizontal flows,* Journal of Hydraulic Research, vol. 1 (l), pp 1-28.

Abdel-Aal, F.M., 1992. *Shoreline change modeling*, In: Computer Modelling of Seas and Coastal Regions, Partridge, P.W. (Eds.), Boston, MA: Computational Mechanics Publications, pp 379-396.

Adkins, G., and Pooch, U.W., 1977. Computer simulation: a tutorial. *Computer*, vol. 10, pp 12-17.

Asp, N.E. 2004. L*ong- to short-term morphodynamic evolution of the tidal channels and flats of the Dithmarschen Bight, German North Sea,* Ph.D. Thesis, Coastal Research laboratory, University of Kiel, Germany, 126 pp.

Asp, N. E., Wilkens, J., Ricklefs, K. & Mayerle, R., 2001. *Geology and Morphodynamics of a Tidal Flat Area of the German North Sea Coast and Its Support to a Medium-scale Morphodynamic Modelling,* In: Proceedings VIII Congresso da ABEQUA. Mariluz/Imbe, Brazil.

Allsop N.W.H., Vann A.M., Howarth M., Jones R.J. & Davis J.P., 1995. *Measurements of wave impacts at full scale: results of fieldwork on concrete armour units*, Proc. Conf. On Coastal Structures & Breakwaters '95, ICE, ISBN 0-7277-2509-2, Thomas Telford, London, pp287-302.

Allsop N.W.H., Vicinanza D. & McKenna, J.E., 1996. *Wave forces on vertical and composite breakwaters*, Research Report SR 443, HR Wallingford, pp 1-94.

Amos, C.L., Feeney, T., Sutherland, T.F., Luternauer, J.L., 1997. *The stability of fine-grained sediments from the Fraser River delta*, Estuarine Coastal and Shelf Science, vol. 45 (4), pp 507-524.

Andersen, T.J., Jensen, K.T., Lund-Hansen, L., Mouritsen, K.N., Pejrup, M., 2002. *Enhanced erodibility of fine-grained marine sediments by Hydrobia ulvae*. Journal of Sea Research, vol. 48, pp 51–58.

Ariathurai, R. and Krone, R.B., 1976. *Finite Element Model for Cohesive Sediment Transport,* Journal of the Hydraulics Division, vol. 102 (3), pp 323-338.

Ariathuri, R. & MacArther, R., Krone, R. B., 1977. *Mathematical model of estuarial sediment transport*, Technical Report D-77-12, US Army Corps of Engineers, Dredged Material Research Program, Vicksburg, Mississipi, USA, 158 pp.

Armanini, A., 1995. *Non-uniform sediment transport: Dynamics of the active layer*, Journal of Hydraulic Research, vol. 33, pp 611- 622.

Aubrey, D.G., 1986. *Hydrodynamic Controls on Sediment Transport in Well-Mixed Bays and Estuaries*, In: Physics of Shallow Estuaries and Bays, J. van de Kreeke (Eds.), Springer-Verlag, pp 245-258.

Austen I., Andersen T.J., Edelvang K. 1999. *The influence of benthic diatoms and invertebrates on the erodibility of an intertidal mudflat, the Danish Wadden Sea*, Estuarine, Coastal and Shelf Science, vol. 49 (1), pp 99-111.

Baart, F., Van der Kaaij, T., Van Ormondt, M., Van Dongeren, A., Van Koningsveld, M., Roelvink, J. A., 2009. *Real-time forecasting of morphological storm impacts: a case study in the Netherlands,* Journal of coastal research, vol. SI56, pp 1617-1621.

Bagnold, R.A., 1966. *An approach to the sediment transport problem from general physics*, Professional Paper U.S. Geological Survey Professional Paper, 422-I, pp 1-37.

Balci, O., 1997. *Principles of simulation model validation, verification, and testing*, Transactions of the Society for Computer Simulation International, vol. 14 (1), pp 3-12.

Balci, O., and Sargent, R.G., 1984. *A bibliography on the credibility assessment and validation of simulation and mathematical models*, Simuletter, vol. 15, pp 15-27.

Barber, R.W. & Pearson, R.V., 1996. *Modelling tide-induced currents and pollutant transport using a generalised curvilinear coordinate system, Computational Mechanics,* INC., 25 Bridge St., Billerica, MA 01821 (USA), pp 263-274.

Bartholomä, A., Kubicki, A., Badewien, T.H., Flemming B.W., 2009. *Suspended sediment transport in the German Wadden Sea - seasonal variations and extreme events*, Ocean Dynamics, vol. 59 (2), pp. 213-225.

Bass, S. J. 2000. *Sand and mud dynamics in shelf seas,* Ph.D. Thesis, University of Cambridge, United Kingdom.

Bass, S. J., Aldridge, J. N., McCave, I. N., & Vincent, C. E., 2002. *Phase relationships between fine sediment suspensions and tidal currents in coastal seas,* Journal of Geophysical Research, vol. 107 (3146), 14 pp, doi:10.1029/2001JC001269.

Bass, S. J., McCave, I. N., Rees, J.M.,Vincent, C. E., 2007. *Sand and mud flux estimates using acoustic and optical back scatter sensors:measurements seaward of the Wash, southern North Sea,* Geological Society, vol. 274, pp 25-35.

Baugh, J.V., Manning, A.J., 2007. *An assessment of a new settling velocity parameterization for cohesive sediment transport modelling*, Continental Shelf Research, vol. 27,pp 1835-1855.

Beheshti, A.A. and Ataie-Ashtiani, B., 2008. *Analysis of Threshold and Incipient Conditions for Sediment Movement*, Coastal Engineering, vol. 55, pp. 423-430.

Bekey, G.A., 1977. *Models and reality: some reflections on the art and science of simulation, Simulation*, vol. 29, pp 161- 164.

Benedet, L. and List, J.H., 2008. *Evaluation of the physical process controlling beach changes adjacent to nearshore dredge pits,* Coastal Engineering, vol. 55, pp 1224-1236.

Besley, P., Stewart, T. and Allsop, N.W.H., 1998. *Overtopping of vertical structures: new prediction methods to account for shallow water conditions*, Proc. Conf. Coastlines, Structures and Breakwaters, I.C.E., publ. Thomas Telford, London, pp 46-58.

Bilgili, A., Swift, M.R., Lynch, D.R., Ip, J.T.C., 2003. *Modelling bed-load transport of coarse sediments in the Great Bay Estuary, New Hampshire*, Estuarine, Coastal and Shelf Science vol. 58, pp 937-950.

Bishop, J.K.B., 1986. The correction and suspended particulate matter calibration of Sea-Tech transmissometer data, Deep-Sea Research, vol. 33, pp 121-134.

Black, K.P., 1995. *The numerical hydrodynamic model 3D and support software,* Occasional Report No.19, In: Department of Earth Sciences, Waikato, N.Z. (Eds.), University of Waikato, 69 pp.

Black, K.P., 2003. *Perspective on Evolution in Sediment Modelling*, Chapter 8 In: Advances in Coastal Modelling, C. Lakhan (Eds.), Elsevier Oceanography Series, Amsterdam, vol. 67, pp 217-235.

Black, K., Green, M., Healy, T., Bell, R., Oldman, J., and Hume, T., 1999. *Lagrangian modeling techniques simulating wave and sediment dynamics determining sand-body equilibria,* In: Computerized Modeling of Sedimentary Systems, Harff, J., Lemke, W., and Stattegger, K. (Eds.), New York: Springer-Verlag, pp 3-22.

Blumberg, A. F., and H. L. Mellor, 1987. *Three-dimensional coastal ocean models*, A Description of a Three-Dimensional Coastal Ocean Circulation Model, N.S. Heaps (Eds.), vol. 4, American Geophysical Union, 208 pp.

Booij, N., R. C. Ris, and L. H. Holthuijsen, 1999. *A third-generation wave model for coastal regions, 1, Model description and validation*, Journal of Geophysical Research, vol. 104 (C4), pp 7649-7666.

Borthwick, A.G.L., Barber, R.W., 1992. *River and reservoir flow modeling using the transformed shallow water equations*, International Journal of Numerical Methods Fluids, vol. 14, pp 1193-1217.

Boudreau, B.P., 1997. *A one-dimensional model for bedboundary layer particle exchange*, Journal of Marine Systems, vol. 11 (3–4), pp 279–303.

Brennan, M. L., May, C. L., Danmeier, D. G., Crooks, S., and Haltiner, J. H., 2008. *Numerical Modeling of Restoration Alternatives in an Erosional Estuary,* Proceedings of the Tenth International Conference on Estuarine and Coastal Modeling, Newport, RI; USA, ASCE, pp 942-960.

Briand M.H.G. and Kamphuis, J.W., 1990. *A Micro Computer Based Quasi 3-D Sediment Transport Model,* Proc. 2nd Int. Conf. on Co. Eng., ASCE, Delft, pp 2159-2172

Briand, M., Kamphuis, J.W., 1993. *Waves and currents on natural beaches: a quasi 3d numerical model*, Coastal Engineering, vol. 20, 101-134.

Bunt, J.A.C., Larcombe, P., and Jago, C.F., 1999. Quantifying the response of optical backscatter devices and transmissometers to variations in suspended particulate matter, Continental shelf research, vol. 19(9), pp 1199-1220.

Burchard, H., Flöser, G., Staneva, J.V., Badewien, T.H., & Riethmüller, R., 2008. *Impact of density gradients on net sediment transport into the Wadden Sea,* Journal of Physical Oceanography, vol. 38, pp 566−587.

Burt, T.L., 1986. *Field settling velocity of estuary muds*, In: Estuarine cohesive sediment dynamics, A. J. Mehta (Eds.), Lecture notes on coastal and estuarine studies, New York: Springer, vol. 14, pp 126-150.

Campbell, C.G., Laycak, D.T., Hoppes,W., Tran, N.T., Shi, F.G., 2005. *High concentration suspended sediment measurements using a continuous fiber optic in-stream transmissometer*, Journal of Hydrology, vol. 311, pp 244-253.

Cancino, L., and Neves, R., 1999. *Hydrodynamic and sediment suspension modelling in estuarine systems. part I: Description of the numerical models*, Journal of Marine Systems, vol. 22, pp 105- 116.

Cancino, L., Neves, R., 1999. *Hydrodynamic and sediment suspension modelling in estuarine systems: Part II. Application to the Western Scheldt and Gironde estuaries,* Journal of Marine Systems, vol. 22, pp 117- 131.

Cacchione, D.A., P.D. Thorne, Y. Agrawal, and N.J. Nidzieko, 2007. *Time-averaged near-bed suspended sediment concentrations under waves and currents: comparison of measured and model estimates*, Continental Shelf Research, vol. 28 (3), pp 470-484.

Carrivick JL. 2007. *Modelling coupled hydraulics and sediment transport of a high magnitude flood and associated landscape change,* Annals of Glaciology, vol. 45, pp 143−154.

Casulli, V., and Cheng, R.T., 1992. *Semi-implicit finite difference methods for three-dimensional shallow water flow*, International Journal for Numerical Methods in Fluids, vol. 15, pp 629-648.

Celik, I., and Rodi, W., 1988. *Modeling Suspended Sediment Transport In Nonequilibrium Situations*, Journal of Hydraulic Engineering, vol. 114 (10), pp 1157–1191.

Cheviet, C., Violeau, D., and Guesmia M., 2002. Numerical Simulation of Cohesive sediment Transport in the Loire Estuary with a Three-Dimensional Model Including New Parameterisatons, In: Fine Sediment Dynamics in the Marine Environment, Winterwerp, J.C. and C. Kranenberg (eds.), Elsevier, Amsterdam, pp 529-544.

Cole, P., & Miles, G. V. (1983). *Two-dimensional model of mud transport*, Journal of Hydraulic Engineering, ASCE, vol. 109, pp 1-12.

Davies, A., Van Rijn, L.C., Damgaard, J., Van de Graaff, J., and Ribberink, J., 2002. *Intercomparison of research and practical sand transport models*, Coastal Engineering, vol. 46, pp 1- 23.

Davies, A. G., and Villaret, C., 2002, *Prediction of sand transport rates by waves and currents in the coastal zone,* Continental shelf research, vol. 22 (18 – 19), pp 2725-2737.

De Vriend, H.J., Stive, M.J.F., 1987. *Quasi-3D modelling of nearshore currents,* Coastal Engineering, vol. 11, pp 565- 601.

De Vriend, H.J., 1991. *Modelling in marine morphodynamics,* In: Computer Modelling in Ocean Engineering 91, Arcilla, A.S., Pastor, M., Zienkiewicz, O.C., and Schrefler, B.A. (Eds.), Rotterdam, The Netherlands: A.A. Balkema, pp. 247-260.

De Vriend, H.J., Zyserman, J., Nicholson, J., Roelvink, J.A., Pe`chon, P., Southgate, H.N., 1993. *Medium-term 2DH coastal area modelling.* Coastal Engineering, vol. 21, pp 193-225.

De Vriend, H.J., and Ribberink, J.S., 1996. *Mathematical modelling of meso-tidal barrier island coasts. Part II: Process-based simulation models,* In: Advances in Coastal and Ocean Engineering, Lui, P.L.-F. (Ed.), Singapore:World Scientific Publishing Co., vol. 2, pp 151-197.

Dean, R.G. and Dalrymple, R.A., 2002. *Coastal Processes with Engineering Applications,* Cambridge, UK, Cambridge University Press, 487 pp.

Dittmer, E., 1938. *Schichtenaufbau und Entwicklungsgeschichte des dithmarscher Alluviums,* Westküste, No. 1 (2): pp 105-150.

Dodd, N., 1998. *Numerical model of wave runup, overtopping and regeneration,* Journal of Waterway, Port, Coastal and Ocean Engineering, vol. 124(2), pp 73-81.

Dankers, N., Binsbergen, M., Zegers, K., Laane, R., & Rutgers Van Der Loeff, M., 1984. *Transportation of water, particulate and dissolved organic and inorganic matter between a salt marsh and the Ems-Dollard estuary,* the Netherlands, Estuarine, Coastal and Shelf Science, vol. 19, pp 143-165.

Denner, w.w., 1989, *Measuring and understanding coastal processes for engineering purposes,* National Academies Press, 119 pp.

Dronkers, J., 1986, *Tidal asymmetry and estuarine morphology*, The Netherlands Journal of Sea Research, vol. 20, pp 117-131.

Dyer, K.R., 1986. *Coastal and Estuarine Sediment Dynamics,* John Wiley and Sons, New York, 342 pp.

Dyer, K.R., 1989. *Sediment processes in estuaries: future research requirements*, Journal of Geophysical Research, vol. 94 (C10), pp 14327-14399.

Dyer K.R., Bale, A.J., Christie, M.J., Feates, N., Jones, S., and Manning, A.J., 2002. *The Turbidity Maximum in a Mesotidal Estuary, the Tamar Estuary, U.K.: I and II*. In: Fine Sediment Dynamics in the Marine Environment, Winterwerp, J.C. and C. Kranenberg (eds.), Elsevier, Amsterdam, pp 203-232.

Echeverry, J., 2004. *Assessment of performance of the Dithmarschen Bight model using the RMAE parameter on cross section measurements*, Master of Science Thesis, Coastal Research laboratory, University of Kiel, Germany, 98 pp.

Eisma, D., 1993. *Suspended matter in the aquatic environment*, Springer-Verlag, ISBN 354055825X, Berlin, 318 pp.

Eisma, D., & Li, A., 1993. *Changes in suspended matter floc size during the tidal cycle in the Dollard Estuary*, Netherlands Journal of Sea Research, vol. 31 (2), pp 107- 117.

Elfrink, B., Broker, I., Deigaard, D., Hansen, E., Justesen, P., 1996. *Modelling of q3d sediment transport in the surf zone*, In: Coastal Engineering, Edge, B.L. (Eds.), ASCE, Orlando, Florida, USA, pp. 3805-3817.

Escobar, C.A. 2007, *Modelling of Sediment Dynamics in the Dithmarschen Bight, German North Sea Coast*, Ph.D. Thesis, Coastal Research laboratory, University of Kiel, Germany, 208 pp.

Escobar S, C. A. Mayerle, R., 2006. *Procedures for Improving the Prediction of Equilibrium Grain Sizes, Bed Forms and Roughness in Tidally-Dominated Areas,* Journal of Coastal Engineering Conference, Conf. 30, vol. 3, pp. 3092-3104

Falconer, R.A., 1980. *Numerical Model of Tidal Circulation in Harbors,* Journal of the Waterway Port Coastal and Ocean Division, ASCE, vol. 106 (11), pp. 31-48.

Fennema, R. J., and Chaudhry, M. H., 1990. *Explicit methods for 2-D transient free surface flows,* Journal of Hydraul. Eng., vol. 116 (8), pp 1013-1034.

Figge, K., 1980. *Begleitheft zur Karte der Sedimentverteilung in der Deutschen Bucht 1:250000 (Nr. 2900),* Bericht des Deutsches Hydrographisches Instituts, In German.

Francisco, J.M., Simoes and Yang, C.T., 2006. *Sedimentation Modeling for Rivers and Reservoirs,* In: Reclamation Managing Water in the West. Erosion and Sedimentation Manual, C.T. Yang (Eds.), U.S. Department of the Interior Bureau of Reclamation, Denver, Colorado, Chapter 5, 92 pp.

Furbringer, J.-M., and Roulet, C.-A., 1999. *Confidence of simulation results: put a sensitivity analysis module in your mode,* The IEAECBCS annex 23 experience of model evaluation, Energy and Buildings, vol. 30, pp 61–71.

Furumai, H., 2010. *Significance of Advanced Monitoring and Application of environmental Numerical Simulation,* In: Advanced Monitoring and Numerical Analysis of Coastal Water and Urban Air Environment, H. Furumai, S. Sato, M. Kamata and K. Yamamoto (Eds.), vol. 3, pp 1-11.

Galappatti, R., & Vreugdenhil, C. B, C.B. 1985. *A depth-integrated model for suspended transport,* Journal of Hydraulic Research, vol. 23, pp 359-377.

Gartner, J. W., Cheng, R., Wang, P.F., & Richter, K., 2001. *Laboratory and field evaluations of the LISST-100 instrument for suspended particle size determinations,* Journal of Marine Geology, vol. 175, pp 199-219.

Goda, Y., 1985. *Random seas and maritime structures,* Univeristy of Tokyo Press.

Gordon, H.R. and Clark, D.K., 1980. *Initial Coastal Zone Color Imagery,* Proceedings of the 14th Symposium on Remote Sensing of Environment, San Jose, Costa Rica, April 23-30.

Green, M. O., Bell, R. G., Dolphin, T. J. & Swales, A., 2000. *Silt and sand transport in a deep tidal channel of a large estuary (Manukau Harbour, New Zealand),* Journal of Marine Geology, vol. 163, pp 217-240.

Groen, P., 1967. *On the residual transport of suspended matter by an alternating tidal current,* Netherlands Journal of Sea Research, vol.3, pp 564- 574.

Haas, K. A., and Warner, J. C., 2009. *Comparing a quasi-3D to a full 3D nearshore circulation model: SHORECIRC and ROMS,* Ocean Modelling, vol. 26, pp 91-103.

Hamrick , J. M. 1992. *A Three-dimensional Environmental Fluid Dynamics Computer Code: Theoretical and Computational Aspects,* The College of William and Mary, Virginia Institute of Marine Science, Special Report 317, 63 pp.

Hartsuiker, G., 1997. *Deutsche Bucht and Dithmarschen Bucht, Set-up and calibration of tidal flow models,* Delft Hydraulics, report no. H1821.

Hawley, N., and Lesht, B. M., 1992. *Sediment resuspension in Lake St. Clair,* Limnol. Oceanogr., vol. 37, pp 1720-1737.

Hill, P.S., Syvitski, J.P., Cowan, E.A., and Powell, R.D., 1998. *In situ observations of floc settling velocities in Glacier Bay, Alaska,* Marine Geology, vol. 145, pp 85-94.

Hill P.S., Milligan, T.G., and Geyer, W.R., 2000. *Controls on effective settling velocity of suspended sediment in the Eel River flood plume,* Continental shelf research, vol. 20(16), pp 2095-2111.

Holmes, P., and Samarawickrama, S.P., 1997. *Tide and wave-induced changes at a coastal lagoon entrance,* In: Computer Modelling of Seas and Coastal Regions III, Arcinas, J.R., and Brebbia, C.A. (Eds.), Coastal 97, Boston, MA: Computational Mechanics Publications, pp. 75-84.

Horn, D.P., 1992. *A numerical model for shore-normal sediment size variation on a macrotidal beach,* Earth Surface Processes and Landforms, vol. 17, pp 755-773.

Houwing, E.J., 1999. Determination of the critical erosion threshold of cohesive sediments on intertidalmud flats along the Dutch Wadden Sea Coast, Estuarine, Coastal and Shelf Science, vol. 49, pp 545-555.

Hsu, Y. L., Dykes, J.D., Allard, R.A., and David, D. W., 2007. *Validation test report for Delft3D,* NRL memorandum report, NRL/MR/7320-08-9079, 42 pp.

Hu, K., Ding, P., Wang, Z., Yang, S., 2009. *A 2D/3D hydrodynamic and sediment transport model for the Yangtze Estuary, China,* Journal of Marine Systems, vol. 77 (1-2), pp 114-136.

Huang, I.T., 2006. Investigation of Sediment Dynamics Using Numerical Model in the Central Dithmarschen Bight, German North Sea Coast, Master Thesis, Coastal Research Laboratory, University of Kiel, 75 pp.

Hwang, K.N., Mehta, A.J., 1989. *Fine sediment erodibility in Lake Okeechobee, Florida,* Coastal & Oceanographic Engineering Dept., University of Florida, Technical Report UFL/COEL-89/019, 140 pp.

Huthnance, J.M., Karunarathna, G., Lane, A., Manning, A.J., Norton, P., Reeve, D., Spearman, J., Soulsby, R.L., Townend, I.H., Wolf, J. and Wright, A., 2007. *Development of estuary morphological models,* R&D Technical Report FD2107/TR, Joint Defra/EA Flood and Coastal Erosion Risk Management R&D Programme.

Jago, C.F. and Bull, C.F., 2000. *Quantification of errors in transmissometer-derived concentration of suspended particulatematter in the coastal zone: implications for flux determinations,* Marine Geology, vol. 169, pp 273–286.

Ji, Z.-G., 2008. *Hydrodynamics and water quality; modeling rivers, lakes and estuaries,* Wiley-Interscience., 704 pp.

Ji, Z.-G., Hamrick, J.H., and Pagenkopf, J., 2002. *Sediment and metals modeling in shallow river*, Journal of Environmental Engineering, vol. 128, pp 105-119.

Jiménez Gonzalez, S., Mayerle, R., and Egozcue, J.J., 2005. *A Proposed Approach for Determination of the Accuracy of Acoustic Profilers in the Field*, Die Küste, Heft 69, pp 409-420.

Katopodi, I. and Ribberink, J.S., 1992. *Quasi-3D modelling of suspended sediment transport by currents and waves,* Coastal Engineering, vol. 18(1&2), pp 83-110.

Kineke, G. C. & Sternberg, R. W., 1989. T*he effect of particle settling velocity on computed suspended sediment concentration profiles,* Marine Geology, vol. 90, pp 159-174.

Kitchen, J.C., Zaneveld, J.R.V., 1980. *Interrelationships between optical parameters, biological parameters and particle size distributions in Monterey Bay,* Oregon State University. Dept. of Oceanography, Technical Report, NAS5-23738, 53 pp.

Krone, R. B., 1962. *Flume studies of the transport of sediment in esturial shoaling processes,* Hydraulic Engineering Laboratory, and Sanitary Engineering Laboratory University of California, Berkeley. 110 pp.

Krone, R.B., 1999. *Effects of bed structure on erosion of cohesive sediments,* Journal of Hydraulic Engineering, vol. 125 (12), pp 1297-1301.

La Valle, P.D., and Lakhan, V.C., 1993. *Comparison between simulated and empirical results on nearshore morphological changes,* Third International Geomorphological Conference. Program with Abstracts, The International Association of Geomorphologists, p. 175.

La Valle, P.D., and Lakhan, V.C., 1997. *Utilizing microcomputer-based models to simulate changes in the nearshore environment,* Environment Modelling & Software, vol. 12 (1), pp 19–26.

Lakhan, V.C., 1986. *Modelling and simulating the morphological variability of the coastal system,* Presented at the *International Congress on Applied Systems Research and Cybernetics* on August 18, 1986 in Baden-Baden, West Germany.

Lakhan, V.C., 1989. *Modeling and simulation of the coastal system,* In: Applications in Coastal Modeling, Lakhan, V.C., and Trenhaile, A.S. (Eds.), Amsterdam, The Netherlands, Elsevier Science Publishers, pp 17-42.

Lakhan, V.C., 1991. *Simulating the interactions of changing nearshore water levels, morphology and vegetation growth on Guyana's coastal environment,* In: Toward Understanding Our Environment, McLeod, J. (Ed.), Simulation Councils, Inc, USA, pp 13–20.

Lakhan, V.C., and Jopling, A., 1987. *Simulating the effects of random waves on concave-shaped nearshore profiles,* Geografiska Annaler, vol. 69 (A), pp 251-269.

Lakhan, V.C., and LaValle, P.D., 1987. *Development and testing of a simulation model for nearshore profile changes,* Presented at the Canadian Association of Geographers, Marine Studies Group, May 28, 1987, Hamilton, Ontario.

Lakhan, V.C., and LaValle, P.D., 1992. *Simulating the onshore–offshore movement of sediment in the coastal environment,* Environmental Software, An International Journal, vol. 7, pp 165-173.

Lakhan, V.C., and Trenhaile, A.S., 1989. *Models and the coastal system,* In: Applications in Coastal Modeling, Lakhan, V.C., and Trenhaile, A.S. (Eds.), Amsterdam, The Netherlands: Elsevier Science Publishers, pp 1-16.

Lakhan, V.C., Trenhaile, A.S., and LaValle, P.D., 1993. *Modelling and simulating morphological changes in the nearshore system,* Third International Geomorphological Conference. Program with Abstracts, The International Association of Geomorphologists, 176 pp.

Lang, G., Schumbert, R., Markofsky, M., Fanger, H.U., Grabemann, I., 1989. *Data Interpretation and Numerical Modeling of the Mud and Suspended Sediment Experiment 1985,* Journal of Geophysical Research, vol. 94 (C10), pp 14381-14393.

Larson, M., Kraus, N.C., and Hanson, H., 1990. *Decoupled numerical model of three-dimensional beach changes,* Proceedings of the 22nd Coastal Engineering Conference, American Society of Civil Engineers, pp 2173-2185.

Lam, N.T.; Stive, M.J.F.; Verhagen, H.J.; Wang, Z.B., 2007. *Morphodynamics of tidal inlets in a tropical monsoon area,* 4th International Conference Port Development and Coastal Environment, PDCE 2007, Varna, Bulgaria.

Launder, B.E., 1991. *Current capabilities for modelling turbulence in industrial flows,* Journal of Applied Scientific Research, vol. 48, pp 247-269.

Law, A.M., and Kelton, W.D., 1982. Simulation Modeling and Analysis, New York: McGraw-Hill Co.

Le Hir, P., 1994. *Fluid and sediment integrated-modelling: Application to fluid mud flows in estuaries,* In: Wallingford editor, Paper 41 in Proc. 4th Nearshore and Estuarine Cohesive Sediment Transport Conference, INTERCOH'94, J. Wiley, Chichester.

Le Hir, P., Bassoullet, P. & L'Yavanc, J., 1993. *Application of a multivariate transport model for understanding cohesive sediment dynamics,* In: Coastal and Estuarine Studies, A. Mehta (Eds.), vol. 42, pp 467-485.

Le Hir, P., Ficht, A., Silva Jacinto, R., Lesueur, P., Dupont, J.-P., Lafite, R., Brenon, I., Thouvenin, B., and Cugier, P., 2001. *Fine sediment transport and accumulations at the mouth of the Seine Estuary (France),* Estuarine Research Federation, vol. 24, pp 950-963.

Lesser, G., Van Kester, J., and Roelvink, J.A., 2000. *On-Line Sediment transport Within Delft3D-Flow,* Waterbouwkundig Laboratorium/Delft Hydraulics, Delft, Netherlands.

Lesser, G., Roelvink, J.A., van Kester J.A.T.M., Stelling, G.S., 2004. *Development and validation of a three-dimensional morphological model,* Coastal Engineering, vol. 51, pp 883-915.

Leybourne, A.E., 2002. Comparison of 2D and 3D Predictions of the FOR3D Acoustic Propagation Model in Shallow Water Flat Bathymetry Environments, Naval Research Lab Stennis Space Center, 130 pp.

Li, M., Fernando, P.T., Pan, S., O'Connor, B.A., Chen, D., 2007. *Development of a quasi-3d numerical model for sediment transport prediction in the coastal region,* Journal of Hydro-environment Res. Vol. 1 (2), pp 143-156.

Li, L., 2010. *A fundamental study of the Morphological Acceleration Factor,* Master Thesis, Delft University of Technology / Deltares, 102 pp.

Lick, W., Lick, J., and Ziegler, C. K., 1994. *The resuspension and transport of fine-grained sediments in Lake Erie,* Journal of Great Lakes Research, vol. 20(4), pp 599-612.

Ludwig, K. A. & Hanes, D. M. 1990. *A laboratory evaluation of optical backscatterance suspended solids sensors exposed to sand-mud mixtures,* Marine Geology, vol. 94, pp 173-179.

Luettich, R. A., Harleman, D. R. F., and Somlyody, L., 1990. *Dynamic behavior of suspended sediment concentrations in a shallow lake perturbed by episodic wind events,* Limnology and Oceanography, vol. 35 (5), pp 1050-1067.

Luthardt, H., 1987. *Analyse der Wassernahen Druck- und Windfelder über der Nordsee aus Routinebeobachtungen*, Hamburger Geophysikalische Einzelzeitschriften, A 83, in German.

Maa, J. P.-Y., Sanford, L.P., and Halka, J.P., 1998. *Sediment resuspension characteristics in the Baltimore Harbor,* Marine Geology, vol. 146, pp 137-145.

Maa, J.P.-Y., Kim, S.C., 2002. *A constant erosion rate model for fine sediment in the York River, Virginia,* Environmental Fluid Mechanics, vol. 1, pp 345-360.

Maa, J. P.-Y. and Lee, D.-Y., 2002. *A preliminary study on the measurement of high resolution marine sediment bed structure,* In: Fine Sediment Dynamics in the Marine Environment, J.C. Winterwerp and C. Kranenburg (Eds), Elsevier, pp 469-482.

Maa, J. P.-Y., Kwon, J.-I., Hwang, K.-N., and Ha, H.K., 2008. *Critical bed shear stress for cohesive sediment deposition under steady flows,* Journal of Hydraulic Engineering, vol. 134(12), pp 1767-1771.

MacIntyre, S., Lick, W., and Tsai, C. H., 1990. *Variablity of entrainment of cohesive sediments in freshwater,* Biogeochem., vol. 9, pp 187-200.

Mahatma, 2004. *The spatial and temporal patterns of erodibility of an intertidal flat in the East Frisian Wadden Sea, Germany,* Ph.D. Thesis, Coastal Research laboratory, University of Kiel, Germany, 129 pp.

Marren, P.M. 2005. *Magnitude and frequency in proglacial rivers: a geomorphological and sedimentological perspective,* Earth- Sciences Review, vol. 70(3−4), pp 203−251.

Mayerle, R., & Palacio, C., 2002. *Open Boundary Condition Approaches for Near Coastal Area Models,* In: 13th Congress of the Asia and Pacific Division of IAHR, Singapore.

Mayerle, R., Pramono, G., and Escobar, C., 2005. *Dimension and Roughness Distribution of Bed Forms in Tidal Channels in the German Bight*, Die Küste, Heft 69, pp 229-252.

Mayerle, R., Razakafoniaina, T., Palacio, C. & Pramono, G., 2002. *Bed forms and equivalent roughness sizes in tidal channels*, Proceedings of the International Conference on Fluvial Hydraulics (River Flow 2002), IAHR, Louvain-la-Neuve. Belgium.

Mayerle, R., Wilkens, J., Escobar, C., and Windupranata, W., 2005. *Hydrodynamic Forcing along Open Sea Boundaries of Coastal Models*, Die Küste, Heft 69, pp 203-228.

Mayerle, R., & Zielke, W., 2005. PROMORPH – Predictions of Medium-Scale Morphodyanimcs: Project Overview and Executive Summary, Die Küste, Heft 69, pp 1-24.

McAnally, W.H., Letter, J.V. and Thomas, W.A., 1986. *Two- and three-dimensional modelling systems for sedimentation*, Proc. Third Int. Symp. River Sedimentation, Mississippi, U.S.A., pp 400-411.

Mehta, A.J., 1986. *Characterization of cohesive sediment properties and transport processes in estuaries,* In: Estuarine Cohesive Sediment Dynamics, Mehta, A.J. (Eds.), Springer-Verlag, pp 290-325.

Mehta, A.J., Partheniades, E., 1975. *An investigation of the depositional properties of flocculated fine sediments,* Journal of Hydraulic Research, vol. 12, pp 361- 381.

Mehta, A.J., and E. Partheniades, 1973. *Depositional Behavior of Cohesive Sediments,* Tech report No. 16, Univ. of Florida, Gainesville, Florida.

Mehta, A. J., & Parchure, T. M., 2000. *Surface erosion of fine-grained sediment revisited,* In: Muddy coast dynamics and resource management, B.W. Flemming, M.T. Delafontaine, & G. Leibezeit (Eds.), Amsterdam, Elsevier, pp 55-74.

Mingham, C.G. and Causon, D.M., 1998. *A High Resolution Finite Volume Method for Shallow Water Flows,* Journal of Hydraulic Engineering, vol. 124 (6), pp605-614.

Mingham, C. G., 2003. *Advanced Numerical Methods for Coastal Hydrodynamics,* Elsevier Oceanography Series, vol.67, pp 73-91.

Mitchener, H. and Torfs, H., 1996. *Erosion of mud/sand mixtures,* Coastal Engineering, vol. 29 (1-2), pp 1-25.

Moody, J. A., Blrrman, B., and BOTHNER, M.H., 1987. *Near-bottom suspended matter concentration on the continental shelf during storms: estimates based on in situ observations of light transmission and a particle size dependent transmissometer calibration,* Continental Shelf Research, vol. 7, pp 609-628.

Mulder, H.P.J., Udink, C., 1991. *Modelling of cohesive sediment transport. A case study: the western Scheldt estuary,* In: Edge, B.L. (Eds.), Proceedings of the 22nd International Conference on coastal Engineering, ASCE, pp. 3012-3023.

Müller, M.J., 1996. *Handbuch Ausgewählter Klimastationen der Erde: 1272 Stationen,* Forschungsstelle Bodenerosion, Mertesdorf, 5th edition.

Neill, S.P., Hashemi, M.R., Elliott, A.J., 2007. *An enhanced depth-averaged tidal model for morphological studies in the presence of rotary currents,* Continental shelf research, vol. 27, pp 82-102.

Nicholson, J., Broker, I., Roelvink, J. A., Price, D., Tanguy, J. M. & Moreno, L., 1997. *Intercomparison of coastal area morphodynamic models,* Coastal Engineering, vol. 31, pp 97-123.

Nix, J. S., 1990. *Mathematical modeling of the combined sewer system, Chapter 2 in Control and treatment of combined sewer overflows,* P. E. Moffa (Eds.), New York, Van Nostrand Reinhold Company, pp 23- 78.

Noda, H., 2003. *Numerical models for nearshore currents,* In: Advances in coastal modelling, Lakhan, V.C. (Ed.), Elsevier Oceanography Series, vol. 67, pp 93-132.

Novak, P. and Cábelka, J., 1981. *Models in Hydraulic Engineering,* Pitman, London, 459 pp.

O'Connor, B.A., and Nicholson, J., 1988. *A three-dimensional model of suspended particle sediment transport,* Coastal Engineering, vol. 12, pp 157-174.

Odd, N.V.M., 1988. *Mathematical modeling of mud transport in estuaries,* In: Physical Processes in Estuaries, J. Dronkers and W. van Leussen (eds.), Springer Verlag, Berlin, pp 503-531.

Odd, N.V.M., Owen, M.W., 1972. *A two-layer model of mud transport in the Tames estuary,* Proceedings of Institute of Civil Engineers, London, pp 195–202.

Ohm, K., 1985. *Optische Messungen zur Bestimmung von Schwebstofftransporten*, Die Küste, Heide/Holstein, vol 42, pp 227–236.

Osinski, R.D., 2007. Numerical Modelling of Sediment Transport with application to the bay of Paranaguá, Brazil, Master Thesis, Technical University of Berlin, Germany, 122 pp.

Owen, M.W., 1970. *A detailed study of the settling velocities of an estuary mud,* Report INT78, Hydraulics Research Station, Wallingford, United Kingdom.

Owen. M.W., 1980. *A three-dimensional model of the Bristol Channel,* Journal of Physical Oceanography, vol. 10, pp 1290-1302.

Owen, M.W., and Odd, N.V.M., 1972. *A mathematical model of the effect of a tidal barrier on siltation in an estuary,* In: Tidal Power, T. J. Gray and O. K. Gashus (eds.), Plenum Press, New York, pp 456-485.

Ouchi, S., 1985. *Response of alluvial rivers to slow active tectonic movement,* Geological Society of America Bulletin, vol. 96, pp 504-515.

Palacio, C.A. 2002. Metodologia para la validación de modelos hidrodinámicos utilizando amplia información de campo: Aplicación a la bahía Meldorf en la costa del mar del norte Alemán, Ph.D. Thesis, Universidad Nacional de Colombia, Medellín, 181 pp.

Palacio, C., Mayerle, R., Toro, M., and Jiménez, N., 2005. *Modelling of Flow in a Tidal Flat Area in the South-Eastern German Bight*, Die Küste, Heft 69, pp 141-174.

Palacio, C., Mayerle, R., and Toro, F., 2002. *Tidal Analysis in the Meldorf Bight, North Sea Coast, Germany*, XV National Seminar of Hydraulic and Hydrology, Colombia.

Panagiotopoulos, I., Voulgaris, G., Collins, M., 1997. *The influence of clay on the threshold of movement of fine sandy beds,* Coastal Engineering, vol. 32, pp 19-43.

Parchure, T.M., 1984. *Effect of bed shear stress on the erosional characteristics of kaolinite,* Ph.D. Thesis, University of Florida, Gainesville, FL, 339 pp.

Parchure, T.M., Mehta, A.J., 1985. *Erosion of soft cohesive sediment deposits,* Journal of Hydraulic Engineering, ASCE, vol. 111, pp 1308- 1326.

Partheniades, E., 1962. *A study of erosion and deposition of cohesive soils in salt water,* Ph.D. Thesis, University of California at Berkeley, 182 pp.

Partheniades, E., 1965. *Erosion and deposition of cohesive soils,* Journal of Hydraulics Div., ASCE vol. 91(HY1), pp 105-139.

Partheniades, E., 2009. *Cohesive sediments in open channels: erosion, transport and deposition,* Butterworth-Heinemann imprint of Elsevier, 358 pp.

Péchon, P., Rivero, F., Johnson, H., Chesher, T., O'Conner, B., Tanguy, J.-M., Karambas, T., Mory, M.,Hamm, L., 1997. *Intercomparison of wave-driven current models,* Coastal Engineering, vol. 31, pp 199-215.

Pejrup, M., Edelvang, E., 1996. *Measurements of in situ settling velocities in the Elbe estuary*, Journal of Sea Research, vol. 36 (1-2), pp 109– 113.

Perillo, G.M. and Sequeira, M.E., 1989. *Geomorphologic and sediment transport characteristics of the middle Reach of the Bahia Blanca estuary (Argentina)*, Journal of Geophysics Research, vol. 94 (C10), pp 14351-14362.

Petersen, O., and Vested, H.J., 2002. *Description of Vertical Exchange Processes in Numerical Mud Transport Modelling,* In: Fine Sediment Dynamics in the Marine Environment, Winterwerp, J.C. and C. Kranenberg (Eds.), Elsevier, Amsterdam, pp 375-392.

Petersen, O., Vested, H.J., Manning, A.M., Christie, M., and Dyer K.R., 2002. *Numerical Modelling of Mud Transport Processes in the Tamar Estuary,* In: Fine Sediment Dynamics in the Marine Environment, Winterwerp, J.C. and C. Kranenberg (Eds.), Elsevier, Amsterdam, pp 643-654.

Phillips, N. A., 1957. A coordinate system having some special advantage for numerical forecasting, Journal of Meteorology, vol. 14, pp 184-185.

Piedra-Cueva, I., Mory, M., 2001. *Erosion of a deposited layer of cohesive sediment,* In: Coastal and estuarine fine sediment processes, McAnally W.H., & Mehta A.J. (eds), Elsevier, Amsterdam, pp 41-51.

Poerbandono, 2003. *Sediment Transport Measurement and Modeling in the Meldorf Bight Tidal Channels, German North Sea Coast,* Ph.D. Thesis. Coastal Research Laboratory, University of Kiel, Germany, 151 pp.

Poerbandono and R. Mayerle, 2005. *Composition and Dynamics of Sediments in Tidal Channels of the German North Sea Coast*, Die Küste, Heft 69, pp 63-92.

Poerbandono and R. Mayerle, 2005. *Effectiveness of Acoustic Profiling for Estimating the Concentration of Suspended Material*, Die Küste, Heft 69, pp 393-408.

Popper, K.R., 1968. *The Logic of Scientific Discovery*. New York: Harper Torchbooks.

Poulos, S.E., Collins, M.B., 2002. *Fluviate sediment fluxes to the Mediterranean Sea: a quantitative approach and the influence of dams,* In: Sediment Flux to Basins: Causes, Controls and Consequences, Jones, S.J., Frostick, L.E. (Eds.), Special Publications, vol. 191. Geological Society, London, pp. 227-245.

Pramono, G., 2005. T*he Study of Bedforms and Equivalent Roughness Sizes in the Central Dithmarschen Bight,* Ph.D. Thesis, Coastal Research Laboratory, University of Kiel, Germany, 136 pp.

Puleo, J.A., Butt, T., Plant, N.G., 2005. *Instantaneous energetics sediment transport model calibration,* Coastal Engineering, vol. 52, pp 647-653.

Puls, W., Kuehl, H., 1989. *The settling velocity of suspended solid matter in the river Elbe at Lauenburg and Bunthaus,* GKSS-Forschungszentrum Geesthacht G.m.b.H., Hamburg, Germany.

Rakha, K.A., 1998. *A quasi-3D phase-resolving hydrodynamic and sediment transport model,* Coastal Engineering, vol. 34, pp 277-311.

Raudkivi, A. J., 1990. *Loose boundary hydraulics,* third ed., Pergamon, Oxford, UK, 512 pp.

Reimers, H.-C, 2003. *Sedimentverteilung und Benthosverbreitung in den Watten der Dithmarscher Bucht als Indikator für morphodynamische Veränderungen,* Abschlußbericht zum Forschungsvorhaben "Sedimorph" im GKSS Hochschulprogramm, Berichte der GKSS 18, 49 pp.

Reimers, H.C., 1999. *Wirkungsweise von Buschlahnungen auf den Sedimenthaushalt von aufwachsenden Deichvorländern,* Research and Technology Centre Westcoast, University of Kiel, Büsum, Germany, Report no. 17.

Ricklefs, C., 1989. *Zur Sedimentologie und Hydrographie des Eider-Ästuars,* Berichte Nr. 35 - Geologisch-Paläontologisches Institut, Christian-Albrechts-Universität, Kiel.

Ricklefs, K., and Asp Neto, N.E., 2005. *Geology and Morphodynamics of a Tidal Flat Area along the German North Sea Coast*, Die Küste, Heft 69, pp 93-128.

Riethmüller, R., Heineke, M., Kühl, H., Keuker-Rüdiger, R., 2000. *Chlorophyll a concentration as an index of sediment surface stabilisation by microphytobenthos?,* Continental Shelf Research, vol. 20, pp 1351-1372.

Ris R.C., Holthuijsen, L.H., and Booij, N., 1999. *A third-generation wave model for coastal regions: II Verification,* Journal of geophysical research , vol. 104 (C4), pp7667-7681.

Rouse, H., 1937. *Modern conceptions of the mechanics of fluid turbulence,* Transactions of ASCE, vol. 102, pp 436-505.

Sanford, L.P., and Halka, J.P., 1993. *Assessing the paradigm of mutually exclusive erosion and deposition of mud, with examples from upper Chesapeake Bay*, Marine Geology, vol. 114, pp 37-57.

Sanford, L. P. and Maa, J. P.-Y., 2001. *A unified erosion formulation for fine sediments,* Marine Geology, vol. 179, pp 9-23.

Sargent, R.G., 1988. *A tutorial on validation and verification of simulation models,* Proceedings of the 1988 Winter Simulation Conference. CA: San Diego, pp 33-39.

Schrottke, K. and Abegg, F., 2005. *Measurements of Near Bed Suspended Sediment Dynamics in a Tidal Channel of the German Wadden Sea*, Die Küste, Heft 69, pp 353-368.

Schwartz, M.L. (Ed.), 2005. *Encyclopedia of Coastal Science,* Springer-Verlag, The Netherlands, 1211 pp.

Schweim, C., Prochnow, J. V., and Köngeter, J., 2002. *Numerical Assessment of Source and Sink Terms for Cohesive Sediments,* In: Fine Sediment Dynamics in the Marine Environment, J.C. Winterwerp and C. Kranenburg (Eds.), Elsevier, New York, pp 671-685.

Shi, Z., Zhou, H.J., Eittreim, S.L., Winterwerp, J.C., 2003. *Settling velocities of fine suspended particles in the Changjiang Estuary China*, Journal of Asian Earth Sciences, vol. 22 (3), pp 245–251.

Sierra, J.P., Azuz, I., Rivero, F., Sanchez-Arcilla, A., and Rodriguez, A., 1997. *Morphodynamic modelling in the nearshore area,* In: Computer Modelling of Seas and Coastal Regions III, Arcinas, J.R., and Brebbia C.A. (Eds.), Coastal 97, Boston, MA: Computational Mechanics Publications, pp 433-442.

Simons, D.B. and Sentürk, F., 1992. Sediment Transport Technology. Water Resource Publications (Littleton, Colo., USA), 897 pp.

Simpson, M.R., 2001. *Discharge Measurements using a Broad-Band Acoustic Doppler Current Profiler,* Open File Report 01-1. USGS, California, USA.

Sorensen, R. M., 2006. *Basic Coastal Engineering,* 3rd ed., Springer, New York, 324pp.

Sottolichio A., Le Hir P. and Castaing P., 2001. *Modeling mechanisms for the stability of the turbidity maximum in the Gironde estuary, France.* In: Coastal and Estuarine Fine Sediment Processes, W.H. McAnally, A.J. Mehta (Eds.), Elsevier, Amsterdam, pp 373-386.

Soulsby, R., 1997. *Dynamics of marine sands,* Telford, London, UK, 248 pp.

Sheng, Y. P., Bulter H. L., 1982. *Modelling coastal currents and sediment transport*, Porceedings of the 18th Coastal Engineering Conference, Cape Town, 14–19 November, pp. 1127-1148.

Stanev, E., Wolff, J.-O., Burchard, H., Bolding, K., and Flöser, G., 2003. *On the circulation in the East Frisian Wadden Sea: Numerical modeling and data analysis,* Ocean Dynamics, vol. 53, pp 27–51.

Stanev, E.V., Brink-Spalink, G., Wolff, J.-O., 2007. *Sediment dynamics in tidally dominated environments controlled by transport and turbulence: a case study for the East Frisian Wadden Sea*, Jurnal of Geophys Research, vol. 112, 20 pp.

Staneva, J., Stanev, E.V., Wolff, J.-O., Badewien, T.H., Reuter, R., Flemming, B., Bartholomä, A., Bolding, K., 2008. *Hydrodynamics and sediment dynamics in the German Bight.Afocus on observations and numerical modelling in the East Frisian Wadden Sea,* Continental Shelf Research, vol. 29, pp 302-319.Stive, M.J.F., and de Vriend, H.J., 1995. *Modelling shoreface profile evolution,* Marine Geology, vol. 126, pp 235-248.

Struiksma, N., 1985. *Prediction of 2-D bed topography in rivers,* Journal of Hydraulic Engineering, ASCE, vol. 111 (8), pp 1169 - 1182.

Talke, S.A.; Swart, H.E., 2006. *Hydrodynamics and morphology in the Ems / Dollard estuary : review of models, measurements, scientific literature and the effects of changing conditions,* Technical Report, IMAU Reports, Issue: R06-01, University of Utrecht, 78 pp.

Teeter, A.M., 2001. *Clay-silt sediment modeling using multiple grain classes: Part II. Application to shallow-water resuspension and deposition,* In: Coastal and estuarine fine sediment processes, McAnally, W.H. et al. (Eds.), Proceedings in Marine Science, vol. 3, pp. 173-187.

Teeter, A.M., and Johnson, B.H., 2005. *Atchafalaya Bar Channel Numerical Hydrodynamic And Fluid / Settled Mud Modeling,* Technical Report, Computational Hydraulics and Transport LLC, PO Box 569, Edwards, Ms 39066, 202 pp.

Ten Brinke, W.B.M. 1994. *Settling Velocities of Mud Aggregates in the Oosterschelde Tidal Basin (the Netherlands), Determined by a Submersible Video System,* Estuarine Coastal Shelf Science, vol. 39, pp 549–564.

Thomas, C., 2000. *1D modelling of the hydrodynamic response to historical morphological change in the Mersey estuary,* In: Modelling Estuary Morphology and Process, EMPHASYS Technical Report, FD1401, paper 9, pp 55-61.

Toorman, E.A., 2001. *Cohesive sediment transport modeling: European perspective,* In: Coastal and Estuarine Fine Sediment Processes, W.H. McAnally & A.J. Mehta, (Eds.), Proceedings in Marine Science, Elsevier Science, Amsterdam, vol. 3, pp.1-18.

Toorman, E.A., Bruens, A.W., Kranenburg, C., & Winterwerp, J.C., 2002. *Interaction of suspended cohesive sediment and turbulence,* In: Fine Sediment Dynamics in the Marine Environment, J.C. Winterwerp & C. Kranenburg (Eds.), Proceedings in Marine Science, Elsevier Science, Amsterdam, vol. 5, pp 7-23.

Torfs, H., 1995. *Erosion of mud/sand mixtures,* Ph.D. Thesis, Catholic Univ. of Leuven, Leuven, Belgium, pp 223.

Torfs, H., Mitchener, H., Huysentruyt, H., Toorman, E., 1996. *Settling and consolidation of mud/sand mixtures,* Coastal Engineering, vol. 29 (1-2), 27–45.

Torfs, H., Jiang, J., Mehta, A.J., 2001. *Assessment of the erodability of fine/coarse sediment mixture*, In: Coastal and Estuarine Fine Sediment Processes, McAnally, W.H., Mehta, A.J. (Eds.), Elsevier, Amsterdam, pp 109-123.

Toro, F., 2003. *A Decision Support System In The Development Of A Hydrodynamic Numerical Models,* Ph.D. Thesis, Coastal Research laboratory, University of Kiel, Germany, 105 pp.

Toro, F., Mayerle, R., Poerbandono, and Wilkens, J., 2005. *Patterns of Hydrodynamics in a Tide-Dominated Coastal Area in the South-Eastern German Bight*, Die Küste, Heft 69, pp 25-62.

Tsimplis, M.N., Josey, S.A., Rixen, M., Stanev, E.V., 2004. *On the forcing of sea level in the Black Sea,* Journal of Geophysical Research, vol. 109 (C8), C08015, 13 pp.

Tung, T.T., Walstra D.J.R., van de Graaff, J., Stive, M.J.F., 2009. *Morphological modelling of tidal inlet migration and closure,* 10th International Coastal Symposium (ICS 2009), APR 13-18, 2009 Lisbon, POLAND, Journal of Coastal Research vol. 2, Special Issue: Sp. Iss., pp 1080-1084.

Uncles, R.J., and Stephens, J.A., 1989. *Distributions of suspended sediment at high water in a macrotidal estuary,* Journal of Geophpical Research, vol. 94, pp 14395-14405.

US Army Corps of Engineers (USACE), 2008. *Coastal Engineering Manual*, EM1110-2-1100, US Army Corps of Engineers, Washington, DC, US, (in six volumes).

Valeur, J.R., Pejrup, M., Jensen, A., 1996. *Particle dynamics in the sound between Denmark and Sweden,* ASCE Conf Proc, Coastal Dynamic '95, pp 951-962.

Van der Lee, W.T.B., 2000. *The settling of mud flocs in the Dollard estuary, The Netherlands,* Ph.D. Thesis, University of Utrecht, 133 pp.

Van der Werf, J.J., 2003**.** *A literature review on sand transport under oscillatory flow conditions in the rippled-bed regime,* Ph.D. Thesis, University of Twente, The Netherlands, 60 pp.

Van Ledden, M. 2002. *A process-based sand mud model,* In: International Conference on Cohesive Sediments, Winterwerp, J.C., Kranenburg, C. (Eds.), Intercok 2000, Delft, The Netherlands. Proceedings of Marine Science, Elsevier, Amsterdam, pp 577-594.

Van Ledden, M., 2000. Sediment segregation in estuaries and tidal lagoons. A literature review., Technical report, TUDelft, October 2000.

Van Leussen, W., and Corneliss, J.M., 1993. The determination of the sizes and settling velocities of estuarine flocs by an underwater video system, Netherlands Journal of Sea Research, vol. 31, pp 231-241.

Van Rijn, L.C., 1993. Principles of Sediment Transport in Rivers, Estuaries and Coastal Seas, Aqua Publications, The Netherlands, 715 pp.

Van Rijn, L.C., 1984a. *Sediment transport, Part I: Bed load transport,* Journal of Hydraulic Engineering, vol. 110(10), pp 1431-1456.

Van Rijn, L.C., 1984b. *Sediment transport, Part II: Suspended load transport,* Journal of Hydraulic Engineering, vol. 110(11), pp 1613-1641.

Van Rijn, L.C., 1984c. *Sediment transport, Part III: Bed forms and alluvial roughness,* Journal of Hydraulic Engineering, vol. 110 (12), pp 1733-1754.

Van Rijn, L.C., 1989. *Handbook of Sediment Transport by Currents and Waves,* Delft Hydraulics. Delft, The Netherlands, 420 pp.

Van Rijn, L.C., 2007a. *Unified view of sediment transport by currents and waves, I: Initiation of motion, bed roughness and bed-load transport,* Journal of Hydraulic Engineering, ASCE, vol. 133 (6), pp 649-667.

Van Rijn, L.C., 2007b. *Unified view of sediment transport by currents and waves, II: Suspended transport,* Journal of Hydraulic Engineering, ASCE, vol. 133 (6), pp 668- 689.

Van Rijn, L.C., 2007c. *Unified view of sediment transport by currents and waves, III: Graded beds.* Journal of Hydraulic Engineering, ASCE, vol. 133 (7), pp 761-775.

Van Rijn, L.C., Walstra, D.J.R., and van Ormondt M., 2007. *Unified view of sediment transport by currents and waves. IV: Application of morphodynamic model,* Journal of Hydraulic Engineering, vol. 133 (7), pp 776-793.

Van Rijn, L.C., and D.J.R. Walstra, 2003. *Modelling of sand transport in delft3d,* Technical Report, Z3624, WL Delft Hydraulics.

Van Rijn, L.C., Meijer, K., 1988. *Three dimensional mathematical modelling of suspended sediment transport in current and waves, IAHR Symposium on Mathematical Modelling of Sediment Transport in the Coastal Zone,* Copenhagen, Denmark, pp 89–99.

Van Wijngaarden, M., Roberti, J.R., 2002. *In situ measurements of settling velocity and particle distribution with the LISSTST,* In: Fine Sediment Dynamics in the Marine Environment, Winterwerp, J.C., Kranenburg, C. (Eds.), Elseiver Science, Amsterdam, pp 295-311.

Vela-Diez, S., 2001. *Sediment Mapping of the Tidal Flat Channels off Büsum,* M.Sc. Thesis, Coastal Research Laboratory, University of Kiel, Germany, 91 pp.

Velegrakis, A.F., Collins, M.B., Bastos, A.C., Phaphitis, D, and Brampton, A., 2007. *Seabed sediment transport pathways investigations: review of scientific approach and methodologies,* In: Coastal and Shelf Sediment Transport, Balson, P.S. and Collins, M.B. (Eds.), Geological Society of London, Special Publication 274, pp 127-146.

Verboom, G.K., De Ronde, J.G., and Van Dijk, R.P., 1992. *A fine grid tidal flow and storm surge model of the North Sea,* Continental Shelf Research, vol. 12, pp 213-233.

Vinzón, S., and Paiva, A.M., 2002. *Modeling the Sediment Concentration Profiles at the Amazon Shelf,* In: Fine Sediment Dynamics in the Marine Environment, J. Winterwerp and C. Kranenburg (Eds.) Proc. Marine Science, Elsevier, vol. 5, pp 687-702.

Violeau, D., Bourban, S., Cheviet, C., Markofsky, M., Petersen, O., Roberts, W., Spearman, J. Toorman, E.A., Vested, H.J., and Weilbeer, H., 2002. *Numerical Simulation of Cohesive Sediment Transport: Intercomparison of Several Numerical Models*. In: Fine Sediment Dynamics in the Marine Environment, Winterwerp, J.C. and C. Kranenberg (Eds.), Elsevier, Amsterdam, pp 75-90.

Walker, T.A., 1981. *Dependence of phytoplankton chlorophyll on bottom resuspension in Cleveland Bay, Northern Queensland,* Australian Journal of Marine and Freshwater Research, vol. 32, pp981-986.

Walstra, D.J.R., Roelvink, J.A., Groeneweg, J., 2000. *3D calculation of wave-driven cross-shore currents,* Proceedings 27th International Conference on Coastal Engineering, July 16-21, Sydney.

Walstra, L.C., Van Rijn, L.C., Blogg, H., and Van Ormondt, M., 2001. *Evaluation of a hydrodynamic area model based on the COAST3D data at Teignmouth 1999*, Report 121-EC MAST Project, MAS3-CT97-0086, HR Wallingford, UK.

Walstra, D.J.R., Sutherland, J., Hall, L., Blogg, H., Van Ormondt, M., 2001. *Verification and comparison of two hydrodynamic area models for an inlet system,* Proceedings of Coastal Dynamics '01, the Fourth Conference on Coastal Dynamics, Lund, Sweden. ASCE, Reston, VA, pp 433-442.

Wang, S.S.Y., and Adeff, S.E., 1986. *Three-Dimensional Modeling of River Sedimentation Processes,* Proceedings of the 3rd Int. Symp. on River Sedimentation, Univ. of Mississippi, Oxford, MS, pp. 496-1505.

Wang, D.-P., 1989. *Model of mean and tidal flows in the Strait of Gibraltar,* Deep Sea Res., 36, 1535- 1548.

Warren, R., 1993. *Development and application of a generic modelling system for coastal processes,* In: Large-Scale Coastal Behavior '93, List, J.H. (Ed.), US Geological Survey Open-File Report 93-381, pp 22-223.

Welsch, C.A., 2002. *Assessment of Delft3D Morphodynamic Model During Duck94,* Master Thesis, Naval Postgraduate School Monterey, Canada, 40 pp.

Whitehouse, R., Basssoullet, P., Dyer, K., Mitchener, H., and Roberts, W., 2000. *The influence of bedforms on flow and sediment transport over intertidal mudflats,* Continental Shelf Research, vol. 20, pp 1099-1124.

Wilkens, J., 2004. *Medium Scale Morphodynamics of the Central Dithmarschen Bight,* Ph.D. Thesis, Coastal Research Laboratory, University of Kiel, Germany, 181 pp.

Wilkens, J., Junge, I., and Hoyme, H., 2005. *Modelling of Waves in a Tidal Flat Area in the South-Eastern German Bight*, Die Küste, Heft 69, pp 175-202.

Wilkens, J., and Mayerle, R., 2005. *Morphodynamic Response to Natural and Anthropogenic Influences in the German Bight*, Die Küste, Heft 69, pp 311-338.

Win-Juinn, C., and Ching-Ton, K., 1991. *Numerical model of beach profile changes,* In: Computer Modelling in Ocean Engineering 91, Arcilla, A.S., Pastor, M., Zienkiewicz, O.C., and Schrefler B.A. (Eds.), Rotterdam, The Netherlands: A.A. Balkema, pp 219-225.

Winter, C., & Mayerle, R., 2003. *Calibration of a sediment transport model using field measurements,* In: Davis RA, Sallenger A, Howd P (Eds.) Proc int symp coastal sediments 2003, 18–23 May 2003, Clearwater Beach, Florida. World Scientific, Hackensack, New Jersey.

Winter, C., Poerbandono, Hoyme, H., and Mayerle, R., 2005. *Modelling of Suspended Sediment Dynamics in Tidal Channels of the German Bight*, Die Küste, Heft 69, pp253-278.

Winterwerp, J.C., 1998. *A simple model for turbulence induced flocculation of cohesive sediment,* IAHR, Journal of Hydraulic Engineering, vol. 36 (3), pp 309-326.

Winterwerp, J.C., 1999. *Hindered settling and self-weight consolidation,* Delft University of Technology and WL|delft hydraulics, Report Z2386, June 1999.

Winterwerp, J.C., 1999. *Flocculation and settling velocity,* Delft University of Technology and WL|delft hydraulics, Report Z2386, June 1999.

Winterwerp, J.C., 2001. *Stratification effects by cohesive and noncohesive sediment,* Journal of Geophysical Research, vol. 106 (C10), pp 22559-22574.

Winterwerp, J.C., 2002. *On the flocculation and settling velocity of estuarine mud,* Continental Shelf Research, vol. 22, pp 1339–1360.

Winterwerp, J.C., Cornelisse, J.M., Kuijper, C., 1992. *A Laboratory study on the behaviour of mud from the Western Scheldt under tidal conditions,* Proceedings of the Workshop on Nearshore and Estuarine Cohesive Sediment Transport, April 1991 1992 , pp 295-313.

Winterwerp, J.C., and Kranenburg, C., 2002. *Fine sediment dynamics in the marine environment,* In: Elsevier Science B.V., editor, Proceedings in Marine, vol. 5, P.O. Box 211, 1000 AE Amsterdam, The Netherlands, 730 pp.

Winterwerp, J.C., Van Kesteren, W.G.M., 2004. *Introduction to the physics of cohesive sediments in the marine environment,* In: Developments in Sedimentology, vol. 56. Elsevier, Amsterdam, 576 pp.

WL | Delft Hydraulics. 2004/2007. D*elft3D-FLOW, Simulation of multi-dimensional hydrodynamic flows and transport phenomena,* including sediments, User Manual, Delft.

Wright, A., and Norton, P., 2000. *Inter-comparison between one, two, and three-dimensional numerical models,* MAFF Project FD1401, Modelling Estuary Morphology and Processes - Final Report, EMPHASYS Consortium.

Xie, M., Zhang, W., & Guo, W., 2010**.** *A validation concept for cohesive sediment transport model and application on Lianyungang Harbor, China,* Coastal Engineering, Elsevier, vol. 57 (6), pp 585-596.

Yang, S. L., Zhang, J., & Zhu, J., 2004. *Response of suspended sediment concentrations to tidal dynamics at a site inside the mouth of an inlet: Jiaozhou Bay (China)*, Hydrology and Earth System Sciences, vol. 8, pp 170–182.

Zaneveld, J.R.V., Spinrad, R.W., & Bartz, R. 1982. *An optical settlingtube for the determination of particle-size distributions*, Marine Geology, vol. 49, pp 357- 376.

Zeigler, B.P., Praehofer, H., and Kim, T.G., 2000. *Theory of Modeling and Simulation,* 2nd ed. New York, Academic Press, 510 pp.

Zerull, R.H., and Weiss, K., 1974. *Scattering properties of irregular dielectric and absorbing particles, In* Atmospheric Aerosols: their Optical Properties and Effects, Optical Society of America, Washington DC.

Ziervogel, K., and Bohling, B., 2003. Sedimentological parameters and erosion behaviour of submarine coastal sediments in the south-western Baltic Sea, Geo-marine letters, vol. 23 (1), pp 43-52.

Erklärung

Hiermit erkläre ich, dass die Abhandlung – abgesehen von der Beratung durch meine akademischen Lehrer, nach Inhalt und Form meine eigene Arbeit ist. Diese Arbeit hat an keiner anderen Stelle im Rahmen eines Prüfungsverfahrens vorgelegen. Außerdem erkläre ich, dass dies mein erster Promotionsversuch ist.

Kiel, den 10. May. 2011
Maryam Rahbani